IAHR YPN Young Professionals Network
Hosted by Spain Water and IWHR, China

IAHR AIRH International Association for Hydro-Environment Engineering and Research
Hosted by Spain Water and IWHR, China

2nd IAHR Young Professionals Congress

Online. 30 Nov. - 2 Dec. 2021

PROCEEDINGS

Editors: David Ferras, Emanuele Quaranta, Eva Fenrich, Gaetano Crispino, José M. Carrillo, Livia Pitorac and Manish Pandey

The papers included in this volume were part of 2nd IAHR Young Professionals Congress cited on the cover and title page. Papers were selected and subject to review by the editors and International Scientific Committee. The papers published in these proceedings reflect the work and thoughts of the authors and are published herein as submitted. The publisher is not responsible for the validity of the information or for any outcomes resulting from reliance thereon.

Proceedings of the 2nd IAHR Young Professionals Congress Online. 30 NOV. – 2 Dec. 2021

Editors: Emanuele Quaranta, Eva Fenrich, Gaetano Crispino, José M. Carrillo, Livia Pitorac, Manish Pandey and David Ferras.

Published by: International Association for Hydro-Environment Engineering and Research - IAHR
Pª Bajo Virgen del Puerto, 3 28005 Madrid, SPAIN
A-1 Fuxing Road, Haidian District, 100038, Beijing, CHINA

ISBN: 978-90-824846-7-0 IAHR publications follow the Ethical Guidelines and Codes of Conduct provided by the Committee of Publication Ethics (COPE).

IAHR, founded in 1935, is a worldwide independent member-based organization of engineers and water specialists working in fields related to the hydro-environmental sciences and their practical application. Activities range from river and maritime hydraulics to water resources development and eco-hydraulics, through to ice engineering, hydro informatics, and hydraulic machinery. IAHR consists of two offices: Madrid Office, Spain and Beijing Office, China.

Foreword

The year 2021 has been a difficult Covid-19 year again. The ups and downs of the health crisis has brought a rise in science skepticism and even denialism. We have been exposed through the social media to a number of grounds that should be of concern to any scientist of any field, such as the cherry picking of data, fabrication of fake controversies or the continuous distortion of scientific claims. Critical thinking might have been blurred by such context, but it is precisely during crises when integrity becomes relevant. Pseudoscience, and especially denialism, is a threat to scientific advance not only in the field of medicine but also in hydro-environment, and the climate-change explanatory war is a good example of it.

Walking the line of science is doing the business of "explaining things at our best". For this purpose the hydro-environment community of researchers and professionals have gathered again during the 2nd edition of the IAHR Young Professionals online Congress, once more connecting the youth with the not-so-youth. The congress has welcomed 840 participants from 90 different countries. The participants have had access to 100 research contributions offered by young professionals who have been supported by 80 IAHR senior members that composed the International Scientific Committee of the congress. Students, young academics and practitioners have had the chance therefore to openly receive advice and mentoring from the top scientists of the IAHR network.

The importance of fundamental physics, the relative relevance of artificial intelligence and big data, the scope of physical and numerical data in providing scientific explanations, the need of urgent actions to solve hydro-environmental problems, or the encouragement to the curiosity-driven pioneers. All these issues have been hot topics during the IAHR Young Professionals congress in which the keynote speakers, session chairs and young professionals provided their critical standpoints. From the organizing committee we are immensely grateful to the parts that contributed to this knowledge sharing, which certainly fed with optimism the young generations who sooner than later will take the floor of hydro-environment's future.

Emanuele Quaranta
Eva Fenrich
Gaetano Crispino
José M. Carrillo
Livia Pitorac
Manish Pandey
David Ferras

ISBN: 978-90-824846-7-0

Table of Contents

Coastal and Maritime Hydraulics

Experimental Methods and Instrumentation

Fluid Mechanics

Fluvial Hydraulics and Reservoir Sedimentation

Hydraulic Machinery and Transient Flows

Hydraulic Structures

IAHR YPN

Young Professionals Network

Hosted by
Spain Water and IWHR, China

IAHR AIRH

International Association for Hydro-Environment Engineering and Research

Hosted by
Spain Water and IWHR, China

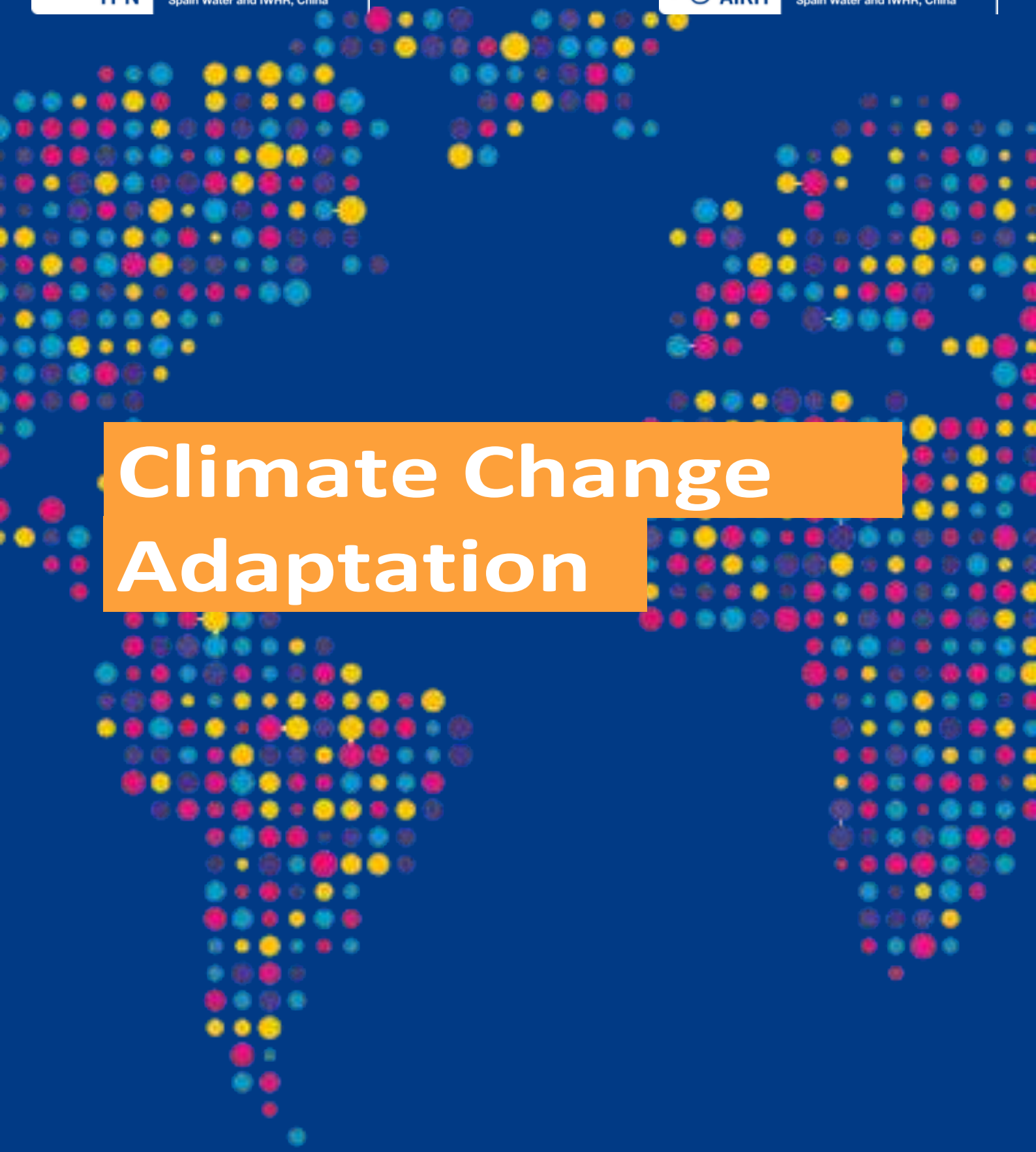

Climate Change Adaptation

Proceedings of the 2nd IAHR
Young Professionals Congress
30 Nov-2 Dec. 2021

Blue-green and red? Identifying the potential synergies in wastewater heat recovery and decentralized wastewater treatment

Madhu K. Murali [1] and Aonghus McNabola [2]

[1] Department of Civil, Environmental and Structural Engineering, Trinity College Dublin, Dublin, Ireland
muralim@tcd.ie

[2] Department of Civil, Environmental and Structural Engineering, Trinity College Dublin, Dublin, Ireland
amcnabol@tcd.ie

ABSTRACT

With an increasing focus on decarbonizing heating energy and improving the adaptability of urban water systems to climate uncertainties, there is an opportunity to identify the synergies between two measures related to addressing these issues: Wastewater Heat Recovery (WWHR) and decentralized wastewater treatment, respectively. As compared to traditional sewer-scale WWHR systems, combining decentralized wastewater treatment with WWHR has one main advantage, there is less uncertainty around wastewater temperatures. This is a key parameter for certain biological treatment processes. The reduced uncertainty is mainly due to the increased proximity between the WWHR and decentralized treatment plant, leading to less retention time in sewers. If a common regulatory framework could be developed around WWHR and decentralized wastewater, there could be significant opportunities for synergy between them.

Keywords: Wastewater Heat Recovery; Drainwater Heat Recovery; Decentralized Wastewater Treatment.

1 INTRODUCTION

With up to 40% of the energy in European cities being used for space and water heating (Garcia Pardo et al., 2012), there is a growing focus on reducing and decarbonizing this significant energy expenditure. Wastewater Heat Recovery (WWHR) is an option to reduce this energy use and involves reclaiming the thermal resource available in wastewater using heat pumps or heat exchangers (Nagpal et al., 2021). WWHR can occur across different scales based on the overall thermal resource available (Figure 1) which depends mainly on wastewater temperature and volumetric flows. Wastewater is warmest at the component or building level and progressively cools as it reaches a treatment plant through the sewer network (Figure 1). Conversely, the highest flows are available further down the network in sewer mains and treatment plants.

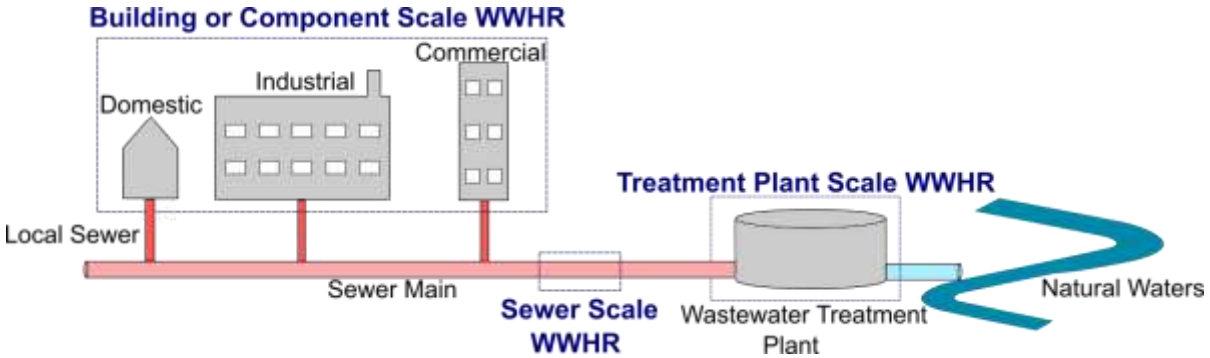

Figure 1. Potential Wastewater Heat Recovery (WWHR) scales across a centralized urban wastewater network. The colour of the pipes represent the relative heat embedded in the wastewater.

It has been suggested that existing centralized urban water systems are not well equipped to deal with the challenges of growing populations and anthropogenic climate change (Brown et al., 2009). Decentralizing wastewater treatment by using smaller community or household scale treatment plants can be one of the solutions in improving the resilience and sustainability of urban water systems. There is a potential for combining decentralized wastewater with WWHR to obtain better outcomes for the sustainability of urban water systems and the decarbonization of heating energy. However, their combined implementation may not necessarily be synergistic. Hence, this paper aims to analyse existing literature to determine the potential synergies in implementing WWHR alongside the use of decentralized wastewater treatment. Further work is also proposed to improve knowledge in this area.

ISBN: 978-90-824846-7-0

2 OPPORTUNITIES FOR SYNERGY

Currently, one of the restrictions in implementing WWHR, particularly in the sewer-scale, is that excess heat removal from wastewater can have an impact on temperature-dependent downstream biological treatment processes, particularly nitrification (Wanner et al., 2005). Further, there is significant uncertainty in wastewater temperature dynamics within sewers, which can depend on the sewer diameter, ground temperature, flow height and other parameters (Abdel-Aal et al., 2015). This contributes to difficulties in predicting inlet wastewater temperature to treatment plants after WWHR in long stretches of sewers. Decentralizing wastewater treatment to the appropriate level combined with WWHR could address some of these issues. For example, by reducing the proximity between WWHR and the treatment plant or even combining them into one facility, the travel time in sewers could be reduced significantly leading to less uncertainties in wastewater temperature. Wastewater temperature optimization could also be easier with closer proximity and/or combined operations with the WWHR system. The ideal scale for this kind of combined system would likely be larger than the residential scale, where WWHR with a heat pump is not yet feasible (Spriet & McNabola, 2019). Some of these advantages also exist in centralized treatment plant-scale WWHR systems, however, these can have other drawbacks such as requiring sufficiently large heating demand close to the treatment plant and potentially lower wastewater temperatures after longer residence times in sewers.

There are some uncertainties within this synergy, mainly to do with the scale of the proposed benefits and difficulties in implementation. Decentralized wastewater and WWHR have both proven to be difficult to implement due to issues related to their governance and interactions with existing infrastructure. This is a complicated issue to address and collaborative governance has been suggested as one of the options to improve outcomes and implementation from these types of projects (Malekpour et al., 2021). In terms of more technical issues, the scale of heat loss in sewers is dependent on the network design and local conditions; this may result in situations where there may be no improvement in thermal resource from decentralized WWHR compared to a centralized treatment plant. Additional work in this area focused on measuring or modelling the temperature across different parts of a wastewater network could address this knowledge gap.

3 CONCLUSIONS

Treating wastewater in smaller scales through decentralization could also have benefits in improving WWHR. These benefits mainly occur through a reduction in uncertainty around wastewater temperature by reducing transit times in sewers before treatment. There may also be a heating improvement by using higher temperature wastewater in upstream parts of the sewer network, but the scale of this improvement is yet to be quantified.

ACKNOWLEDGEMENTS

This research was part funded by the ERDF Interreg Ireland-Wales Programme 2014-2020, through the Dŵr Uisce Project (80910).

REFERENCES

Abdel-Aal, M., Mohamed, M., Smits, R., Abdel-Aal, R. E., De Gussem, K., Schellart, A., & Tait, S. (2015). Predicting wastewater temperatures in sewer pipes using abductive network models. *Water Science and Technology*, *71*(1), 89–96. https://doi.org/10.2166/wst.2014.398

Brown, R. R., Keath, N., & Wong, T. H. F. (2009). Urban water management in cities: Historical, current and future regimes. *Water Science and Technology*, *59*(5), 847–855. https://doi.org/10.2166/wst.2009.029

Garcia Pardo, N., Vatopoulos, K., Krook Riekola, A., Perez Lopez, A., & Olsen, L. (2012). *Best available technologies for the heat and cooling market in the European Union*. Publications Office of the European Union. https://data.europa.eu/doi/10.2790/5813

Malekpour, S., Tawfik, S., & Chesterfield, C. (2021). Designing collaborative governance for nature-based solutions. *Urban Forestry & Urban Greening*, *62*, 127177. https://doi.org/10.1016/j.ufug.2021.127177

Nagpal, H., Spriet, J., Murali, M. K., & McNabola, A. (2021). Heat Recovery from Wastewater—A Review of Available Resource. *Water*, *13*(9), 1274. https://doi.org/10.3390/w13091274

Spriet, J., & McNabola, A. (2019). Decentralized drain water heat recovery: A probabilistic method for prediction of wastewater and heating system interaction. *Energy and Buildings*, *183*, 684–696. https://doi.org/10.1016/j.enbuild.2018.11.036

Wanner, O., Panagiotidis, V., Clavadetscher, P., & Siegrist, H. (2005). Effect of heat recovery from raw wastewater on nitrification and nitrogen removal in activated sludge plants. *Water Research*, *39*(19), 4725–4734. https://doi.org/10.1016/j.watres.2005.09.026

Proceedings of the 2nd IAHR
Young Professionals Congress
30 Nov-2 Dec. 2021

Impacts of particulate matter on the Arabian Sea tropical cyclones - Pollutants from India are a major concern

Gobishankar Sathiyamohan[1]

[1]University of Sri Jayewardenepura 1, Nugegoda, Sri Lanka,
gobishankarsathiyamohan@gmail.com

ABSTRACT

Tropical cyclones (TC) are one of the most catastrophic natural disasters in the Northern Indian Ocean (NIO) including the Arabian Sea and the Bay of Bengal which brings floods, strong winds and landslides. The formation, intensification and inhibition of TC depend on environmental factors. The increase in frequency of TC could be due to climate change and air pollution. Particulate matter (PM) and aerosols released into the ambient air are transported through the wind and accumulate over the ocean surface. This directly and indirectly affects the TC formation and intensification. We used the forecast data from Whole Atmospheric Community Climate Model (WACCM) to observe the PM over the Arabian Sea surface during the cyclonic events and archived meteorological data from HYSPLIT to observe the pollutant trajectories. Our results suggest there is a positive relationship between TC and PM. Also, PM from India is a contributor to cyclone formation and intensification.

Keywords: Tropical cyclones; particulate matter; Arabian Sea; HYSPLIT; WACCM.

1 INTRODUCTION

Tropical cyclones are a type of extreme weather event. They form as result of several environmental conditions such as wind shear, warm sea surface temperature, humidity, and atmospheric instability. This is particularly true in Northern Indian Ocean where the Bay of Bengal and the Arabian Sea are becoming hotspots for frequent tropical storms. Sudden weather changes such as floods, landslides and strong winds have dire consequences that would lead to the loss of lives and livelihood, displacement of climate refugees, and property loss worth billions in countries like India, Bangladesh, Iran, Pakistan, and Sri Lanka. Anthropogenic emissions such as particulate matter and aerosols can also impact tropical cyclone formation and inhibition. According to Evan *et al.*,2011 from 1997 to 2010 cyclone frequency in the Arabian Sea was increased. Black carbon and particulate matter clouds block the sun's radiation above the surface leading to cooling in the upper ocean surface relative to the equatorial Indian Ocean. This environment enhances the formation of a deep depression which then intensifies into more violent tropical cyclones. Ultimately the strength of the cyclones and their direction are affected by particulate matter and aerosols. Anthropogenic emissions from the countries surrounding the northern Indian Ocean contribute to this situation often. Considering major air pollutant particulate matter from the Indian subcontinent, their impact on tropical cyclones is studied here. Our objective is to predict the movement of air parcels and identify their locality to study their impact on tropical cyclone formation.

2 DATA

The Cyclonic data for the last four cyclones Tuktae, Gati, Nisarga, and Pawan which occurred in the Arabian Sea data was collected from the Indian Meteorological Department's published documents. Data for WACCAM analysis- Web-based sea surface particulate matter data were used for the WACCM model and were obtained from National Centre for Atmospheric Research. Data for HYSPLIT analysis - Web-based HYSPLIT model was obtained from NOAA READY site. The gridded archive meteorology data available within READY prevail during the storm event and were obtained from the archived GDAS data, which is using vertical pressure coordinates with a spatial resolution of 1°and temporal resolution of 12-hour version was used to run the web-based HYSPLIT model to track the pollutant dispersion into the Arabian sea.

3 METHODOLGOY

We used the web version of WACCM to create the map for particulate matter composition in the Arabian Sea. Also, we used the web version of HYSPLIT to run backward pollution movement in the Arabian sea region at 100m, 500m, and 1000m vertical heights.

ISBN: 978-90-824846-7-0

4 RESULTS AND DISCUSSION

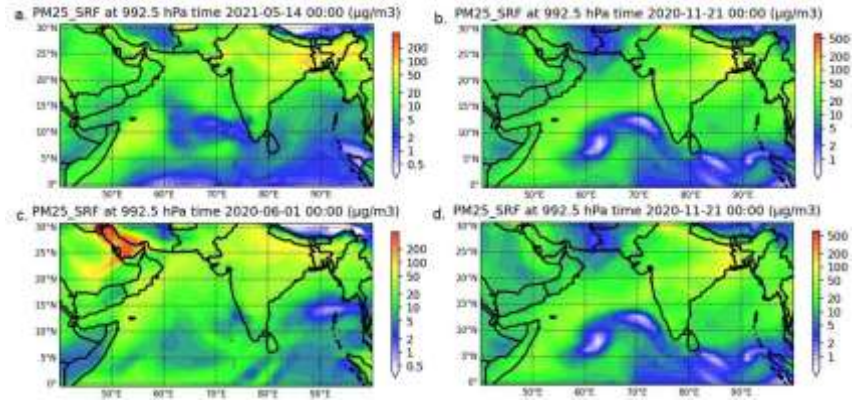

Figure 1. WACCM outputs a,b,c,d shows PM concentration over the Arabian Sea for tropical cyclones Tuktae, Gati, Nisarga, Pawan during deep depression stage.

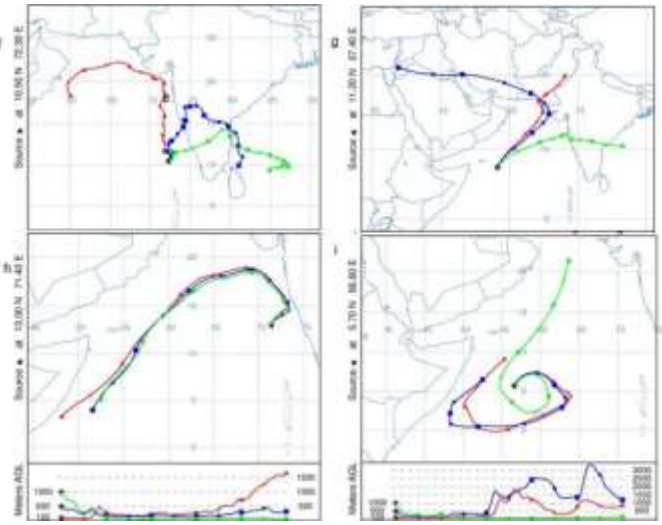

Figure 2. HYSPLIT output f,g,h,i indicates air parcel movement of backward trajectories for five consecutive days from the moment of formation of deep depression for cyclones Tuktae, Gati, Nisarga, and Pawan.

WACCM output show the particulate matter was very high in India relative to other countries. During the cyclonic event, the particulate matter forms a thick layer and high concentration in the outer periphery of the deep depression. Also, all the deep depressions formed are intensified to tropical cyclones over the sea surface indicate there is a clear connection between particulate matter pollution and cyclone formation and intensification. The HYSPLIT output indicates during Tuktae, Gati air pollution originated from Indian states and for Nisarga, and Pawan shows the air pollutants were carried from Arabian Sea itself.

5 CONCLUSIONS

The trend shows that the occurrence of cyclones is favored by regional climate shifts caused by the emission of particulate matter. The pollutant particulate matter, and black carbon were emitted by several countries and India is a large contributor to it. The findings point out hazardous effects of particulate matter far off health impacts. If anthropogenic pollutants significantly affect the cyclone formation and intensification the main contributor to this man-made hazard is India in the Indian Ocean region.

REFERENCES

Evan, A.T., Kossin, J.P. and Ramanathan, V. (2011). Arabian Sea tropical cyclones intensified by emissions of black carbon and other aerosols. *Climate change* Nature, 479(7371), pp.94-97.

ISBN: 978-90-824846-7-0

The influence of extremely shallow conditions on rock slope stability

Stefano Marino [1], Giuseppe Roberto Tomasicchio [2] , Leonardo Damiani [1] , Antonio Francone [1] , Giulio Scaravaglione [1] and Alessandra Saponieri [2]

[1] Dept. of Civil, Environmental, Building Engineering and Chemistry, Polytechnic University of Bari, Bari, Italy, stefano.marino@poliba.it, leonardo.damiani@poliba.it, antonio.francone@poliba.it, giulio.scaravaglione@poliba.it

[2] Dept. of Engineering for Innovation, University of Salento, , Lecce, Italy, roberto.tomasicchio@unisalento.it , alessandra.saponieri@unisalento.it

ABSTRACT

The aim of this research is to investigate the influence of the extremely shallow foreshores on the slope stability of a rubble mound breakwater. New tests have been performed on a 2D physical model in presence of a mild slope foreshore (1:30), in order to evaluate the damage of the structure with varying stones diameter. Furthermore, 4 different water depths have been tested allowing to evaluate the damage of the structure with a surf-similarity parameter ξ_m greater than 10. Indeed, experimental data on structure stability available in literature refer to a breaker parameter between 0.7 – 7.6. The analysis of the experimental results show that the structure stability is still constant in the surging domain ($\xi_m > 10$), whereas it seems to increase when ξ_m reaches values greater than 20.

Keywords: rubble mound breakwater, shallow waters, wave-structure interaction, slope stability.

1 INTRODUCTION

The hydraulic stability of a rubble mound breakwater is a key topic in coastal engineering, widely studied over the years. The stability is expressed through the well-known Hudson formula (Hudson et al., 1959), which relates the stability number ($N_s = H_{s,t}/\Delta D_{n50}$) to the wave height at toe of the structure, the reduced relative density (Δ), the nominal diameter of the armour layer (D_{n50}), the angle of the front slope of the structure and a dimensionless parameter that depends on the damage level of the armour layer. Van deer Meer (1988) improved the Hudson's formula, through a large experimental campaign aimed at investigating the influence of several parameters (e.g., porosity, number of waves, wave steepness, type of armour layer) on the structure stability mainly in deep and shallow water conditions. More recently, new tests (e.g., Van Gent et al., 2004, Eldrup et al., 2019) have been performed in order to evaluate the armour stability in shallow foreshore under different wave conditions (e.g. breaking waves) and foreshore slope (m = 1:100).

2 EXPERIMENTAL SET-UP

An experimental campaign on a 2D physical model has been carried out at the European Maritime and Environmental Research (EUMER) Laboratory of the University of Salento (Lecce, Italy). The wave flume is 45 m long, 1.5 m wide and 2 m high. The flume is equipped with a piston-type wave paddle which can generate both regular and irregular waves. The maximum irregular wave height that can be generated is 0.35 m, with a maximum water depth equal to 1.50 m.

Four different structure's layout have been tested. Both the main wave parameters of the physical model and the calculated stability number are reported in Table 1.

Table 1. Main parameters of tests.

	Test Serie WL1	Test Serie WL2	Test Serie WL3	Test Serie WL4
Number of tests	7	13	10	10
Water depth h_t [m]	0.40	0.20	0.10	0.05
Relative Depth, $H_{m0,o}/h_t$	0.43-0.78	0.75-1.48	1.55-2.56	2.94-4.74
Wave steepness, s_{m0}	0.024-0.048	0.024-0.048	0.024-0.048	0.024-0.048
Breaker parameter, ξ_m	2.71-4.47	2.95-9.10	5.20-15.71	11.07-23.67
Stability number, N_s	2.21-3.80	2.67-2.90	2.36-2.51	2.62-3.31

The shallowness condition is based on the classification reported in Hofland et al. (2017) and depends on the ratio between the deep spectral wave height ($H_{mo,o}$) and the water depth at toe of the structure (h_t). In table 1 the wave steepness (s_{m0}) calculated offshore is also reported.

ISBN: 978-90-824846-7-0

Figure 1 shows the sketch of the physical model, with all the dimensions in flume scale. From the wave paddle, the bottom is horizontal for 13 m, followed by a 1:5 transitional slope for about 1 m.
The foreshore is 1:30 for 13 m, up to the toe of breakwater. The structure is 0.9 m high and it has a front slope of 1:2. Waves transformation along the flume has been evaluated by 7 resistive wave gauges (WG1-WG7,Figure 1). The wave run-up has been measured by means of a wave gauge installed over the armour layer. The sampling acquisition frequency is 40 Hz. The damage of the structure has been estimated through the comparison between initial and final profiles measured by a laser bed profiler system.

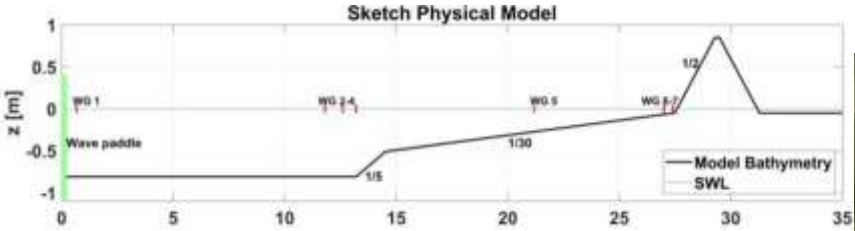

	Test Serie WL1	Test Serie WL2	Test Serie WL3	Test Serie WL4
D_{n50} - armour [m]	0.046	0.034	0.24	0.138
D_{n50} - under layer [m]	0.024	/	/	/
D_{n50} - core [m]	0.01	0.01	0.01	0.01

Figure 1. Sketch of the physical model. The dimension of the stones are reported in model scale (1:10).

3 RESULTS AND CONCLUSIONS

40 tests have been executed in extremely foreshore, to understand the response of the structure when the breaker parameter become greater than 10. Experimental results reveal that the stability trend is quite constant (Figure 2) in line with previous study (e.g., Eldrup et al., 2019). Anyway, in case of $\xi_m > 20$, the stability number slightly increases, so further experimental investigations are needed to confirm this trend.

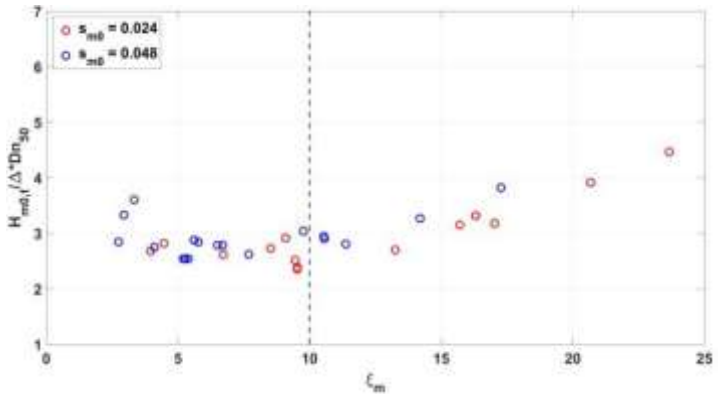

Figure 2. Stability results for the two different wave steepness tested.

REFERENCES

Eldrup, M. R., & Andersen, T. L. (2019). Extension of shallow water rock armour stability formulae to nonlinear waves. *Coastal Engineering*, *153*, 103536.

Hofland, B., Chen, X., Altomare, C., & Oosterlo, P. (2017). Prediction formula for the spectral wave period Tm-1, 0 on mildly sloping shallow foreshores. *Coastal Engineering*, *123*, 21-28.

Hudson, R. Y. (1959). Laboratory investigation of rubble-mound breakwaters. *Journal of the waterways and Harbors division*, *85*(3), 93-121.

van der Meer, J. W. (1988). Deterministic and probabilistic design of breakwater armor layers. *Journal of waterway, port, coastal, and ocean engineering*, *114*(1), 66-80.

Van Gent, M. R., Smale, A. J., & Kuiper, C. (2004). Stability of rock slopes with shallow foreshores. In *Coastal Structures 2003* (pp. 100-112).

ISBN: 978-90-824846-7-0

Proceedings of the 2nd IAHR
Young Professionals Congress
30 Nov-2 Dec. 2021

Estimating urban flood resilience under climate change

Roberta Padulano [1], Guido Rianna [2], Pierfranco Costabile [3], Carmelina Costanzo [4], Giuseppe Del Giudice [5] and Paola Mercogliano [6]

[1,2,6] Regional Models and Geo-Hydrological Impacts Division, Fondazione Centro Euro-Mediterraneo sui Cambiamenti Climatici, Via T.A. Edison 81100, Caserta, Italy. E-mail: roberta.padulano@cmcc.it, guido.rianna@cmcc.it, paola.mercogliano@cmcc.it
[3,4] Department of Environmental Engineering, University of Calabria, via P. Bucci 42/B, 87036 Rende (CS), Italy. E-mail: piefranco.costabile@unical.it, carmen.costanzo@unical.it
[5] Department of Civil, Architectural and Environmental Engineering, University of Naples 'Federico II', via Claudio 21, 80125 Naples (Italy). E-mail: delgiudi@unina.it

ABSTRACT

A simple but effective methodology is proposed to quantitatively estimate flood resilience of urban areas under climate change. The approach relies on the use of a large ensemble of Euro-CORDEX climate projections for climate change modelling, and on the use of CADDIES Caflood for flood simulation. Results are analyzed in terms of lumped flood indicators describing overall flood conditions over the domain; normalization with respect to current climate conditions is proposed to highlight the effect of climate change. Results show that the relation between normalized flood indicators and normalized rainfall intensity is linear, with a non-unitary slope. The approach can be effectively applied for scenario analysis. Different indicators can be adopted to analyze different flood impacts, such as flood hazards on urban sub-systems. With different reference conditions for normalization, the approach is also valuable for expeditious viability analysis of adaptation measures and drainage solutions.

Keywords: CADDIES Caflood; climate change; Euro-CORDEX; urban flooding; urban flood resilience.

1 INTRODUCTION

Urban flood resilience can be defined as "the ability to absorb, accommodate to and recover from the effects of the hazard in a timely and efficient manner, including through the preservation and restoration of its essential basic structures and functions" (Johnson & Blackburn, 2012). A resilient domain can be defined as an area where an increase in the severity of rainfall does not necessarily entail a similar increase in the severity of consequent flooding. Conversely, a domain is not resilient, or poorly resilient, when even a small increase in the severity of rainfall entails a significant increase in the severity of flooding. The concept of resilience is particularly important in a context of climate change (Padulano et al., 2021). The present research aims at exploring novel methodologies to estimate urban flood resilience in a climate change perspective. The estimation of flood resilience is driven by the following question: *how does the urban environment as a whole respond to extreme rainfall?*, which, in a climate change perspective, can be further attuned in the following: *to what extent do flooding conditions change when extreme rainfall changes?* (Padulano et al., 2021).

2 MATERIALS AND METHODS

The proposed approach is made up of two separate modules, targeting climate change estimation and rainfall-runoff transformation respectively. The estimation of climate change effects on the extreme rainfall regime is performed according to the procedure proposed by Padulano et al. (2019), whereas the rainfall-runoff transformation is performed relying on the CADDIES Caflood tool (Ghimire et al., 2013). The model is able to provide spatially distributed surface water depth over the domain with a user-defined time step as well as in peak conditions (enveloping the most critical flood conditions experienced throughout the event for each cell of the domain). Process parameters were set to simulate a data-limited condition regarding the size and location of the sewer system, which is very common in urban areas. Results of the rainfall-runoff transformation were expressed by means of two lumped indicators, namely the peak Flood Area Index (FAI) and the peak Runoff Volume Index (RVI) (Padulano et al., 2021), quantifying the extent and amount of water present in the domain under envelope conditions. The proposed approach is tested on a domain located in the City of Naples (Italy), about 2 km^2 wide (about 40% impervious areas, 30% buildings, 30% green areas), with a population of about 40'000 and a number of highly relevant strategic assets particularly prone to the adverse consequences of flooding.

ISBN: 978-90-824846-7-0

3 RESULTS

FAI and RVI indicators were computed for two different return periods (10 and 200 years, describing a "common" and an "exceptional" event), considering, for each return period, one rainfall intensity provided by local IDF curves (used as reference for normalization) and 19 rainfall intensities corresponding to 19 Euro-CORDEX climate projections (Jacob at al., 2021) for 2100 under RCP4.5 and 8.5 concentration scenarios (total 78 flood simulations). The duration of all rainfall events was set to 1 hr. For each return period, results show that the transformation of rainfall into runoff can be represented by a linear relation between the normalized variables. The slope of the regression lines is such that a unitary increase in rainfall does not imply a unitary change in flooding conditions, in terms of either runoff volume or flooded area. This confirms the recognized non-linearity of the rainfall – runoff transformation, which corresponds to unitary slope. For both indicators, regression lines of data points for T_2 show a lower slope than T_1, implying that the more critical is the baseline scenario, the lower is the increase in criticality due to an increase in rainfall with respect to baseline. In particular, in cases with slope<1, flood severity increases more slowly than rainfall severity.

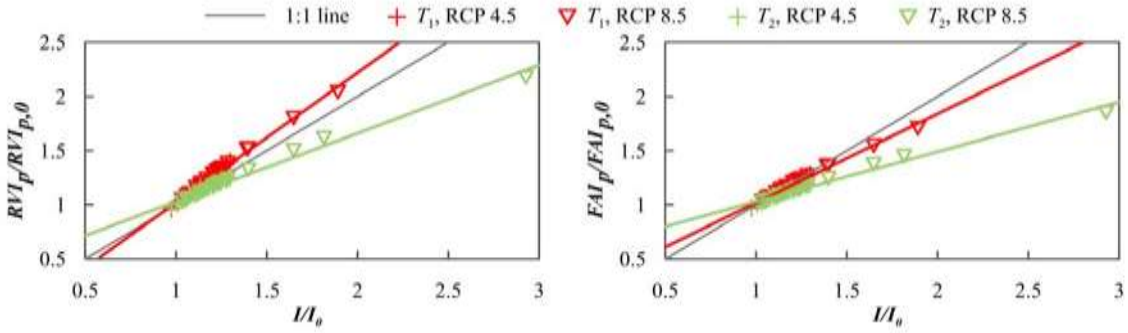

Fig. 1: Normalized peak flood indicators as a function of normalized intensity for T_1=10 yr and T_2=200 yr ("0" points to current climate)

4 CONCLUSIONS

The proposed methodology provides a simple but effective approach to quantitatively estimate flood resilience of urban areas. The approach is flexible with respect to available data (whose amount and variety can drive the choice of the flood modelling tool) and to the targeted definition of flood resilience (implying that the approach can be adjusted to analyze any specific urban sub-system of interest such as pedestrian/vehicular traffic, buildings, etc. by considering additional indicators, such as hazard classifications). The proposed normalization allows to disregard possible inaccuracies caused by the flood inundation model, such as governing equations, numerical scheme, parametrizations for simplified processes. Additionally, baseline for normalization can be tailored to identify different effects other than that of climate change, such as the use of adaptation measures and drainage solutions.

REFERENCES

Ghimire, B., Chen, A.S., Guidolin, M., Keedwell, E.C., Djordjevíc, S., and Savíc, D.A. (2013). Formulation of a fast 2D urban pluvial flood model using a cellular automata approach. *Journal of Hydroinformatics*, 15 (3), 676-686.

Jacob, D., Teichmann, C., Sobolowski, S. et al. (2021) Regional climate downscaling over Europe: perspectives from the EURO-CORDEX community. Regional Environmental Change 20, 51.

Johnson, C., and Blackburn, S. (2012). My city is getting ready! A global snapshot of how local governments reduce disaster risk. Making Cities Resilient Report 2012.

Padulano, R., Reder, A., and Rianna, G. (2019). An ensemble approach for the analysis of extreme rainfall under climate change in Naples (Italy). *Hydrological Processes*, 33 (14), 2020-2036.

Padulano, R., Rianna, G., Costabile, P., Costanzo, C., Del Giudice, G., and Mercogliano, P. (2021). Propagation of variability in climate projections within urban flood modelling: a multi-purpose impact analysis. Journal of Hydrology, 126756.

ISBN: 978-90-824846-7-0

Proceedings of the 2nd IAHR
Young Professionals Congress
30 Nov-2 Dec. 2021

Non-stationary frequency analysis of extreme rainfall series in a typical urbanized basin

Mingming Song [1,2]
[1] State Key Laboratory of Hydrology-Water Resources and Hydraulic Engineering, Nanjing Hydraulic Research Institute, Nanjing, China, email (smmjy1228@126.com)
[2] Research Center for Climate Change, Ministry of Water Resources, Nanjing, China.

ABSTRACT

This study examined the extreme rainfall non-stationary characteristics in urban area and investigated the relationships between urbanization and extreme rainfall frequency. Extreme rainfall series were generated from rainfall observations for 1979-2015 in a typical urbanized basin located in the Yangtze River delta, China. A novel framework consisting of series stationarity reconstruction and Generalized Additive Model for Location, Scale and Shape (GAMLSS) were proposed for non-stationary frequency analysis. The Results revealed that extreme rainfall showed significant non-stationary characteristics. The GAMLSS framework developed with impervious area ratio as covariate showed higher accuracy than that with time as covariate. The design value calculation method based on stationary hypothesis is no longer suitable for non-stationary condition.

Keywords: non-stationarity, frequency, extreme rainfall, urbanization, GAMLSS, climate change

1 INTRODUCTION

In the backdrop of climate change and urbanization, precipitation extremes have been reported to become more frequent and intense across the globe, although with varying spatial characteristics (Myhre G, 2019; Shi, 2019). These evidence of variations in extreme events have attracted debates about whether the stationarity assumption is still valid basis for water resources planning. The methods on which these debates are based includes two main aspects, i.e., the approach based on the backward reconstruction or forward reconstruction, and that directly based on the non-stationary extreme series (Liang, 2011). The Generalized Additive Model for Location, Scale and Shape (GAMLSS) was proposed to address the modeling of non-stationary observations directly (Rigby, 2005). Urbanization area responses to the extreme rainfall events more sensitively with more intervention in the hydrological cycle due to the human activities. However, the non-stationary characteristics of rainfall extremes and frequency in urbanized areas have not been fully understood. This study focused on urban extreme rainfall events and proposed a novel framework consisting of series stationarity reconstruction (Hu, 2014) and GAMLSS model for comparison and comprehensive analysis of non-stationary frequency characteristics. Findings would motivate the urban flood risk management and mitigation strategies.

2 MATERIAL AND METHODS

2.1 Study area and datasets

Qinhuai River Basin is located in the lower plain of the Yangtze River, China. It extends between 118°39′and 119°19′E, 31°34′and 32°10′N. The drainage area is 2,631 square kilometers. The elevation ranges from 0 to 417 meters. The river basin has been influenced by a subtropical monsoon climate and the precipitation variability is large. In recent years, the Qinhuai River basin experienced extreme floods in 1931, 1954, 1969, 1991, 2016 and 2020.The rapid urbanization process in recent years increases the flood risk of the basin. The extreme rainfall series were generated from 10 rainfall gauge observations for 1979-2015 based on 5 extreme indexes: R_{1d}, R_{3d}, R_{7d}, R_{95p} and R_{99p}.

2.2 Methods

The non-stationary frequency analysis framework consists of comparison and comprehensive analysis of extreme rainfall frequency based on both stationary and non-stationary assumptions. The characteristics of non-stationary extreme rainfall and relationships between urbanization and extreme rainfall frequency were analyzed based on this framework.

ISBN: 978-90-824846-7-0

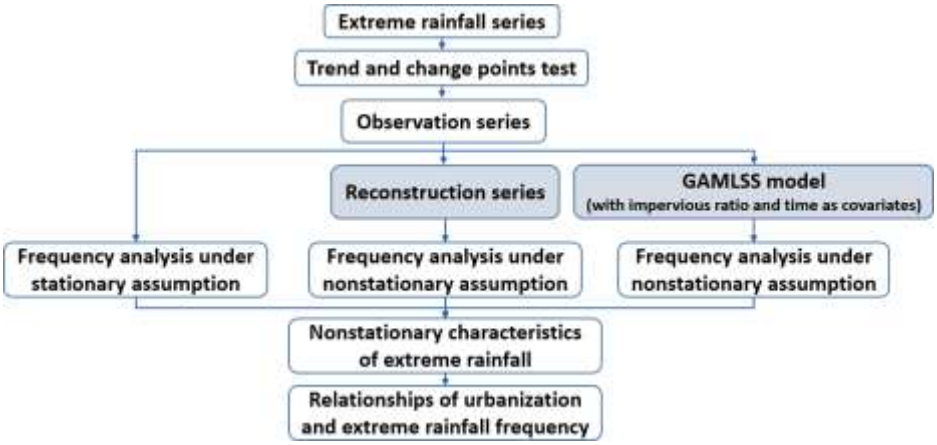

Fig.1 Non-stationary frequency analysis framework

3 Results and Discussion

The trend and change points test revealed that all the extreme rainfall series in Qinhuai River basin showed significant increasing trends. The inverse Gumbel (RG) distribution were identified as the best fitting model through the Akaike information criterion (AIC) and worm plots. The GAMLSS model of the non-stationary extreme rainfall series developed with impervious area ratio as covariate showed higher accuracy than that with time as covariate. It indicated that urban impervious ratio has a significant correlation with rainfall extremes. There exists obvious differences between the design values calculated based on stationary and non-stationary assumptions(Table1). Thus, the design value calculation method based on stationary hypothesis is no longer suitable for non-stationary condition.

Table.1 Non-stationary frequency analysis framework

Return period/a	Observation series results (mm)					Reconstruct series results (mm)					GAMLSS model results (mm)				
	R_{1d}	R_{3d}	R_{7d}	R_{95p}	R_{99p}	R_{1d}	R_{3d}	R_{7d}	R_{95p}	R_{99p}	R_{1d}	R_{3d}	R_{7d}	R_{95p}	R_{99p}
100	178	281	409	864	697	191	284	404	918	548	100	153	229	421	128
50	164	259	373	785	552	178	262	371	830	477	99	152	226	417	127
10	128	204	284	587	292	144	206	289	618	310	92	143	209	388	126
2	82	130	175	346	96	101	136	190	374	130	71	111	148	272	121

4 Conclusions

All the extreme rainfall series in Qinhuai River basin showed significant non-stationary characteristics. The GAMLSS framework developed with impervious area ratio as covariate showed higher accuracy than that with time as covariate. The design value calculation method based on stationary hypothesis is no longer suitable for non-stationary condition. The physical mechanism of the relationship between urbanization and extreme rainfall needs further study.

REFERENCES

Hu YM, Liang ZM, Zhao WM, et al.(2014). Study on frequency analysis method of non-stationary observation based on jump analysis. Yellow River, 36(6): 51-53, 57.

Rigby RA, Stasinopoulos DM. (2005). Generalized additive models for location, scale and shape. J Stat Softw, 54(3):507-554.

Shi J, Cui L, Wang J , et al.(2019). Changes in the temperature and precipitation extremes in China during 1961-2015. Quaternary International, 527(Aug.30):64-78.

Liang ZM, Hu YM and Wang J. (2011). Advances in hydrological frequency analysis of non-stationary time series. Advances in water science, 22(06):864-871.

Myhre G, K Alterskjær, Stjern CW , et al.(2019). Frequency of extreme precipitation increases extensively with event rareness under global warming. Scientific Reports, 9(1):16063.

ISBN: 978-90-824846-7-0

Proceedings of the 2nd IAHR
Young Professionals Congress
30 Nov-2 Dec. 2021

Influences of monsoon regime, flooding events and headlands on Tien Chau tidal inlet

Duy Truong Nguyen [1], Son Hong Truong [2] and Trung Hai Le [3]

[1] ThuyLoi University, Hanoi, Vietnam,
duynt45@wru.vn
[2] ThuyLoi University, Hanoi, Vietnam,
truonghongson@tlu.edu.vn
[3] ThuyLoi University, Hanoi, Vietnam,
trung.l.h@tlu.edu.vn

ABSTRACT

This paper studies the influences of the monsoon and flooding regime on the hydrodynamics and morphodynamics of a sheltered tidal inlet. Located south of Xuan Dai Bay, the Tien Chau tidal inlet connects the Ky Lo river with the South East Sea. This inlet anchors next to a headland and is bordered on its opposite side by a sandspit. This sandspit continuously moves and fluctuates toward the southern headland. In order to obtain more insight into the physical processes of this system, field measurements were conducted at different stations across the inlet system. In addition, a schematized model of the inlet was constructed in the state-of-the-art Delft3D model. The results suggest that while seasonal wave climate is the main driving factor causing the modification of the sandspit toward the south side, the short-term flooding even is the leading cause of the sudden opening of the inlet.

Keywords: Monsoon; flooding events; sheltered tidal inlets; field measurement; numerical model.

1 INTRODUCTION

Tien Chau tidal inlet is known as the only entrance for fishing boats to approach the Tien Chau Port, one of the four major ports in Phu Yen Province, Viet Nam. Located inside Xuan Dai Bay, this tidal inlet is one of the three main channels that connect the Ky Lo river with the South East Sea. The southern headland shelters the south side of the Tien Chau inlet and a sandspit border the north side (see Fig 1). The study area locates in a tropical monsoon region with a distinct dry and wet season. According to the report provided by the ThuyLoi University (TLU, 2020), the Tien Chau inlet is filling with sediment, and its profile is rapidly shifting. During the low tide level, the water depth is shallow of approximately 1m. The width of the inlet's entrance is approximately 15m, making only small boats capable of entering the port. As a result, this phenomenon has negative impacts on the local environment and fishery resources. Lack of proper studies, data, and necessary knowledge about the Tien Chau inlet make it challenging to propose proper solutions for the inlet's stability and the safe and efficient operation of the harbor. Therefore, the main objectives of this study are to investigate the physical processes of the Tien Chau tidal inlet under the influences of the seasonal monsoon factor and the short-term flooding events

Figure 1. General locations of Tien Chau tidal inlet with the zoom-in descriptions including the inlet, the fishing port, the updrift sandspit and Ong Ngon Mountain as the southern headland.

ISBN: 978-90-824846-7-0

2 METHODS

Tien Chau inlet's primary field measurement data set includes the detailed topography of the study area, the water level, the flow at tidal inlet, and the wave height along the Tien Chau coast. A schematized model was built in a coupled model of Delft3D-FLOW and Delft3D-WAVE with a well-structured, orthogonal curvilinear grids for the sea, estuary and the river region (Figure 1). The model results were then validated using the measured data sets.

3 RESULTS

Different major morphological features of Tien Chau tidal inlet were determined using satellite images and topography data (Fig 1). Figure 2 shows simulation results, validated with the field measured data (a) and the velocity field during the northeast monsoon season during the flood period (b). There is a good agreement between the model and the measured data. It is suggested that wave- and tide-induced currents divide into two parts. One part flows over the flood tidal delta to enter the main channel. Another part of these currents which is blocked by the sand spit flows along the shore toward the North.

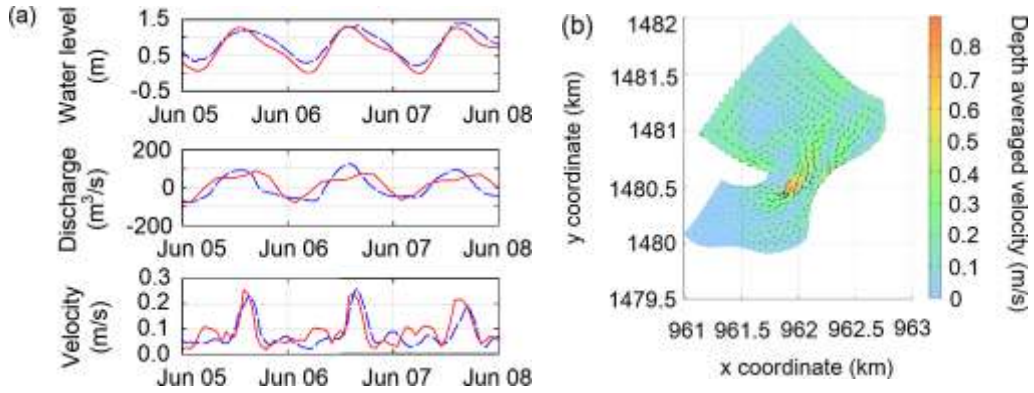

Figure 2. (a) Comparisons of time series of observations (dashed blue lines) and model results (solid red lines) at different stations, including water levels, discharge at the tidal inlet, and depth-averaged streamwise velocity. (b) The flow field of averaged velocity in the inlet area under the influence of waves during the northeast monsoon season is also included.

4 CONCLUSIONS

Different main features of the inlet were identified. The northern and southern headlands of the Xuan Dai Bay offer a natural barrier blocking the southeast and north coming waves. On the other hand, the human constructions block the development of the downdrift sand barrier island. Consequently, the width of the inlet usually increased within a month right after the flood. These observations suggest that the sand spit fluctuated continuously toward the seaside, and the width of the tidal inlet strongly depends on temporal flooding events. Later, when the annual maximum discharge is reduced, the wave takes advantage, the sand spit can shift back to the "equilibrium" position, and the width of the inlet will decrease. The equilibrium width-depth ratio of the Tien Chau tidal inlet is about 8m.

REFERENCES

J. Bosboom and M. Stive (2021). Coastal Dynamics. *Delft University of Technology,* Delft, Netherlands, 595 pp.

Bruun P. (1986). Morphological and navigational aspects of tidal inlets on littoral drift shores*. Journal of Coastal Research*, vol 2, no 2, pp. 123-145.

Miles O. Hayes and Duncan M. FitzGerald (2013). Origin, Evolution, and Classification of Tidal Inlets. *Journal of Coastal Research*, vol 69, pp. 14-33.

ThuyLoi University (2020). Tien Chau Investigation project report [in Vietnamese]. *Thuy Loi University*, Hanoi, Vietnam.

ISBN: 978-90-824846-7-0

Design strategies and Life Cycle Assessment for the improvement of environmental sustainability of OBREC

Giuseppina Colaleo [1], Pasquale Contestabile [2] and Diego Vicinanza [3]
[1] Department of Engineering, University of Campania "Luigi Vanvitelli," Aversa, Italy, giuseppina.colaleo@unicampania.it
[2] Department of Engineering, University of Campania "Luigi Vanvitelli," Aversa, Italy, pasquale.contestabile@unicampania.it
[3] Department of Engineering, University of Campania "Luigi Vanvitelli," Aversa, Italy, diego.vicinanza@unicampania.it

ABSTRACT
The environmental consequences due to the construction and installation of energy conversion systems that exploit the waves of the sea have not so far been taken into great consideration. This work aims to frame the Overtopping BReakwater for Energy Conversion (OBREC) system, implemented and tested in the port of Naples (Italy), to identify design, construction and maintenance strategies to improve its sustainability performance. To select economical and environmentally friendly construction products for the OBREC prototype, an application was created using the BEES (Building for Environmental and Economic Sustainability) software. The tool measures the environmental performance of construction products using the LCA approach specified in the ISO 14040 series of standards.

Keywords: Eco-design; Life Cycle Assessment; wave energy converter.

1 INTRODUCTION

Fundamental structural change in energy sources, structures, size, economy and energy policy is occurring around the world through a transition from fossil fuels to renewable energy.
Interest in the wave of energy as a renewable energy source is growing around the world. Currently electricity conversion technologies are not economically competitive with other technologies, such as those used for wind energy, however we are witnessing a rapid phase of development which is attracting the interest of governments and industries.
At the same time, humanity's ever-increasing awareness of the importance of the environmental issue has gone hand in hand with an extension of design's interest in product and service innovation (no longer just process). from an ecological point of view. Wave energy converters have significant advantages in this regard, as they can be integrated into existing coastal structures, minimizing costs and simplifying maintenance by forming an attractive system that provides the necessary protection to coastal regions along with power generation. .
Following this innovative approach to the design of sea dams, an innovative device developed called OBREC, acronym for Overtopping BReakwater for Energy Conversion, was created, which uses the overflow of waves to produce electricity, installed in the port of Naples (Italy) in 2015. (Figure 1). The following work aims to identify design, construction and maintenance strategies to improve the sustainability characteristics of the OBREC device in the industrial production phase with a view to sustainable design, or Eco-design, and Life Cycle Assessment (LCA).

Figure 1. Full-scale device installed at the port of Naples in Italy after Contestabile et al. (2017).

ISBN: 978-90-824846-7-0

2 MATERIALS AND METHODS

The Overtopping BReakwater for Energy Conversion, or OBREC, consists of a dam equipped with a cistern which, placed in a higher position than sea level, collects water from a hydroelectric ramp in front to convert it into potential energy. The difference in hydraulic load between the tank and the average sea level generates a flow that drives low-load turbines, located behind the tank and coupled to a generator, transforming the energy of the water flow into electrical energy. It was decided to compare five different types of cement to evaluate their environmental sustainability, considering the entire life cycle of the materials. software provided by "The National Institute of Standards and Technology" (NIST), an agency of the United States Department of Commerce, was used. The software is called BEES (Building 8for Environmental and Economic Sustainability) and measures the environmental performance of construction products, using the LCA approach specified in the ISO 14040 (2006a) and ISO 14044 (2006b) series of standards. The life cycle took into consideration all the phases of the entire production chain: acquisition of raw materials, processing, transport, installation, use, recycling and waste management. They were considered:

1. generic concrete, or the classic pozzolanic concrete (called anonymous IP)
2. Portland-type concrete (based on internationally standardized specifications
3. concrete with a percentage of recycled aggregates in the amount of 20%
4. concrete with a percentage of recycled aggregates in the amount of 35%
5. concrete with a percentage of recycled aggregates in the amount of 50%. In the various cements a content of secondary constituents (fillers or other materials) not exceeding 5% is allowed. The distance was set at 20 miles (32 km) based on the actual distance from a probable cement plant to the site.

3 RESULTS AND CONCLUSIONS

The results (Figure 2A – 2B) show Portland Normal cement as the best green solution if the supply source is at the same distance. In fact, for cements with coarse aggregates partly deriving from recycling, gradually increasing acidification phenomena occur, thus making their selections uncertain and risky. In addition to being an ethical choice, Ecodesign is the first step towards a Circular Economy because it considers the environmental impact that a particular product will have throughout its life cycle, from its conception to its disposal. Indeed, Ecodesign and Circular Economy together constitute the first step towards a sustainable economy.

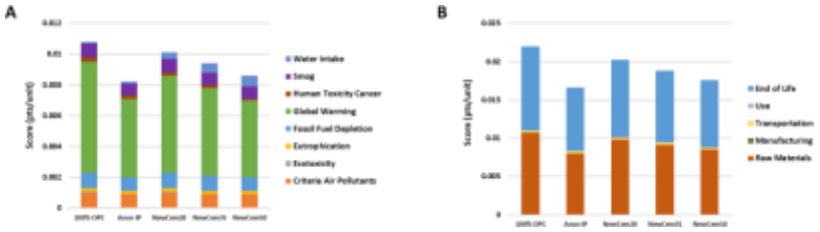

Figure 2. A) Results in terms of environmental performance for the alternatives considered. B) Environmental performance of the different types of cement considered: from production to end of life

REFERENCES

Contestabile, P., Iuppa, C., Di Lauro, E., Cavallaro, L., Lykke Andersen, T., Vicinanza, D. (2017). "Wave loadings acting on innovative rubble mound breakwater for overtopping wave energy conversion", Coastal Engineering, ISSN 0378-3839, vol. 122, pp. 60–74.

Falcao, A. F. D. O. (2010). Wave energy utilization: a review of the technologies. *Renew. Sustain. Energy Rev.* 14, 889–918. doi: 10.1016/j.rser.2009.11.003

Spangenberg JH., Joachim H., Alastair F.L., Blincoe K. (2010). Design for Sustainability (DfS): the interface of sustainable production and consumption. Journal of Cleaner Production 18: 1485–1493

Vicinanza D., Norgaard J., Contestabile P. e Lykke Andersen T. (2013a) - Wave loadings acting on Overtopping BReakwater for Energy Conversion, Journal of Coastal Research, ISSN 0749-0208, SI 65, pp. 1669-1674.

ISBN: 978-90-824846-7-0

IAHR YPN

Young Professionals Network

Hosted by
Spain Water and IWHR, China

IAHR AIRH

International Association for Hydro-Environment Engineering and Research

Hosted by
Spain Water and IWHR, China

Ecohydraulics

Proceedings of the 2nd IAHR
Young Professionals Congress
30 Nov-2 Dec. 2021

Using integrated hydrology simulations to understand runoff generation mechanisms in the presence of micro-topography at the hillslope scale

Rachel M. Johnson[1], Ilhan Özgen-Xian[2] and Sergi Molins[3]
[1] University of Colorado Colorado Springs, Colorado Springs, Colorado, USA,
rachelmjohnso@gmail.com
[2,3] Lawrence Berkeley National Laboratory, Berkeley, California, USA,
iozgen@lbl.gov, smolins@lbl.gov

ABSTRACT

Runoff generation results from the non-linear interaction between rainfall, climate, soil properties, topography, and vegetation. In particular, the effect of micro-topography on runoff partitioning and runoff generation is widely documented. In this work, we aim to understand the control that micro-topography exerts on rainfall generation through integrated hydrological modeling. We analyze the results of 864 rainfall-runoff simulations at the hillslope scale, considering different soil types, hillslope geometries, and rainfall intensities. Each simulation is run until the steady state is reached. Specifically, we are interested in the effect of micro-topography on the dominant runoff generation mechanism of the hillslope. We find that at the steady state, soil type is the most dominant control on the type of runoff generation mechanism, while the impact of micro-topography is only local. Further, at the steady state, we observe only runoff generated by subsurface stormflow and excess runoff. Infiltration excess runoff is not observed.

Keywords: integrated hydrology; runoff generation; hydrological modeling; hillslope; micro-topography.

1 INTRODUCTION

Runoff generation is a multi-factor process, consisting of a large number of localized and interconnected processes. Commonly recognized mechanisms for runoff generation are (i) saturation excess runoff (Dunne flow), (ii) infiltration excess runoff (Hortonian flow), and (iii) subsurface stormflow. While saturation excess runoff occurs when the soil is fully saturated (Dunne, 1978), infiltration excess runoff occurs when the rainfall intensity exceeds the saturated hydraulic conductivity and thus, creates an inverted zone of saturation near the surface (Horton, 1933). Subsurface stormflow occurs in permeable soils, where the water can flow rather fast near the surface, such that no overland flow is observed. Depending on the catchment characteristics, the dominant runoff generation mechanism in the catchment switches between these three mechanisms (Dunne, 1991).

The effect of micro-topography on runoff generation has been investigated in (Thompson *et al.*, 2010), using hillslopes with a superimposed one-dimensional sine-wave shaped micro-topography. Overland flow is simulated with a fully dynamic shallow flow solver to simulate coupled to an empirical infiltration model. Thompson *et al.* (2010) find that micro-topography creates spatial patterns in the ponding water depth, which increases the infiltration rate locally. Caviedes-Voullième *et al.* (2021) confirm and expand these findings on hillslopes with a two-dimensional sine-wave shaped micro-topography, using a similar conceptual model. In both of these investigations, the interplay between surface and subsurface water is greatly simplified. The importance of explicitly representing surface-subsurface interplay is discussed in (Frei *et al.*, 2012), where it is shown that micro-topography causes spatial heterogeneities in the potential head, which leads to local variations in the infiltration rate and biogeochemical hotspots.

This contribution studies the effect of micro-topography on the dominant runoff generation mechanism using an integrated surface-subsurface hydrology model at the hillslope scale. Specifically, we investigate whether micro-topography can lead to a switch in the dominant runoff generation mechanism at the hillslope. This is a natural extension of the work in (Thompson *et al.*, 2010; Caviedes-Voullième *et al.*, 2021). In contrast to (Frei *et al.*, 2012) we focus on the influence of micro-topography on the dominant runoff generation mechanism at the hillslope rather than on the spatial patterns of geochemical hotspots.

	Amplitude (m)	Wavelength (m)
A	0.0125	2.0
B	0.025	1.0
C	0.05	0.5
D	0.0125	0.5
E	0.05	2.0

ISBN: 978-90-824846-7-0

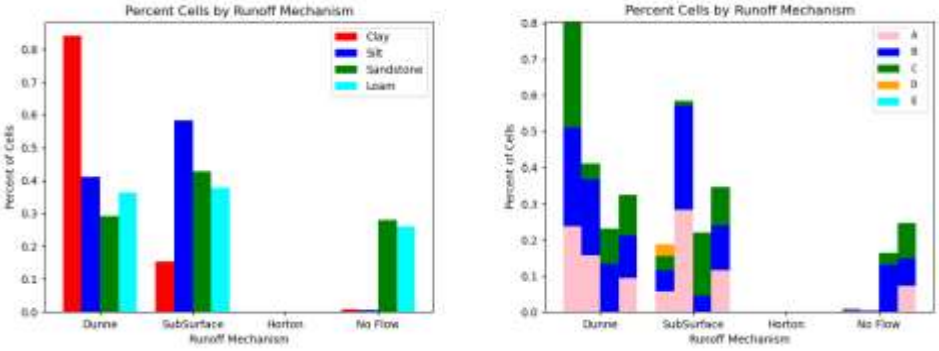

2 MATERIALS AND METHODS

In this study, we use the Advanced Terrestrial Simulator (ATS) (Coon *et al.*, 2021) to simulate the surface-subsurface hydrology, which solves the governing equations (zero-inertia and Richards equations) in a fully-coupled manner. Micro-topography is described through a one-dimensional sine-wave, superimposed on the hillslope with constant slope. The sine-wave properties for different micro-topography (A to E) are summarized in the above table. We consider three different slopes: 0.1, 0.01, and 0.001. In addition, we investigate four different soil types: sandstone, silt, loam, and clay. All simulations are forced with a constant and unceasing rainfall. We study three rainfall intensities: 10^{-6} m/s, 10^{-7} m/s, and 10^{-8} m/s. Simulations are run for 1 year, which is sufficient for the hillslope to converge to a steady state. Preliminary results are shown in the above figures.

3 CONCLUSIONS

Simulation results suggest that at the steady state, the dominant runoff generation mechanism switches between saturation-excess runoff and subsurface stormflow, while infiltration-excess runoff is not observed. The control on this switch is the soil type, specifically the soil permeability. Microtopography causes local deviations in the runoff generation mechanism, but the effect does not manifest itself at the hillslope scale. These findings are supported by Dunne *et al.* (1991), who report that soil properties and slope control the runoff generation at steady states. Potential engineering applications for mitigating runoff are conceptual, but microtopography should be viewed as a control on reducing overland flow.

ACKNOWLEDGMENT

This work is supported as part of the Watershed Function Scientific Focus Area, funded by the U.S. Department of Energy, Office of Science, Office of Biological and Environmental Research under Award Number DE-AC02-05CH11231. R. M. Johnson acknowledges the support by the U.S. Department of Energy, Office of Science, Office of Workforce Development for Teachers and Scientists (WDTS) under the Science Undergraduate Laboratory Internship (SULI) program.

REFERENCES

Caviedes-Voullième, D., Ahmadinia, E., and Hinz, C. (2021) Interactions of microtopography, slope and infiltration cause complex rainfall-runoff behaviour at the hillslope scale for single rainfall events. *Water Resources Research,* 57, e2020RW028127.

Coon, E., Berndt, M., Jan, A., Svyatsky, D., Atchley, A.L., Kikinzon, E., Harp, D.R., Manzini, G., Shelef, E., Lipnikov, K., Garimella, C., Xu, J., Moulton, J.D., Karra, S., Painter, S.L., Jafarov, E., and Molins, S. (2020). Advanced Terrestrial Simulator. US Department of Energy, USA. Version 1.0.

Dunne, T. (1978). Field studies of hillslope flow processes. In: M.J. Kirkby (ed), *Hillslope Hydrology.* John Wiley, New York, USA.

Dunne, T., Zhang, W., and Aubry, B.F. (1991). Effects of rainfall, vegetation, and microtopography on infiltration and runoff. *Water Resources Research*, 27, 2271-2285.

Frei, S., Knorr, K.H., Pfeiffer, S., and Fleckenstein, J.H. (2012). Surface micro-topography causes hot spots of biogeochemical activity in wetland systems: A virtual modeling experiment. *Journal of Geophysical Research*, 117, G00N12.

Thompson, S.E., Katul, G.G., and Porporato, A. (2010). Role of microtopography in rainfall-runoff partitioning: An analysis using idealized geometry. *Water Resources Research*, 46, WR008835.

ISBN: 978-90-824846-7-0

Proceedings of the 2nd IAHR
Young Professionals Congress
30 Nov-2 Dec. 2021

Interaction of V baffle weir on turbulence kinetic energy on fish passage with CFD model

Maryam Shahabi[1] Marjan Narimousa [1] Javad Ahadiyan[1] Mehdi Ghomeshi [1] and Hossein Azizi Nadian [1]

[1] Faculty of Water Sciences Engineering,Shahid Chamran University of Ahvaz, Ahvaz, Iran

m-shahabi@stu.scu.ac.ir, m-narimousa@stu.scu.ac.ir, j.ahadiyan@scu.ac.ir, ghomeshi@scu.ac.ir, Hossein.azizi@kmsu.ac.ir

ABSTRACT

The structure of the fishway, by discharging the energy of the water flow, is a way for the fish to migrate upstream of the obstacles. In this study, a V-shaped weir with an angle of 22.5 degrees was used for the fishway, this weir was tested at a flow rate of 0.029 m3/s and three different slopes of 4, 7, and 10% with three relative distances 1.3, 2.6, and 4 m. The results showed that increasing the slope and distance has a direct effect on TKE. On the other hand, in order to reduce the implementation costs, the Relative distance 4 in the slope of 4% and the relative distance of 2.6 in the slope of 10% were selected as the most optimal conditions.

Keywords: fishway, turbulent kinetic energy, energy depreciation

1 INTRODUCTION

The construction of dams to use surface water resources has caused environmental problems of rivers. In order to reduce these destructive effects, the hydraulic-environmental structure called fishway structure was presented and studied. The structure of the fishway creates the conditions for fish to migrate to their desired habitat (kim et al., 2016). Turbulent kinetic energy (TKE), its distribution, and volume are the most important reasons for the low efficiency of fishway (Puzdrowska, M., Heese, T,. 2019). Turbulence studies on fish behavior and swimming energy have shown that fish can be affected by flow circulation patterns, especially the size and rapidity of eddies in fishways (Duguay et al., 2018). Ghaderi et al (2020) investigated experimentally and numerically the effect of the v-shaped weir on changes in flow velocity and TKE. The results of the experiments showed that as the distance between structures increased, the flow velocity increased and consequently the energy loss decreased. Also, changing the angle did not have much effect on the hydraulic parameters. Due to limited studies on the fishway with a V-shaped weir, In this study, the effect of V-shaped Weir fishway on turbulent kinetic energy (TKE) is investigated.

2 MATERIALS AND METHODS

Experiments were performed in a laboratory flume 10m long, 0.50m high and 0.25m wide at Shahid Chamran Laboratory to calibrate the CFD model. Figure 1 shows the v-shaped weirs arrangement in the flume. By calibrating the flow depth with three turbulence models $k-w$, RNG and $k-\varepsilon$, it was found that numerical model RNG with R^2=0.99 is the closest to laboratory data. According to Table 1, the experiments at a flow rate of 0.029m3/s were studied with three different slopes of 4, 7 and 10% at three relative distances of 1.3, 2.6 and 4.

Table 1. Scenarios of calculation

Θ(Degree)	D/L	D(m)	S(%)	Q(m^3/s)
22.5	1.3	0.3	4	0.029
	2.6	0.6	7	
	4	0.9	10	

Figure 1: The view of V shaped weirs in flume with details

ISBN: 978-90-824846-7-0

3 RESULTS AND CONCLUSIONS

According to Figure 2, the value of TKE increases with an increasing slope. Also, the amount of TKE near the structure i is more than upstream of the structure i + 1. It should be noted that at D / L = 1.3 between slopes of 4 and 7% , the increase in turbulence is significant, but between slopes of 7 and 10% is not significant change occurs so it can be concluded that at slope of 7% to maximum turbulence Has reached itself. Also, Examining Figure 2, it can be seen that on all slopes, maximum turbulence or peak points occurs at the water level, which has increased by 20% compared to lower depths (0.02, 0.04 and 0.06 m). However, at intervals of D / L = 2.6 and 4, this difference is much smaller. At a distance of D / L = 1.3 from the range of 0.10 to 0.15 m relative to the structure i, maximum TKE occurs, this sharp state can cause the most damage to fish. It then goes through a fixed routine, which is called the equilibrium length. Then from the point 10 cm to the structure i + 1, a steady state was observed. So we can say that slope of 10% is suitable because it is cost effective. At D / L = 4, slopes of 7 and 10%, TKE value is more than 0.05 m^2/s^2 and according to the criterion (Shahabi et al., 2021) TKE value is more than 0.05 m^2/s^2 out of fish tolerance, so these two models are not recommended. The results showed that the RNG turbulence model has a good capability for hydraulic flow simulation. Also, due to the high cost of building a physical model and saving time, Flow3D software can be used.

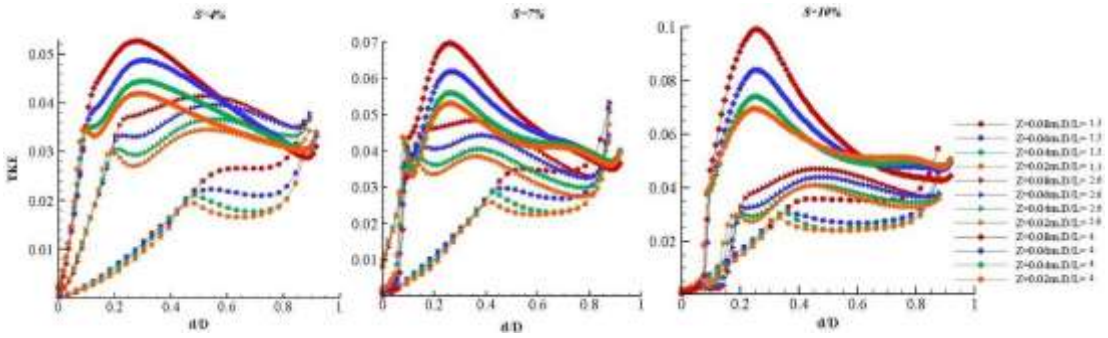

Figure 2: Variation of longitudinal turbulent kinetic energy (TKE; m^2/s^2) corresponding to a: distances D/L of 1.3, 2.6 and 4 in slope of 4% b: distances D/L of 1.3, 2.6 and 4 in slope of 7% c: distances D/L of 1.3, 2.6 and 4 in slope of 10%

Nomenclature	
D	Distance between apex of weir i to i+1
d	Distance of each custom point from i
S	Slope
L	Projection length
D/L	Distance ratio for spacing between weirs
d/D	Relative longitudinal distance

REFERENCES

Kim, J. H., Yoon, J. D., Baek, S. H., Park, S. H., Lee, J. W., Lee, J. A., & Jang, M. H. (2016). An efficiency analysis of a nature-like fishway for freshwater fish ascending a large Korean river. Water, 8(1), 3.

Puzdrowska, M., & Heese, T. (2019). Detailed Research on the Turbulent Kinetic Energy's Distribution in Fishways in Reference to the Bolt Fishway. Fluids, 4(2), 64.

Duguay, J., Foster, B., Lacey, J., & Castro-Santos, T. (2018). Sediment infilling benefits rainbow trout passage in a baffled channel. Ecological Engineering, 125, 38-49.

Li, S., Yang, J., Ma, X., & Li, X. (2020). Flow features in a pooled fishway with V-shaped weir formation. Engineering Applications of Computational Fluid Mechanics, 14(1).

Ghaderi, A., Dasineh, M., Aristodemo, F., & Ghahramanzadeh, A. (2020). Characteristics of free and submerged hydraulic jumps over different macroroughnesses. Journal of Hydroinformatics, 22(6), 1554-1572.

Shahabi, M., Ghomeshi, M., Ahadiyan, J., Mohammadian, T., & Katopodis, C. (2021). Do fishways stress fish? Assessment of physiological and hydraulic parameters of rainbow trout navigating a novel W-weir fishway. Ecological Engineering, 169, 106330.

ISBN: 978-90-824846-7-0

Proceedings of the 2nd IAHR
Young Professionals Congress
30 Nov-2 Dec. 2021

Incipient motion of compact-shape microplastics: experimental design and expected results

Arianna Varrani [1], Massimo Guerrero [2], Magdalena Mrokowska [3] and Lukasz Przyborowski [4]
[1,3,4] Institute of Geophysics, Polish Academy of Sciences, Warsaw, Poland,
e-mail[1] avarrani@igf.edu.pl
e-mail[3] m.mrokowska@igf.edu.pl
e-mail[4] lprzyborowski@igf.edu.pl
[2] Università di Bologna, Bologna, Italy,
e-mail massimo.guerrero@unibo.it

ABSTRACT

In this study, we present the experimental setup for laboratory tests on the incipient motion of microplastic particles made at the Hydrodynamic Models Laboratory at the Institute of Geophysics, together with some very preliminary results. The experiments see a movable bed of plastic particles (ellipsoidal, 3-mm sized) subject to free surface flow, with UVP-based characterisation of the flow field and image-based characterisation of the bed changes. The dataset will serve as a reference for further experiments with more "natural" configurations, namely with microplastic particles moving on a clastic sediment bed.

Keywords: microplastics, incipient motion, open channel flow, image analysis, UVP

1 INTRODUCTION

Microplastics pollution of freshwater bodies is recently attracting much attention and the number of studies assessing microplastics presence is rapidly increasing, covering most environments from polar regions (Obbard et al., 2014) to mangrove systems (Nor et al., 2014) down to ocean trenches (Jamieson et al., 2019). There is a clear need in understanding their transport dynamics and interactions with biota, and this contribution addresses the first point. Microplastic particles, small plastic fragments ranging in size from 1 μm to 5 mm, entering rivers and streams are transported downstream by the current, and they are part of the present riverine transport together with other clastic sediments (Stubbins et al., 2021). Sediment transport studies focussed their attention on the onset of motion and transport since their early years, and a large body of literature testifies the decades-long efforts in defining incipient motion conditions for natural particles (Dey and Ali, 2019). The presence of plastic fragments and microplastics in rivers and streams, for their unique properties in terms of density and shape, opens new paths for sediment research. Building upon present knowledge, we are conducting incipient motion experiments with plastic particles, to define their motion threshold in transitional to turbulent flow conditions. The presented experiments partially complement the work by Waldschläger and Schüttrumpf (2019) adding another plastic material to the picture.

2 METHODS

Experiments of microplastic particle mobilisation are performed in a 5-m-long, 0.25-m-wide flume at the Hydrodynamic Models Laboratory at the Institute of Geophysics, Polish Academy of Sciences. The experimental setup consisted of a 3-cm thick bed layer of PA6 (polyamide 6) 3-mm ellipsoidal particles. All tests are made in steady flow conditions and zero slope. Flow field measurements are carried out via the Ultrasonic Velocity Profiler (UVP) UB-Lab P, with two, 60 mm-spaced, transducers fixed to a side wall and which project two acoustic beams converging towards the opposite wall while crossing the flume with angles of 70° and 110° to the flume axis. This setup allowed measuring horizontal profiles of the longitudinal velocity at different depths. The bed conditions are mapped from videos (shot at 60fps), via image-analysis techniques. The full dataset consists of four cross-sections (1,2,3,4 respectively at 2.0, 2.5, 3.0, 3.5 m from the inlet) mapped in terms of flow conditions and bed movements. Five UVP measurements are sampled along the vertical, the first one starting at 0.5 cm from the bed, up to about half of the flow depth, around 3.5 cm from the bed surface. Positioning of the UVP probe aims at measuring the near-bed flow field, assuming a logarithmic profile of the longitudinal velocities. Videos of the bed are shot with a GoPro Hero 9 camera, focussing perpendicular to the bed surface (Figure 1).

ISBN: 978-90-824846-7-0

Figure 1. Experimental setup at the first cross-section.

The first velocity profile, at 5 mm from the bed, is coupled with the video recordings to identify single particles detachment. The other profiles are then used to derive the 1D velocity field between the first and last measurements' sections.
The particles' motion is derived from bed changes at different times. The bed cover variations are identified from the difference between consecutive frames, adapting the temporal resolution of the analysis to the rate of the bed morphology changes.

3 EXPECTED RESULTS

The results of the tests in terms of changes in bed cover derived from videos will be related to the near-bed flow field characteristics averaged over the observation period. This data will serve to estimate the mean erosion expected for the tested hydraulic parameters (e.g. discharge, Reynolds number). Future tests will be carried out with other plastic materials, as well as with other types of bed substrate (sand and gravel beds), with the aim to identify the erosional threshold of microplastics resting on different beds.

ACKNOWLEDGEMENTS

This research was partially funded by NCN National Science Centre Poland–call PRELUDIUM 19, Grant Number 2020/37/N/ST10/01828, a subsidy from the Polish Ministry of Education and Science for the Institute of Geophysics, Polish Academy of Sciences and an internal grant for young scientists at IG-PAS number 500-10-51. This project was also supported by UBERTONE's UVP Innovation Springboard. We would like to thank the UBERTONE team for the free rental of a UB-Lab P and their full technical support, especially to Marie Burckbuchler.

REFERENCES

Dey, S., and Ali, S.Z. (2019). Bed sediment entrainment by streamflow: State of the science. *Sedimentology*, *66*(5), 1449-1485.

Jamieson, A.J., Brooks, L.S.R., Reid, W.D., Piertney, S.B., Narayanaswamy, B.E., and Linley, T.D. (2019). Microplastics and synthetic particles ingested by deep-sea amphipods in six of the deepest marine ecosystems on Earth. *Royal Society open science*, *6*(2), 180667.

Nor, N.H.M., and Obbard, J.P. (2014). Microplastics in Singapore's coastal mangrove ecosystems. *Marine pollution bulletin*, *79*(1-2), 278-283.

Obbard, R.W., Sadri, S., Wong, Y.Q., Khitun, A.A., Baker, I., and Thompson, R.C. (2014). Global warming releases microplastic legacy frozen in Arctic Sea ice. *Earth's Future*, *2*(6), 315-320.

Stubbins, A., Law, K.L., Muñoz, S.E., Bianchi, T.S., and Zhu, L. (2021). Plastics in the Earth system. *Science*, *373*(6550), 51-55.

Waldschläger, K., and Schüttrumpf, H. (2019). Erosion behavior of different microplastic particles in comparison to natural sediments. *Environmental science & technology*, *53*(22), 13219-13227.

Proceedings of the 2nd IAHR
Young Professionals Congress
30 Nov-2 Dec. 2021

Preliminary assessment of quantifying fish injury in pipe flow

Reilly X. Cox[1*], Owen Lee [1], William L. Peirson[1], Hiruni Kammanankada[1], Maryam Farzadkhoo[1], John H. Harris[2] and Stefan Felder [1]
[1] Water Research Laboratory, School of Civil and Environmental Engineering, UNSW Sydney, Australia
*reilly.cox@unsw.edu.au
[2] Centre for Ecosystem Science, School of Biological, Earth and Environmental Sciences, UNSW Sydney, Australia

ABSTRACT

Tube Fishways aim to improve fish passage by piping fish over steep barriers using a water surge with considerable velocity. To ensure safe operation and prevent fish harm, investigation of hydraulic stressors present in pipe flows is required to quantify thresholds for fish injury. Preliminary experiments were conducted assessing impacts of shear stresses, acceleration and pressure in steady flows in pipes. Sensor data in conjunction with tests of juvenile Australian bass and silver perch with length of ~120mm indicate no observable injury for all flow conditions of present tests. Maximum values for brief exposure to stressors were 35 Pa wall shear stress, acceleration of 16G and Ratio of Pressure Change of 1.25. These preliminary results suggest piping fish over barriers is a plausible solution to current fishway limitations. Further research will determine potential threshold values to provide safe limits for the operation of the Tube Fishway and other closed conduit systems.

Keywords: Tube Fishway; fish passage; shear stress; acceleration sensor; native Australian fish.

1 INTRODUCTION AND METHODOLOGY

Fish passage allows the continuation of fish migration over man-made barriers. Fishways have performed poorly across the world (Harris et al., 2017) and much of the common infrastructure such as fish ramps, ladders and vertical slot fishways are costly to build (Mallen-Cooper et al., 2008). A new type of fishway, the Tube Fishway, aims to overcome these issues. This system transports fish through pipes at considerable velocities using an unsteady water surge. Previous experiments have shown effective attraction and lifting of fish (Harris et al., 2020; Peirson et al., 2021). Despite initial successes, systematic research is needed to quantify thresholds of fish injury before field operation. Current information regarding fish injury in closed conduits is limited and mostly associated with downstream fish movements through turbines and across flow conveyance structures. Key stressors with potential to harm fish include shear and turbulence, acceleration and impact as well as barotrauma (Cada et al., 1997). There is currently no distinct information on any of these stressors in closed conduit flows including straight pipes, flow contractions and bends, which are of high relevance for the operation of a Tube Fishway. Herein preliminary steady flow experiments investigated acceleration, pressure changes and wall shear stress through a pipe system with contraction at UNSW Water Research Laboratory (Figure 1).

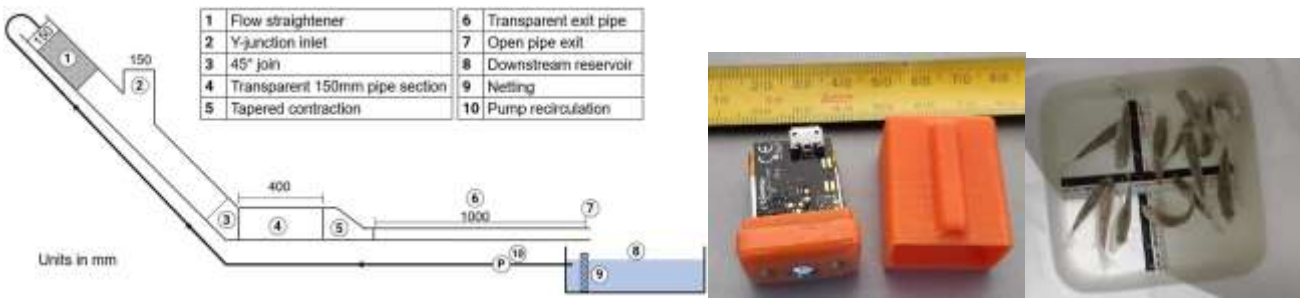

Figure 1. Side view of experimental setup (left). Disassembled sensor (middle). Juvenile silver perch (right).

Steady flows allowed for consistency of trials providing guidance on expected threshold values for fish injury in the unsteady surge during Tube Fishway operations. The neutrally buoyant sensors measured accelerations in 3 degrees of freedom at 400 Hz and pressures at 250 Hz. Following this, juvenile Australian bass and silver perch with mean length of 120 mm were used for trials (n=20). Figure 1 shows a side view of the experimental setup, as well as the pressure and acceleration sensor and examples of tested fish. Steady flows were established in a recirculation system between the start of the pipe system and an exit reservoir downstream of the pipe exit. Discharges of 5.5 L/s and 8.4 L/s, corresponding to Reynolds numbers of 1.4×10^5 and 2.1×10^5

ISBN: 978-90-824846-7-0

were used. Sensors were gently inserted into the flow at the Y-junction. This was repeated afterwards withliv fish. Contraction ratios of 3 and 3.75 were tested with Perspex exit pipes of 50mm and 40mm diameter respectively. Observations of fish behaviour were conducted with two GoPro cameras (30fps), a high-speed camera (457fps) and these observations were paired with recorded acceleration and pressure values along the system.

2 RESULTS AND CONCLUSION

Sensor data captured accurately pipe flow theory (Figure 2) with a pressure drop at the contraction and friction losses through the straight exit pipe. Initial experiments have considered the effects of acceleration and pressure changes through a contraction and wall shear stress on fish. For tested flow rates, maximum values experienced were 35 Pa of wall shear stress in the exit pipe (Location 6), 16G of acceleration and a ratio pressure change (RPC) of 1.25 in the contraction (Location 5). Live fish experiments showed only minor bruising injuries and no mortality in juvenile Australian bass or silver perch, during the experiments, immediately after and for the next two consecutive observation weeks. Silver perch spent an average of 0.36 seconds within the smaller diameter pipe compared to Australian bass with 0.48 seconds on average. This was due to differences between behaviour of species with Australian bass observed to swim against the flow more often than silver perch. These preliminary experiments showed brief exposure to stressors did not harm native juvenile fish and are consistent with thresholds presently used for UNSW Tube Fishway design (Peirson et al., 2021).

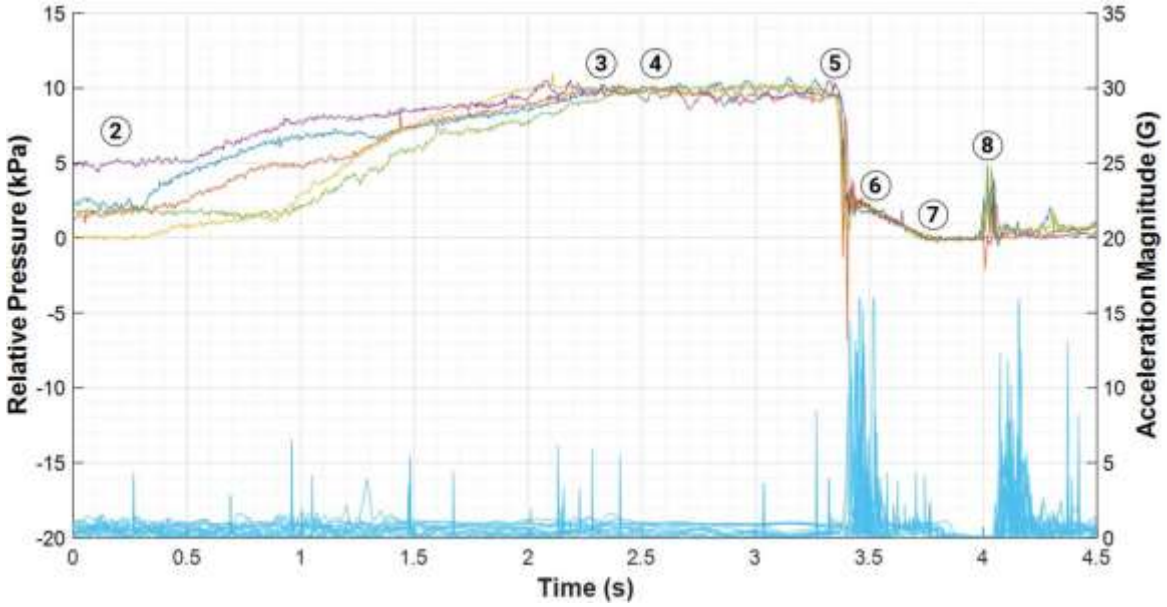

Figure 2. Combined sensor data for 50 mm exit pipe Q=8.4 L/s (Pressure upper curves, Acceleration lower curves), corresponding locations are found in Figure 1.

REFERENCES

Cada, G.F., Coutant, C.C. & Whitney, R.R. (1997). *Development of biological criteria for the design of advanced hydropower turbines*. U.S. Department of Energy Idaho Operations Office, United States.

Harris, J.H., Kingsford, R.T., Peirson, W. & Baumgartner, L.J. (2017). Mitigating the effects of barriers to freshwater fish migrations: the Australian experience. *Marine and Freshwater Research*, 68, 614.

Harris, J.H., Peirson, W.L., Mefford, B., Kingsford, R.T. & Felder, S. (2020). Laboratory testing of an innovative tube fishway concept. *Journal of Ecohydraulics*, 5, 84-93.

Mallen-Cooper, M., Zampatti, B., Stuart, I. & Baumgartner, L. (2008). *Innovative Fishways – Manipulating turbulence in the vertical-slot design to improve performance and reduce cost.* Arthur Rylah Institute for Environmental Research.

Peirson, W.L., Harris, J.H., Kingsford, R.T., Mao, X. & Felder, S. (2021). Piping fish over dams. *Journal of Hydro-environment Research*. 39, 71-80.

ISBN: 978-90-824846-7-0

Proceedings of the 2nd IAHR
Young Professionals Congress
30 Nov-2 Dec. 2021

Fish tracking in laboratory simulated hydropeaking

Robert Naudascher[1], Luiz G. M. Silva[1], Robert Boes[2] & Roman Stocker[1]

[1] Department of Civil, Environmental and Geomatic Engineering, Institute of Environmental Engineering, ETH Zurich, Zurich, Switzerland
[2]Laboratory of Hydraulics, Hydrology and Glaciology (VAW), ETH Zurich, Zurich, Switzerland

ABSTRACT

In this study, we present a novel laboratory flume setup, which allows to quantify 2D-movement trajectories of individual small-bodied fish during varying flow conditions. By combining a semi-transparent substrate with infrared-light illumination we managed to create sufficient contrast to deploy existing imaging-based tracking techniques. First experiments revealed active relocation behavior along lateral depth gradients. The tracking algorithm successfully tracked fish in 97% of the acquired frames for both, low and high discharge situations. Challenges mainly arise from surface waves perturbing the images, however the here presented setup allows to shed light on the fundamental mechanisms and timescales of movement behavior in temporarily altered open-channel flow-fields.

Keywords: hydropeaking, infrared-based imaging, ramping-rates, laboratory hydraulic flume, tracking

1 INTRODUCTION

High-head storage hydropower is deemed to be the ideal renewable energy source to meet the increasing demand for daily peak electrical energy. However, the accompanying release of discharge peaks - called hydropeaking - can affect aquatic biota downstream of such facilities on a daily basis (Schmutz et al., 2015; Auer et al., 2017). Despite more then 30 years of hydropeaking research, the fundamental movement behavior of individuals towards flow changes has never been quantified. It is not known if fish recognize locally decreasing water-levels or flow velocities and relocate towards deeper waters to avoid stranding. The aim of our study was to develop a laboratory setup which allows to quantify such fine scale relocation movement behavior in an automated fashion.

Several imaging-based tracking approaches have been developed over the last decade (Panadeiro et al., 2021), however most of their applications have been limited to still water settings or quasi stationary 2D-flow fields where surface waves are quasi absent. Imaging-based tracking approaches are in principle analogous in the sense that their performance fundamentally rely on (i) good contrast between moving object and its background and (ii) a stationary and therefore non-moving background. Ensuring these conditions in laboratory hydropeaking experiments was the goal of the here presented approach.

2 METHODS

We developed a novel laboratory setup which allows to derive 2D-fish-trajectories for varying discharge conditions on a semi-natural gravel bed. A transparent base-layer of epoxy and glass wedges is illuminated with infrared-light through the glass bottom of the flume. Cameras are equipped with infrared pass filters so that only


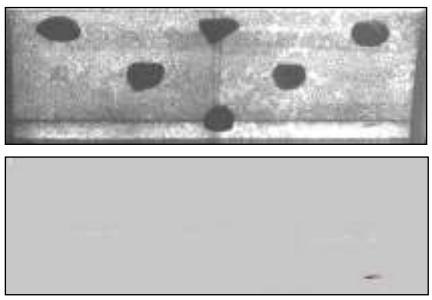
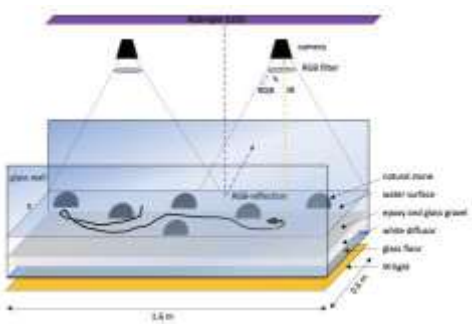

ISBN: 978-90-824846-7-0

Figure 1. Left: Gravel bed; Center: Stitched raw image and output from the tracking code; Right: Setup

wavelength in the range 750-1000 nm reach their sensor. The infrared light is blocked by the fish which therefore appears dark. The raw images are recorded at 15 fps and pre-processing steps include stitching and subtracting the median background. The resulting frames are processed with the open source software "Tracktor" (Sridhar et al., 2019). We run "soft" and "rough" hydropeaking experiments only differing in their ramping-rates (2 and 6 cm/min) and by using N = 15 individual hatchery trout. The tracking performance was evaluated for the base-flow period (Q_{base} = 1.5 L/s) and the peak-flow period (Q_{peak} = 16.5 L/s) with present surface water waves.

3 RESULTS

The tracking performance was evaluated as the fraction of successfully tracked frames. For base-flow and peak-flow a tracking performance above 97 % was achieved. During peak-flow fish was observed to hold station behind larger stones in the shallow water of the laterally inclined gravel bed.

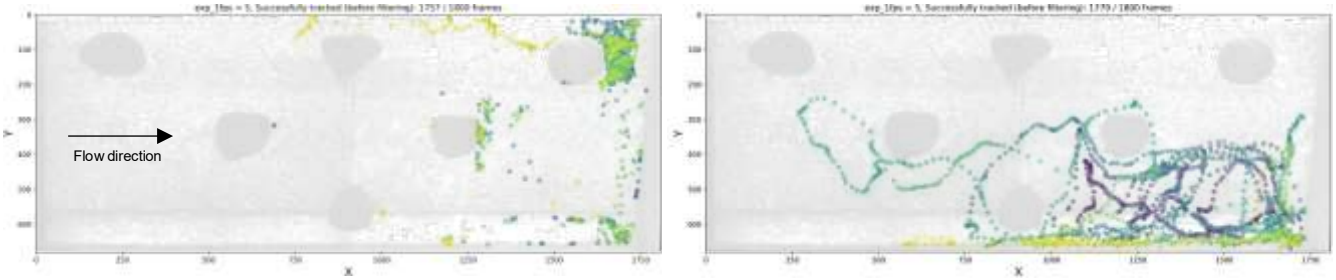

Figure 2. Left: Tracked positions of one individual during 6 minutes of peak-flow conditions; Right: Fish positions during 6 minutes of constant base-flow conditions.

4 DISCUSSION

Fish trajectories could be derived both for base-flow and peak-flow conditions. The trajectories revealed distinct hydrodynamic space use for the tested flow conditions and species. While exploratory behavior with higher swimming velocities could be observed during base-flow conditions, fish retrieved to shallow areas potentially minimizing energy expenditure during peak-flow conditions. Tracking performance was reduced by surface waves appearing as similar sized objects as the fish's body and areas of poor contrast along the flume walls.

5 CONCLUSIONS

The here presented approach allowed to quantify hydrodynamic space use of early-life stage trout. Our results reveal high movement rates during baseflow and prolonged station holding at distinct location behind stones during peak flow. Infrared pass filters and a transparent gravel bed were crucial to minimize to reflections and distortions at the air-water interface. The approach might be adopted in future laboratory experiments with aquatic biota in turbulent open-channel flow.

REFERENCES

Auer, S., Zeiringer, B., Führer, S., Tonolla, D. & Schmutz, S. (2017) Effects of river bank heterogeneity and time of day on drift and stranding of juvenile European grayling (Thymallus thymallus L.) caused by hydropeaking. *Science of The Total Environment*, **575**: 1515–1521.

Panadeiro, V., Rodriguez, A., Henry, J., Wlodkowic, D. & Andersson, M. (2021) A review of 28 free animal-tracking software applications: current features and limitations. *Lab Animal*, **50** (9): 246–254.

Schmutz, S., Bakken, T.H., Friedrich, T., Greimel, F., Harby, A., Jungwirth, M., Melcher, A., Unfer, G. & Zeiringer, B. (2015) Response of Fish Communities to Hydrological and Morphological Alterations in Hydropeaking Rivers of Austria. *River Research and Applications*, **31** (8): 919–930.

Sridhar, V.H., Roche, D.G. & Gingins, S. (2019) Tracktor: Image-based automated tracking of animal movement and behaviour L. Börger ed. *Methods in Ecology and Evolution*, **10** (6): 815–820.

ISBN: 978-90-824846-7-0

Proceedings of the 2nd IAHR
Young Professionals Congress
30 Nov-2 Dec. 2021

Macroplastic monitoring in the urban water system of the city of Florence (Italy)

Lorenzo Innocenti [1] and Luca Solari [2]
[1,2] Department of Civil and Environmental Engineering of the University of Florence, Florence, Italy
lo.innocenti@unifi.it

ABSTRACT

Urban areas are the main source of plastic leakage into the natural environment (i.e. rivers, lakes, and oceans), although data on plastic pollution in urban water systems are scarce. In this work, we present a monitoring activity of macroplastics carried out in the urban area of the city of Florence (Italy). Through visual observations, macroplastic abundance and polymer categories are determined using available citizen science tools. The visual observation of lying waste on the riverbanks is conduced for the two main rivers that flow thought the city, the Arno River and the Mugnone River, respectively. The observed waste density on the Arno riverbanks is of 145 items/km, comparable with previous works, while, for the Mugnone riverbanks the density increase to 581 items/km. These observations highlight the difference between the two considered rivers and represent the first attempt for quantify the production of macroplastics from the city of Florence.

Keywords: citizen science; macroplastic; plastic pollution; Florence; visual observation.

1 INTRODUCTION

Rivers play a key role in transport of plastics from sources to sea, yet, even in some of the world's most polluted river systems, the plastic emission to other water bodies is only 3% of the plastic waste generated within the river basin (Van Emmerik *et al.*, 2019). Thus, the large part of the plastic waste remains entrapped within the river system, particularly on vegetated riverbanks and at in-channel structures (Tasseron *et al.*, 2020; van Emmerik and Schwarz, 2020).
Urban areas has been recognized as the main sources for plastic waste into the river networks. For this reason, in recent years, many studies have been performed in order to understand the and quantify the spatiotemporal variations of plastics in urban water systems (van Emmerik and Schwarz, 2020). As highlighted by Tasseron *et al.* (2020) a long-term data collection are needed to further understand the role of a city into the river plastic budget. For this reason the importance of the citizen science was spotted.
In the present work, the focus is on the city of Florence (Italy), particularly on the riverbanks of the Arno River and the Mugnone River. The main aim of the work is the characterization of the plastic pollution for the city. In order to achieve this goal, a visual observation of lying plastic waste on the riverbanks was carried out. Then, results were compared with similar study cases.

2 METHODOLOGY

The study area extends over 10 km along the Arno River and 4 km along the Mugnone River, a major tributary of the Arno in the municipality of Florence. The Arno River flows thought the historical city center of the city, for this reason not the entire riverbed is accessible (about 1 km of the entire reach). Upstream and downstream the city center the river is surrounded by gardens and parks. On the contrary, the Mugnone River (a tributary of the Arno River) flows through many residential and industrial areas of the city. It is very much embedded between large dike walls (5 m high), above these walls there are mostly roads, sometimes with heavy traffic.
The study area was divided into 240 sections of 100 m in length and between 2 and 10 m in width depending on the possibilities.
The data collection has been done using the mobile citizen science app CrowdWater, which includes a module for measuring plastics in urban and natural water systems (van Emmerik *et al.*, 2020). Macroplastics were characterized following the CrowdWater classification, seven typologies were considered: PET, PO-soft, PO-hard, PS, EPS, Multilayer, and others.

ISBN: 978-90-824846-7-0

3 RESULTS

The density along the two monitored rivers resulted really different, for the Arno River a density of 145 item/km was observed, while for the Mugnone River the density grew up to 575 items/km. Despite the difference in the density, the classification of the macroplastics resulted comparable (Figure 1). For both rivers, the PO-soft resulted to be the greater part of the total observed waste.
In addition, on the Arno riverbanks, four hotspots were identified, all of them located in the central part of the reach in which the presence of numerous bridges increase the blocking probability of the transported macroplastics. However, the observed density of plastic waste for the Arno River resulted comparable with previous studies for similar water bodies (Tasseron *et al.*, 2020; van Emmerik and Schwarz, 2020).

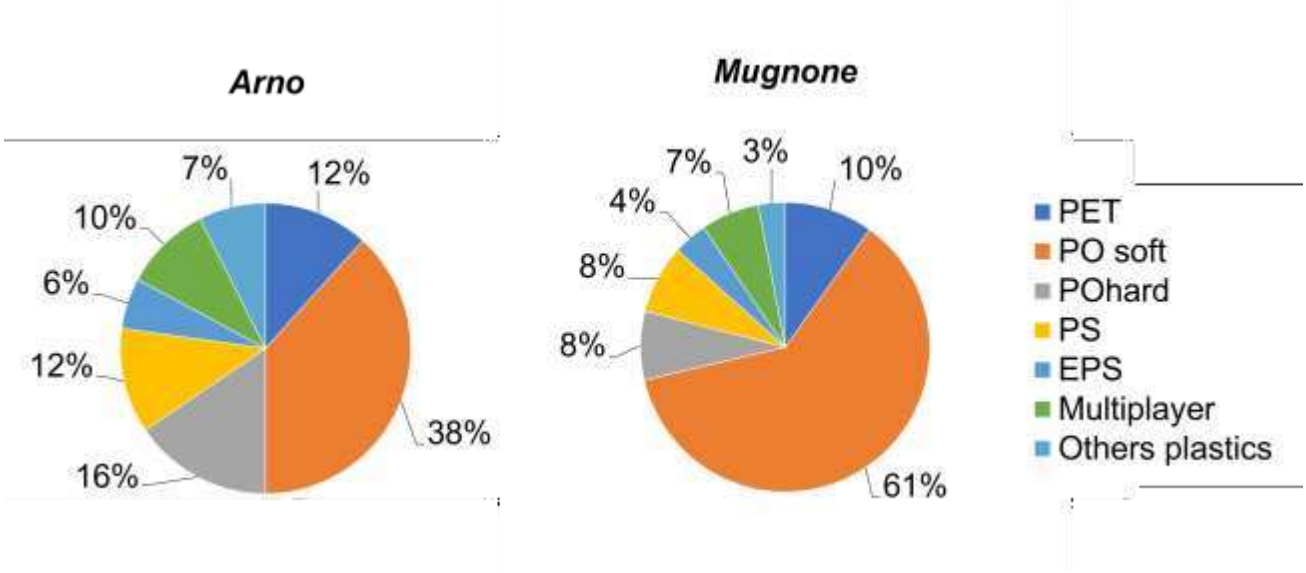

Figure 1. Resulting macroplastics classification.

4 CONCLUSIONS

Data collection on the riverbanks of the Arno River and Mugnone River has been highlighted the most plastic-polluted areas of the city of Florence. Four hotsposts were identified along the Arno reach, located around the main city center. On the contrary, for the Mugnone River the observed density did not highlighted hotspots, while it was greater in the entire reach than for the Arno. The latter means that an high number of macroplastic elements goes from the city to the river and remain entrapped into the riverbed.
The waste classification showed that the most present plastic type was the PO-soft (i.e. plastic bags and other light plastics), while plastic bottles (PET), rigid plastics (PO-hard), plastic cutlery (PS) and multilayer packaging were represented in relatively comparable parts.
Monitoring the evolution of these findings would be particularly interesting through participatory science by encouraging the population to contribute to scientific research.

AKNOWLEDGEMENTS

The authors thank Yann Lenormand and Tommaso Guarnieri for their work done through curricular internship in the Hydraulic Engineering laboratory of the Department of Civil and Environmental Engineering of the University of Florence.

REFERENCES

van Emmerik, T. *et al.* (2020) 'Crowd-Based Observations of Riverine Macroplastic Pollution', *Frontiers in Earth Science*, 8(August), pp. 1–12. doi: 10.3389/feart.2020.00298.
Van Emmerik, T. *et al.* (2019) 'Riverine plastic emission from Jakarta into the ocean', *Environmental Research Letters*. IOP Publishing, 14(8). doi: 10.1088/1748-9326/ab30e8.
van Emmerik, T. and Schwarz, A. (2020) 'Plastic debris in rivers', *Wiley Interdisciplinary Reviews: Water*, 7(1), pp. 1–24. doi: 10.1002/wat2.1398.
Tasseron, P. *et al.* (2020) 'Plastic hotspot mapping in urban water systems', *Geosciences (Switzerland)*, 10(9), pp. 1–11. doi: 10.3390/geosciences10090342.

A novel open-source, freely redistributable algorithm for detrending river DEMs

Beatriz Negreiros [1], Ricardo Barros [1], Sebastian Schwindt [1], Silke Wieprecht [1]
[1] Institute for Modelling Hydraulic and Environmental Systems, Stuttgart, Germany,
beatriz.negreiros@iws.uni-stuttgart.de

ABSTRACT

River detrending involves removing the valley slope from a river Digital Elevation Model (DEM) to obtain non-slanted topographic data. The resulting detrended DEM is a fundamental parameter for geomorphic analyses. Despite recent advances in remote sensing and measuring techniques, which have revolutionized the access to free topographic data, accessible detrending tools are still needed. Current detrending tools are either not open-source or require expensive proprietary software. The objective of this study is to develop an open-source, freely redistributable algorithm for detrending river DEMs. The algorithm is developed in Python and applied to a residual stretch of the Inn River in Germany. The results show that the algorithm satisfactorily removes the valley slope, and therefore, constitutes a valuable tool for fluvial analyses. Anyone interested in using the novel algorithm can download it.

Keywords: Digital Elevation Model, detrending, fluvial geomorphology, Python, Thalweg.

1 INTRODUCTION

Rivers follow a longitudinal valley slope, but many ecological functional relationships can be attributed to lateral slope, which is truncated by valley slope. Thus, for eco-geomorphic analyses, longitudinal slope is removed from river Digital Elevation Models (DEMs) in a process called detrending. To this end, detrending methods are 'levelling the DEM to the horizontal' (Brigante et al., 2017). This is achieved by determining an inclined plane that is tilted along the valley slope. Then, elevations (of the inclined plane) are subtracted from the DEM to tilt it toward a horizontal, non-skew plane. Detrended elevation is valuable information for a variety of geomorphic analysis, such as landform and geomorphic unit classification (Pasternack et al., 2018). However, detrending tools are either not open-source or require expensive proprietary software such as ArcGIS. Thus, current tools are, to the Author's best knowledge, not freely accessible. Therefore, this study introduces the novel, freely available algorithm *riodetrend* (Barros, 2021), which is coded in Python.

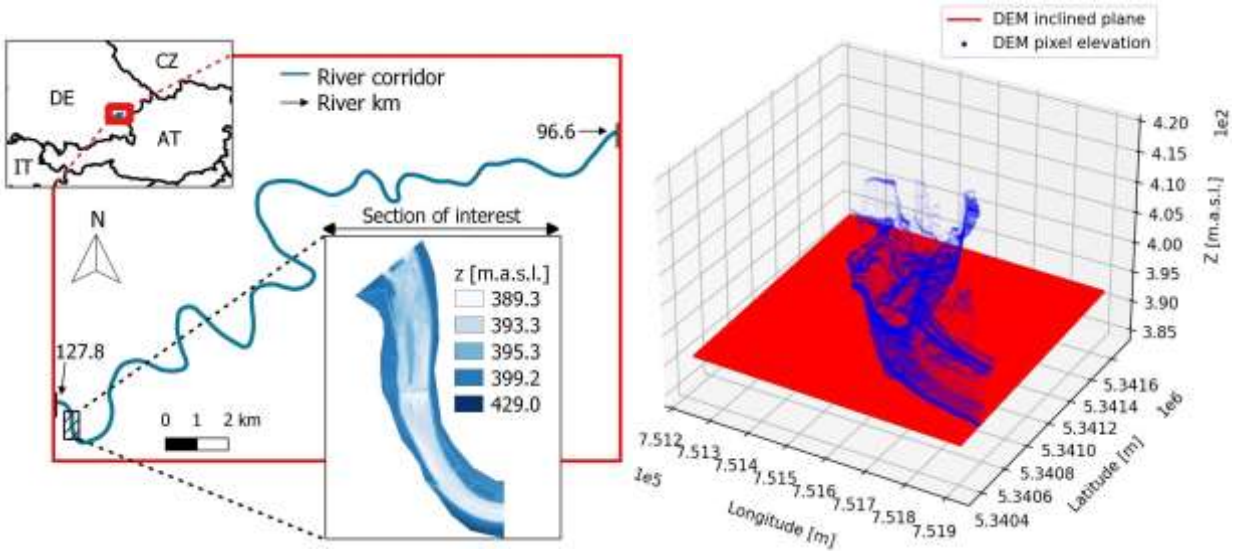

Figure 1: Location of the section of interest at the Inn River, Germany (left), and 3d view of an inclined plane (in red) of the section of interest (right).

2 METHODS

The workflow of the novel algorithm involves computing a regression inclined plane following the Thalweg slope and performing raster operations to subtract the computed plane from the pixels elevation. Thus, the novel algorithm requires input data in the form of a DEM (i.e., raster) and river thalweg points (i.e., xyz shape points).

ISBN: 978-90-824846-7-0

For geomorphic analyses, it has been argued that the Thalweg is less representative than the centerline because Thalweg sinuosity may not align with bank sinuosity (Pasternack et al., 2018). However, this aspect is only relevant for analyses related to subjective bankfull flow theories. The novel algorithm computes a regression plane for every river section independently (see Figure 1, left). To this end, river sections are clipped from the DEM according to expert assessment. The algorithm performs an automated piecewise detrending over all input river sections of the informed directory. Furthermore, gravel bars and other structures such as groins precludes the centerline to represent the valley slope correctly.

A residual stretch of the Inn River (MQ = 106.0 m³/s), Germany (Figure 1), is used as testbed to exemplify the usage of the novel algorithm. A lidar-based topographic survey from January 2020 enabled to obtain a DEM with a pixel size of 0.5 m. The Thalweg is computed with a least-cost algorithm (with the *scikit-image* library) and then smoothened in QGIS to avoid excessive point density resulting from wiggly lines. In the following, we present the result of detrending the section of interest showed in Figure 1 (right).

3 RESULTS AND CONCLUSIONS

Figure 2 illustrates the results of detrending the section of interest with the novel algorithm. The figure shows that the algorithm reduces the valley slope from -0.19% to a residual slope of -0.02%. The residual slope is an artifact of the regression line fitted to the new detrended elevation points of the Thalweg. Even though the inclined plane is removed from the DEM, the detrended Thalweg may still have a slight longitudinal slope, which is not related to the valley slope. As a whole, the results indicate that the algorithm satisfactorily removes valley slope, and therefore, it is a valuable tool for river analyses.

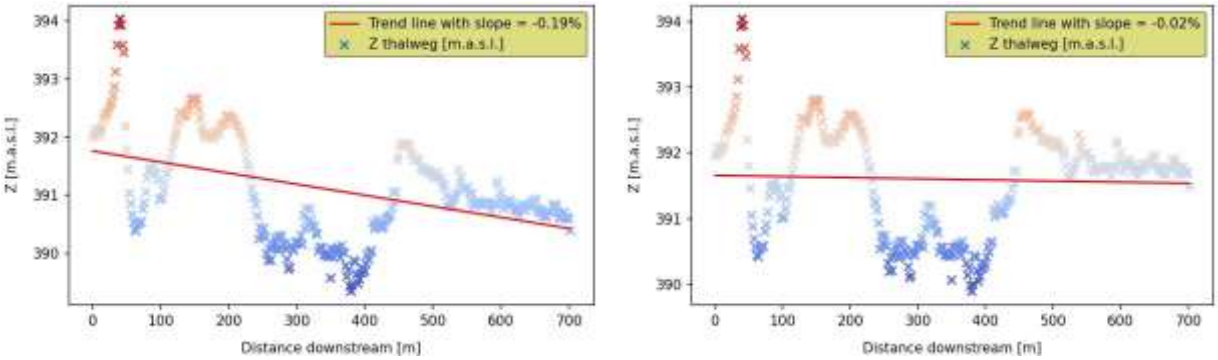

Figure 2: Longitudinal profile of the section of interest before detrending (left) and after detrending (right).

4 RECOMMENDATIONS AND OUTLOOK

Clipping the DEM in several river sections is not a trivial task and it depends on subjective expert assessment. The aim of clipping the DEMs is to fit an inclined plane that best describes every section individually, and thus, to produce a better approximation of the valley slope than by using only one inclined plane for an entire DEM. Following this idea, inflection points along the river corridor provide excellent break criteria for clipping.

Another approach for generating a Thalweg line consists of running a hydrodynamic model with very low discharge. Such simulations were, however, beyond the scope of this study. Future research will focus on implementing an automated, non-subjective geometric river corridor analysis to clip the DEM, and on adding a feature to obtain the river's Thalweg via DEM-only methods.

REFERENCES

Barros, R. (2021, July). *riodetrend.* https://github.com/ricardovobarros/riodetrend (release version 0.0.1). GitHub.

Brigante, R., Cencetti, C, De Rosa, P., Fredduzzi, A., Radicioni, F. and Stoppini, A. (2017). Use of aerial multispectral images for spatial analysis of flooded riverbed-alluvial plain systems: the case study of the Paglia River (central Italy), Geomatics, Natural Hazards and Risk. 8:2, 1126-1143.

Pasternack, G. B., Baig, D., Weber, M. D., & Brown, R. A. (2018). Hierarchically nested river landform sequences. Part 1: Theory. Earth Surface Processes and Landforms, 43(12), 2510-2518.

ISBN: 978-90-824846-7-0

Evaluation of the Physical Habitat Suitability (PHS) for 3 species of fish downstream the Arroyito Dam, in Limay River, Argentina

Brea Francisco José[1], Zombori Mateo [2] and Lopardo María Cecilia[3]

[1,3] Instituto Nacional del Agua (INA) 1, Buenos Aires, Argentina,
: breafranciscojose@gmail.com, mateozombori@gmail.com, mclopardo@gmail.com

ABSTRACT

In this study we evaluated the suitability of the physical habitat for the adult stage of 3 species of fish inhabiting the Limay River, using an ecohydraulic methodology. Using the Telemac 2D program, we evaluated 3 discharges of interest, showing as a result a low exploitation of the modeled site for all the studied species. We intend to continue with the development of Telemac 2D in its new habitat suitability module, generating biological information on fish fauna in Argentina and their habitat preferences.

Keywords: Limay River, ecohydraulic, habitat suitability, Telemac 2D

INTRODUCTION

The science behind environmental water allocations (environmental flow assessment science or environmental water science) is based on quantifying the linkages between hydrological processes and components and various ecological variables.
Analysis of these linkages supports the establishment of a water regime necessary to manage rivers, and other water system, in a more ecologically and socially sustainable manner.
The objective of this study was to evaluate the Physical Habitat suitability (PHS) for the adult stage of 3 fish species inhabiting the Limay River using an ecohydraulic methodology. The habitat suitability models evaluate habitat quality based on abiotic parameters (in this case velocity and depth), which are derived from the modeling results of the Telemac 2D software. The relationships between these parameters and habitat suitability are represented as zones of different coloration, indicating better or worse habitat use by the species studied.

MATERIALS AND METHODS

The study was carried out in the Limay River, in the province of Neuquén.
The software Telemac 2D was use to generate the hydromophodynamic modeling. Its main fields of action are hydromorphological and water quality processes, lacking an ecological approach. This is why we developed an ecohydraulic model in which using the Telemac 2D modeling results, and from the information on the biological knowledge of the species, it is possible to obtain the results of the habitat preference conditions.
This study focuses on three species of fish: *Galaxias maculatus* and *Percichthys trucha,* who are endemic, and *Salmo trutta,* who is invasive. In Argentina, in spite of having a great biodiversity, there are not enough ecological studies for the construction of the preference curves necessary for this type of models.
Therefore, it is common to use habitat preference curves developed in other rivers, previously testing that the transfer of information is possible.
Based on topo-bathymetric information obtained from previous works carried out by the Institute, representing 10 km of extension downstream of Arroyito dam, we used the Blue Kenue program to generate a grid of the area and perform the hydraulic calibration. We then inserted the information from the habitat preference curves for two variables, depth and velocity (Sanz-Ramos et al., 2019, Garcia et al, 2012), and ran the program evaluating 3 discharges of interest: 224 m3/s (average river flow), 300 m3/s (turbined flow from the dam) and 624 m3/s (incoming flow from the dam).

RESULTS

The modeling results showed similar responses for the 3 species: the PHS in all cases indicated a low utilization of the represented site. In the case of *Salmo trutta* we can see that the suitability in relation to

velocity decreases in relation to the increase of represented flows (Fig 1 A-B), while the depth variable shows opposite results (Fig 1 C-D).

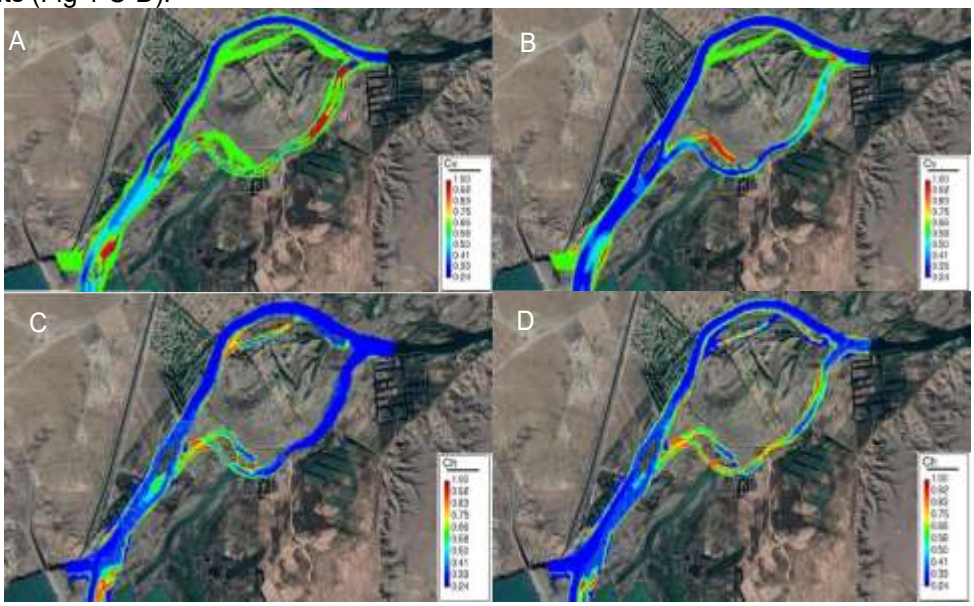

Fig 1- Suitability maps for the velocity (A-B) and depth (C-D) of Salmo trutta with two discharges: A-C:224 m^3/s (left) and B-D: 624 m^3/s (right).

Regarding *Galaxias maculatus* and *Percichthys trucha*, both showed a decrease in habitat suitability in both parameters evaluated in relation to an increase in modeled flow rates (Fig 2 A-B).

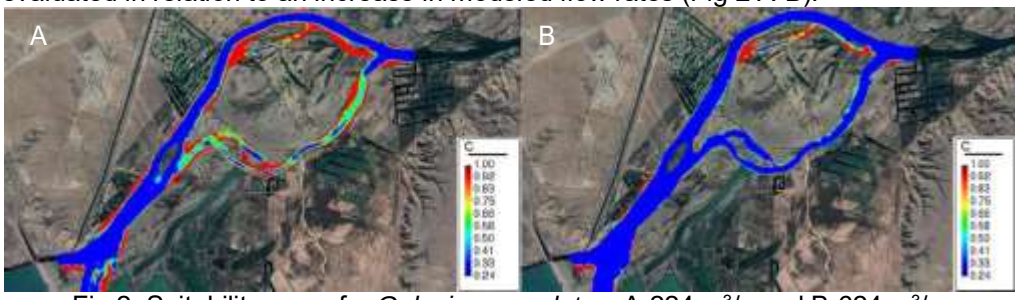

Fig 2 -Suitability maps for *Galaxias maculatus*: A-224 m^3/s and B-624 m^3/s.

CONCLUSIONS

The results obtained showed a low utilization of the habitat represented for the species studied. The Limay River presents a great diversity in terms of habitat types and tributary rivers, in which fish can find refuge, reproduction and breeding areas, so one hypothesis could be that the species studied would prefer these secondary courses in relation to the aforementioned activities.

In Argentina, studies of ecological flows with an ecohydraulic approach are just beginning, little is known about the habitat preferences for the ichthyic fauna of our region, as well as the impact caused by the construction of dams and reservoirs in their life cycles and reproductive patterns. Therefore it is of vital importance to achieve a correct understanding of the dynamics of our rivers, advancing for this aspect in the development of Telemac 2D in its new habitat function, in order to achieve a better regulation of water resources by the population, protecting the different species of the river and their normal life cycles.

REFERENCES

García, A.; González, J. & Habit, E. (2012). "Caracterización del hábitat de peces nativos en el río San Pedro (cuenca del rio Valdivia, Chile)", Gayana Especial: 36-44.

Sanz-Ramos, M; Bladè Castellet, E; Palau Ibars, A; Querol, D.V & Ramos Fuertes, A. (2019): "IberHabitat: evaluación de la Idoneidad del Hábitat Físico y del Hábitat Potencial Útil para peces. Aplicación en el río Eume", Ribagua, DOI:10.1080/23863781.2019.1664273.

ISBN: 978-90-824846-7-0

IAHR YPN

Young Professionals Network

Hosted by
Spain Water and IWHR, China

IAHR AIRH

International Association for Hydro-Environment Engineering and Research

Hosted by
Spain Water and IWHR, China

Urban Drainage & Groundwater Hydraulics

Proceedings of the 2nd IAHR
Young Professionals Congress
30 Nov-2 Dec. 2021

Assessment of groundwater contamination by pesticides using the PRZM-GW model in Júcar River Basin (Spain)

Ricardo Pérez-Indoval [1], Eduardo Cassiraga [2] and Javier Rodrigo-Ilarri [3]
[1] Universitat Politècnica de València (UPV), Valencia, Spain
e-mail: hidroindoval@gmail.com

ABSTRACT

Pesticides are commonly used to control weeds and prevent no desirable grow of algae, fungi and bacteria in many agricultural applications. A number of models have been developed to predict the behavior, mobility, and persistence of pesticides. These models should account for key hydrological and agricultural processes, such as crop growth, pesticide application patterns, transformation processes and field management practices. This work shows results obtained by the Pesticide Root Zone Model for GroundWater) (PRZM-GW) model to simulate the behavior of pesticides. The model uses a whole set of parameters to solve a modified version of the mass transport equation considering the combined effect of advection, dispersion and reactive transport processes. PRZM-GW is used to estimate the daily concentrations of chlorpyrifos in Júcar River Basin (Spain). Results of the PRZM-GW model obtained in this study represents a crucial first step towards the development of a pesticide risk assessment in Júcar River Basin (Spain).

Keywords: pesticide, hydrological and transport processes, models, risk assessment

1 INTRODUCTION

Following USEPA (2005), pesticides are “substances or organisms used to eliminate, incapacitate, modify, inhibit growth of or repel pests. They can be natural or synthetic chemicals, mixtures of these, or living organisms that act as biological control agents. Depending largely on the amount of product used, as well as the physicochemical characteristics of the environment, pesticides can infiltrate the soil and eventually affect the aquifer. If the infiltration is carried out slowly through the unsaturated soil, there are possibilities of retention and some biological degradation, although their accumulation continues to pose a potential risk to plantations. If they reach the aquifer directly, their elimination by biological actions is very slow or null, and it can end up giving concentrations of pollutant not suitable in abstractions destined for drinking water. The mobility of pesticides in aquifers depends greatly on their structure and their chemical composition. In areas where groundwater levels are deep - with a very long transit time for pollutants in the vadose zone - the problem in groundwater may be deferred in time. The use of numerical models is one of the available alternatives to understand the consequences of using pesticides on soil and groundwater. Pesticides transport simulations have been widely studied (Francaviglia and Capri (2000)). Some other authors such as Brusseau and Rao (1989, 1991), Brusseau and Reid (1991) or Brusseau et al. (1989), focused their research on understanding the behavior of organic pollutants in the vadose zone. In order to carry out an evaluation of the impact of the choice of the numerical model chosen, the present work compares the results obtained by applying the model of resolution of the transport equation in unsaturated porous media to the same set of input data which refers to a certain area on Júcar River Basin (Spain).

PRZM-GW (Pesticide Root Zone Model for GroundWater) is a USEPA computer model that simulates the movement of contaminants in unsaturated soil systems within and immediately below the root zone. It is used as a groundwater risk assessment tool. The model considers different formulations that analyze the transport processes of pesticides in the vadose zone. The groundwater flow is described by Richard’s equation:

$$\frac{\partial \theta}{\partial t} = \frac{\partial}{\partial z}\left[K(\theta)\frac{\partial h}{\partial t}\right] \qquad [1]$$

2 MODEL SETUP AND RESULTS

The concentrations in soil of the chlorpyrifos was computed using PRZM-GW for the different applications and types of soil (Figure 1). The numerical modeling was design to simulate the behavior of chlorpyrifos on a certain area on Júcar River Basin were the peak concentrations of chlorpyrifos were measured to be 0.90 ppb for single dose and for annual application until 7.36 ppb.

ISBN: 978-90-824846-7-0

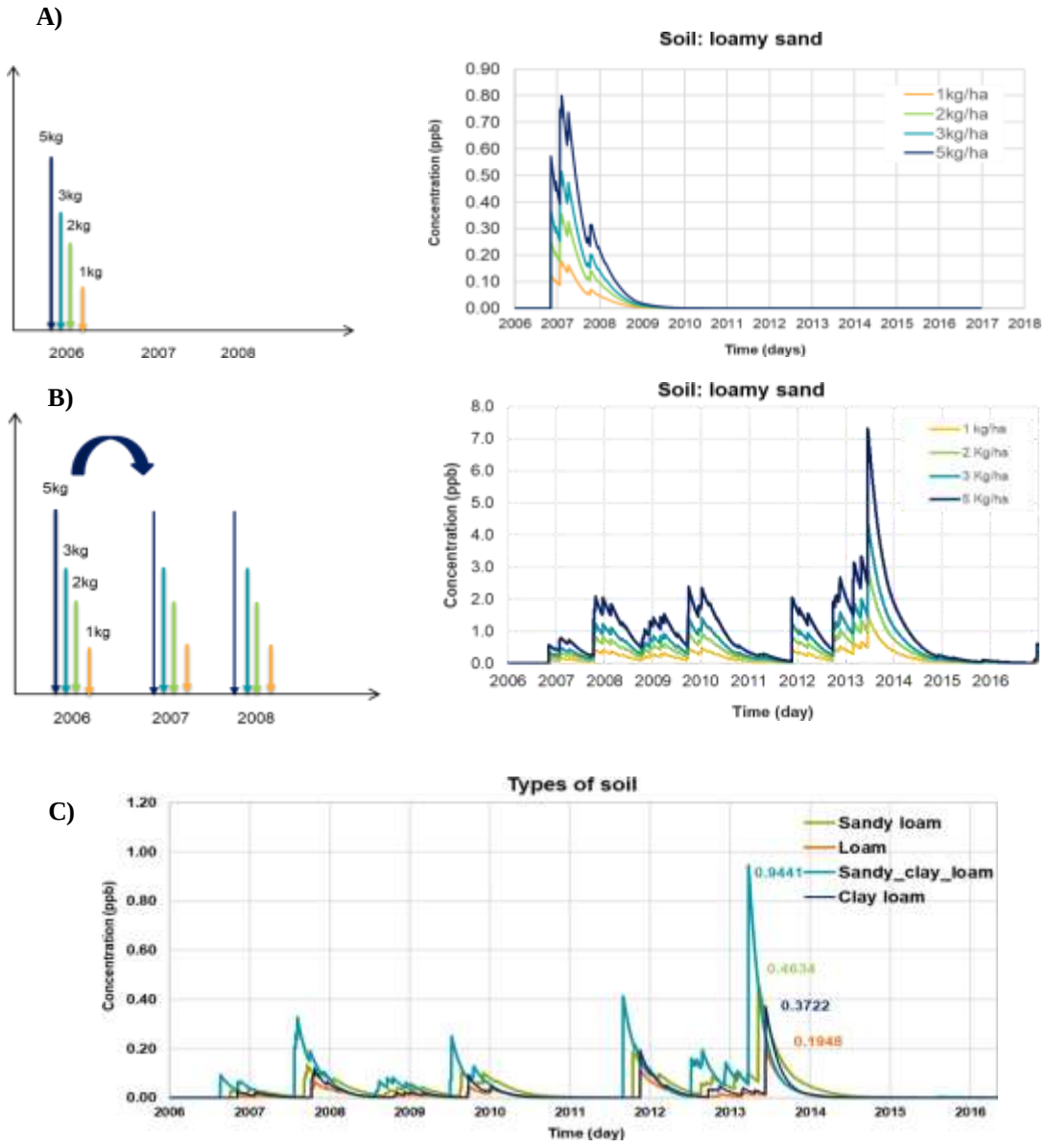

Figure 1. PRZM-GW simulation results for the different applications chlorpyrifos; a) single dose b) annual application and c) types of soil (below)

3 CONCLUSIONS

In conclusion, results show that numerical simulation is a valid tool for the analysis and prediction of the fate and transport of pesticides in the groundwater.

REFERENCES

Brusseau, M.L. and Rao, P.S.C. (1989): Sorption nonideality during organic contaminant transport in porous media. CRC Critical Reviews in Environ. Contro., 19:33.

Brusseau, M.L. and Rao, P.S.C. (1991): Influence of sorbate structure on nonequilibrium sorption of organic compounds. Environ. Sci. Technol., 25:1501.

Brusseau, M.L. and Reid, M.L. (1991): Nonequilibrium sorption of organic chemicals by low organic carbon aquifer materials. Chemosphere, 22:341.

Francaviglia, R. and Capri, E. (2000): Lysimeter experiments in Tor Mancina (Italy). Agricultural Water Management, 44, 63-74.

USEPA (2005). Guidelines for Responsible Pesticide Use. Adelaide, South Australia.

ISBN: 978-90-824846-7-0

Proceedings of the 2nd IAHR
Young Professionals Congress
30 Nov-2 Dec. 2021

Analysis of spatio-temporal evolution of hydrogeochemical properties in the central zone of the Morroa aquifer

Ermys D. Monterroza[1], Valery Polo[2]
[1,2] Universidad del Norte, Barranquilla, Colombia,
[1]ermysm@uninorte.edu.co
[2]vmpolo@uninorte.edu.co

ABSTRACT

Morroa aquifer is the main source of water supply in Sucre, Colombia. It's used in domestic, agricultural and industrial areas, generating overexploitation and affecting the quality of the aquifer environment. Objective of this study is to analyze hydrogeochemical variables and their behavior in spatio-temporal domain in the Morroa aquifer for 2007-2019. Descriptive and multivariate statistical analysis, Piper, Stiff and bivariate diagrams and isoconcentration maps for main ions and physico-chemical parameters were implemented to 40 wells and 107 groundwater samples. Results indicate the aquifer is dominated by $NaHCO_3$ and $Ca(HCO_3)_2$ facies controlled by ion exchange, silicate weathering and carbonate dissolution processes. Origin of ions, anomalies and aquifer contamination sources were identified. Also, 50% of deep wells exceed admissible values of drinking water standards in Colombia. Finally, the presence of chloride alterations associated with anthropic processes constitutes a threat to Morroa aquifer and to all population who are supplied with this resource.

Keywords: hydrogeochemistry, physico-chemical parameters, aquifer, ion exchange, groundwater.

1 INTRODUCTION

In the department of Sucre, in northwestern Colombia, groundwater from the Morroa aquifer is the main source of drinking water for approximately 500,000 inhabitants. Due to the increase in population and the implementation of industrial activities, the demand for water has increased and during the last 6 decades the aquifer has been intensively exploited, leaving a consequence in the quantity and quality of water. In addition, the Morroa aquifer has a medium-high vulnerability, because its recharge area is crossed by streams of domestic wastewater discharges such as the Grande de Corozal stream (CARSUCRE, 2017). Likewise, the presence of agrochemicals in the recharge zone product of the development of agricultural activities, generates long-term changes in their original chemical composition spatially and temporally (Mora Marín et al., 2017). Therefore, the objectives of this study are: a) Determine temporal changes in the hydrogeochemical parameters of the central zone in the Morroa aquifer for 2007-2019. And b) Identify the processes that have influenced the hydrogeochemical characteristics of the study area and their relationship to the geological environment.

2 METHODS

This investigation is analyzed from descriptive statistical analysis, multivariate statistical analysis, generation of Piper, Stiff, bivariate diagrams. Also, isoconcentration maps for the main ions Ca^{+2}, Mg^{2+}, K^{+}, Na^{+}, Cl^{-}, SO_4^{2-}, HCO_3^{-}, CO_3^{2-} and physico-chemical parameters such as pH, electrical conductivity and total dissolved solids were implemented. A total of 40 wells and 107 groundwater samples were used. The data used in this paper were obtained from the files corresponding to the deep well groundwater concessions that belong to the Regional Autonomous Corporation of Sucre (CARSUCRE) for 2007 - 2019.

3 RESULTS

Descriptive statistical analysis indicates that 50% of deep wells exceed admissible values of drinking water standards in Colombia. As well, the multivariate statistical analysis allowed the identification of 3 processes represented by subcomposition data. The first two (Mg and Na) and (HCO_3, K and Ca) can be interpreted as sets of processes, which influence the hydrochemistry of the aquifer and subcomposition 3 (Cl and SO_4) defines an unusual variation that is considered a process of independent influence on the original hydrochemistry of the

aquifer. The piper diagram suggests that the aquifer is dominated by sodium bicarbonate and calcium bicarbonate waters. However, a third type of water was presented in each period of years, defined by local processes as dissolution of carbonates or contamination, this type of water refers to the variations of chlorides and sulphates. The spatial variation maps show that the studied ions and parameters present similar conditions, most of the concentrations are highest in the western sector of the study area, except for the pH, since the deepest wells are in the east, presenting higher pH in that area.

4 DISCUSSIONS

4.1 Ion exchange

The ion exchange is one of the processes that contributes the most to groundwater chemistry. First of all, a recharge source with high concentrations of Ca^+ and a presence of minerals with high cation exchange capacity (CEC) as well as Na^+ is needed at their exchange sites. For this reason, the exchange of cations between Ca^+, Mg^+, Na^+, is the process responsible for the increase in sodium to the SW in the study area and the decrease in calcium and/or magnesium from the recharge zone to the discharge zone. The Piper and Stiff diagrams show the hydrogeochemical facies changes in the cations, their concentrations have an order of magnitude $Na^+ > Ca^+ > Mg^+ > K^+$. The presence of potassium in these samples is moderate, but K^+ may come from weathering of feldspars, micas, and clay minerals.

4.2 Silicate weathering

The weathering of silicate minerals is the cause of the predominance of HCO_3^- in the aquifer system, a possible source of bicarbonate is due to the dissolution of silicates by reacting with H_2CO_3 or from CO_2 in the soil at the time of bedrock minerals weathering. Because HCO_3^- is the dominant ion in the Morroa aquifer, it indicates an initial source of alkalinity in groundwater. Indeed, some pH concentrations exceed the limit established by the Colombian drinking water standard, presenting pH values > 9.0, located in the NW of the area.

4.3 Carbonate dissolution

Dissolution and precipitation of minerals may be one of the secondary processes that control chemistry in the Morroa aquifer. To determine the chemical balance between calcite mineral and groundwater, the saturation index (IS) of calcite calculated by the Diagrammes software was used. If groundwater is saturated (IS>0) with respect to a mineral, it is prone to deposit part of the solute charge (precipitation). Whereas, if it is unsaturated (IS<0) it will take up more mineral in the solution (dissolution).

5 CONCLUSIONS

The graphical methods and multivariate analysis techniques were able to identify specific hydrogeochemical characteristics in the Morroa aquifer, showing two main types of groundwater by sodium bicarbonate and calcium bicarbonate waters controlled by cation exchange and silicate weathering processes which are responsible for the high concentrations of Na and HCO_3^- in the aquifer. The calcite saturation index diagram establishes a response time of 3 - 4 years for the aquifer in the case of the ENSO phenomenon (El Niño – Southern Oscillation) and the wells of shallower depths. Finally, contamination sources present in the wells were identified, such as leaching, untreated sewage and sewer leaks that can cause an increase in chlorides. Indeed, anthropogenic contamination has a representative influence on the hydrogeochemistry of the aquifer environment and has repercussions throughout the department of Sucre, especially in the communities that supply from this source.

REFERENCES

Corporación Autónoma Regional de Sucre. (2017). Estudio técnico del acuífero Morroa. Grupo de Aguas Subdirección de Gestión Ambiental. Sincelejo.

Mora Marín, M. A., Ríos Pescador, L., Ríos Ramos, L., & Almario Charry, J. L. (2017). Impacto de la actividad ganadera sobre el suelo en Colombia. Ingeniería Y Región, 17, 1-12. https://doi.org/10.25054/22161325.1212

ISBN: 978-90-824846-7-0

Proceedings of the 2nd IAHR
Young Professionals Congress
30 Nov-2 Dec. 2021

Addition of drinking water treatment sludge into permeable pavements for phosphorus control in infiltrated runoff water

Eduardo García-Haba[1], Carmen Hernández-Crespo[2], Miguel Martín[3] and Ignacio Andrés-Doménech[4]
[1,2,3,4]Instituto Universitario de Ingeniería del Agua y Medio Ambiente – Universitat Politècnica de València, Camí de Vera s/n, 46022 València, Spain
e-mail: [1]edgarha@iiama.upv.es, [2]carhercr@upv.es, [3]mmartin@hma.upv.es, [4]igando@hma.upv.es

ABSTRACT

Sustainable Urban Drainage Systems (SUDS) are effective solutions for stormwater management. In particular, permeable pavements (PPs) allow water quality improvement. However, its capacity of treatment can be enhanced through the addition of drinking water treatment sludge (DWTS) to the filter media. This low-cost adsorbent material, provides high retention capacity of phosphorus among other pollutants. The study aims to investigate the effect of DWTS on the treatment capacity of PPs. The response of two permeable pavements, one of them with DWTS, are tested and compared under the average rainfall regime of Valencia (Spain). The results show a reduction of 33% in total phosphorus (TP) and 55% in phosphate concentrations in infiltrated water. Thus, the addition of DWTS into the filter media improves the treatment capacity of permeable pavements. This finding might suppose valorization of DWTS and integration of the circular economy principles in the urban water cycle.

Keywords: sustainable urban drainage systems; permeable pavements; drinking water treatment sludge; phosphorus control; circular economy.

1 INTRODUCTION

Sustainable urban drainage systems (SUDS) are nature-based solutions to manage stormwater in a sustainable way by reducing the urban runoff production, thus reducing the risk of combined sewer overflows (CSO). SUDS include green swales, green roofs, infiltration basins and permeable pavements (PPs), among others. SUDS in general, and PP concretely, provide with other environmental benefits such as water quality improvement, groundwater recharge or mitigation of urban heat island effect (Hernández-Crespo et al. 2019). Several studies have demonstrated the ability of PPs to significantly improve the water quality (WQ) of the water infiltrating through them, compared to the corresponding surface runoff that would be generated if the pavement were impermeable (Hernández-Crespo et al. 2019; Razzaghmanesh and Borst, 2019). This capacity to improve WQ can be enhanced by using reactive media in the structure of PPs. Drinking water treatment sludge (DWTS) is the main waste generated in drinking water treatment plants (DWTPs), as a result of the coagulation-flocculation and sedimentation treatments. However, it should be considered as a by-product to be valorized because it constitutes a low-cost adsorbent material with high retention capacity of phosphorus, as well as other pollutants such as metals and semimetals (Zhao et al. 2020). In this study, the following hypothesis was set up: PPs treatment capacity can be enhanced by introducing a small proportion of DWTS in the filling medium of permeable interlocking concrete pavement (PICP).

2 MATERIAL AND METHODS

The experimental setup consists of two infiltrometers with permeable pavement, structured by the following layers, from the bottom to the top: geotextile, 25 cm of coarse gravel (25-40 mm size), geotextile, 5 cm of fine gravel (2-4 mm size), and interlocking concrete pavement. A special interlocking concrete pavement, called FIT-BLOCK, donated by (QUADRO), was used. The interlocking separation is 3,75 mm and it is filled with fine gravel (3-6 mm size). In one of the infiltrometers (PICP), the separation was filled with this fine gravel, according to the manufacturer and, in the other infiltrometer (PICP-DWTS), the separation was filled with a mixture of fine gravel (80% mass of the mixture) and DWTS (20% remaining mass). The rainfall simulator consists of a water storage tank, provided with a pump (Multi-1300 SICCE) and a grid of drip irrigation pipes.

The simulated rainfall reproduces the average rainfall regime of Valencia (Spain): events with a rainfall volume of 16 mm and 30 min duration (32 mm/h), every two weeks for a 6 months period. The influence of progressive pollution build-up was studied by dry sprinkling sediments (real dust and dirt) on the pavement surface. The applied sediments were collected using a mechanical sweeper (dry conditions) at Universitat Politècnica de València. The deposition rate on the pavement (5 g/m^2/d) was selected according to Hernández-Crespo et al.

ISBN: 978-90-824846-7-0

(2019). Deionized water was used to simulate rainwater. A container was placed below the infiltrometer to collect the infiltrated water. Then, infiltrated water was continuously weighed in order to obtain the output hydrograph, and physico-chemical variables were subsequently analyzed.

3 RESULTS AND CONCLUSIONS

During a six month-experiment, PICP and PICP-DWTS were able to retain a significant volume of simulated rainfall. Concretely, both systems retained an average volume of 6,6 l/m^2, which represents 41% of the total volume applied (16 l/m^2). Conversely, there were significant differences regarding the concentration of total phosphorus (TP) and phosphates in the infiltrated water (Figure 1). In terms of accumulated mass, TP infiltrated through PICP was 9,0 mg/m^2 and 6,0 mg P/m^2 through PICP-DWTS, while phosphates were 3,8 and 1,7 mg P/m^2 respectively. This means that the addition of DWTS enhances the treatment capacity by 33% for TP and 55% for phosphates.

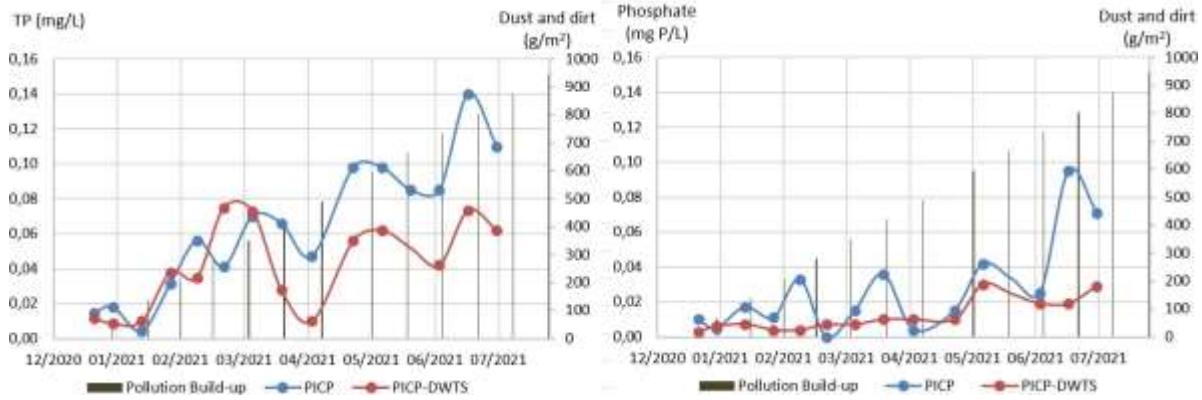

Figure 1.Infiltrate concentrations of TP and Phosphates through PICP and PICP-DWTS

4 CONCLUSIONS

Valorization of DWTS as filling material of PICP, enhances the treatment capacity of this SUDS technique, while promotes integration of the circular economy principles in the urban water cycle. PICP-DWTS is able to retain a significantly higher quantity of phosphorus than PICP. This supposes an important advantage for receiving water bodies, sensitive to eutrophication, as phosphorus is the main limiting nutrient.

ACKNOWLEDEGEMENTS

This research receives funding from the Ministry of Science and Innovation of the Spanish Government (Ref. PRE2019-089409). The study has been developed within the framework of the ENGODRAIN project (Ref. RTI2018-094217-B-C31) funded by the Spanish National Research Agency through the General State Budgets and the European Regional Development Fund (ERDF). Eduardo García-Haba appreciates the funding for pre-doctoral contracts for doctors training.

REFERENCES

Hernández-Crespo, C., Fernández-Gonzalvo, M., Martín, M., Andrés-Doménech, I. (2019). Influence of rainfall intensity and pollution build-up levels on water quality and quantity response of permeable pavements. Sci. Tot. Environ. 684, 303-313; 2019. doi.org/10.1016/j.scitotenv.2019.05.271.

Razzaghmanesh, M., Borst, M. (2019). Long-term effects of three types of permeable pavements on nutrient infiltrate concentrations. Sci. Tot. Environ. 670, 893-901. https://doi.org/10.1016/j.scitotenv.2019.03.279.

Zhao, Y., Nzihou, A., Ren, B., Lyczko, N., Shen, C., Kang, C., & Ji, B. (2020). Waterworks Sludge: An Underrated Material for Beneficial Reuse in Water and Environmental Engineering. Waste and Biomass Valorization, 0123456789. https://doi.org/10.1007/s12649-020-01232-w.

Proceedings of the 2nd IAHR
Young Professionals Congress
30 Nov-2 Dec. 2021

Comparative analysis of radar and rain gauge-based runoff in urban drainage system of damhusaen catchment, Copenhagen

Husnain Tansar[1,2], Mukand Babel[2], Huan-Feng Duan[1]

[1]Department of Civil and Environmental Engineering, The Hong Kong Polytechnic University, Hung Hom, Kowloon, Hong Kong,
husnain.tansar@connect.polyu.hk

[2]Water Engineering and Management, Asian Institute of Technology,
P.O. Box 4, Klong Luang, Pathumthani, Thailand

ABSTRACT

The investigation of rain gauge and radar-based runoff has become essential due to advantages and disadvantages of both types of rainfall measurement methods. A comparative analysis was made in this study based on both types of rainfall-based forecast using three different types of storm events. The rain gauge-based forecast performed better than radar with limited ability to capture spatial variation of rainfall in urban catchment. The radar-based forecast showed potential to simulate spatial rainfall dynamics but could not reasonably performed well, might be due to presence of uncertainties from multiple sources.

Keywords: urban drainage; radar; uncertainty; rainfall dynamics; spatial variation.

1 INTRODUCTION

The principle of rainfall measurement is different in case of rain gauge and radar. The rain gauge measurement method is a direct, continuous, and point-based approach, while radar measures rainfall with indirect, discrete, and spatial measurement approach. Both types of rainfall measurement methods have pros and cons that significantly change urban runoff simulation results (Quirmbach & Schultz, 2002). In case of short- and long-term radar-based rainfall, the accuracy and reliability of radar-based flow forecasts are essential for efficient control and operation of urban drainage system. Therefore, the uncertainties in radar-based rainfall needs to be rectified before using it as a forcing in urban drainage models (UDMs). In another scenario, the rain gauge measures point rainfall with high accuracy because of direct measurement method, but they are unable to represent the spatial variation of rainfall within catchment. Based on pros and cons of both methods, both rainfall measurement approaches simultaneously used considering accuracy, reliability, and spatial variability of rainfall in urban catchment (Ochoa-Rodriguez et al., 2019).

2 MATERIALS AND METHODS

The damhusaen catchment is located in Copenhagen, Denmark, having total population and area of 0.26 million and 55.7 km^2, respectively. The UDM of damhusaen catchment is based on 90 pumps, 4423 nodes, 268 weirs, 1698 sub-catchments and 81 orifices. Two upstream boundaries were specified as input forcing in the model (B1 & B2). D1, D2, D3 and D4 are flow measurement locations, longitudinally distributed from upstream to downstream of catchment on main drainage network, as shown in Figure 1.

The C-band Doppler radar is used with its total coverage range of 360km and spatial resolution of 500 × 500 m^2. Radar data is converted into rainfall depth by using Marshall Palmer empirical power-law equation (Eq.1) and standard values of parameters (a & b) were used. Total 864 radar grids were selected that captured rainfall over catchment domain. The bias correction of radar rainfall was performed using mean field bias (MFB) correction method.

The expression used for conversion process is:

$$Z = aR^b \quad (1)$$

The equation (1) is converted to equation (2) to calculate the rainfall intensity.

$$R = \left(\frac{Z}{a}\right)^{1/b} = \left(\frac{10^{(dBZ/10)}}{a}\right)^{1/b} \quad (2)$$

Where, R = Rainfall rate (mmh^{-1}); Z = Radar reflectivity factor (mm^{6}m^{-3}); a = Conversion constant, default value 200; b = Conversion constant, default value 1.6.

The equation (3) represents mean field bias correction method, the correction factor MFB is estimated to adjust the raw radar rainfall.

$$MFB = \frac{\sum_{i=1}^{N} G_i}{\sum_{i=1}^{N} R_i} \quad (3)$$

ISBN: 978-90-824846-7-0

Where MFB is bias correction factor; G_i and R_i are measured rainfall at gauge i and radar grid paired with gauge i (mm). For comparison of radar and rain gauge-based runoeff, th volume error was calculated with the v following formula.

$$\text{Volume error (\%)} = \frac{Vsim - Vobs}{Vobs}$$

Where, V_{sim} and V_{obs} are simulated and observed volumes, respectively.

Figure 1. Damhusåen drainage system with the locations of rain gauges, discharge observations (D1, D2, D3, D4), water level observations and boundary locations

3 RESULTS AND DISCUSSION

The correction factor was estimated based on twelve rain gauges and their nearer radar grids, and average correction factor 0.8437 of all rain gauges were applied to correct radar rainfall. The coefficient of correlation between radar and rain gauge rainfall was selected to validate radar rainfall. Furthermore, the nine rain gauges showed quite good correlation above 0.4 and remaining three presented less than 0.4. Overall, the maximum and minimum correlation were estimated up to 0.6171 and 0.1776 for all grids, as four of them is represented in Figure 2.

Overall, radar-based runoff forecast represented higher volume error compared to corrected radar and rain gauge-based runoff in three different (short, medium and large) rainfall events at all observation locations within catchment, as shown in Figure 3. A significant reduction in volume error of 2-8% noticed in total outflow of catchment (D4) because of corrected radar rainfall during three events. Among three scenarios, the rain gauge-based flow forecast proved to be the best for accurate flow prediction and capturing spatial representation of rainfall dynamics.

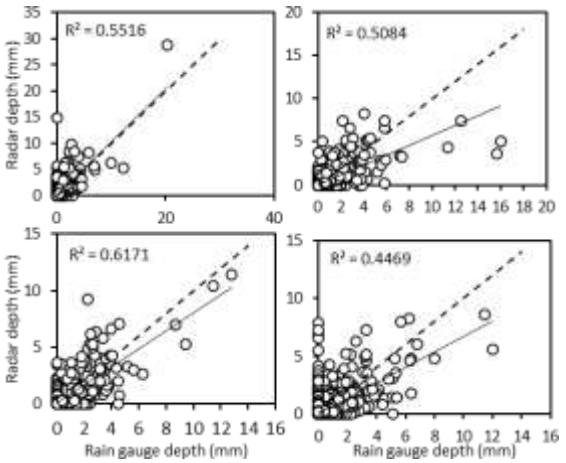

Figure 2. Scatter plots of hourly accumulated radar rainfall and rain gauge observations;

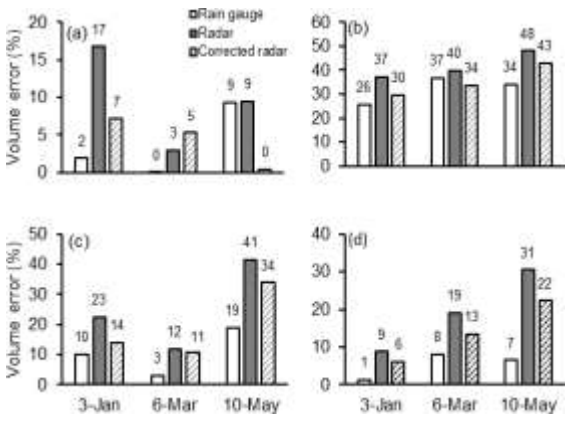

Figure 3. Comparison of volume error of radar, corrected radar and rain gauge-based flow forecasts at (a) D1, (b) D2, (c) D3 and (d) D4

4 CONCLUSIONS

The rain gauge-based runoff predictions presented higher confidence on its performance compared to radar-based rainfall measurement method. The major advantage of radar-based rainfall measurement is to capture spatial variations of rainfall processes, however, this method compromised accuracy of required outputs because of its indirect measurement method, uncertainties from multiple sources and limited ability of rainfall correction methods.

REFERENCES

Ochoa-Rodriguez, S., Wang, L. P., Willems, P., & Onof, C. (2019). A Review of Radar-Rain Gauge Data Merging Methods and Their Potential for Urban Hydrological Applications. *Water Resources Research*, *55*(8), 6356-6391. https://doi.org/10.1029/2018wr023332.

Quirmbach, M., & Schultz, G. A. (2002). Comparison of rain gauge and radar data as input to an urban rainfall-runoff model. *Water Science and Technology*, *45*(2), 27–33.

ISBN: 978-90-824846-7-0

Proceedings of the 2nd IAHR
Young Professionals Congress
30 Nov-2 Dec. 2021

Reconstruction of a digital elevation model in a lab-scale urban drainage facility applying LiDAR and SfM techniques

Manuel Regueiro-Picallo[1], Esteban Sañudo [1], Luis Cea[1] and Jerónimo Puertas[1]
[1] Universidade da Coruña, Water and Environmental Engineering Group, Elviña, 15071 A Coruña, Spain.
e-mail (manuel.regueiro1@udc.es, e.sanudo@udc, luis.cea@udc.es, jeronimo.puertas@udc.es)

ABSTRACT

The use of visualization techniques for obtaining elevation maps with simple and relatively low-cost procedures, apart from conventional topographic methods, is widespread. In the field of urban drainage systems, numerical models require greater grid detail to solve complex hydraulic problems. This study presents the use of Structure from Motion (SfM) and Light Detection And Ranging (LiDAR) techniques to obtain the roof and pavement elevations of an urban drainage experimental module. The digital reconstructions obtained are both satisfactory, in terms of the detail of the elements, and similar between each other, with a mean vertical error for both surfaces less than 2 mm. The main discrepancies between both procedures lie in collecting and processing point clouds and meshes.

Keywords: urban drainage; photogrammetry; Structure from Motion (SfM); Light Detection And Ranging (LiDAR).

1 INTRODUCTION

Urban runoff-rainfall models are commonly used to study the performance of urban drainage systems. High spatial resolution models, such as detailed grids of the surface elevations, should be used as input geometries in numerical models to accurately analyse the hydraulic processes that occur in these systems. As the computational capabilities of commercial computers increase, they will make it possible to solve more complex problems with larger mesh sizes. Visualization tools are a suitable mechanism to obtain a better approach to the model elevation map, assessing surface macro-roughness (e.g., roofs and pavers within urban drainage systems). A comparison of the elevation map acquisition with LiDAR and SfM procedures in part of an urban drainage experimental module is shown in this study. The use of photogrammetric techniques to obtain elevations by the authors is noteworthy, especially on impervious surfaces and accumulation of sediments in sewer pipes. Further information regarding these applications can be found in Naves et al. (2019) and Regueiro-Picallo et al. (2020).

2 MATERIAL AND METHODS

This study was carried out in a water-sensitive urban design (WSUD) facility located in the Hydraulic Engineering Laboratory of the Center for Technological Innovation in Construction and Civil Engineering (CITEEC) at the University of A Coruña (Spain). This facility is included in the WSUD experimental models of the laboratory, which were built mainly for research as well as high-education purposes (Puertas et al., 2020). For the present study, one of the roofs of the WSUD experimental model and part of the paved surface have been selected. The elevation map of these surfaces was obtained by applying SfM and LiDAR techniques (Figure 1). To obtain the elevations with the SfM technique, the surfaces were first photographed with a conventional digital camera (Canon EOS 2000d, EF-S 18-55mm f/3.5-5.6 IS). Since these are surfaces with uniform textures, it was necessary to project a texture onto the surfaces so that the SfM technique could detect the pairs of points between the photographs. VisualSfM software was used for the digital reconstruction of the model and MeshLab software was used for point cloud processing and mesh generation. On the other hand, an Intel RealSense LiDAR Camera L515 together with the commercial software RecFusion have been used to directly obtain the digital reconstruction of the installation using the LiDAR technique.

3 RESULTS

The final products consist of two Digital Elevation Models (DEM) with a 5 mm spatial resolution. Differences between Digital Elevation Models (DEM) obtained with each technique were quantified using the Root Mean Square Error (RMSE) using the LiDAR topography as reference. The RMSE obtained between roof topographies was 8 mm while for paved topographies was 5 mm. In addition, the mean vertical error obtained for roof and paved surface topographies was less than 2 mm. These differences agree with the results in Naves et al. (2019) where a topography with a similar resolution was used and validated in a hydraulic numerical model. Therefore, no significant differences can be considered regarding DEM resolution and accuracy between both techniques for this research scope.

ISBN: 978-90-824846-7-0

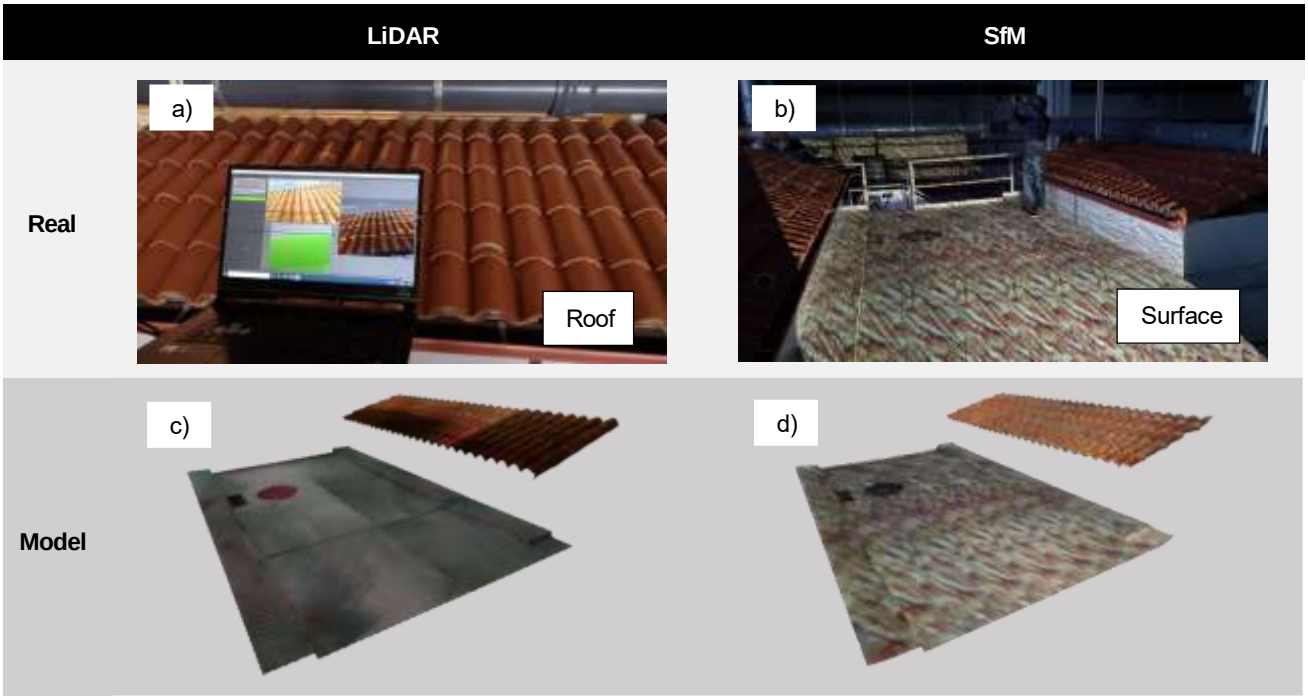

Figure 1. Snapshots of the roof (a) and the surface (b) of the WSUD facility, and LiDAR (c) and SfM (d) reconstruction models.

4 CONCLUSIONS

LiDAR and SfM techniques show significant advances in reconstructing highly detailed (mm/cm scale) urban drainage surfaces, such as pavements and roofs, to increase the performance of numerical models. The comparison of the elevations in the facility shows that the result is similar regardless of the technique used. Nevertheless, as main differences, it should be noted that the SfM technique allows to obtain a greater detail of the surface macro-roughness, such as roof tile channels, mainly due to the higher density of points. On the other hand, the LiDAR technique shows greater advantages when processing point clouds since the mesh can be obtained directly by using the sensor-software combination, and within a known coordinate system and scale.

ACKNOWNLEDGEMENTS

The work developed by Manuel Regueiro-Picallo is funded within the postdoctoral fellowship programme from the Xunta de Galicia (Consellería de Cultura, Educación e Universidade). The contract of Esteban Sañudo is funded by the INTERREG ATLANTIC AREA program through the project AA-FLOODS (EAPA_45/2018).

REFERENCES

Naves, J., Anta, J., Puertas, J., Regueiro-Picallo, M., Suárez, J. (2019). Using a 2D shallow water model to assess Large-Scale Particle Image Velocimetry (LSPIV) and Structure from Motion (SfM) techniques in a street-scale urban drainage physical model. *Journal of Hydrology,* 575, 54-65.

Puertas, J., Hernández-Ibáñez, L., Cea, L., Regueiro-Picallo, M., Barneche-Naya, V., Varela-García, F.-A. (2020). An Augmented Reality Facility to Run Hybrid Physical-Numerical Flood Models. *Water,* 12, 3290.

Regueiro-Picallo, M., Suárez, J., Sañudo, E., Puertas, J., Anta, J. (2020). New insights to study the accumulation and erosion processes of fine-grained organic sediments in combined sewer systems from a laboratory scale model. *Science of The Total Environment,* 716, 136923.

Laboratory assessment of long-term clogging of a porous concrete pavement system

Juan Naves[1], Jose Anta[1], Joaquín Suárez[1], Angélica Goya[1], Damián Pazos[1], Alfredo Jácome[1], and Raquel Viturro[1]
[1]Universidade da Coruña, Water and Environmental Engineering Group (GEAMA), A Coruña, Spain, juan.naves@udc.es

ABSTRACT

Clogging can reduce the stormwater management and treatment capacity of permeable pavements and understanding this process is key to improve their maintenance and foster their development. In this work, a laboratory analysis of the long-term performance of a porous pavement system was carried out using a laboratory rainfall simulator. First, the hydrologic behavior of the system was characterized comparing results with an equivalent impervious surface, resulting in a retaining capacity of 5 L/m^2 that allows intercept light rains by itself. Clogging process was then assessed using road dust sediments with three different granulometries. Using a realistic granulometry was resulted as key, and porous concrete slabs was observed to work as sediment traps up to 1.5 kg/m^2 without reducing the hydraulic performance of the system, keeping joints from clogging for higher loads.

Keywords: permeable pavement; clogging; rainfall simulator; urban drainage.

1 INTRODUCTION

The installation of permeable pavements in an urban environment involves the reception of dust and dirt from atmospheric deposition, leaf fall, runoff and degradation of the filter media materials themselves, in addition to other inputs. This dust and dirt, consisting of materials of different sizes, is partially retained. Retention is a favorable process because the particles may be associated with contamination. However, retention also implies clogging of the permeable pavement, reducing its proven effectiveness in stormwater management and treatment. Given the great uncertainty in how the clogging affects their long-term performance, this work assesses the affectation of different sediment loads and grain sizes in a permeable pavement system using a 1 m^2 rainfall simulator under laboratory-controlled conditions.

2 METHODOLOGY

A realistic rainfall simulator (Naves et al., 2020), showed in Figure 1a, was used to analyze long-term clogging of a porous concrete pavement system. The permeable pavement (dps-system.com) consists of porous concrete slabs with joints, geotextile layer and geocells structure (Figure 1b and 1c).

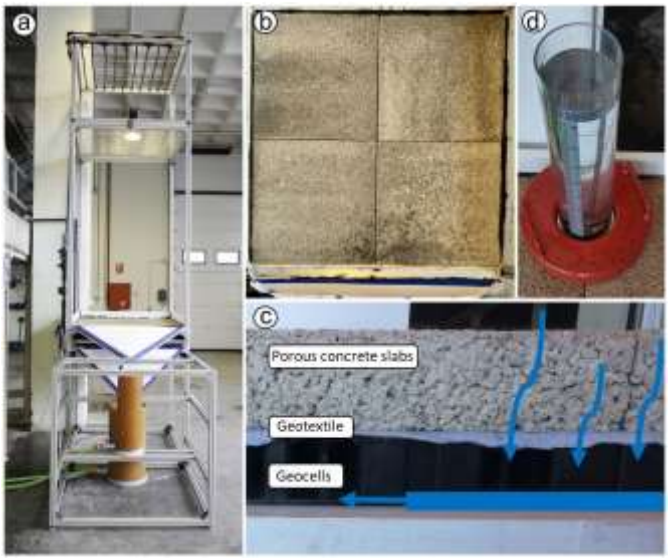

Figure 1. a) Rainfall simulator, b) pavement system top view and c) cross-section, and d) LCS permeameter.

ISBN: 978-90-824846-7-0

The porous pavement system was installed on an impervious surface with a 2% slope to drain the filtered water and potential runoff to two collection tanks. The runoff discharges from uniform rainfall of 80 mm/h and different durations were first used to perform a hydrological characterization of the pavement system, allowing comparison of the results with those obtained on an equivalent impervious surface. Then, the clogging process was evaluated using three different granulometries of road dust sediments, two of them uniform and the other realistic with ranges of 63-125 µm, 250-500 µm and 0-1000 µm respectively. Increasing sediment loads were distributed over the pavement and drained discharges were recorded to evaluate the effect of retained sediment on the permeable pavement's filtration capacity. The pavement condition was also measured using an LCS permeameter (Figure 1d) for a cumulative sediment load of 1 kg/m^2 in order to assess the influence of grain size on clogging process. In addition, the effect of higher sediment loads on filtered and runoff flows was analysed for sediment loads of 2 and 3 kg/m^2 using the realistic granulometry. Finally, a mass balance was also performed by vacuuming the different parts of the pavement system.

3 RESULTS AND CONCLUSIONS

The porous pavement system resulted in a water retention capacity of 5 L/m^2 without considering the additional capacity that geocells can provide. This was also observed in the results of the drained discharges since there was a significant delay and a reduction of the peak flow for simulated 80 mm/h rainfalls up to 15 minutes. In terms of clogging assessment, Figure 2 shows the permeameter results and demonstrate the importance of considering realistic sediment granulometries. While the finer sediments reduced permeability of the porous concrete slabs to 30% of the initial permeability, the coarser and realistic grain sizes clogged the slabs to a greater degree, resulting in permeability reductions of 85 and 92% for a cumulative sediment load of 1 kg/m^2.

The test with the realistic granulometry was continued up to 3 kg/m^2 cumulative load over the pavement surface. A reduction in filtered discharge was observed from a cumulative load of 1.5 kg/m^2. At this point, the slabs began to be unable to fully drain the 80 mm/h rainfall, producing a small amount of runoff. This can also be seen in Figure 2, where the slabs were completely clogged for 2 and 3 kg/m^2 of realistic grain size. The reduction in filtered discharge was occurred because the runoff produced by the two downwards slabs drained to the runoff collection tank since no joint was configured at the perimeter of the system. The remaining runoff generated was still drained by the joints, which were kept from clogging since sediments were retained by the porous concrete slabs. Future research will be oriented to further extend the knowledge of the process by optimizing the presented methodology and testing other typologies.

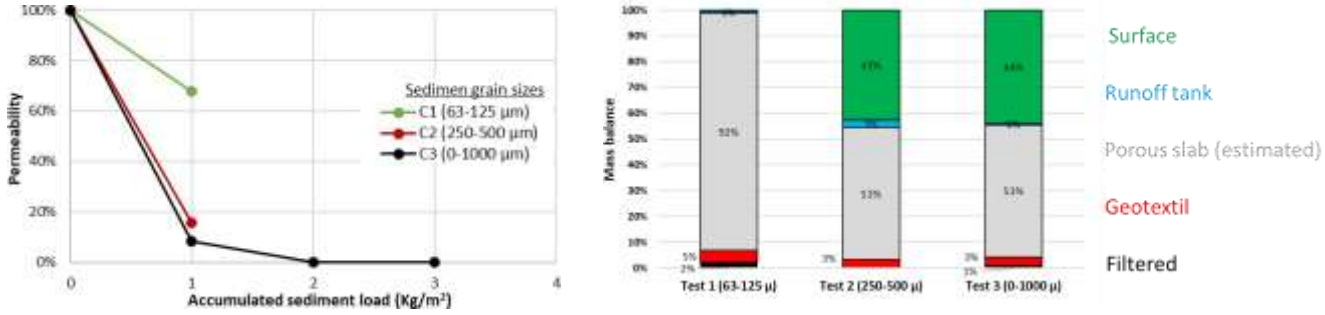

Figure 2. Mean permeability measures on the center of the concrete slabs for different grainsizes and sediment loads (left). Mass balances obtained at the end of the three tests (right).

ACKNOWLWDGES

This work was partially founded by companies HIDROSTANK, Pavimentos de Tudela (PVT) and ah asociados, by the Spanish Ministry of Science and Innovation (grant no. RTI2018-094217-B-C33), and by the EU under the Horizon 2020 program within a contract for Integrating Activities for Starting Communities (Ref. 101008626).

REFERENCES

Naves, J.; Anta, J.; Suárez, J.; and Puertas, J. (2020). Development and Calibration of a New Dripper-Based Rainfall Simulator for Large-Scale Sediment Wash-Off Studies. *Water*, 12, 152. https://doi.org/10.3390/w12010152

Proceedings of the 2nd IAHR
Young Professionals Congress
30 Nov-2 Dec. 2021

Flooding vulnerability and SuDS suitability in a heterogeneous catchment in Brazil

Luma Gabriela Alves[1], Maria Eduarda Veiga[1], Camila Silva[1] and Bervylly Santos[1]
[1] Federal University of Campina Grande, Campina Grande, Brazil,
lumagabriela2010@hotmail.com, eduardav83@gmail.com, cmlsantos91@gmail.com and bervylly.santos@gmail.com

ABSTRACT

The rapid urbanization of developing countries produces areas characterized by heterogeneous urban configurations (UCs). The UCs are usually not coincident with catchments. They are characterized by different urban patterns, and can determine the generation of runoff and decisions on stormwater control, including the design and implementation of Sustainable Urban Drainage Systems (SuDS). This study investigates the influence of different UCs on flooding vulnerability and SuDS suitability, in a small but heterogeneous catchment located in Brazil. We used hydrological modeling to understand the distribution of flooding spots throughout the catchment and simulate different SuDS scenarios, among which we considered permeable pavements, bioretention systems, infiltration trenches, and rainwater harvesting. The results demonstrate that the majority of flooding spots are located in a UC with high block density and impermeable paved streets. Likewise, we could identify appropriate SuDS for each UC, reinforcing the importance of such analysis in urban drainage projects.

Keywords: hydrological simulation; drainage systems; urban configurations.

1 INTRODUCTION

Urban drainage projects are subject to the particularities of each type of Urban Configuration. These projects have been designed and implemented for rapid drainage of stormwater, through massive engineering works of gray infrastructure, many times ignoring the urban configuration patterns. In this sense, an appropriate approach has emerged, the Sustainable Urban Drainage Systems (SuDS). However, SuDS design and implementation are complex, particularly in areas characterized by heterogeneous urban configurations, given the different patterns of surface permeability, vegetation cover, street network, and distribution of public and private open spaces. Such patterns affect surface runoff generation, inhabitants' quality of life, and decisions about the SuDS allocation (Palme et al. 2020). Thus, we propose that the evaluation of flooding vulnerability and SuDS suitability in the urban space must consider the different spatial configurations and their characteristics.

2 METHODOLOGY

The Ramadinha catchment (128 ha), located in the city of Campina Grande in the Brazilian northeast, is characterized by 4 urban configurations (UC):

- UC1: 80% of the roads are impervious, and 78% of the sidewalks are regular; the majority of block densities does not surpass 43%; there are few open public spaces and vacant lots.
- UC2: existence of precarious settlements, and a portion is composed of a Special Social Interest Zone, with high building density; 73% of the roads are unpaved, only 54% of sidewalks are regular, and there are no open public spaces.
- UC3: high building density, with 100% of paved roads and regular sidewalks; the majority of block density surpasses 60%; there are large permeable open spaces.
- UC4: low building density and many vacant lots; the majority of block density does not surpass 40%; there are 74% of unpaved roads and 62% of absent or irregular sidewalks.

Hydrological simulations were performed using the Storm Water Management Model (SWMM) for an extreme rainfall event. The parameterization of the current land use and occupation considered several physical characteristics of the catchment, such as area, slopes, flow directions, and surface imperviousness. For this simulation, we discretized the catchment according to the boundaries of each block, totaling 199 sub-catchments endowed with each parameter analyzed.

Three urban characteristics were taken into consideration to analyze how flooding vulnerability may be influenced by the catchment spatial heterogeneity: paved and unpaved roads, block density and permeable open spaces.

SuDS suitability varies according to these urban characteristics:

- Permeable pavements (PP): absent or irregular sidewalks, parking areas and unpaved roads where the slopes are smaller than 10% (County of LA, 2014);
- Bioretention systems (BS): open spaces with slopes under 20% (Woods Ballard, 2015);

ISBN: 978-90-824846-7-0

- Infiltration trenches (IT): side roads with slopes under 5% (Woods Ballard, 2015);
- Rainwater harvesting systems (RH): open spaces available.

We simulated SuDS on SWMM, modifying the subcatchment's parameters according to each SuDS specificity and using SUDS data from the literature (Woods Ballard, 2015; Rossman, 2008; Brown, 2009). Furthermore, SuDS were placed in the existing sub catchments working in parallel, each one "treating a different portion of the runoff generated from the fraction of the sub-catchment without SUDS measures" (Rossman, 2008).

3 RESULTS

The simulation results (Figure 1) have shown that the high density of the blocks are direct causes of the occurrence of flooding in their contribution outlets, due to the high degree of imperviousness. 33% of the flooded spots are outlets of blocks that have >60% density. The urban configuration that presented the majority of flooding hotspots in the outlet of high dense blocks was UC3.

Paved roads with traditional (impervious) pavement can aggravate flooding downstream, being a direct cause of the occurrence in the catchment, represented by the occurrence of 66% of the flooding spots located downstream of paved roads. The urban configuration that presented the majority of flooding spots in the outlet of paved roads was UC3.

The allocation of SuDS in the catchment demonstrated that PP are more suitable in UC2, due to the prevalence of unpaved streets; IT are more suitable for UC1 e UC2, according to the terrain slopes; BS for UC3 e UC4, due to the presence of large public and vacant spaces; and RH for UC2, since the density of houses would provide an appropriate application of the technique.

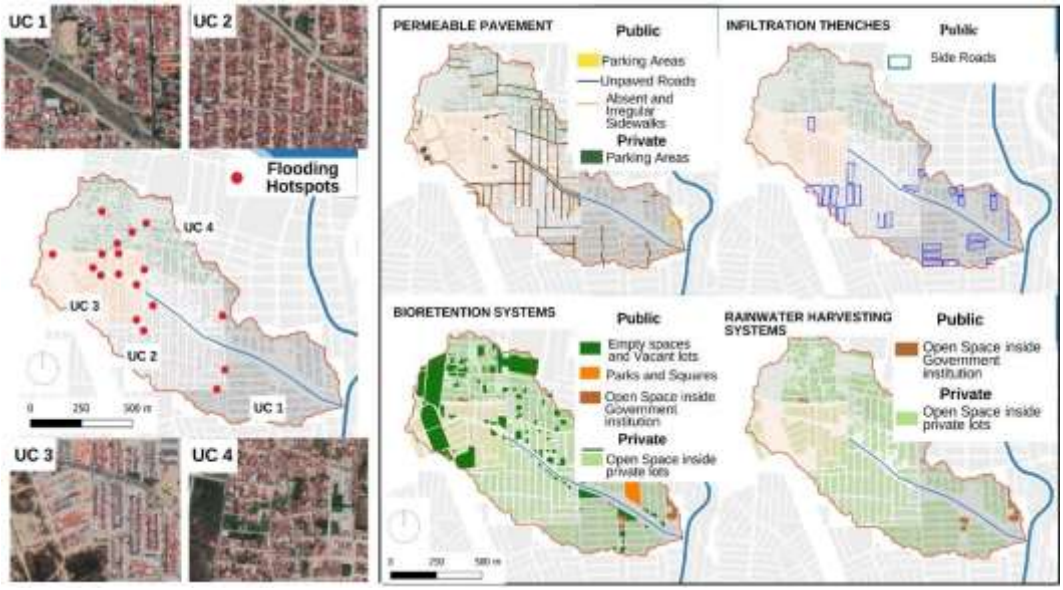

Figure 1. Flood spots and distribution of SuDS techniques

4 CONCLUSIONS

The study highlights the need to implement drainage projects considering the urban configurations, since they determine not only the generation of runoff but also the options and decisions for interventions. Furthermore, despite the complexity of designing SuDS in heterogeneous catchments, it is possible to incorporate appropriate SuDS techniques, considering such heterogeneities.

REFERENCES

Brown, S. A.; Stein, S. M.; Warner, J. C. (2009) Urban Drainage Design Manual. Hydraulic Engineering Circular 22, Second Edition. Federal Highway Administration Washington, D. C.

County of Los Angeles Department of Public Works. (2014). Low impact development standards manual. Los Angeles, USA.

Palme, M., Privitera, R., & La Rosa, D. (2020). The shading effects of Green Infrastructure in private residential areas: Building Performance Simulation to support urban planning. *Energy and Buildings*, 229.

Rossman, L. (2008). Storm Water Management Model User's Manual Version 5.0. U.S. Environmental Protection Agency. Cincinnati.

Woods-Ballard, B., Wilson, S., Udale-Clarke, H., Illman, S., Scott, T., Ashley, R., Kellagher, R. (2015). The SuDS manual. *CIRIA*. London, United Kingdom.

ISBN: 978-90-824846-7-0

Proceedings of the 2nd IAHR
Young Professionals Congress
30 Nov-2 Dec. 2021

Physically-guided neural network model for real-time prediction of urban flood

Lin Zhang[1], Huapeng Qin[1] and Junqi Mao [1]

[1] Peking University Shenzhen Graduate School, Shenzhen, China
zhanglin@stu.pku.edu.cn

ABSTRACT

Urban flood is an evitable threat for urban development. In this study, a new hybrid model is proposed to enhance real-time prediction of flooded points. Physical parameters have been constructed to provide theoretical constraints for the data-driven algorithm. Input factors were combined with the attention mechanism by weight, and the measured data of rainfall and water depth trained by neural network. A comprehensive evaluation framework has been built up as the optimization objective. The specific values of physical parameters and hyperparameters were automatically optimized by multi-objective genetic optimization algorithm. Guided by physical mechanism, the long short-term memory (LSTM) network combined with attention mechanism has been successfully applied to the real-time prediction in two different flooded points in Futian District of Shenzhen, China. The hybrid model used in this study effectively bridges the gap of data-driven model in physical explanation, parameter revision, as well as illustrates certain reliability.

Keywords: urban flood; real-time prediction; hybrid modeling; deep learning.

1 INTRODUCTION

Urban flood disasters occur frequently and are destructive especially in developing regions (Li et al., 2020). Urban flood forecast plays an essential role in flood control by providing effective information for decision makers and residents. The potential application value of deep learning methods in hydrology and water science only receives increasing focus in recent years(Shen et al., 2018). Compared with hydrologic and hydrodynamic models, data-driven models show universality and high computational efficiency, which match flood prediction timelines, but lack of physical interpretation. At present, for urban flood forecast research based on deep learning method, due to the difficulty in obtaining measured data, most studies adopt rainfall and water depth simulation data as learning samples. The time resolution of prediction could be low since only the maximum water depth prediction of a single flood event is carried out (Reichstein et al., 2019). Thus, this study combined physical mechanisms of urban flood generation with the deep learning method to build up a new hybrid model for the real-time prediction of flooded points.

2 MATERIALS AND METHODS

Combined with attention mechanism, the long short-term memory network (LSTM) (Hochreiter & Schmidhuber, 1997) guided by physical mechanism is proposed in this study as new hybrid model. Guided by physical mechanism, a rainfall input database was constructed with three processes as the start, accumulation and hydropeak. Three physical parameters have been built up, namely, rainfall start threshold, rainfall window size and centroid. LSTM with cellular unit and gated structure, was used to memorize historical data, and the weight of each physical process input factor was assigned by combining with attention mechanism. Multi-objective genetic optimization algorithm (NSGA Ⅱ) was applied to find the optimal combination of physical parameters and hyperparameters of neural network automatically (figure 1). The evaluation function system has been defined as the optimization objective:

Nash efficiency coefficient ($\boldsymbol{NSE}$)
$$NSE = 1 - \frac{\sum_{t=1}^{T}(y_o^t - y_m^t)^2}{\sum_{t=1}^{T}(y_o^t - y_o)^2} \quad (1)$$

Oscillation degree ($\boldsymbol{O_d}$)
$$O_d = \frac{f_m}{f_o} \quad (2)$$

Peak error ($\boldsymbol{E_p}$)
$$E_p = \frac{(y_{o,p} - y_{m,p})}{y_{o,p}} \times 100\% \quad (3)$$

Time error to peak ($\boldsymbol{E_t}$)
$$E_t = t_{o,p} - t_{m,p} \quad (4)$$

In the above formulas, $\boldsymbol{y}$ is the depth of water in decimeter dm, $\boldsymbol{f}$ is the number of shocks, $\boldsymbol{y_p}$ is the maximum depth of water, $\boldsymbol{t_p}$ is the time to reach the maximum depth of water in minutes, subscript $\boldsymbol{o}$ is the observed value,

ISBN: 978-90-824846-7-0

subscript m is the simulated value. The evaluation function takes into account not only the overall fitting trend and oscillation, but also the most concerned peak simulation in flood events to realize the overall optimization of the training process. Optimal parameters were substituted into hybrid model for fast prediction.

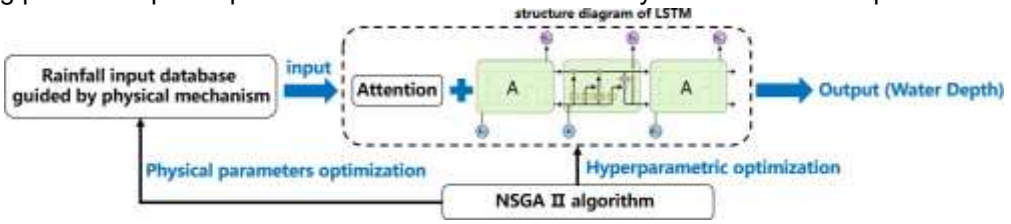

Figure 1 flowchart of algorithm combing physically guided LSTM network and attention mechanism

3 RESULTS AND DISCUSSION

The hybrid model was applied to the fast prediction of flooded points of intersection and overpass types in Futian District of Shenzhen, China. Each point provided four minute-level records of flood events as samples, which were divided into training set, validation set and testing set in the ratio of 12:3:5. The forecast result (table 1 & figure 2) shows that the new method properly predicted the occurrence time and value of the maximum water depth in the minute-level urban flood forecasts.

Table 1 Evaluation function value of urban flood forecast results

Flooded point's type	NSE	Od	Ep	Et（min）
Intersection	0.78	1.8	0.25	-11
Interchange	0.88	3.8	-0.56	-3

Figure 2 Training effect and forecast results of two types of flooded points

4 CONCLUSIONS

This study proposed a new hybrid model combing LSTM network guided by physical and attention mechanisms, which could effectively learn the relationship between rainfall and flood response in urban regions to automatically update and optimize parameters under data assimilation. The prediction results show that the hybrid model is reliable, and has been successfully applied to different types of flooded points and has universal adaptability. Therefore, the method could be applied to the real-time forecast of urban flood. The model is expected to be further interpreted according to the physical parameters after optimization.

REFERENCES

Hochreiter, S., & Schmidhuber, J. (1997). Long Short-Term Memory. *Neural Computation*, *9*(8), 1735–1780.

Li, L., Collins, A. M., Cheshmehzangi, A., & Chan, F. K. S. (2020). Identifying enablers and barriers to the implementation of the Green Infrastructure for urban flood management: A comparative analysis of the UK and China. *Urban Forestry & Urban Greening*, *54*, 126770.

Reichstein, M., Camps-Valls, G., Stevens, B., Jung, M., Denzler, J., Carvalhais, N., & Prabhat. (2019). Deep learning and process understanding for data-driven Earth system science. *Nature*, *566*(7743), 195–204.

Shen, C., Laloy, E., Elshorbagy, A., Albert, A., Bales, J., Chang, F. J., Ganguly, S., Hsu, K. L., Kifer, D., Fang, Z., Fang, K., Li, D., Li, X., & Tsai, W. P. (2018). HESS Opinions: Incubating deep-learning-powered hydrologic science advances as a community. *Hydrology and Earth System Sciences*, *22*(11), 5639–5656.

ISBN: 978-90-824846-7-0

IAHR YPN

Young Professionals Network

Hosted by
Spain Water and IWHR, China

IAHR AIRH

International Association for Hydro-Environment Engineering and Research

Hosted by
Spain Water and IWHR, China

Coastal & Maritime Hydraulics

Proceedings of the 2nd IAHR
Young Professionals Congress
30 Nov-2 Dec. 2021

Effect of falling circular dense jets on concentration changes in shallow stagnant ambient water

Hossein Azizi Nadian[1], Nima Shahni karamzadeh [1], Javad Ahadiyan [2] and Morteza Bakhtiari[1]

[1]Faculty of Marine Engineering, Khorramshahr University of Marine Science and Technology, Khuzestan, Iran
hossein.azizi@kmsu.ac.ir, n.karamzadeh@kmsu.ac.ir, bakhtiari@kmsu.ac.ir

[2]Faculty of Water Sciences Engineering, Shahid Chamran University of Ahvaz, Ahvaz, Iran
j.ahadiyan@scu.ac.ir

ABSTRACT

In this study to investigate laboratory the effect of falling circular dense jets on the concentration changes on the ambient water surface, series of experiments in 3 nozzle diameters, 2 discharges, constant fall height, and constant concentration jet, in a laboratory flume with a 3.2 m long, 0.9 m high, and 0.6 m wide was done in Shahid Chamran University of Ahvaz. The results of the experiments showed that increasing the densimetric Froude number has an effective effect on reducing the concentration of the water surface. So that increasing densimetric Froude number, reduce the wastewater concentration on the water surface.

Keywords: falling circular jet, dense jet, concentration surface water, densimetric Froude number, laboratory model

1 INTRODUCTION

The construction and use of desalination plants to compensate for the shortage of freshwater resources needed for drinking water and agriculture have grown significantly in recent years (Heidari et al., 2019). On the other hand, after purification and supply of freshwater, these factories discharge wastewater in the form of saltwater into the receiving environment (ambient water), which leads to destructive effects on the environment river and Habitat of living organisms. To reduce and control these destructive effects, using jet flow is an effective method (Abessi and Roberts, 2018). Depending on the distance from the nozzle outlet to the water surface, jets can be divided into three groups: submerged, surface, and falling. In the case of surface jets, (Heidari et al., 2019) pointed to the direct effect of the slope on the spread of the jet downstream of the point of impact to the bed surface. In the field of submerged jets, (Papakonstantis and Tsatsara, 2019) reported the correlation between the discharge angle and the dimensionless trajectory and the linear dependence of the dimensionless trajectory on the densimetric Froude number. With the review of the conducted researches, the shortage of studies on falling dense jets and their performance in the concentration changes in the ambient water level was felt. Therefore, in the present study, the effect of falling circular dense jet flow on concentration changes on the ambient water surface will be investigated in the laboratory.

2 MATERIALS AND METHODS

In order to plan the experiments, first, Parameters governing the present study were identified that shown in Eq.1.

( ) [1]

: initial velocity of the jet flow at the outlet of the discharge nozzle, : inner diameter of the nozzle discharging the jet flow, : outflow rate of the jet flow, : falling height of the jet flow, : specific mass of the jet flow, : absolute viscosity of the initial fluid of the jet flow, : acceleration of gravity, : depth of the ambient water, : specific mass of the ambient water, : Water surface concentration, : Initial concentration the jet flow and :time for jet flow to reach water surface. Then dimensional analysis was performed using the Buckingham π method to extract dimensionless parameters and Finally, Eq.2 introduces important dimensionless parameters of the present study.

(–) [2]

where is densimetric Froude number of the jet flow and — is concentration normalized (ratio of the Water surface concentration to Initial concentration the jet flow). Characteristics of experiments include diameters of 0.02 m, 0.016 m, and 0.013 m and flow rate of 0.0002 m3/s, 0.0001 m3/s, falling height, and constant initial concentration were selected as 0.36 m and 20 g / l, respectively. The experiments were performed on a model

located in the hydraulic laboratory of the Faculty of Water and Environmental Engineering, Shahid Chamran University of Ahvaz, Iran. Salinity and temperature were measured using a laboratory EC meter (HACH, ECO 20). Figure 1 shows flume and figure 2 shows an example of an experiment performed.

Figure 1. flume used in this study

Figure 2. Example of conducted experiment

3 RESULTS

Figure 3 shows the effect of densimetric Froude number on changes in the water surface concentration normalized of the ambient water.

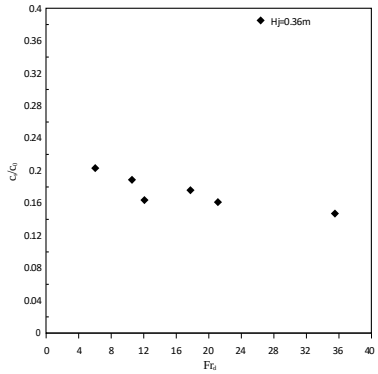

Figure 3. Effect of densimetric Froude number on concentration normalized

Examining Figure 3, the direct effect of the densimetric Froude number is observed on the trend of changes in the concentration normalized in the water surface. Because by increasing the densimetric Froude number of the jet flow, the turbulence in the water surface increases, and the mixing velocity and mixing power of the jet flow and ambient water increases, as a result of which the jet flow with ambient water dilutes more. For example in Figure 3, increasing the densimetric Froude number landings from 6.05 to 35.33, the dimensionless concentration normalized of jet flow decreases by 85.28%. Also, due to the fixed fall height, the time to reach the water level is also a function of the densimetric Froude number.

4 CONCLUSIONS

The present experimental study showed the effect of increasing the densimetric Froude number of the falling jet flow cause to reduce the wastewater concentration at the water surface and thus reduce their destructive effects on the environment of water bodies.

REFERENCES

Heidari, T., Karamzadeh, N. S., & Ahadiyan, J. (2019). An experimental investigation of convergent rectangular surface jets: spreading characteristics of horizontal flow over the bed of deep and stagnant ambient water. International Journal of Civil Engineering, 17(3), 443-456..

Abessi, O., & Roberts, P. J. (2018). Rosette diffusers for dense effluents in flowing currents. Journal of Hydraulic Engineering, 144(1), 06017024.

Papakonstantis, I. G., & Tsatsara, E. I. (2019). Mixing characteristics of inclined turbulent dense jets. Environmental Processes, 6(2), 525-541.

ISBN: 978-90-824846-7-0

Proceedings of the 2nd IAHR
Young Professionals Congress
30 Nov-2 Dec. 2021

Study of erosion control measure using an open source software at Bay of Bengal

Md.Tawhidur Rahaman[1], Dr.Umme Kulsum Navera[2]
[1,2] Bangladesh University of Engineering and Technology, Dhaka, Bangladesh,
e-mail: tawhidbuet066@gmail.com

ABSTRACT

The natural shape of Bangladesh coastal and marine areas is controlled by dynamic processes such as tides wave actions, strong winds, and it faces continuous land erosion and accretion. This study prioritizes the most vulnerable erosion-prone locations in Bangladesh, which is near the coastline of Cox-Bazar. There are a few measures have been taken by the local authority using geotubes, tetrapods, and concrete blocks. However, those systems do not stand appropriately. As a result, the area is still vulnerable due to coastal erosion. This study will analyze the nearshore hydrodynamics by a two-dimensional model named Delft3D. At the same time, we will incorporate Breakwater and Groins in this model to oversee the structure's performance to protect the shoreline due to erosion.

Keywords: Bay of Bengal model, Delft3d, breakwater, hydraulic structure

1 INTRODUCTION

Among the three coastal regions (a) The eastern zone, (b) The central zone, (c) Western zone in Bangladesh, the most significant location due to coastal erosion is at the eastern zone near the Cox Bazar coastline in Bay of Bengal. The cox-bazar is the longest uninterrupted sea beach which is facing continuous erosion due to high wave action and the marine drive road is under vulnerable situation. This road has enormous importance because of livelihood of the local people is mostly depending on sea fishing, salt cultivation, aquaculture, and tourism where all of these activities lies around that area. The socio-economic condition of the area solely depends on the connectivity of the road. Three locations named Harchery para, Himchari and Inani beach area is under continuous threat due to continuous erosion problem. Nearly one kilometer in length road are completely washed out near Kalatoli due to severe wave action during a storm surge event. Different structural intervention such as revetment and concrete blocks are the only protecting measures taken earlier along the shoreline which resulted insufficient to protect the area. A proper understanding of the nearshore hydrodynamics needs to analysis for any kind of protection measures. In this work, a coupled Delft3D-Flow Wave model has been used to simulate the nearshore hydrodynamics and different structures(Breakwater and Groin) incorporated as a structural measure for erosion control. The Delft3D-Flow Wave model is tested by different research works (Vlijm, 2011; James and Dykes, 2008) and also widely used in large coastal projects. The flow model is calibrated by observed water level data and wave model is calibrated by the observed wave data. To calibrate and validate the Bay of Bengal model we have used the GEBCO bathymetry data, global tidal data, historical wind and wave data, tidal constituents for the boundary condition and sediment data. After calibration and validation of the model Breakwater have been incorporated in the model for observing the wave energy reduction near the interventions for protection against the erosion. There is huge knowledge gap of structural interventional work in a calibrated model where a very few works have been done worldwide. Finally, this work can contribute to the decision maker for solving the erosion problem at Cox Bazar marine drive as well as it can be a valuable reference work for other erosion prone coastal part of Bangladesh.

ISBN: 978-90-824846-7-0

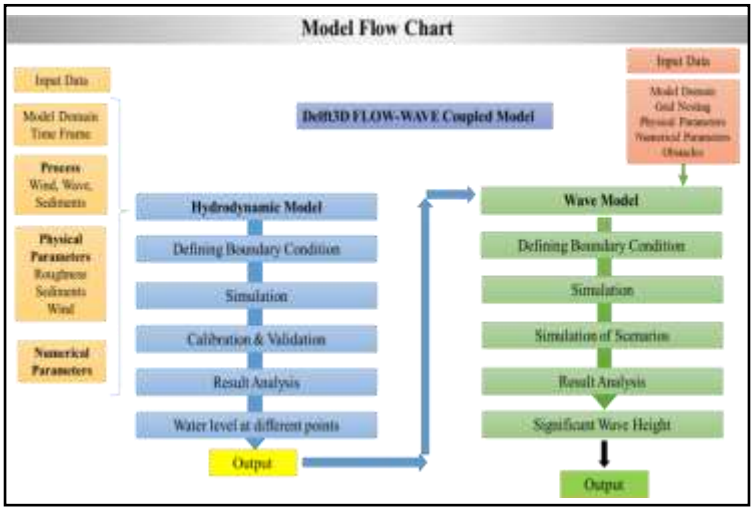

Figure 1: Delft3D FLOW-WAVE Coupled Model Flow chart

2 STUDY AREA

In our study of the Bay of Bengal model, the upstream boundary is from Vishakhapatnam (Latitude:18.904° Longitude:93.865°) in Odisha coast in India to Gwa Bay (Latitude:17.686° Longitude: 83.299°) near sittwe in Myanmar, where the downstream boundary is at Barurua (Latitude:23.46°; Longitude : 89.48°) in the confluence of lower Jamuna river and Padma river. The Breakwater is incorporated at Latitude: 21°24'13 N; Longitude : 91°59'28 E near the Hatcharipara, which is continuously eroded by high wave action. During a storm surge event, one kilometer of marine drive road was totally washed out near the kolatoli beach area.

3 CONCLUSIONS

It is observed from the analysis that to protect site 1, which is 1.7 km long with series of Breakwater, the wave height reduction rate is 27 % - 53 %, and the wave energy reduction rate is 47% -78%. It shows good results to reduce wave height and energy at those interventions. The further analysis illustrates a mixed result, where two of the Breakwater shows continuous erosion, and one Breakwater shows continuous sedimentation in the vicinity of the structure. To protect the site1 with series of Breakwater is not a feasible option because it requires additional maintenance work with sand nourishment to make the beach stable. One the other hand, with series of Groin, the wave height reduction rate is 9 % - 76 % and wave energy reduction rate is 17% -91%, which also shows low to moderate reduction rate of the wave height and energy. The sediment analysis depicts positive results, where six Groins shows continuous sedimentation, and one shows erosion. To protect site 1 with series of Groin is a good option because six groins among seven show positive results to accumulate sediment along the shoreline to make the beach stable. This study is one of the first in Bangladesh to examine the nearshore structural intervention with Breakwater and Groin and can be used as a reference for field implementation or further research work.

REFERENCES

Vlijm, R. J. (2011), Process-based modelling of morphological response to Submerged breakwaters, MSc Thesis, Delft University of Technology, The Netherlands.

Hossain, D.(2012), Application of 2D Mathematical Model for Verification of Water Velocity at Coastal Area of Bangladesh, MSc Thesis, Department of Water Resource Engineering, BUET.

Komol, K. M. (2011), Numerical Simulation of Tidal Level at Selected Coastal Area of Bangladesh, MSc Thesis, Department of Water Resource Engineering, BUET, 2011

ISBN: 978-90-824846-7-0

Proceedings of the 2nd IAHR
Young Professionals Congress
30 Nov-2 Dec. 2021

Preliminary design of an Innovative Floating Breakwater/WEC

Sara Russo [1,2], Claudio Lugni [3], Pasquale Contestabile[1,2] and Diego Vicinanza [1,2,3]

[1] University of Campania "Luigi Vanvitelli", Via Roma 29, 81031 Aversa, Italy
e-mail: sara.russo@unicampania.it; pasquale.contestabile@unicampania.it; diego.vicinanza@unicampania.it
[2] Inter-University National Consortium for Marine Sciences (CoNISMa), P.zzale Flaminio, 00144, Rome, Italy
[3] CNR-INM, Institute of Marine Engineering, Via di Vallerano 139, 00128 Roma, Italy
e-mail: claudio.lugni@cnr.it

ABSTRACT
A recent concept of offshore energy archipelago in the Mediterranean Sea has led to the definition of an innovative floating breakwater, with the aim of creating a protected area where new kind of blue energy devices can be installed. However, the possibility of implementing an alternative use of this module as wave energy converter represents an extremely challenging task. The dual functioning is achieved by properly varying the draft of the module, depending on the sea states. In extreme ones, the module should strictly work as breakwater, being almost fully submerged and dissipating the incoming waves; in mild sea states instead, where it should work as wave energy converter, larger device motions are required, resulting in lower drafts. In this study, through the linear potential flow theory, the feasibility of its dual use is investigated. Results allow the identification of the optimal draft values satisfying the two different functionalities.

Keywords: hybrid floating breakwater; Wave Energy Converter; linear potential flow theory; draft-varying device.

1 INTRODUCTION

The European Union has highlighted the importance of offshore marine renewable energies in achieving climate neutrality by 2050 (European Commission, 2020). In this context, a new concept of energy HUB specifically designed for Mediterranean Sea has been proposed by the Institute of Marine Engineering of the National Research Council of Italy (INM-CNR). The concept refers to an energetic archipelago where various devices for exploiting marine renewable energy can coexist in a modular way. The archipelago is spatially defined in a closed circle constituted by a line of floating breakwater modules. This protected sea area allows the installation of blue energy devices, while outside, floating wind turbines are possibly positioned. The whole produced energy can be stored and can support the development of new productive activities. The present work focuses on a preliminary numerical study on the floating breakwater/WEC.
Currently, these structures are categorized in function of the Wave Energy Converter (WEC) type system that is combined with the breakwater (Zhao et al.,2019). Often the coupling between the double functioning has been achieved by attaching WECs at the weather side of floating breakwaters (Martinelli et al., 2016). However, although these studies demonstrated the possibility for these devices to function as WECs, their main purpose remained the coastal protection. In this study instead, the module alternatively works as one or another function, depending on its draft.

2 MATERIALS AND METHODS

The preliminary concept was designed as a truncated lower cylinder, connected to an upper trapezoid. The double functioning of the device was strictly dependent from the draft, that increased passing from WEC to breakwater usage (Figure 1). Four drafts were given to the module to simulate its behaviour.

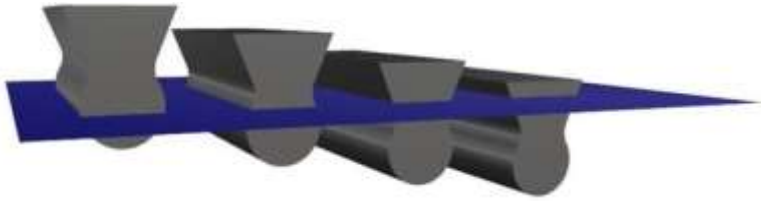

Figure 1.Sketch of simulated drafts. The first two refer to a WEC functioning, third and fourth simulate a breakwater behavior.

Usually, the first stage in modelling wave/structure interaction of a WEC, is carried out in frequency domain (Penalba et al.,2017), by solving the equation of motion [1], where M and A(ω) are respectively the structural

mass and the added mass matrixes, B(ω) is the radiation damping coefficient matrix, K is the restoring coefficient matrix. F(ω) is the vector of the excitation forces, ξ(ω) represents the vector of the frequency domain displacements. Dividing the module of ξ(ω) by the wave amplitude A, allows the definition of the Response Amplitude Operator (RAO) for each degree of freedom. In this study, an in-house Boundary Element Method numerical solver, based on the solution of the linear potential flow model was used.

$$[-\omega^2 (M + A(\omega)) + iB(\omega) + K] \cdot \xi(\omega) = F(\omega) \qquad [1]$$

3 RESULTS AND DISCUSSION

The RAOs of the module in heave and roll motions have been derived for the four values of draft, and their shapes compared to representative sea states of the Mediterranean Sea (Figure 2). Concerning the WEC behavior, the maximum energy is harvested when the floating module motions are in resonance with the waves. However, the choice of the prevalent motion to be exploited will depend on the power-take-off (PTO) system. In extreme sea states instead, the module works as breakwater, absorbing the incoming waves and protecting the devices installed in the archipelago. For this aim, when the module is almost fully submerged, the significant decreasing in the heave peak intensity presupposes a duality heave motion-wave energy flux absorption.

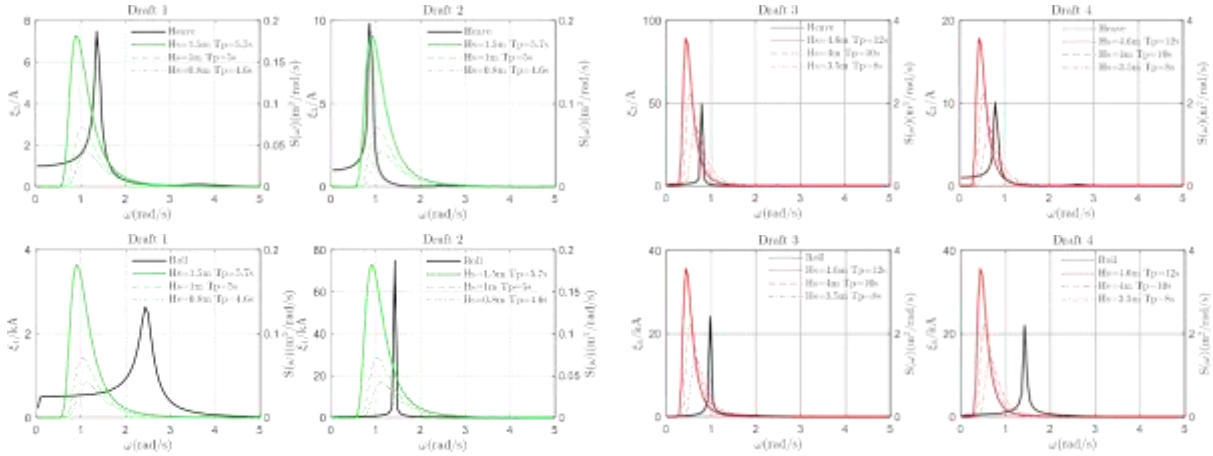

Figure 2. Heave and Roll RAOs of the module compared to mild sea load cases (left-side, WEC behavior) and extreme ones (right-side, Breakwater behavior).

4 CONCLUSION

The numerical simulation presented in this study showed the feasibility of an innovative module that, depending on its draft can behave as WEC or as breakwater. However, several limitations need to be fixed, such as the neglection of both mooring lines and PTO system that will affect the interaction between the structure and the waves. Moreover, ongoing laboratory tests on the proposed module will provide detailed validation of numerical observations, allowing to evaluate the functioning of multiple modules, considering their mutual influence, needs to be carried out.

REFERENCES

European Commission (2020). An EU Strategy to harness the potential of offshore renewable energy for a climate neutral future.

Martinelli, L., Ruol, P., & Favaretto, C. (2016, June). Hybrid structure combining a wave energy converter and a floating breakwater. In *The 26th International Ocean and Polar Engineering Conference*. OnePetro.

Penalba, M., Kelly, T., & Ringwood, J. (2017). Using NEMOH for modelling wave energy converters: A comparative study with WAMIT.

Zhao, X. L., Ning, D. Z., Zou, Q. P., Qiao, D. S., & Cai, S. Q. (2019). Hybrid floating breakwater-WEC system: A review. *Ocean engineering*, *186*, 106126.

ISBN: 978-90-824846-7-0

Proceedings of the 2nd IAHR
Young Professionals Congress
30 Nov-2 Dec. 2021

River-sea system connectivity: analysis of sediment dispersal in the northern Adriatic Sea

Rossella Belloni [1], Claudia Adduce [2], Federico Falcini [3], Vittorio Ernesto Brando [4], Giovanni La Forgia [5]
[1,2] Roma Tre University, Rome, Italy,
e-mail: rossella.belloni@uniroma3.it, claudia.adduce@uniroma3.it
[1,2,3,4] National Research Council – Research Institute of Marine Sciences (CNR-ISMAR), Rome, Italy,
e-mail: federico.falcini@cnr.it, vittorio.brando@cnr.it
[5]Università degli Studi di Cassino e del Lazio Meridionale, Cassino (FR), Italy,
e-mail: g.laforgia@unicas.it

ABSTRACT

Connectivity describes the efficiency of material transfer between system components, the definition of which varies from one discipline to another. Specifically, in this study, a spatio-temporal analysis of river plume dispersal in the area of the Po River prodelta (northern Adriatic Sea, Italy) was performed to investigate the degree of sediment connectivity of the river-sea system. The analysis was carried out coupling high-resolution multispectral satellite data from the Copernicous Sentinel-2 mission, with in situ measurements of the main environmental forcings affecting sediment dynamics in the study area. Although with some intrinsic limitations, the analysis showed the good potential of high-resolution remotely sensed data to capture the main features of sediment dynamics, and therefore their relevance for a better understanding of the processes that govern sediment connectivity in coastal areas.

Keywords: Remote sensing, sediment connectivity, river plumes, coastal geomorphology

1 INTRODUCTION

Connectivity describes the efficiency of materials transfer between the components of a system (Wohl et al., 2019). Definition of components varies between disciplines and in relation to the material under consideration. In fluvial and coastal geomorphology, connectivity essentially is a measure of how efficiently and undisturbed is the transport of sediment through the river-sea system. A river-sea system includes the whole river basin and the surrounding coastal area which extension is determine by the extent of the riverine influence in the receiving waters (river plume). In recent years, many techniques have been developed to quantify sediment connectivity (Najafi et al., 2021) however, because of the challenges involved in monitoring coastal sediment dynamics, so far there are limited applications in coastal environments despite the huge impact of sediment connectivity on the ecology and morphology of coastal areas. The main objective of this work was therefore to investigate the potential of high-resolution remote sensing data from optical sensors to investigate the degree of sediment connectivity of a river-sea system in its final section (coastal area), using as a case study the area of the Po River prodelta in Italy.

2 MATERIALS AND METHODS

Level-1C Sentinel-2 images were collected and processed for the study area in the period June 2015 – April 2018 selecting those without any source of disturbance (clouds and sun glint effect) and showing a clear visible river plume. The images selected were later processed using a generic processor developed for atmospheric correction and processing for coastal and inland water applications, ACOLITE (Vanhellemont and Ruddick, 2016). The processor can also output several parameters derived from water reflectance. In this study, it was used to obtain ten-meters resolution turbidity maps (Dogliotti et al., 2015), a key parameter both in water quality and sediment transport monitoring of coastal and inland waters, in order to investigate the spatio-temporal variability of river plume dispersal in the study area (Falcini et al., 2012; Brando et al., 2015; Braga et al., 2017). Turbidity maps were then coupled with in situ measurements of the main environmental forcings affecting sediment transport in the study area (wind and river discharge) to evaluate their role in affecting river plume morphologies.

ISBN: 978-90-824846-7-0

3 RESULTS AND CONCLUSIONS

The analysis of satellite-derived turbidity maps along with the in situ hydro-meteorological data showed plume patterns with a moderate spatio-temporal variability and confirmed the major role of wind and river discharge in affecting their overall structure, and therefore sediment connectivity (Figure 1). Long-lasting northerly winds tend to compress the plume against the coast promoting the sediment supply on the surrounding coastal areas, whereas the southerly winds determine a sediment transport towards the open sea. The highest river discharge events seem instead to limit the wind influence.

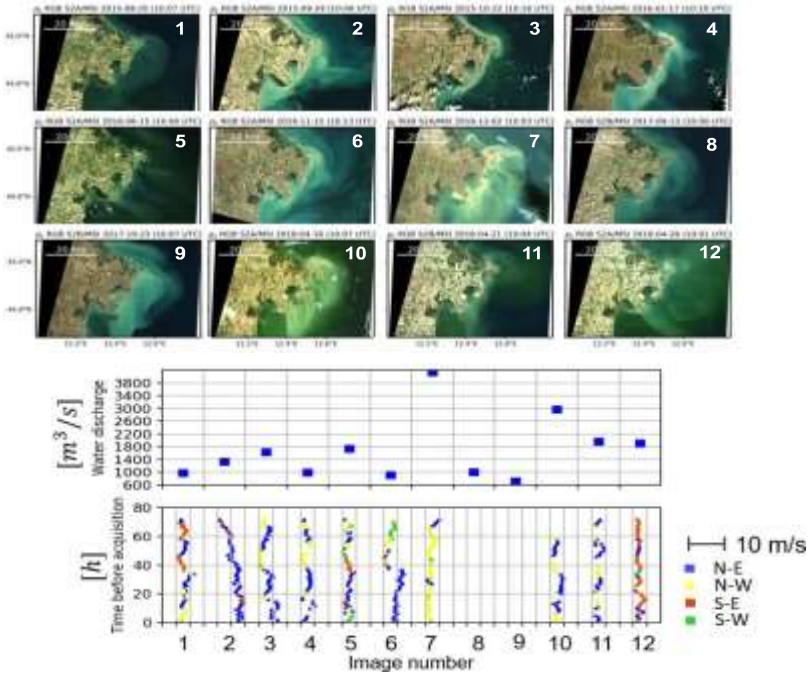

Figure 1. True colour Po river plume images with river discharge and hourly wind data

REFERENCES

Braga, F., Zaggia, L., Bellafiore, D., Bresciani, M., Giardino, C., Lorenzetti, G., ... & Brando, V. E. (2017). Mapping turbidity patterns in the Po river prodelta using multi-temporal Landsat 8 imagery. *Estuarine, Coastal and Shelf Science, 198*, 555-567.

Brando, V. E., Braga, F., Zaggia, L., Giardino, C., Bresciani, M., Matta, E., ... & Carniel, S. (2015). High-resolution satellite turbidity and sea surface temperature observations of river plume interactions during a significant flood event. *Ocean Science, 11*(6), 909-920.

Dogliotti, A. I., Ruddick, K. G., Nechad, B., Doxaran, D., & Knaeps, E. (2015). A single algorithm to retrieve turbidity from remotely-sensed data in all coastal and estuarine waters. *Remote Sensing of Environment, 156*, 157-168.

Falcini, F., Khan, N. S., Macelloni, L., Horton, B. P., Lutken, C. B., McKee, K. L., ... & Jerolmack, D. J. (2012). Linking the historic 2011 Mississippi River flood to coastal wetland sedimentation. Nature Geoscience, 5(11), 803-807.

Najafi, S., Dragovich, D., Heckmann, T., & Sadeghi, S. H. (2021). Sediment connectivity concepts and approaches. *Catena, 196*, 104880.

Vanhellemont, Q., & Ruddick, K. (2016, May). Acolite for Sentinel-2: Aquatic applications of MSI imagery. *In Proceedings of the 2016 ESA Living Planet Symposium, Prague, Czech Republic* (pp. 9-13).

Wohl, E., Brierley, G., Cadol, D., Coulthard, T. J., Covino, T., Fryirs, K. A., ... & Sklar, L. S. (2019). Connectivity as an emergent property of geomorphic systems. *Earth Surface Processes and Landforms, 44*(1), 4-26.

ISBN: 978-90-824846-7-0

Proceedings of the 2nd IAHR
Young Professionals Congress
30 Nov-2 Dec. 2021

Analysis of ship-induced waves in the near-bank area of a large river via LSPIV

Gábor Fleit [*1,2] and Sándor Baranya [3]

[1] MTA-BME Water Management Research Group, Eötvös Loránd Research Network, Budapest, Hungary
[2] Budapest University of Technology and Economics, Budapest, Hungary
[*] Correspondence: fleit.gabor@emk.bme.hu

ABSTRACT

Large-scale particle image velocimetry (LSPIV) has become a popular tool in the hydraulic engineering community in the last decades due to its cheapness and straightforward applicability. In this study, an application of LSPIV is presented for the analysis of ship-induced waves in the near-bank area of a large river. This shallow area of rivers is of high importance from the aspects of sedimentology and ecology as well. However, conventional measurement techniques are usually not applicable due to shallow water depths and temporary wetting/drying during wave events. The consequent lack of ground truth data for the verification of the LSPIV results is overcome with results from a previously validated, high-resolution numerical wave model.

Keywords: ship waves, large river, LSPIV, CFD modeling, surface velocities

1 INTRODUCTION

The rapid development of imaging tools and computational capacities in the past decade implied the rapid development of image-based measurement and data acquisition techniques in a wide range of industrial and scientific applications. From the aspects of the hydraulic and mechanical engineering community, one of the most important tools arising from these newfound disciplines was particle image velocimetry (PIV). The adaptation of such practical image-based techniques to field conditions is usually much desired by hydraulic engineers, as they tend to offer fast, cheap, non-intrusive measurements. Since its first applications in the 1990s, large-scale PIV (LSPIV) has been successfully used in various hydraulic engineering tasks (e.g., Muste et al. (2008)).

Although many examples can be found for the detailed PIV-based analysis of various types of waves, these are usually performed in laboratory conditions, with conventional PIV setups. These setups are complex and costly systems, consisting of cameras, lasers, lenses, synchronizers, etc. The direct application of PIV in field environments is possible, however, it is still expensive, and the complex instrumentation makes its use cumbersome (e.g., Cameron et al., 2013; Nimmo Smith et al., 2002). In this study, LSPIV is used to quantify the near-bank hydrodynamic impacts of ship-induced waves in a large river based on regular video recordings. Velocities and the related shear stresses in these shallow areas are of high importance from sedimentological and ecological aspects as well.

2 METHODS

Field measurements of ship-induced wave were performed in a Hungarian section of the Danube River. Acoustic Doppler velocimeters (ADV) and a pressure gauge were used to directly investigate the hydrodynamic impacts, while complementary video recordings were also taken of the near-bank area. These videos were analyzed via LSPIV, while the pressure and ADV data was used to parametrize and verify a high-resolution CFD model.

A general use, in-house PIV code (Fleit and Baranya, 2019) was used for the quantification of wave related surface velocities. After the necessary pre-processing steps (image enhancement, orthorectification, etc.) the LSPIV analysis provided the distribution of 2D horizontal velocity vectors with a temporal resolution of 30 Hz. Considering that no measurement tools are applicable in the direct proximity of the bank due to very shallow water depths and temporary wetting-drying, image velocimetry results were compared with results obtained with the CFD model REEF3D (Bihs et al., 2016). The numerical model was previously built up and validated against own field data (GPS surveying, pressure and velocity measurements) from the near-bank area and showed reliable and consistent performance (see e.g., Fleit et al. (2021)).

ISBN: 978-90-824846-7-0

3 RESULTS

The tracer for the PIV algorithm was naturally provided by the breaking waves in a form of foam, patches of resuspended sediments and turbulent boils. LSPIV manages to capture surface wave velocities in the near-bank area both during wave runup and retreat (Figure 1a) – the results are considered plausible. In order to compare the calculated velocities with the numerical model results, the same wave event was simulated based on the field pressure data. Surface velocities were extracted from both the midline (parallel to *x*-axis) of the LSPIV and CFD results and stacked up over time, resulting in space-time velocity distributions (Figure 1b). Considering the complexity of the hydrodynamics and the necessary simplifications made during the modeling, the agreement is considered promising.

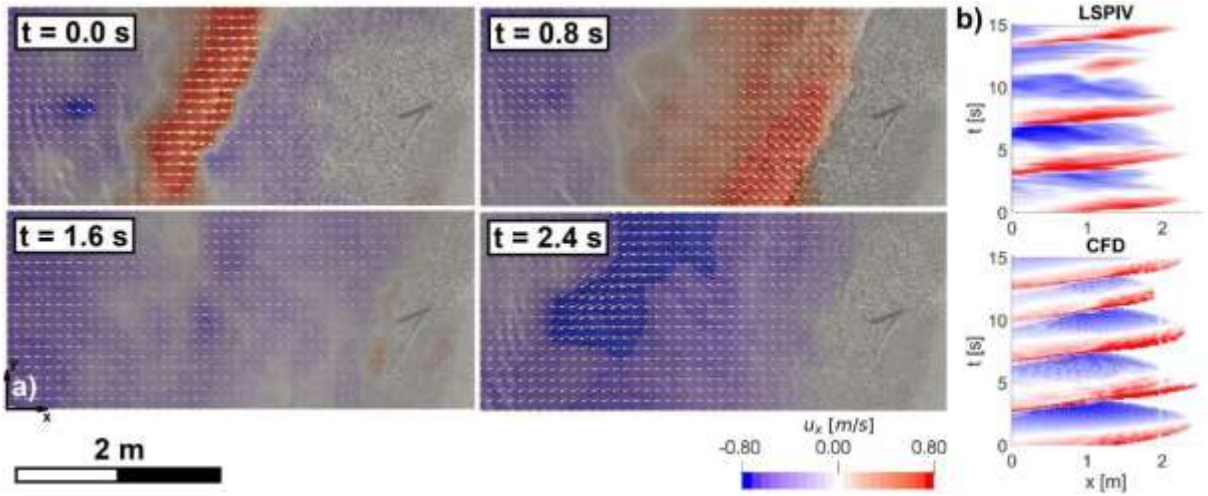

Figure 1. a) LSPIV results for a wave runup to the riverbank colored by the cross-shore velocity component (u_x), velocity vectors are also presented. b) Comparison of the space-time distribution of u_x calculated with CFD and LSPIV.

4 CONCLUSIONS

An in-house PIV code was used to quantify surface wave velocities in the littoral zone. As conventional velocity measurements techniques (e.g., acoustic Doppler velocimetry) are no longer applicable in this area due to temporary wetting/drying and shallow water depths, the results wish to fill a knowledge gap.

A previously validated CFD model was successfully used to verify the image velocimetry results. While the results offer a promising perspective, the question is not considered resolved. The derivation of surface velocities is of great importance, the complexity and non-linearity of near-bank wave runup and breaking calls complementary image-based methods, such as stereoscopic imagery.

ACKNOWLEDGEMENTS

The first author acknowledges the support of the ÚNKP-21-4 New National Excellence Programs of the Ministry of Innovation and Technology, respectively. The second author acknowledges the support of the Bolyai János research fellowship of the Hungarian Academy of Sciences.

REFERENCES

Bihs, H., Kamath, A., Chella, M.A., Aggarwal, A. and Arntsen, Ø.A. (2016) A New Level Set Numerical Wave Tank with Improved Density Interpolation of Complex Wave Hydrodynamics. *Computers and Fluids*, 140, 191–208.

Cameron, S.M., Nikora, V.I., Alayrak, I., Miler, O., Stewert, M., Siniscalchi, F. (2013) Interactions between aquatic plants and turbulent flow: a field study using stereoscopic PIV. *Journal of Fluid Mechanics*, 743:345–372.

Fleit, G. and Baranya, S. (2019) An improved particle image velocimetry method for efficient flow analyses. *Flow Measurement and Instrumentation*, 69:101619, 9p.

Fleit, G., Hauer, C. and Baranya S. (2021) A numerical modeling-based predictive methodology for the assessment of the impacts of ship waves on YOY fish. *River Research and Applications*, 37:373–386.

Muste, M., Fujita, I. and Hauet, A. (2008) Large-scale particle image velocimetry for measurements in riverine environments. *Water Resources Research*, 46(4)1:14.

Nimmo Smith, W.A., Atsavapranee, P., Katz, J., and Osborn, T.R. (2002) PIV measurements in the bottom boundary layer of the coastal ocean. *Experiments in Fluids*, 33(6):962–971.

Proceedings of the 2nd IAHR
Young Professionals Congress
30 Nov-2 Dec. 2021

Scour assessment on detached rubble-mound breakwaters using advanced measurement techniques

Francisco Pinto, Paulo Rosa-Santos and José Victor Ramos
Faculty of Engineering of the University of Porto (FEUP), Porto, Portugal
Interdisciplinary Centre of Marine and Environmental Research (CIIMAR), Porto, Portugal
Hydraulic and Water Resources Institute (IHRH), Porto, Portugal.
ftaveirapinto@fe.up.pt, pjrsantos@fe.up.pt, jvr@fe.up.pt

ABSTRACT

This study presents the preliminary developments of different techniques for scour hole analysis. A physical model was built on the Hydraulics Laboratory of the Hydraulics, Water Resources and Environment Division of the Faculty of Engineering of the University of Porto (FEUP) representing a case study located in Esposende, on the northern Portuguese coastal stretch. This study aims to explore the capabilities of the Laser Scanner equipment to characterize scour nearby rubble-mound breakwaters, namely in terms of its geometry and shape. Through multiple post processing software, the scour depth was quantified and newer parameters are proposed to better characterize scour phenomena in future works.

Keywords: laser scanner; physical model; coastal erosion, CloudCompare.

1 INTRODUCTION

Given the present significant knowledge gap on detailed scour characterization at rubble-mound structures, high resolution Laser Scanner surveys are being used to obtain new insights (Sumer et al., 2001; Den Bieman et al., 2019). The present work uses as case study the sandspit of Ofir, along with the ocean-facing beach-dune system and adjacent Cávado estuary, which compose the coastal protection system of Esposende city, in Portugal. A mobile bed, 3D physical model of the area was built on a geometric scale of 1/100, which includes all existing rubble-mound structures, such as the longitudinal dike and the northern groin (Figure 1). The bathymetry was realized based on the Navionics database and survey campaigns carried out over the navigation channel. Two scenarios were considered: the present situation and the one resulting from the construction of new structures to control local sediment dynamics and improve the resilience of the fragile sandspit to extreme maritime conditions. That intervention includes a longitudinal rubble-mound dike built along the inner side of the sandspit up to the Cávado river mouth and two detached breakwaters: a central one (with blue rock, Figure 1a) and another one located to its left, designated as breakwater 2 (with white rock). This study focused only on the morphological changes near the second detached breakwater proposed to protect the Ofir sandspit.

Figure 1. (a) Illustration of the physical model versus (b) the real case study.

ISBN: 978-90-824846-7-0

2 SCOUR HOLE CHARACTERIZATION

During the physical model experiments, different hydrodynamic conditions were considered, namely: five water levels, eight significant wave heights, five wave periods and three river discharges. In this way, the proposed coastal protection structures were exposed to approximately 30 000 waves. All scans were processed through the software SCENE (SCENE, 2020) and afterwards using the *CloudCompare* and *Matlab software*. Given the complexity of scour assessment, this study quantified the evolution of the scour hole near the right head of the breakwater 2 (Figure 2) and proposes parameters that could be used in the characterization of scour. In addition, Figure 2 presents the cross section, accompanied by the respective spatial location of the cross section, to provide a better interpretation of the morphologic change. This figure shows the evolution of the scour depth as a function of the number of waves. Thus, it is possible to analyze the evolution and location of the maximum depth of the scour hole.

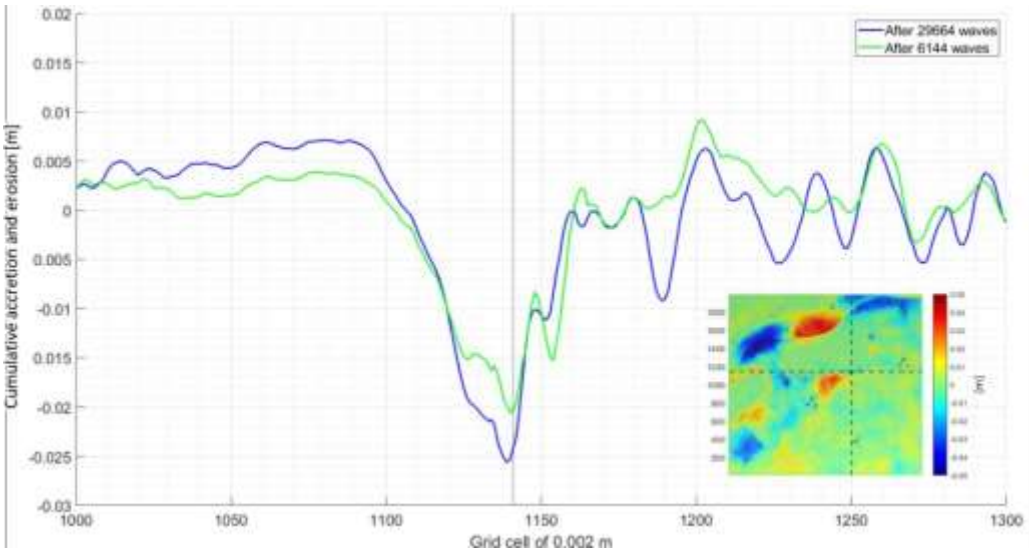

Figure 2. Scour depth analysis near the right head of the second detached breakwater.

At present scour holes still remain with a rather scarce characterization in the literature. Thus, it is important to monitor them in future research physical models according to the following geometrical and shape parameters. The parameters are the following: the extension of the scour hole according to the orthogonal and parallel direction to the wave propagation, its area, volume and the inclination of both the rear and front slopes of the scour hole according to the cross-section along the orthogonal and parallel directions to the wave propagation.

3 CONCLUSIONS

This study has allowed the application of several tools capable of characterizing the scour holes as a result of a detailed analysis of laser scanner measurements, using different software packages with very detailed point cloud processing capabilities. This work became quite extensive as it was divided into 4 phases: the practical phase where the scans were carried out, the phase of processing the scans into files compatible with the CloudCompare software, the phase of filtering and exporting the data into matrices and, finally, the phase of creating maps and graphs which allowed quantifying some scour holes observed in one of the structures implemented in the model.

REFERENCES

SCENE (2020). FARO Focus Laser Scanners – Training Workbook. USA.

Den Bieman, Joost P., van Gent, Marcel R.A., HoonHout, Bas M. (2019). Physical model of scour at the toe of rock armoured structures. Coastal Engineering, 154, 0378-3839.

Sumer, B. Mutlu; Torum, Alf; Whitehouse, Richard J.S. (2001). Scour around coastal structures: a summary of recent research. Coastal Engineering. 44: 153-190. ISSN 0378-3839/01.

ISBN: 978-90-824846-7-0

Proceedings of the 2nd IAHR
Young Professionals Congress
30 Nov-2 Dec. 2021

Performance analysis of an U-OWC device

Lilia Carlo[1], Claudio Iuppa [2] and Carla Faraci [3]

[1,2,3] University of Messina, Messina, Italy,
lcarlo@unime.it

ABSTRACT

This document aims at studying the interaction of a wave flow field with an U-OWC type marine energy conversion device. To this end an experimental campaign was carried out, in which the physical model of the U-OWC was forced to the action of regular waves within a flume. The tests were carried out varying the geometric characteristics of the caisson and the hydrodynamic parameters of the wave, acquiring pressure and velocity measurements in the air chamber and oscillation measurements of the free surface along the channel and inside the U-OWC.
The experimental approach aims to perform analysis of both reflection and energy efficiency.

Keywords: reflection; wave energy, U-OWC device.

1 INTRODUCTION

The continuous growth in the consumption of fossil fuels have led science to a greater interest in renewable energies. In this framework, in recent times, one of the leading sectors is marine energy. Among the energy conversion devices called WEC (Wave Energy Converter), the most commonly used are the OWC (Oscillating water column) devices or U-OWC, which add a U duct to the original OWC. The choice of these devices to be integrated in port structures must be based on careful evaluations regarding the energy aspects; as well the structural stability and the reflection phenomenon must be taken into account, especially for those devices that are inserted in structures near the coast.
In the literature there are several studies on the geometric optimization of OWC systems for energy production (Simonetti et al., 2017, Elhanafi et al., 2017), while fewer are those carried out on U-OWCs. In fact, the latter devices have been developed over the last two decades and the first prototypes were built only a few years ago (for example the Port of Civitavecchia started in 2017), so there is still a lot of uncertainty on how to maximize energy efficiency in order to be at the same time economically convenient. The present study addresses some of the mentioned issues.

2 ANALYSIS OF RESULTS

2.1 Methodology

The study of the interaction between the wave flow and an U-OWC was performed within the flume of the Laboratory of Hydraulics at the University of Messina. The U-OWC caisson, reproduced in 1:30 scale with dimensions of 82.0 x 40.0 x 47.0 cm, was made with plexiglass plates. The U-OWC was subject to the action of regular waves in different geometric configurations obtained by progressively changing the position of the front wall of the caisson. The caisson has a 2.5 cm diameter orifice in the pneumatic chamber in order to simulate the housing of a turbine. To measure the velocity of the air, two Pitot tubes were placed at the orifice of the pneumatic chamber, while the oscillations of the free surface inside the U-OWC were measured by means of a video camera.
4 pressure transducers were placed on the vertical walls of the device, one being positioned in correspondence of the air chamber.
For the measurements of the free surface oscillation along the channel, 5 level probes were used, 3 were placed at a distance equal to approximately one wavelength from the U-OWC to measure wave reflection, while the other 2 probes were placed further away from the caisson to evaluate the wave height along the flume.
Experimental studies led to interesting results regarding the reflection and the energy efficiency. The analyses were conducted varying the width of the vertical duct and the hydrodynamic characteristics of the wave.

2.2 Results

Figure 1a shows the trend of the reflection coefficient k_r, calculated with the method of the three probes of Mansard & Funke (1980), as a function of the relative depth *kd* and for fixed values of *b/W*, being *k* the wave number, *d* the water depth, *b* the width of the vertical duct at the opening of the U-OWC and *W* the width of the internal chamber. The graph shows an increasing trend of k_r as *kd* increases and *b/W* decreases.

Similarly, Figure 1b shows the trend of the energy efficiency coefficient k_e evaluated as the ratio between the energy extracted from the PTO system and the incident wave energy. It has a decreasing trend as the relative depth increases; moreover, it is influenced by the relative width of the vertical duct for low *kd* values.

This behavior suggests that when the width of the vertical duct decreases, the device assumes a behavior similar to a vertical wall.

Empirical formulations for evaluating the reflection coefficient and the energy efficiency coefficient as a function of the relative depth *kd* and relative width of the vertical duct *b/W* were obtained.

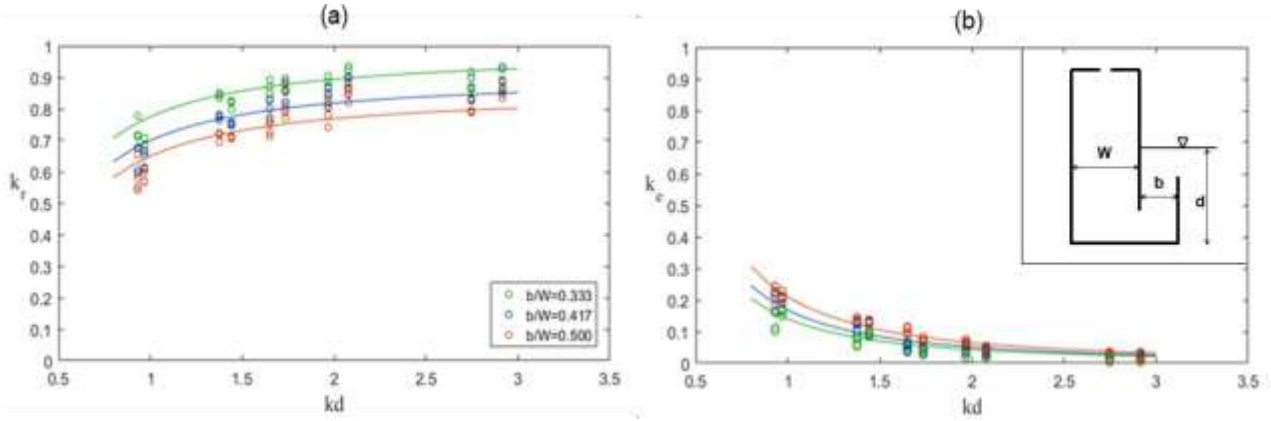

Figure 1. a) Reflection coefficient k_r and b) energy efficiency coefficient k_e as a function of relative depth *kd*.

3 CONCLUSIONS

The experimental study of the interaction of wave flow with an U-OWC showed that the reflection coefficient and the energy efficiency of the U-OWC are strongly influenced by the relative depth and the width of the vertical duct. Furthermore, the maximum extractable energy from the PTO system with respect to the incident wave energy is 23% for *kd*=0.93 and *b/W*=0.50.

ACKNOWLEDGEMENTS

This work has been partly supported by the project TETI - TEcnologie innovative per il controllo, il monitoraggio e la sicurezza in mare (code ARS01_00333) and by the project ISYPORT - Integrated SYstem for navigation risk mitigation in PORTs (code ARS01_01202).

REFERENCES

Ashlin, S.J., Sundar, V., Sannasiraj, S.A. (2016). Effects of bottom profile of an oscillating water column device on its hydrodynamic characteristics. *Renewable Energy*, 96, 341-353.

Elhanafi, A., Fleming, A., Macfarlane, G., Leong, Z. (2017). Numerical hydrodynamic analysis of an offshore stationary–floating oscillating water column–wave energy converter using CFD. *Int. J. Nav. Archit. Ocean Eng.*, 9 (1), 77–99.

Mansard, E. & Funke, E. (1980). The measurement of incident and reflected spectra using a least squares method. *Proc., 17th Int. Coastal Engineering Conf*., ASCE, New York, 154–172.

Simonetti, I.; Cappietti, L.; Elsafti, H.; Oumeraci, H. (2017). Optimization of the geometry and the turbine induced damping for fixed detached and asymmetric OWC devices: a numerical study. *Energy*, 139, 1197-1209.

Simonetti, I. & Cappietti, L. (2021). Hydraulic performance of oscillating water column structures as anti-reflection devices to reduce harbour agitation. *Coastal Engineering*, 165, 103837.

Proceedings of the 2nd IAHR
Young Professionals Congress
30 Nov-2 Dec. 2021

Collinear interaction of wave and current over a rippled bed

Alessia Ruggeri [1], Carla Faraci [1]

[1]University of Messina, Messina, Italy
e-mail: aleruggeri@unime.it

ABSTRACT

In this paper, ripple formation and evolution along with vortex separation along the bedform profile were investigated in a U-Tube in the presence of wave only, current only and collinear wave plus current. Experiments involved both live bed and fixed bed conditions.
It was observed that when the current superimposes to the wave, it reduces the vortex separating at the ripple crest in the wave only case. In the fixed rippled bed case, velocity measured in the current only case is larger than in the wave plus current flow.

Keywords: ripples; sea bottom morphology; vortices; mean velocity.

1 INTRODUCTION

Interaction of waves and currents on cohesionless sandy bottoms can induce morphological variations of the bed, with the consequent appearance of sedimentary structures. The presence of large and regular roughness, such as ripples, leads also to the appearance of large regular vortices along the water column, which present a repeatability both in space and time.
The presence of ripples on the seabed significantly affects the flow field in the presence of collinear waves and currents (Andersen and Faraci, 2003). In this regard, Faraci et al. (2008) observed that the presence of vorticity in the bottom boundary layer generates a modification of velocity profile with an inversion of the velocity itself. Vortex formation over bedforms was also numerically studied by Scandura et al. (2000), who observed the generation of vortices over ripples during the first stage of flow transition.
Aim of the present work is to show preliminary analyses carried out in the framework of the experimental campaign on collinear interaction of wave and current over a rippled bed concerning the evolution of ripples and the dynamics of the vortex structure generation when the current superimposes to the wave.

2 METHODOLOGY AND EXPERIMENTAL RESULTS

An experimental campaign was carried out at the Hydraulics Laboratory of the University of Messina, reproducing steady and oscillating flow within a U-tube. This apparatus allowed both oscillating flow and currents to be contemporarily generated, in order to reproduce the collinear interaction between waves and currents on a rippled bed. During the experimental campaign, tests in the presence of movable and fixed bed in three different flow conditions were carried out: current only (CO), wave only (WO) and waves and currents (WC).
Varying the hydrodynamic parameters, analyses of morphodynamic evolution of ripples with particular attention to the separation of vortices at the crests were carried out. The wave only case and the wave plus current case were compared. In particular, by means of a video camera, frames of the videos were extrapolated (one every 10s) allowing the study of temporal evolution of the two ripple characteristics (length, $\lambda_t(t)$ and height $\eta_t(t)$) as shown in Figure 1a. The latter two were determined as the mean of the height and length of the single ripple, that can be identified in each of the images obtained during the experiment duration. It was found that the two geometric characteristics remain fairly constant. In the case shown in Figure 1, they are about 6 and 1 cm respectively for length λ and height η. It was also found that in the presence of waves and currents, longer times are required for the sedimentary structures to stabilize than in the wave only case.
As regards the vortex shedding, according to Fredsøe et al. (1999), the motion of vortices at different phases of the wave cycle was analysed comparing the cases of wave only and collinear wave and current. At the 90° phase a well-defined clockwise vortex that grows and detaches at the crest was created, extending up to 2.5 cm at the 120° phase (see Figure 1b). These vortices are smaller when the current superimposes to the wave. These results were confirmed by velocity data, extrapolated through the Vectrino Profiler in presence of a fixed ripples bed (λ = 125 mm e η = 18.5 mm). More specifically, over fixed rippled bed, 3 different measuring points were considered along a ripple between crest and trough for the three flow conditions. Analyses showed that

ISBN: 978-90-824846-7-0

the mean velocity in the current only case always shows higher values with respect to those observed in wave and current. Near the bed, in the presence of wave only at all measuring points, a velocity inversion was identified, which confirms the formation of vortices as already found in the presence of moveable bed.

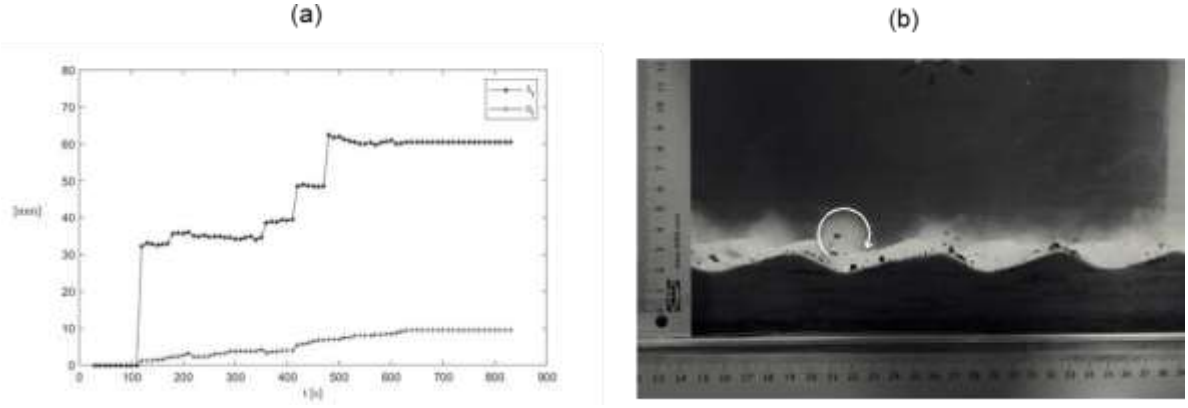

Figure 1. a) Time evolution of ripple characteristics ($\lambda_t(t)$ and $\eta_t(t)$); b) the motion of the vortex in ripple bed.

3 CONCLUSIONS

This work investigated the collinear wave and current interaction over movable and fixed rippled bed acquired in the framework of the experimental campaign in the U-tube. The results discussed in this paper showed that:

- in WC case the sedimentary structures reach stable conditions in longer times with respect to the WO case;
- the superposition of current reduces the extension of the vortex that detaches at the ripple crest in wave only case;
- the separation of vortices observed over movable bed was confirmed by the velocity profiles acquired on the fixed rippled bed, showing a flow inversion at the bottom.

ACKNOWLEDGEMENTS

This work has been partly supported by the project TETI - TEcnologie innovative per il controllo, il monitoraggio e la sicurezza in mare (code ARS01_00333) and by the project ISYPORT - Integrated SYstem for navigation risk mitigation in PORTs (code ARS01_01202).

REFERENCES

Andersen, K. H. and Faraci, C. (2003). The wave plus current flow over vortex ripples at an arbitrary angle. *Coastal Engineering,* 47(4):431–441.

Faraci C., Foti E., and Musumeci RE. (2008). Waves plus currents at a right angle: The rippled bed case. *Journal of Geophysical Research: Oceans*, 113(C7).

Fredsøe, J., Andersen, K.H., Sumer, B.M. (1999). Wave plus current over a ripple-covered bed. *Coastal Engineering*. 38, 177–221.

Scandura, P., Vittori, G., and Blondeaux, P. (2000) Three-dimensional oscillatory flow over steep ripples. *Journal of Fluid Mechanics*, 412:355–378.

ISBN: 978-90-824846-7-0

Proceedings of the 2nd IAHR
Young Professionals Congress
30 Nov-2 Dec. 2021

Analysis of the Hydro – Morphodynamic of the Salaverry Port (Peru) through Numerical Modelling

Luiggi Anthony Cardenas Acuña [1]

[1] IAHR Peru Young Professionals Network, Lima, Peru,
luigg.cardenas08@gmail.com

ABSTRACT

The Port of Salaverry, located northern of Peru, with a longitudinal transport of around 1 million m^3/year of sediments, has generated the formation of shallow water depths close to the head of the breakwater, which influences the calm conditions of the terminal. In response to this hydro – morphodynamic nature, it has been analysed distinct configurations of the terminal by means of using the modelling software package Delft3D WAVE – FLOW, principally evaluating the accumulation of sediment around the head of the shelter structure and the interior wave conditions. Concluding that the most conservative alternative is the one that contemplates the current breakwater structure and a deepening dredging, which reduces the wave heights in nearly 50% in the docking area, hence declining the number of inoperative days.

Keywords: *hydro – morphodynamic; port; breakwater; dredging; Delft3D*

1 INTRODUCTION

The Port of Salaverry, located in the Department of La Libertad – Peru 8° 13' 27" S 78° 59' 52" W, with a hinterland integrated by the departments of La Libertad, Ancash, Lambayeque, Cajamarca and San Martin generated a National GDP of 14.7% in 2018 (Instituto Nacional de Estadistica e Informatica, 2019). In spite of its strategic location it has suffered sedimentation issues throughout its lifespan; implementing a breakwater and a transversal groin that has lost its capacity of retaining the 1 – 1.2 x 10^6 m^3/year of sediments (Consorcio Internacioal AC – INC, 2015), resulting in the accumulation of material around the head of the breakwater and the occurrence of anomalous wave conditions. In consequence, it is proposed the analysis of four configurations of the terminal in response to the hydro – morphodynamic conditions, moreover determine the best alternative and give recommendations for its application.

2 METHODOLOGY

The next alternatives were modelled in the software Delft3D Flow – Wave during a tidal range of 12h30min for both normal and energetic offshore sea conditions, including sediment transport and bed level change.
Alternative 0: Current design of the breakwater and pre dredging bed levels of October 2018.
Alternative 1: Current design of the breakwater and post dredging bed levels of January 2019.
Alternative 2: Extension of the breakwater and pre dredging bed levels of October 2018.
Alternative 3: Extension of the breakwater and post dredging bed levels of January 2019.

Table 1. Offshore sea states for propagation.

	Hs [m]	Tp [m]	HDir [°]	U [m/s]	UDir [°]
NORMAL	1	8	202.5	1.625	157.5
ENERGETIC	2.4	13	202.5	6.5	157.5

Calibration of the model was undertaken, estimating a time step (Δt) of 0.1 min by considering a Courant Number (CFL) and the term of horizontal viscosity stability less than 10 and 1 respectively (Deltares, 2016), further steps involved the calculation of the breakwater Kr = 0.6 by means of applying the refitted formula of Seeling & Ahrens (Zanuttigh, B. and Van der Meer, J.W., 2007), the roughness coefficients (n) of 0.0375 $m^{-1/3}$/s and 0.03 $m^{-1/3}$/s for the normal and energetic sea states respectively, and the application of a Neumman boundary type to solve fluctuations inside the model (Roelvink, D. and Walstra, D.J.,2005).

ISBN: 978-90-824846-7-0

3 RESULTS

- Alternative 0 and 1 show the tendency of the material to move into the sheltered area, however the sediment trap in the lee side of the breakwater has affected either the extension of the accumulation and the wave height in the docking area by reducing it in around 50% with respect to Alternative 0.

Table 2. Wave height under energetic conditions

	Docking Area [m]	Maneuvering Area [m]
ALT. 0	0.4 – 0.8	0.8 – 1.6
ALT. 1	0.2 – 0.6	0.6 – 1.4
ALT. 2	0.2 – 0.4	0.4 – 1.0
ALT. 3	0.1 – 0.35	0.35 – 0.8

- Alternative 2 and 3 present accumulation of sediment around the extended head of the breakwater. On the other hand, in terms of the interior wave conditions both illustrate a declining wave height in approximately 30% and 40% with respect to Alternative 1 respectively.

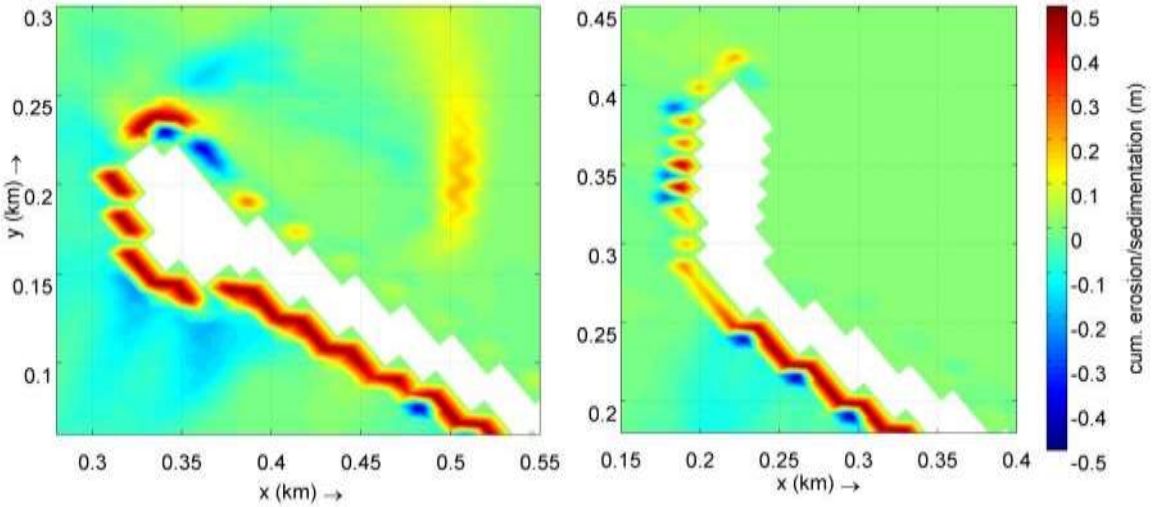

Figure 1. Sedimentation in Alternatives 0 (left) and 2 (right)

4 CONCLUSIONS

- Alternative 1 is the most conservative alternative, because it is known beforehand the extension and shape of the mass of sediment around the head of the breakwater and its influence in the hydrodynamic. In contrast, the sedimentation shown in the remaining 2 alternatives would induced wave conditions different from the ones obtained in the present study.
- According to the statistics published in the portal web of the port concessionaire a downtime reduction of 72.9% was registered in 2019 with regard of 2018, which proves the benefit of Alternative 1.

REFERENCES

Consorcio Internacional AC – INC (2015). Regeneración del borde costero de los balnearios de las Delicias, Buenos Aires y Huanchaco. Ministerio de Transportes y Comunicaciones del Perú. https://portal.mtc.gob.pe/transportes/acuatico/estudios.html

Deltares (2016). *Delft3D – FLOW User Manual Simulation of multi – dimensional hydrodynamics flows and transport phenomena, including sediments.* http://www.deltares .nl

Instituto Nacional de Estadística e Informática (2019). Producto Bruto Interno por Departamentos 2018 (cifras preliminares). https://www.inei.gob.pe/biblioteca-virtual/boletines/pbi-departamental/2019/1/

Roelvink, D. and Walstra, D.J. (2005). Keeping it simple by using complex models. *Advances in Hydro-Science and Engineering, Volume VI*. https://www.researchgate.net/publication/233752032

Zanuttigh, B. and Van der Meer, J.W. (2007). Wave Reflection from Coastal Structures. *Coastal Engineering 2006, pp. 4337 – 4349.* https://doi.org/10.1142/9789812709554_0364.

IAHR YPN

Young Professionals Network

Hosted by
Spain Water and IWHR, China

IAHR AIRH

International Association for Hydro-Environment Engineering and Research

Hosted by
Spain Water and IWHR, China

Experimental Methods & Instrumentation

Proceedings of the 2nd IAHR
Young Professionals Congress
30 Nov-2 Dec. 2021

Assessing the performance of high capacity submersible pumps used in waterways: experimental tests and computational model calibration

Joris HARDY[1], Pierre DEWALLEF[1], Sébastien ERPICUM[1], Michel PIROTTON[1],
Darren PARKINSON[2], Nigel TAYLOR[2], Chris BARNET[2], Paula TREACY[3],
Olivier THOME[1], Pierre ARCHAMBEAU[1] and Benjamin DEWALS[1]
[1] Université de Liège, School of Engineering, Liège, Belgium, joris.hardy@uliege.be
[2] Canal & River Trust (CRT), UK; [3] Waterways Ireland (WI), Ireland

ABSTRACT
Worldwide, navigation is made possible in artificial waterways thanks to the support of a considerable number of high capacity pumps. In terms of energy-efficiency, many of these pumps do not operate optimally. Main reasons for this include pump oversizing and the absence of variable speed drive. In this communication, we present a hybrid modelling approach for assessing the actual performance of high capacity submersible pumps used in waterways. It is based on a novel, large experimental test bench and a computational model of the motor and pump system. The computational model achieves an accuracy of about 10% for predicting the flow rate, energy consumption and system efficiency. This hybrid tool may be valuably exploited to assess full scale pumping systems and lead to energy savings, for instance by improving the selection of the frequency applied to the motor considering the actual losses in suction and discharge pipes.

Keywords: numerical pump model; nalibration using optimization interior point technic; performance-assessment of large submersible pumps; off-design pump operation; Best Efficiency Point (BEP)

1 INTRODUCTION

Navigation in most artificial waterways relies on energy-demanding pumping operations, but a suitable tool to evaluate the actual on-site energy efficiency of these systems is missing. Indeed, pump manufacturers generally provide detailed information on a curve of pump efficiency at nominal rotation speed with the nominal characteristics of the motor, which includes the best efficiency point (BEP). No or little information is available concerning off-design pump operation, while variable speed drives are known to enable increasing the overall efficiency of the pumping system, which is precisely what matters for the end-users. A hybrid modelling approach is presented here. It involves a large experimental test bench (Hardy et al., 2021) used for calibrating a computational model of the whole system, including the motor, the pump and the hydraulic setting.

2 METHOD

A process-based computational model of pumping system is used to simulate the operation of an asynchronous motor (Hardy, 2018), a pump, and the hydraulic system connected to the considered pump. The model involves 13 dimensionless nonlinear equations, including two of them linking the pumping head, torque, flow rate and frequency:

$$H_p = a\,Q^2 + b\,Q\,\omega + c\,\omega^2 \qquad [1]$$

$$T_p = d\,Q^2 + e\,Q\,\omega + f\,\omega^2 \qquad [2]$$

where H_p, T_p, Q and ω represent ratios between the actual value and the nominal value of the pumping head, torque, flow rate, and frequency. Coefficients a, b, c, d, e and f are used to characterize each specific pump. The model considers as inputs: the frequency, the voltage, the elevation head and a head loss coefficient in the pipes. It provides: the flow rate, the rotation speed, the motor efficiency, pump efficiency, hydraulic efficiency, total efficiency and the power. The computational tool is coded in Python.

The novel laboratory test bench is represented in Figure 1d, and it was described in detail by Hardy et al. (2021), together with the procedure followed to collect experimental data. It involves a 4.5 m high tank with a storage capacity of 30 m^3, which can accommodate pumps with a maximum power of 300 kW, a maximum flow rate of 0.3 m^3/s a maximum weight of 2 tons. In the present setting of the test bench, the accuracy of the flow rate, power and differential pressure measurements are 0.4%, 0.5% and 0.075%, respectively. The variable frequency drive is assumed to run at constant efficiency of 90 % (U.S Department of Energy, 2012).

The calibration of the computational model consists in identifying the 13 model parameters by minimizing the root mean square error between predicted and observed flow rate and power consumption. A non-linear optimization algorithm under constraints is used for this calibration. It relies on the interior point method and the Wolf line search conditions. In the tests presented here, 51 measuring points were recorded. For each point, the flow rate, the power consumption as well as the head were registered. The frequency applied to the motor was varied between 15 Hz and 50 Hz, and for each frequency, the opening of a valve was modulated to change the head. The calibration takes as inputs, the frequency, the pump head measured, the power and the flow rate measured.

ISBN: 978-90-824846-7-0

3 RESULTS

The measurements collected on the test bench for a submersible pump, Amarex KRT D 250-400/206UG-S, are displayed in Figure 1a-b, together with results of the computational model. The root mean square differences between computations and measurements are in average 9 %, 3 % and 2 % for the flowrate, the electric power and the total efficiency. The new test bench highlights that the actual efficiency of the engine-pump system peaks around 63 %, which is lower than the efficiency expected from manufacturer data and characteristic of the variable frequency drive (76 % × 90 % ≈ 68 %). This may certainly be explained by the time in operation of this pump (11 years) but possibly also by an initial difference between the actual efficiency and the documented one.

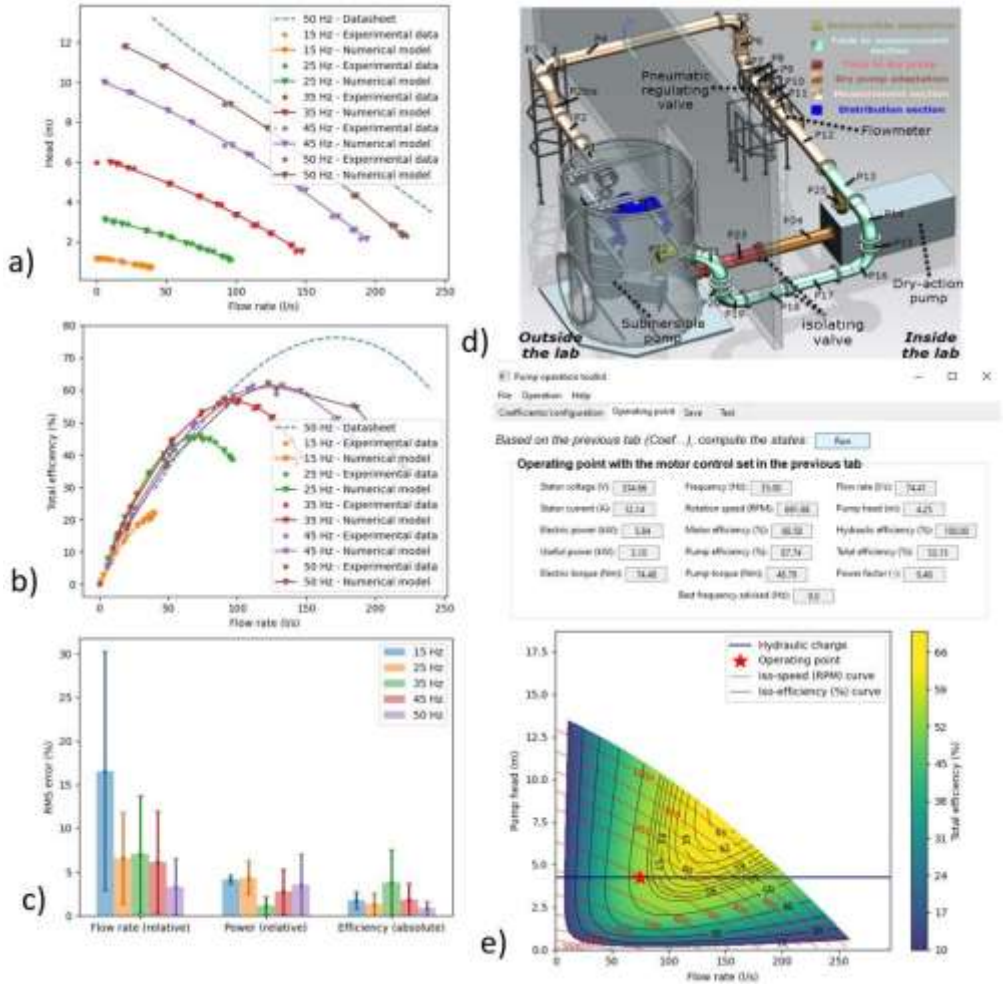

Figure 1 : Results measured by varying the frequency during the pump tests: head as a function of flow rate (a), pump total efficiency as a function of flow rate (b), RMS error and standard deviation between numerical model and measurements for flow rate, power consumption and total efficiency (c), pump test bench CAO (d), and iso-efficiency curves obtained with the numerical model (e).

4 CONCLUSIONS

The actual on-site energy efficiency of pumping stations can be estimated by end-users using the developed computational tool, calibrated thanks to experimental observations in the novel test bench. Accurate information on the pumping efficiency and its evolution over time is of critical importance for guiding decision-making in terms of new investments for pumps maintenance, upgrade or replacement.

ACKNOWLEDGMENTS. This research is partly supported by ERDF funding in the framework of the Interreg NWE project Green WIN. CRT and WI are gratefully acknowledged.

REFERENCES

Hardy, J., et al. , 2021. Experimental Test Bench for Performance-Assessment of Large Submersible and Dry-Action Pumps Used in Waterways. Publ. Inst. Geophys. Pol. Acad. Sci. Geophys. Data Bases Process. Instrum. 434, 101–103.

Hardy, J., 2018. Speed regulation of a compressor test bed using electrical drives. Master Thesis, University of Liège, Liège, Belgium.

U.S Department of Energy, A.M.O., 2012. Adjustable Speed Drive Part-Load Efficiency.

Proceedings of the 2nd IAHR
Young Professionals Congress
30 Nov-2 Dec. 2021

'Noise-Free' Stereoscopic Particle Image Velocimetry

Nijmeh Marouf[1], and Stuart Cameron[2], Vladimir Nikora[3]

[1]University of Aberdeen, UK, n.marouf.19@abdn.ac.uk, [2,3] University of Aberdeen, UK

ABSTRACT

When handling stereoscopic particle image velocimetry (PIV) data, measurement errors associated with image capture and processing are unavoidable. However, if two independent velocity component estimates are available, the noise contribution to second order statistics can be significantly reduced by considering the covariance of the redundant measurements. For stereoscopic PIV, such redundant measurements can be obtained by adding an additional pair of cameras to simultaneously view the light sheet from a different angle. In practice, some correlation is expected and assessment of this is the focus of our study. Simulated PIV image sets suggest that while 'aliasing' and 'camera noise' errors are highly independent, 'gradient' induced errors are strongly correlated between PIV setups. The correlation between 'change of brightness' errors depended on particle image diameter and light sheet thickness, with an optimum camera displacement angle found to minimise noise correlation. Using this approach, a significant reduction in noise contribution to measured velocity statistics is possible.

Keywords: noise-free stereoscopic PIV; noise reduction

1 INTRODUCTION

Stereoscopic Particle Image Velocimetry (PIV) is a widely used method for measuring instantaneous velocities and turbulence statistics across a two-dimensional slice of a flow field. However, the presence of measurement uncertainties clouds the interpretation of data, especially in highly complex and three-dimensional flows. The use of redundant velocity estimates to significantly reduce the measurement error contribution to second order velocity statistics proposed in Cameron et al. (2013) is promising, but not yet well tested. This study therefore aims to assess the performance of the redundant PIV method by generating and analyzing a set of simulated PIV images.

2 THEORY OF NOISE-FREE PIV

When considering PIV measurement errors, it is convenient to work in terms of particle image displacement $\boldsymbol{\Delta_x}$ (pixels) rather than velocity $\boldsymbol{u = \Delta_x M/\Delta_t}$ (m/s), as the time separation $\boldsymbol{\Delta_t}$ (s) between light sheet illumination pulses and the image scale factor $\boldsymbol{M}$ (m/pixel) are constant for a particular measurement setup. Instantaneous displacement fluctuations Δ'_x may be represented as the sum of the actual displacement fluctuation Δ'_{x_a} and measurement noise ε'_x such that $\Delta'_x = \Delta'_{x_a} + \varepsilon'_x$. For two redundant measurements, $\Delta'_{x[1]}$ and $\Delta'_{x[2]}$, the displacement covariance may be decomposed as:

$$\overline{\Delta'_{xi[1]}\Delta'_{xi[2]}} = \overline{(\Delta'_{x_a} + \varepsilon'_{x[1]})(\Delta'_{x_a} + \varepsilon'_{x[2]})} = \overline{\Delta'_{x_a}\Delta'_{x_a}} + \overline{\Delta'_{x_a}\varepsilon'_{x[1]}} + \overline{\Delta'_{x_a}\varepsilon'_{x[2]}} + \overline{\varepsilon'_{x[1]}\varepsilon'_{x[2]}} \quad [1]$$

where the second and third terms on the right-hand-side tend to zero if the fluctuating error is not correlated with the displacement fluctuation. Earlier tests by Cameron et al. (2013) show that this is likely to be the case for typical measurement conditions. Therefore, the noise co-variance $\overline{\varepsilon'_{x[1]}\varepsilon'_{x[2]}}$ remains as the sole noise contribution to $\overline{\Delta'_{x[1]}\Delta'_{x[2]}}$. The correlation coefficient $C_{\varepsilon_{x[1]}\varepsilon_{x[2]}} = \overline{\varepsilon'_{x[1]}\varepsilon'_{x[2]}}/(\varepsilon_{x[1]}\ \varepsilon_{x[2]})$ is a useful metric determining the extent of noise reduction with $C_{\varepsilon_{x[1]}\varepsilon_{x[2]}} = 0$ indicating a near 'noise-free' estimate and $C_{\varepsilon_{x[1]}\varepsilon_{x[2]}} = 1$ indicating no noise reduction.

3 METHODOLOGY

For this investigation, synthetic PIV images generated from randomly distributed particles which follow prescribed motions (e.g. Raffel et al. 2018) were used. The imposed displacement Δ'_{x_a} is therefore known, the measured displacement Δ'_x is obtained by cross-correlation PIV image processing, and the error $\varepsilon'_x = \Delta'_x - \Delta'_{x_a}$

subsequently calculated. Image conditions which may be controlled include: the displacement field (Δ_x , Δ_y , Δ_z), the relative angle Δ_β between a pair of stereoscopic PIV cameras (Figure 1a), particle image diameter D, light sheet thickness L, particle image concentration c_p, and the standard deviation σ_N of additive random image noise. We propose that the total measurement error can be decomposed into four key contributions including: 'aliasing' error ε'_{xA} associated with under-sampling of PIV images; the 'change of brightness' error ε'_{xB} associated with out-of-plane displacement; 'camera noise' error ε'_{xN} associated with the random component of pixel brightness due to camera thermal effects; and 'gradient' error ε'_{xG} reflecting the uncertainty associated with each particle within the PIV sampling volume having a different displacement. We generated a set of simulations for the steady state condition to isolate each of these errors and in each case the correlation coefficient $C_{\varepsilon_x[1]\varepsilon_x[2]}$ was computed.

4 SAMPLE RESULTS AND DISCUSSION

Figure 1b shows the error correlation coefficient as a function of relative stereoscopic camera angle for simulation cases with large out-of-plane displacement Δ_y relative to the light sheet thickness L which isolates the 'change of brightness' error ε'_{xB} At zero relative angle the images and therefore errors from each camera pair are identical and the $C_{\varepsilon_x[1]\varepsilon_x[2]}$ is one. As the relative angle increases, differences in the projections of the three-dimensional particle cluster seen by each camera become significant and the displacement errors obtained from each pair de-correlate. The correlation coefficient crosses zero at a particular relative camera angle indicating potentially 'noise-free' estimates of the displacement variance. The optimum angle depends on the particle image diameter D and the light sheet thickness L as shown in Figure 1c. Other simulations isolating the 'aliasing' and 'camera noise' errors show near zero error correlation for all practical relative camera angles. The 'gradient' error, however, was found to be strongly correlated for all imaging conditions.

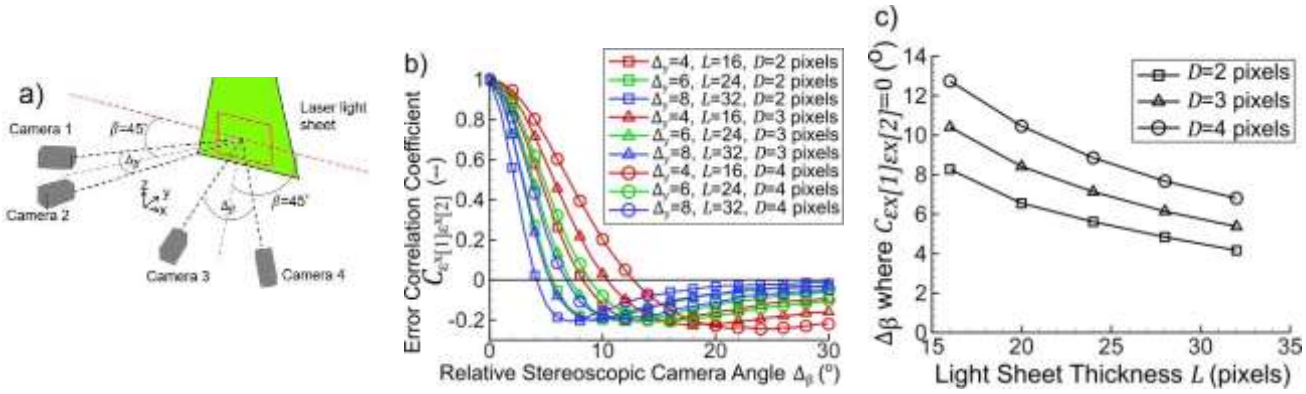

Figure 1. Stereoscopic camera configuration (a); error correlation coefficient $C_{\varepsilon_x[1]\varepsilon_x[2]}$ versus relative stereoscopic angle Δ_β for simulations with large, uniform out-of-plane displacements; legend values are in pixels (b); and optimum relative stereoscopic camera angle versus light sheet thickness (c)

5 CONCLUSIONS

Our study suggests that the 'noise-free' PIV technique utilizing four stereoscopic cameras instead of the conventional two, has potential to significantly reduce the measurement noise contribution to second order velocity statistics. The technique relies on the measurement errors from one pair of cameras being un-correlated with the measurement errors from a second pair. Our simulations suggest that with careful control of the PIV setup, an order of magnitude reduction in the noise contribution to the velocity variance is possible. We plan to further evaluate the method by comparing simulation results to those obtained in an open-channel flume.

REFERENCES

Cameron, S.M., Nikora, V.I., Albayrak, I., Miler, O., Stewart, M., and Siniscalchi F. (2013). Interactions between aquatic plants and turbulent flow: a field study using stereoscopic PIV. *Journal of Fluid Mechanics*, 732:345–372.

Raffel, M., Willert, C.E., Scarano, F., Kähler, C.J., Wereley, S.T. and Kompenhans, J., (2018). Particle image velocimetry: a practical guide. Springer.

Proceedings of the 2nd IAHR
Young Professionals Congress
30 Nov-2 Dec. 2021

Numerical modelling to estimate the hydraulic efficiency of continuous transverse grates

A. Paindelli [1,3], J.D.Tellez-Alvarez [1],M.Gomez [1] and B.Russo [1,2,3]

1 Institute Flumen, Department of Civil and Environmental Engineering, Technical University of Catalonia, Jordi Girona St.,1-3, 08034, Barcelona, Spain.

3 Research Group in Hydraulic and Environmental Engineering, Technical College of La Almunia (EUPLA, University of Zaragoza), Mayor St., n.5, La Almuia de Doña Godina, 50100, Zaragoza, Spain

4 AQUATEC - Suez Advanced Solutions. Ps. Zona Franca 46-48, Barcelona, 08038, Spain.

*Corresponding author email: a.paindelli@aquatec.es or andrea.paindelli@gmail.com

ABSTRACT

The lack of knowledge regarding the interaction efficiency between upper and underground urban drainage system is one of the most undervalued aspects for increasing cities' resilience to cope with pluvial floods. Gomez M. and Russo B. started more than a decade ago investigating over this topic and developing newer approaches to estimate inlet drainage efficiency in function of its geometry. The document presents just a small part of this study area, exposing how experimental data were compared with numerical results obtained from CFD 3D simulations.

Keywords: urban drainage; CFD; hydroinformatics; 3D model; Inlet hydraulic efficiency.

1 INTRODUCTION

Most of the climate projections for the Mediterranean area up to the end of the Century show a significant increase in the number of extreme events, while it is expected a decrease in the total amount of rainfall along the year [8]. Heavy rainfall events usually happen between August and November, after periods without significant precipitations, where foliage and other urban sediments have a higher potential to generate clogging while settling inside the conduits and covering the inlets. This latter could represent one of the most problematic aspects for maintaining a healthy and efficient drainage system, as inlets and manholes are direct responsible for connecting surface and underground system. In this sense, at Universitat Politecnica de Catalunya (from now on UPC), been years investigating on how to quantify and improve the inlet capturing efficiency estimations [3][4][6], while exploring new methodologies and theories with the help of a 1:1 scale platform (1,5 m width, 4,5 m long) located in the UPC's hydraulic laboratory [10]. One of the main achievements was to prove the directly relation between approaching flow behaviors design and the inlet hydraulic capturing efficiency [5], where this latter is intended as the ratio between intercepted and approaching flow, expressed per meter of grate.
A considerable number of tests were completed for this study, employing the above-mentioned UPC platform and a total of 7 common grates were investigated to develop and validate the just presented efficiency equation. The equation was improved to refine geometries dependencies and to ease the adoption at a large scale for untested squared grates too [5]. To speed up implementations and validations for any type of inlet geometries, it was chosen to attempt numerical solutions with the expectancy to swap laboratory tests with computer equivalent simulations. In this sense and following previous experiences [2][9], a hybrid 2D/3D model of the UPC platform was built with the commercial CFD software Flow3D [1].

2 METHODOLOGY

The numerical model pretends to replicate the UPC platform with details in all its elements: upper tank, water source, platform and grate. Specific effort was given to the inlet modelling by using Google SketchUp to obtain a solid Stereolithography (STL) copy, which was the required format to work with Flow3D. Different meshing criteria were applied to the various part of the model, gaining efficiency and decreasing computational cost. The biggest improvement was reached by nesting the fully 3D model (based on Navier Stokes Equations) with the approximated 2D Shallow Water Equations in some specific areas such as over the platform. A mesh sensitivity analysis was performed finding optimal mesh dimension and time step, considering available hardware capabilities (Case computer Intel Core 2 Duo, 2.3 GHz and 12 GB RAM). The maximum cell size was set at 4cm for the tank, 2cm for the platform area, while decreasing down to 1 cm around the inlet zone, resulting into a total number of 1.162.355 cells. The model was forced to adopt the Re-Normalization Group (RNG) to emulate turbulence variability as the most suited for these studies, following Flow3D User manual indications. Initial Conditions (IC) were set as needed, ensuring constant inflow rate (50 l/s and 100 l/s) through the water source,

as well as Boundary Conditions (BC) to emulate reasonable flow behaviors at computational mesh limits (wall, outflow, symmetry). Simulations were performed for a wide range of combinations of transversal and longitudinal slopes, trying to reproduce the most common road existing geometries. Hence, varying the model slope from 0 to 10% towards the direction of the flow and from 0 to 4% perpendicularly, it was possible to emulate exactly how the real UPC platform behaves and thus comparing numerical with experimental results.

3 RESULTS AND DISCUSSION

Simulations were conducted after model calibration, which was achieved by comparing a pair of lab tests with model simulations and leaving the others for model validation. Postprocessing was used to transform results from 1,5 meters length to unit value (1-meter length), simplifying implementation and eventual comparison in further studies. Hydraulic efficiency of continuous transverse grates is usually higher than single lateral inlets; the effect they produce over the flow pattern is far greater and thus more effective if compared with conventional catching elements. Despite this, its applications are strictly limited to large paved areas such as squares, parkings and airstrips. The results can be considered as satisfactory, showing high level of correlation between experimental and numerical data and confirmed also by the value of the R coefficient which is equal to 0.98 (Figure 1). The comparison and the validation between the two methods, opened a brand-new era for laboratory tests, offering a path to shift from traditional 1:1 scale lab equipment to the about-limitless possibility provided by modern CFD software. Results analysis also revealed a high level of accuracy with respect to water depth and velocities distribution all along the whole platform. Although the computational time required to perform the simulations was quite high (due to hardware limitations), the accuracy of the results is extremely satisfying, justifying the adoption of the 3D modelling. Offering CFD solutions has an alternative to common lab procedures, opened new horizons for the adoption of these models in the field of urban hydrology, whilst any good modelling needs to be validated before being implemented, this paper could provide valid references to anybody approaching the topic.

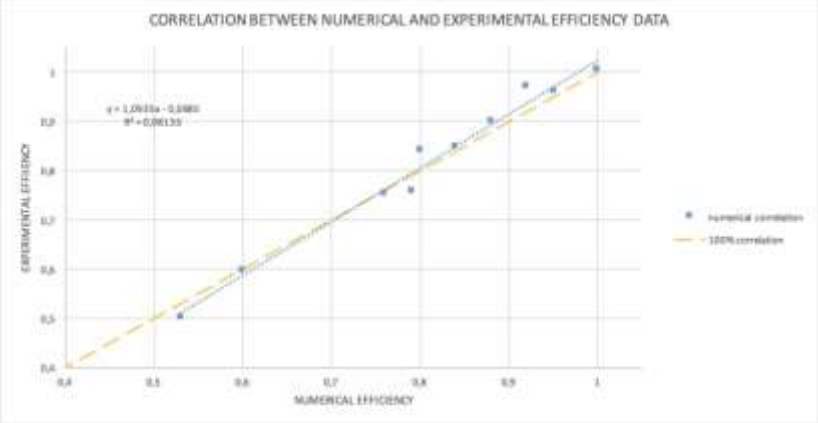

(Figure 1)

REFERENCES

Alvarez, J.T.; Gómez, M.; Russo, B. Hydraulic efficiency and spatial distribution of intercepted flow rate along grated inlet. (2019)
Begum, S.; Rasul, M.G.; Brown, R.J.; Subaschandar, N.; Thomas, P. An experimental and computational investigation of performance of the green gully for reusing stormwater. *J. Water Reuse Desalin.* **2011**, *1*, 99–112.
GómezV, M & Parés, Joan & Russo, B & Martínez-Gomariz, E. (2018). Methodology to quantify clogging coefficients for grated inlets. Application to SANT MARTI catchment (Barcelona). Journal of Flood Risk Management. 12. 10.1111/jfr3.12479.
Gómez V, M & Rabasseda, G & Russo, B. (2012). Experimental campaign to determine grated inlet clogging factors in an urban catchment of Barcelona. Urban Water Journal - URBAN WATER J. 10. 1-12. 10.1080/1573062X.2012.690435.
Gómez, M., and Russo, B. (2009). Hydraulic efficiency of continuous transverse grates for paved areas. Journal of Irrigation and Drainage Engineering. 135(2), 225–230.
Gómez, M., and Russo, B. (2011). Methodology to estimate hydraulic efficiency of drain inlets. Institution of Civil
Gómez, M., Russo B and J Tellez-Álvarez. "Experimental investigation to estimate the discharge coefficient of a grate inlet under surcharge conditions." *Urban Water Journal* 16 (2019): 85 - 91.
IJC 2013 INTERNATIONAL JOURNAL OF CLIMATOLOGY Int. J. Climatol. 34: 643–654 (2014) Published online 6 May 2013 in Wiley Online Library (wileyonlinelibrary.com) DOI: 10.1002/joc.3712
Lopes, P., Leandro, J., Carvalho, R. F., Páscoa, P. & Martins, R. (2013). Numerical and experimental investigation of a gully under surcharge condition. Urban Water Journal 13 (6), 468-476.
Russo, B & V, M & Tellez Alvarez, J. (2013). Methodology to Estimate the Hydraulic Efficiency of Nontested Continuous Transverse Grates. Journal of Irrigation and Drainage Engineering. 139. 864-871. 10.1061/(ASCE)IR.1943-4774.0000625.

ISBN: 978-90-824846-7-0

Proceedings of the 2nd IAHR
Young Professionals Congress
30 Nov-2 Dec. 2021

Drag coefficient of a body-like shape: experiments in two complementary laboratory setups

Delhez Clément[1], Erpicum Sébastien[1], Jašić Radomir[1], Andrianne Thomas[1] , Rivière Nicolas[2], Pirotton Michel[1], Archambeau Pierre[1] & Dewals Benjamin[1]
[1] University of Liege, Liege, Belgium
[2] INSA Lyon, Lyon, France

ABSTRACT

This study focuses on the experimental determination of the drag coefficient of a body-like shape, with the aim of calibrating a computational model to simulate the motion of drowning victims in rivers. The influence of various parameters corresponding to real-life drowning conditions (morphology, clothing, flow depth, limbs position and orientation of the body to the flow) was analyzed and the sensitivity of the drag coefficient to each parameter was evaluated. A range of drag coefficient values was obtained: $0.9 \leq C_D \leq 2.5$. Statistical tests suggest that more robust results are obtained when the drag coefficient is evaluated based on a reference frontal area instead of an area accounting for the variations in the morphology, limbs position or body orientation.

Keywords: body-like shape, drag, drowning, laboratory experiments.

1 INTRODUCTION

Worldwide, around 80 thousand cases of drowning in rivers are reported every year (Word Health Organization, 2014). Current methods to search for a drowning victim are unsatisfactory due to the uneven river bottom and water turbidity. Additionally, existing literature focused mostly on the time of resurfacing and there is a gap of knowledge on the displacement of the victim between the drowning and the time of resurfacing. The objective of this research is to identify the values of parameters necessary for feeding computational models of the displacement of a drowning victim over time. Coefficient determined in this work is drag coefficient C_D that is a basic coefficient to be put in equations that allow modeling a drifting object or drowning victim.

2 EXPERIMENTAL SETUPS

Drag was measured in two complementary experimental facilities: a 20 m long hydraulic flume and a 100 m long towing tank (Table 1). In the former, rigid body models (dummies) at a scale of approximately 1:6 were used, and the covered range of particulate Reynolds number Re_p spans between 2.8×10^4 and 5.2×10^4. In the towing tank, a prototype-scale rigid body model was used, with a particulate Reynolds number varying between 10^5 and 5×10^5. These facilities allow testing the influence of various parameters on the drag of a body-like shape: orientation, morphology, depth, limbs position and clothing. For each configuration, a representative value of the drag was estimated by averaging the values obtained for 5 to 8 different Reynolds values taken in a narrow range (Table 1).

Drag coefficients were calculated from Eq. [1] (Bixler et al., 2007; Chu et al., 2018):

$$F = \frac{1}{2}\rho C_D A U^2 \qquad \text{or} \qquad F = \frac{1}{2}\rho \hat{C}_D A_{ref} U^2 \qquad [1]$$

with F the measured drag, ρ the fluid density, C_D the standard drag coefficient (computed based on A), $\hat{C}_D$ an alternate drag coefficient (computed based on A), A_{ref} a reference frontal area, A the frontal area of the body model depending on the morphology, position, etc. and U the relative velocity in the streamwise direction. The use of the alternate drag coefficients $\hat{C}_D = C_D A / A_{ref}$ enables attenuating the effect of uncertainties in the estimation of the frontal area for each configuration.

Table 1. Complementary laboratory facilities used to measure drag on a body like shape

	Hydraulic flume	Towing tank
Fluid	Flowing water	Water at rest
Body model	1:6 scale model (fixed / drifting)	Full scale, prescribed motion
Velocity	0.09 – 0.2 m/s	0.1 – 0.5 m/s
Water depth	0.62 m	4 m
Range of Reynolds R_p	$2.8 \times 10^4 – 5.2 \times 10^4$	$10^5 – 5 \times 10^5$
Measurements	Load sensor, ADVP	6 load sensors measuring forces and torque in three directions

ISBN: 978-90-824846-7-0

3 RESULTS AND DISCUSSION

The results are first presented for a reference configuration, and next the influence of each individual parameter is described (Table 2). The reference configuration corresponds to a naked dummy, with a standard morphology, positioned close to the water surface, limbs hanging down, spine aligned with the main flow direction, head downstream and face down. In this case, $A = A_{ref} = 85.2$ cm^2 and a value of $C_D = \hat{C}_D \approx 1.6$ is obtained.

Table 2. Drag coefficients and p-value for each tested configuration

Configuration	C_D	$\hat{C}_D$	*p-value* C_D	*p-value* $\hat{C}_D$
Reference	1.6	1.6	-	-
Fat model	2.5	2.2	7×10^{-6}	1×10^{-5}
Model at mid depth	1.1	1.1	4×10^{-6}	4×10^{-6}
Perpendicular to the flow	1.7	2.32	0.4	2×10^{-5}
Horizontal limbs	0.9	0.34	8×10^{-6}	8×10^{-6}
Dressed (sweater + pants), horizontal limbs*	1.7	1.7	-	-

* These results were obtained in the towing tank, while all other data were collected in the hydraulic flume.

Table 2 highlights the influence of each parameter.

- Changing the dummy morphology (fat instead of standard) alters the drag coefficient by 40 % to 60 %.
- Positioning the dummy at mid-depth instead of close to the free surface reduces the drag coefficients by about 30 %.
- When the dummy is oriented in the direction normal to the main flow direction, the standard drag coefficient C_D is increased by just 6 %, whereas the alternate drag coefficient $\hat{C}_D$ rises by about 45 %. This is due to the considerable change in the frontal area, which is accounted for separately for the evaluation of C_D, while it is incorporated in the value of $\hat{C}_D$. Note that in this case, the change in C_D is the only one that appears as statistically not significant based on the calculated p-value. In other words, the effect of modifying the body orientation is properly reflected by the change in the frontal areas, and the value of the standard drag coefficient is virtually not affected. Note also that a misalignment of the body regarding the flow direction leads to the apparition of a lateral force, which is not taken into account at the present stage of the research.
- Similarly, when the limbs are positioned horizontally instead of downward, the standard coefficient C_D shrinks by around 40 %, whereas the alternate one $\hat{C}_D$ is reduced by a factor 5. Again, this stronger variation stems from the change in the frontal area which is taken into account differently in the evaluation of C_D and $\hat{C}_D$.

While the previous results were obtained in the hydraulic flume, the experiments with a dressed body were conducted in the towing tank, with a full scale dummy and limbs positioned horizontally. In this case, several parameters were changed simultaneously, due to experimental constraints. Nonetheless, tests showed that the increase in drag induced by clothing is closely related to the body orientation with respect to the flow due to the inflation of clothes in some positions (parachute effect).

4 CONCLUSIONS

Experiments carried out in two complementary experimental facilities suggest that it is not possible to assign a clear-cut value for the drag coefficient C_D of a body-like shape, but a range of values can be identified. This is a valuable outcome to feed computational modelling of the drift of the body of a drowning victim. The body morphology, body positioning over the water depth and limbs positioning have all a significant effect on the drag coefficient. Re_p is expected to have a significant effect on the drag and will be the subject of further studies.

REFERENCES

Bixler, B., Pease, D., & Fairhurst, F. (2007). The accuracy of computational fluid dynamics analysis of the passive drag of a male swimmer. *Sports Biomechanics*, *6*(1), 81–98.

Chu, C.-R., Lin, Y.-A., Wu, T.-R., & Wang, C.-Y. (2018). Hydrodynamic force of a circular cylinder close to the water surface. *Computers & Fluids*, *171*, 154–165. https://doi.org/10.1016/j.compfluid.2018.05.032

World Health Organization. (2014). *Global report on drowning: Preventing a leading killer*. World Health Organization. https://apps.who.int/iris/handle/10665/143893

ISBN: 978-90-824846-7-0

Proceedings of the 2nd IAHR
Young Professionals Congress
30 Nov-2 Dec. 2021

Detection of pointwise impulsive contaminations in rivers by a moment-based inverse method

Mariano Letizia [1] and Michele Iervolino [1]
[1] Università degli Studi della Campania "Luigi Vanvitelli", Aversa (CE), Italy,
mrnletizia@gmail.com, michele.iervolino@unicampania.it

ABSTRACT

The paper presents an analytical inverse method for the identification of the distance and the entity of impulsive contaminations of rivers, based on the temporal moments of the concentration measured in a cross-section. The proposed method is benchmarked with reference to several small to large rivers and tested against the uncertainty of the governing parameters and the presence of noise in the measures. In most of the considered applications, the method provides reliable solutions at a very limited computational cost.

Keywords: river pollution, water quality, inverse problems, methods of moments, contaminant transport.

1 INTRODUCTION

The detection of relevant pollution sources is essential for the management of water bodies and related infrastructures. In principle, for water bodies subjected to time-continuous monitoring, the entity and the origin of the contamination may be inferred starting from the measured pollutant concentration. From the mathematical point of view, however, this inverse problem is often ill-posed and the achievement of reliable solutions may be very challenging (Kirsch, 2011).
In the present paper we propose a simple method for the detection of instantaneous pointwise contamination events in rivers. The problem was addressed by repeated solution of the solute transport equation (Bencala, 1983; Nordin & Troutman, 1980), and by means of geostatistical Bayesian approaches (Boano et al., 2005; Ferrari et al., 2018). Despite their generality and effectiveness, the above methods turn to be very demanding from the computational point of view.
The proposed method assumes uniform values of the propagation parameters (advection velocity and diffusion coefficient). Based on these assumptions, the closed-form expression of the temporal moments of the pollutant concentration are used as the starting point of the inverse problem solution.

2 MATERIALS AND METHODS

The proposed method estimates the distance from the contamination source, x, and the released contaminant mass, m, by inverting the relations between these unknowns and the temporal moments of the concentration distribution measured in a cross section. The inverse relations are obtained by assuming the validity of the analytical solution of the Advective-Convective-Equation for the case of instantaneous release of a finite mass of non-reactive contaminant (Sauty, 1980) in a channel under uniform flow, and they read as follows:

$$x = \frac{-M_2 u_o^2 - 6M_1 D_o + \sqrt{M_2^2 u_o^4 - 4M_2 u_o^2 M_1 D_o - 12 M_1^2 D_o^2}}{2M_1 u_o} \quad [1]$$

$$m = \frac{2M_1^2 u_o^3}{M_2 u_o^2 - 2M_1 D_o + \sqrt{M_2^2 u_o^4 - 4M_2 u_o^2 M_1 D_o - 12 M_1^2 D_o^2}} \quad [2]$$

in which u_o denotes the uniform flow velocity and D_o the diffusion coefficient, whereas M_1 and M_2 represent the measured first- and second-order temporal moments of the concentration distribution. These moments are estimated by numerical integration of the measured signal over a suitably large time window.
The performance of the proposed method has been tested on a large set of simulated contamination events, occurring in small to large rivers (Di Nardo et al., 2017; Nordin & Troutman, 1980)

ISBN: 978-90-824846-7-0

Moreover, the effect of the uncertainty on the propagation parameters u_o and D_o has been analyzed, showing errors on the estimation of the true distance and mass generally smaller than the parameter uncertainty, except that very close to the contamination source (Figure 1). Similar results (not shown for sake of brevity) have been found when measures are polluted by random noise.

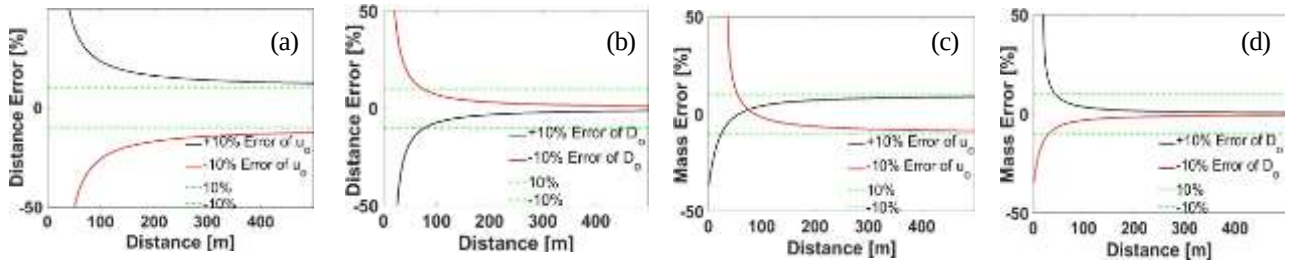

Figure 1. Error in the detection of the distance (a, c) from the pollution source and pollutant mass (b,d) considering a $\pm$ 10% uncertainty in the values of u_o and D_o for the Volturno river ($u_o = 0.70\ \mathrm{m/s}$, $D_o = 10.0\ \mathrm{m^2/s}$).

Finally, the method has been applied to the contamination experiment concerning the Chillàn river (De Smedt et al., 2005; van Genuchten et al., 2013). For the considered example, the flow velocity and diffusion coefficient values are $u_o = 0.426\ \pm 0.003\ \mathrm{m/s}$ and $D_o = 11.4\ \pm 1.4\ \mathrm{m^2/s}$, respectively. The proposed method estimates a distance from the contamination point and a released contaminant mass equal to $x = 4750.5\ \mathrm{m}$ and $m = 166.8\ \mathrm{g}$ with percent errors of 3.1 and 5.8 of the experimental values, respectively.

3 CONCLUSIONS

The method based on temporal moments gives promising results – over a wide range of river size - also in presence of uncertainty in the estimation of the parameters of the propagation model and of measurement errors of the monitoring system, with a very low computational cost.

REFERENCES

Bencala, K.E. (1983). Simulation of solute transport in a mountain pool-and-riffle stream with a kinetic mass transfer model for sorption. *Water Resour. Res.*, *19*(3), 732–738. doi:10.1029/WR019i003p00732

Boano, F., Revelli, R., & Ridolfi, L. (2005). Source identification in river pollution problems: A geostatistical approach. *Water Resour. Res.*, *41*(7). doi:10.1029/2004WR003754

De Smedt, F., Brevis, W., & Debels, P. (2005). Analytical solution for solute transport resulting from instantaneous injection in streams with transient storage. *J. Hydrol.*, *1–4*(315), 25–39. doi:10.1016/j.jhydrol.2005.04.002

Di Nardo, A., Di Natale, M., Iervolino, M., Musmarra, D., & Santonastaso, G. F. (2017). Convolution integral vs. Finite difference for the inverse problem of detection of a contamination source in rivers. *Des. Water Treat.*, *86*, 277–284. doi:10.5004/dwt.2017.20876

Ferrari, A., D'Oria, M., Vacondio, R., Dal Palù, A., Mignosa, P., & Tanda, M. G. (2018). Discharge hydrograph estimation at upstream-ungauged sections by coupling a Bayesian methodology and a 2-D GPU shallow water model. *Hydrol. Earth Syst. Sci.*, *22*(10), 5299–5316. doi:10.5194/hess-22-5299-2018

Kirsch, A. (2011). *An Introduction to the Mathematical Theory of Inverse Problems* (2ª ed.). Springer-Verlag. doi:10.1007/978-1-4419-8474-6

Nordin, C.F., & Troutman, B.M. (1980). Longitudinal dispersion in rivers: The persistence of skewness in observed data. *Water Resour. Res.*, *16*(1), 123–128. doi:10.1029/WR016i001p00123

Sauty, J.-P. (1980). An analysis of hydrodispersive transfer in aquifers. *Water Resour. Res.*, *16*(1), 145–158. doi:10.1029/WR016i001p00145

van Genuchten, M. Th., Leij, F.J., Skaggs, T.H., Toride, N., Bradford, S.A., & Pontedeiro, E. M. (2013). Exact analytical solutions for contaminant transport in rivers 1. The equilibrium advection-dispersion equation. *J. Hydrol. hydromech.*, *61*(2), 146–160. doi:10.2478/johh-2013-0020

ISBN: 978-90-824846-7-0

Proceedings of the 2nd IAHR
Young Professionals Congress
30 Nov-2 Dec. 2021

Analysis of the performance of an air-water flows conductivity probe in a calibration rig

Patricio R. Ortega[1,2], José M. Carrillo[1], Daniel Valero[3], Luis G. Castillo[1] & Juan T. García[1]

[1] *Hidr@m Group, Civil Engineering and Mining Engineering School, Universidad Politécnica de Cartagena, Cartagena, Spain.*
[2] *Civil and Environmental Engineering Department, Escuela Politécnica Nacional, Quito, Ecuador.*
[3] *Water Resources and Ecosystems Department, IHE Delft Institute for Water Education, Delft, the Netherlands.*
patricio.ortega@epn.edu.ec, jose.carrillo@upct.es, d.valero@un-ihe.org, luis.castillo@upct.es, juan.gbermejo@upct.es

ABSTRACT

Conductivity probes have been largely used for measuring air-water flow properties in hydraulic structures. To evaluate the accuracy of different phase-detection probes, a calibration facility has been built, providing controlled flows of water and air by flow meters. Hence, the void fraction value in the facility can be determined and compared with that recorded by the phase-detection probes. In this study, a dual-tip conductivity probe has been tested. The probe tips were made of platinum wire, and measurements were sampled from 20 to 100 kHz during 90 s. The results suggest deviations on the void fractions detected, being more relevant at low concentrations. This indicates the need of calibrating a conductivity probe for accurate air concentration estimations.

Keywords: air-water flows; conductivity probe; circular jet, instrumentation.

1 INTRODUCTION

Most high-velocity air-water flows are characterized by large amounts of entrained air (Straub and Anderson 1958, Wood 1991, Felder and Chanson 2014). In air-water flows, the measurement devices may be affected by air bubbles and air-water interfaces; e.g., Pitot tube or Acoustic Doppler velocimeter (see Frizell 2000, and Matos et al. 2002). Phase-detection probes are commonly used to measure air-water flow properties (e.g., conductivity/resistivity and optical fiber probes), being recommended when the void fraction C exceeds 5 to 10% and/or is less than 90 to 95%. In the recent years, different studies have analyzed the performance of conductivity probes in the detection of air bubbles (Borges et al. 2010, Bung 2012, Kramer et al. 2020, Hohermuth et al. 2021). These studies suggest that conductivity probes may be affected by: 1) hardware limitations and 2) analysis algorithms. These factors merit further analysis.

2 MATERIALS AND METHODS

Measurements were carried out in a calibration rig designed and built at the Universidad Politécnica de Cartagena UPCT (Spain). The structure (Figure 1, left) has a transparent methacrylate tube (diameter ϕ = 110 mm, length 2.0 m), which allows the mixing of water and air, being the distance large enough for the mixed flow to be uniform. Two independent flowmeters are used to measure the air (CS Instruments GmbH & Co. KG, tolerance $\pm$1.5% with temperature correction) and water (Yokogawa, tolerance $\pm$0.5%) flow rates. At the end of the main pipe, there is a contraction and an exit nozzle (diameter D_t = 20.4 mm) (Fig. 1, right). The setup allows to analyze jets with outlet velocity up to 18 m/s and void fractions up to 0.85. In addition, a dual-tip conductivity phase-detection probe was designed and built at the UPCT. The probe tips were made of platinum wire with a diameter ϕ = 0.25 mm. Measurements were sampled at different frequencies (20, 40, 80, 100 kHz) during 90 s. The conductivity probe was used for measuring the local void fraction distributions C in the center of the circular jet, and in the entire cross section located at a distance of $1D_t$ = 20.4 mm from the outlet nozzle.

3 RESULTS AND DISCUSSION

We compared the void fraction measured in the centerline of the jet with that corresponding to the air flow meter recording. Whereas some differences may be acknowledged (for instance, a mean cross-sectional concentration is more relevant), deviations between both estimations may indicate either: 1) a change in the void fraction distribution (non-uniform) or limitations from the conductivity probe. The air flow meter is deemed more accurate and thus herein accepted as ground truth.

For void fraction below C < 0.20 the recorded points by the conductivity probe systematically depart from the 1:1 linear trend (relative to air flowmeter), therefore obtaining lower values of void fraction than those generated by the calibration device (Fig. 2 left). This may be related to difficulties in detecting bubbles at low concentrations (Borges et al. 2010). At the lowest concentrations, absolute errors of 0.20 can be reached (with the conductivity probe omitting the *real* concentration). The obtained results show a similar behavior to those reported by other authors (Matos & Frizell 1997, Borges et al. 2010). As the void fraction increases (C > 0.30), the points tend to behave linearly; however, the data dispersion also tends to increase. This behavior in the void fraction detection

ISBN: 978-90-824846-7-0

seems to be independent of the sampling frequency as, in the tests carried out, no remarkable differences are observed when the recording frequency is changed between 20 and 100 kHz.
Figure 2 (right) presents the void fraction distribution with two different setting values (C = 0.233 and 0.632) in the cross section located at distance $1D_t$ from the nozzle (measurements inside the nozzle indicated negligible entrainment of air from $0D_t$ to $1D_t$). In the central part of the jet, the void fraction values tend to a constant value, hence supporting the uniformity hypotheses to a certain extent. As the points move away from the center, the trend changes due to the ambient air and water strong interactions (Valero and Bung 2016). In summary, the used conductivity probe has difficulties detecting air bubbles at low air concentrations, which is also supported by previous research (Matos & Frizell 1997, Borges et al. 2010).

Figure 2. Void fraction in the jet centerline (left), void fraction profile for different air concentration (right).

ACKNOWLEDGMENTS
The authors express their gratitude for the financial aid received from the “Ministerio de Ciencia, Innovación y Universidades” (MCIU), the “Agencia Estatal de Investigación” (AEI) and the “Fondo Europeo de Desarrollo Regional” (FEDER), through the Project “La aireación del flujo en el vertido en lámina libre por coronación de presas a nivel de prototipo y su efecto en cuencos de disipación de energía”, grant number RTI2018-095199-B-I00, and by the “Comunidad Autónoma de la Región de Murcia” through the “Programa Regional de Fomento de la Investigación Científica y Técnica (Plan de Actuación 2019) de la Fundación Séneca, Agencia de Ciencia y Tecnología de la Región de Murcia”, grant number 20879/PI/18.

REFERENCES
Borges, J.E., Pereira N., Matos J. and Frizell K.W. (2010). Performance of a combined three-hole conductivity probe for void fraction and velocity measurement in air–water flows. *Exp Fluids*. 48: 17-31.
Bung, D.B. (2012). Sensitivity of phase detection techniques in aerated chute flows to hydraulic design parameters. In: *Proc., 2nd European IAHR congress*, 27–29, June 2012, Munich.
Felder, S., and Chanson H. (2014). Phase-detection probe measurements in high-velocity free-surface flows including a discussion of key sampling parameters. *Experimental Thermal and Fluid Science*. 61 (2015) 66-78.
Frizell, K.H., Ehler D.G., & Mefford, B.W. (1994). Developing air concentration and velocity probes for measuring highly-aerated, high-velocity flow. *Technical Report. U.S. Bureau of Reclamation*.
Frizell, K.W. (2000). Effects of aeration on the performance of an ADV. *2000 Joint Conf. on Water Resources Engineering and Water Resources Planning & Management*, ASCE, Minneapolis, USA.
Hohermuth, B., Kramer, M., Felder, S., and Valero, D. (2021). Velocity bias in intrusive gas-liquid flow measurements. *Nat Commun* 12, 4123 (2021). https://doi.org/10.1038/s41467-021-24231-4
Kramer, M., Hohermuth, B., Valero, D., and Felder, S. (2020). Best practices for velocity estimations in highly aerated flows with dual-tip phase-detection probes. *International Journal of Multiphase Flo*w, Volume 126.
Matos, J. and Frizell, K.H. (1997). Air concentration measurements in highly turbulent aerated flow. *Proc. 28th IAHR congress*, Vol. 1, Ed. Sam S.Y. Wang and Torkild Carstens, San Francisco, EUA, pp. 149- 154.
Matos, J., Frizell, K.H., André, S., Frizell, K.W. (2002). On the performance of velocity measurement techniques in air-water flows. In: *Proceedings of the Hydraulic Measurements and Experimental Methods Conference*, EWRI/ASCE & IAHR, Estes Park, USA.
Straub, L.G., and Anderson, A.G. (1958). Experiments on Self-Aerated Flow in Open Channels. *Jl of Hyd. Div*., ASCE, Vol. 84, No. HY7, pp. 1890-1 to 1890-35
Valero, D., Bung, D. (2016). Development of the interfacial air layer in the non-aerated region of high-velocity spillway flows. Instabilities growth, entrapped air and influence on the self-aeration onset. *International Journal of Multiphase Flow,* Vol 84, pp. 66-74
Wood, I.R. (1991). Air Entrainment in Free-Surface Flows. *IAHR Hydraulic Structures Design Manual No. 4, Hydraulic Design Considerations*, Balkema Publ., Rotterdam, The Netherlands, 149 pages.

Proceedings of the 2nd IAHR
Young Professionals Congress
30 Nov-2 Dec. 2021

Impact force of a floating woody debris on a masonry arch bridge

Eda Majtan*, Benedict D. Rogers and Lee S. Cunningham

University of Manchester, Manchester, UK,

*Correspondence: eda.arikan@manchester.ac.uk

ABSTRACT

This paper presents an experimental investigation of flood-induced hydrodynamic and floating woody debris impact on a scaled arch bridge based on a typical single-span masonry arch bridge geometry in the UK. A substantial proportion of masonry arch bridges spanning watercourses has been damaged or destroyed due to flood-induced loads in many parts of the world. Although the scour has been well understood, there are limited studies investigating the highly transient loads on the superstructures and associated responses due to a floating debris inside the flow. To represent a typical river flow situation, an experimental investigation used a 1:10 model in a flume such that the bridge abutments were fully submerged with the impact force from floating debris measured. Results indicate that the debris impact load exerted on the arch bridge was approximately 4.3 times higher than the hydrodynamic force with short impact duration, ~0.01s.

Keywords: *flood events, debris impact, masonry arch bridge, open channel flow, physical model*

1 INTRODUCTION

The majority of masonry arch bridges were built in the nineteenth century with simple design rules. This bridge form is still in daily use in many countries corresponding to approximately 45% of the bridge stock in Spain, 40% in the UK and 32% in Germany (Sarhosis et al., 2016). Although this bridge form has shown high load carrying capacity under vertical loads, many of them have been damaged or destroyed during recent flood events. While the effect of scour has been studied in detail, neither flood-induced hydrodynamic and debris impact loads on the superstructure of masonry arch bridges e.g. abutment, pier, arch barrel and spandrel wall, nor their response to these loads have yet to be investigated properly. An experimental study to complement numerical investigation has been performed at the University of Manchester (UK) to investigate this type of complex interface problem including fluid-solid and solid-solid interaction. This paper presents results from the experimental study to evaluate the drag forces exerted by hydrodynamic and floating debris impact on a scaled single-span arch bridge where the abutment was fully submerged.

2 PHYSICAL FLUME SETUP

Hydraulic experiments were carried out using an existing re-circulating flume at the University of Manchester (UK) with the dimensions of 4.88 m in length, 1.22 m in width and 0.61 m in height as shown in Figure 1(a). A representative masonry arch bridge was chosen according to geometrical properties of many masonry arch bridges (Majtan et al., 2021; Mathews & Hardman, 2017). Thus the prototype bridge was a single-span masonry arch bridge equivalent to an 8 m span, 0.25 rise to span ratio and 4 m stream-wise width in relation to a one-vehicular lane bridge. The model bridge with 1:10 scale was used for experiments corresponding to 0.8 m span and 0.4 m width considering the geometric similarity. Due to the presence of the debris and unknown location of the debris impact, the bridge was suspended using an aluminum beam and elbow joiner keeping an approximately 5 mm gap between the flume surface and bridge bottom. Another beam was mounted behind the bridge to carry the steel plates and load cells. To represent a tree log in the rivers, a cylindrical wooden debris, specifically English Oak, was used based on the span length of the bridge and the ratio between the length and diameter of the debris with 0.059 (Ebrahimi et al., 2016). The debris initial orientation was parallel to the bridge span and its initial distance from the bridge was 1.5 m. The free surface velocity was kept as 0.2 m/s at 1.75 m upstream of the bridge with 0.208 m flow depth corresponding to 0.043641 m^3/s. This represent the free surface velocity of 0.63 m/s in the prototype considering Froude scaling law, which is the main limitation of this experimental study compared to the velocity values observed during flooding cases (Mathews & Hardman, 2017).

3 RESULTS AND DISCUSSIONS

Figure 1(c) and Figure 1(d) show the drag force on a single-span arch bridge without and with the debris impact where the debris orientation was almost the same with its initial orientation (Figure 1(b)). To assess repeatability, three experiments were conducted for each case. Standard deviations of 1.42 N and 7.97 N based on the mean

values of 12.33 N and 52.51 N were observed in the experiments for the cases without and with debris, respectively. The results reveal that the debris impact load on the bridge was 4.3 times higher than the case without the debris with short impact time, approximately 0.01 s. Despite this short impact duration, this significant increase in horizontal load may result in fissures and cracks in the masonry arch bridge. The bridge response to these loads is now under investigation to provide useful insight for assessing masonry arch bridges.

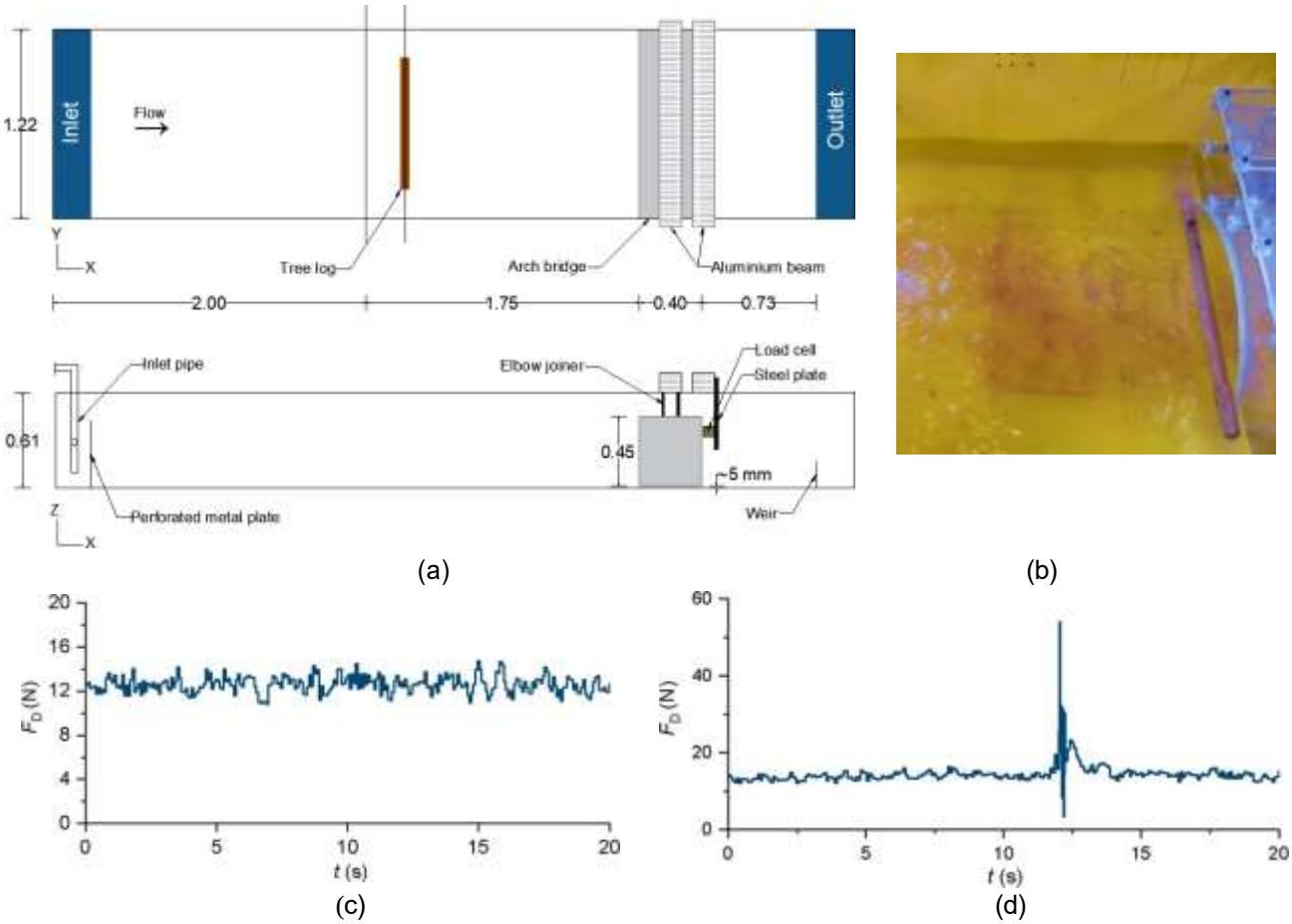

Figure 1: (a) Experimental setup (measures in m), (b) debris orientation around the bridge (c) drag force on the bridge in hydrodynamic case and (d) combination of hydrodynamic and debris impact case

4 CONCLUSIONS

Flood-induced hydrodynamic and debris impact loads were obtained experimentally. The results show that the debris impact results in significantly higher loading on the bridge within shorter duration compared to the hydrodynamic loads which may cause local failure e.g. fissures and cracks in the structure.

REFERENCES

Ebrahimi, M., Kripakaran, P., Djordjević, S., Tabor, G., Kahraman, R., Prodanović, D. M., & Arthur, S. (2016). Hydrodynamic effects of debris blockage and scour on masonry bridges: Towards experimental modelling. *Scour and Erosion - Proceedings of the 8th International Conference on Scour and Erosion, ICSE 2016*, *Rssb 2005*, 743–750. https://doi.org/10.1201/9781315375045-93

Majtan, E., Cunningham, L. S., & Rogers, B. D. (2021). Flood-induced Hydrodynamic and Debris Impact Forces on Single-span Masonry Arch Bridge. *Journal of Hydraulic Engineering*, *147*(11). https://doi.org/DOI: 10.1061/(ASCE)HY.1943-7900.0001932

Mathews, R., & Hardman, M. (2017). Lessons learnt from the December 2015 flood event in Cumbria, UK. *Proceedings of the Institution of Civil Engineers: Forensic Engineering*, *170*(4), 165–178. https://doi.org/10.1680/jfoen.17.00009

Sarhosis, V., De Santis, S., & de Felice, G. (2016). A review of experimental investigations and assessment methods for masonry arch bridges. *Structure and Infrastructure Engineering*, *12*(11), 1439–1464. https://doi.org/10.1080/15732479.2015.1136655

ISBN: 978-90-824846-7-0

Proceedings of the 2nd IAHR
Young Professionals Congress
30 Nov-2 Dec. 2021

Experimental study of cavitation in bottom outlet

Federico Romero [*1], Constanza Fernández Gorostidi [2]
[1,2] Instituto Nacional del Agua, Ezeiza, Argentina,
[*] email: fromero@ina.gob.ar

ABSTRACT

Hydraulic structures subjected to high velocity flows could be exposed to cavitation risks because of surface irregularities, however flow aeration by means of air-entrainment can strongly reduce that risk. The present article shows air concentration profiles at different locations of the rectangular cross section channel of the outlet bottom that was analyzed in a 1:12 length scale physical model. The sectors of the structure where the highest risk of cavitation initiation could be developed where evaluated from the results obtained for the maximum discharge capacity, and possible measures to reduce avoid this are considered.

Keywords: cavitation; aeration; physical model; air-water flow; bottom outlet.

1 INTRODUCTION

Bottom outlet are structures designed for, among other purposes, reduce reservoir level in cases where maintenance operations are required on the dam. The hydraulic head in large dams causes high speed flows that, in the presence of irregularities on the surface of the structure, generate a drop in the flow pressure. If the local pressure equals the water vapor pressure, the cavitation phenomenon will occur, generating potential surface damage and progressively eroding the concrete surface.

The bottom outlet under study has a conduction of 5.8 m wide and approximately 200 m large, built through a tunnel discharge channel with four step aerators of 1.5 m high each. The maximum specific discharge reaches to 32 m^2/s, with flow speeds from 27 m/s at the beginning of the channel, to 18 m/s at the end. The coefficient known as cavitation index of the flow (equation 1) was used to determine the hydrodynamic property that define the potential risk of cavitation, which is defined as:

$$K = \frac{H - H_v}{V^2/2g} \quad [1]$$

where; H refers to the absolute pressure at the point of interest and Hv to the vapor pressure of water, V is the flow velocity and g is the gravitational acceleration.

Once estimated it compared with a critical cavitation index (Kc) to estimate the potential risk cavitation. In this study case the criteria developed by the United States Bureau of Reclamation (USBR) was adopted, which define maximum surface offset irregularities and slope tolerance to prevent damage of cavitation, by linking the cavitation index and the existence or not of aeration in the flow. These tolerance surface parameters recommended are shown in Table 1.

Table 1. Specification of Flow Surface Tolerance

TOLERANCE	OFFSET	SLOPE	CAVITATION INDEX OF THE FLOW	TOLERANCE WITHOUT AERATION	TOLERANCE WITH AERATION
T1	25 mm	1:4	>0.6	T1	T1
T2	12 mm	1:8	0.4 to 0.6	T2	T1
T3	6 mm	1:16	0.2 to 0.4	T3	T1

2 METHODS

The present work was carried out on a physical model, disposed at the Hydraulics Laboratory of Instituto Nacional del Agua (INA, Ezeiza - Argentina), at 1:12 length scale which allow the adequate study of air incorporation phenomenon. By records of velocities and mean pressures, the cavitation coefficients were determined in different sections throughout the entire structure. The air concentrations values were measured by a specific device which has a needle capable of piercing the bubble and, comparing the difference in electrical resistivity between the two flows, the void fraction of the flow is estimated.

ISBN: 978-90-824846-7-0

Because of the characteristic of the phenomenon, the accumulated average concentrations registered up to 0.20 m above the bottom of the channel was considered as a reference.

3 RESULTS

Different authors, including Peterka (1953) and Russell and Sheenan (1974), consider that average air concentrations of the order of 7% would avoid superficial damage. However, values between 1 to 2%, although not fully protective, reduce substantially cavitation erosion (Chanson 1988). Besides, studies on air-entrainment device to reduce cavitation risks in stilling basin developed by INA shows that 2% bottom concentration contributes to strongly reduce cavitation risk associated to pressure fluctuations (Angelaccio, et al 1994).
The results obtained, exposed in Figure 1, determine the region susceptible to the beginning of cavitation by joint evaluation of the cavitation index and the accumulated average concentrations of air.

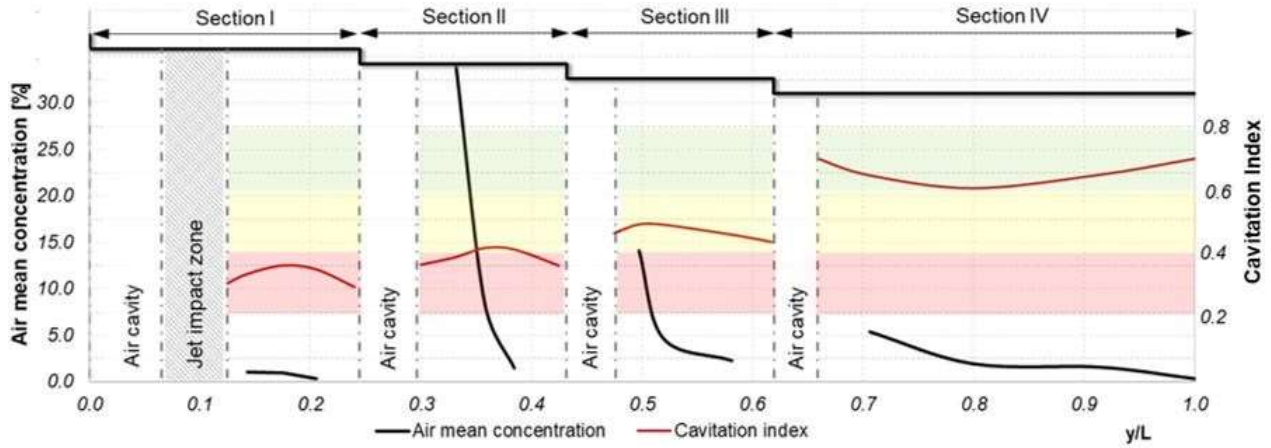

Figure 1. Correlation between mean accumulated concentration, at 0.20 m, and flow cavitation index.

As show in the previous figure in the first section low values mean concentration (0.4% to 1%) and cavitation index in the order of 0.30 was recorded, presenting a potential cavitation damage.
The following sections exhibit a similar behavior to each other with a progressive decrease on the air concentration downstream of each aerator offset. Although in the final zone of each section the air concentration decreases, the values surveyed are high enough in most of its extension. Also, a growing trend of the cavitation index is observed, allowing to conclude that there would be no potential risks of erosion by cavitation despite the absence of air at the final length of the structure. Particularly, along these three referred sections, only at the final sector of the second section there is a low air concentration and cavitation index.

4 CONCLUSIONS

In this study, the section that would be most exposed to the risk of cavitation initiation were determined such as those where the air concentration is less than 2% and the cavitation index is less than 0.4. As a design recommendation to prevent the phenomenon of cavitation in these areas minimum air concentrations must be ensured, adopting structural measures, and/or guarantee surface irregularities less than the maximum admissible on site, which according to the criteria of the U.S.B.R. must be less than 6 mm.

REFERENCES

Angelaccio, C., Bacchiega, J., Barrionuevo, D., Fattor, C. (1994); *Effect of air entrainment on macroturbulent pressure fluctuations in stilling basin* (in spanish). XVI Latin American Hydraulic Congress.
Chanson, H. (1988). *Study of air entrainment and aeration devices on spillway model*. Christchurch: University of Canterbury.
Falvey, H.T. (1990). *Cavitation in chutes and spillways.* Denver: A Water Resources Technical Publication.
Peterka, A.J. (1953). *The effect of entrained air on cavitation pitting.* Denver: Hydraulic Engineer, Design and Construction Division.

ISBN: 978-90-824846-7-0

Numerical analysis of contaminant transport through porous

Sinara Camelo[1], Rita F. Carvalho [2] and Fernando Vieira[3]

[1,3] Universidade Estadual da Paraíba, Campina Grande, Brasil, sinara__@hotmail.com
[2] Universidade de Coimbra, MARE, Coimbra, Portugal, ritalmfc@dec.uc.pt

ABSTRACT
Groundwater is a valuable resource, that can be threatened by the discharge of various polluting sources. Computational Fluid Dynamics (CFD) has been widely used to predict, visualize and evaluate the way fluids may behave under certain conditions. The aim of this work was evaluated CFD techniques to mimic a saturated porous medium and its behavior against the discharge of polluting water. The model was used to analyze the flow regime for four different velocities of discharge of the dye solution. The careful examination of flow patterns showed that the extent and form of contamination depends considerably on the rate of leakage and the rate of entry of water (natural infiltration). Future work will focus on analyzing an analogous physical model to corroborate the numerical results through qualitative comparison and performing new simulations by varying the porosity values

Keywords: contaminant transport; numerical model; porous media, CFD.

1 INTRODUCTION

According to Patil and Chore (2014), groundwater is a valuable natural resource. Its contamination is one of the most typical hydro-geological and environmental problems. Tracking fate of contaminants is a hard, long-term, and sometimes an impossible process (Samadi and Shamshiri, 2019). Therefore, it is essential to understand the process of transporting contaminants through subsurface porous media. For this, in recent years, several analytical equations for free and porous flows have been propounded by researchers in fluid mechanics, water resource management, and hydrogeology (Akowuah and Ampofo, 2016) and many numerical models have been developed to be used to solve equations of dispersion and simulation of the transport of contaminants through the soil (Seyedpour *et al.,* 2019; Wu and Jrng, 2017; Gharedaghloo *et al*., 2018). The aim of this work was evaluated computational fluid dynamic (CFD) techniques to mimic a saturated porous medium and its behavior against the discharge of polluting water

2 METHODOLOGY

The numerical technique which is used within Ansys Fluent considers a porous media model to define the sand region, which is represented by an empirically determined flow resistance, translated as an added momentum sink in the governing momentum equations. A computational fluid dynamics (CFD) model in Ansys Fluent® was built up to analyze a horizontal flume in which a section (50cm x 50 cm x 25 cm) was filled with fine sand, treated so that it could be characterized by known physical properties, namely porosity and permeability. The contained section of sand was crossed by a constant flow to become saturated. The discharge of the dye solution (soluble pollutant) from the top into the soil in order to obtain a constant flow, was carried out by a structure equipped with a trop-plein (Figure 1).
The two-dimensional CFD model was built up defining experimental work. The boundary and initial conditions were satisfied by the following points: 1. the inlet, water head at the left, 2. the inlet with a constant concentration at the top; 3. the outlet with atmospheric pressure, at the right; 4. the wall no slip at the bottom. A structured rectangular quadrilateral mesh was considered. To be sure that the mesh was not affecting the study, three different meshes were tested.

3 RESULTS

The simulations allow the analysis of the velocity distribution of dye and its transportation along through the porous media, for velocity of water V_{water}=0,002 m/s and V_{dye} = 0,02 m/s of discharge of polluted water from

ISBN: 978-90-824846-7-0

the top (Figure 2). The meshes – M1 (0.005m×0.005 m) with 5,000 cells, M2 (0.0035m× 0.0035m) with 10,153 cells, M3 (0.0025m×0.0025m) with 20,000 cells – were tested (Figure 3). The results obtained for the velocity profile showed reliability on M2 (0.0035m× 0.0035m). To analyze the impact of discharge of pollutants, four different velocities of V_{dye} were simulated, V_1 = 0,001 m/s, V_2 = 0,004 m/s, V_3 = 0,008 m/s and V_4 = 0,016 m/s.

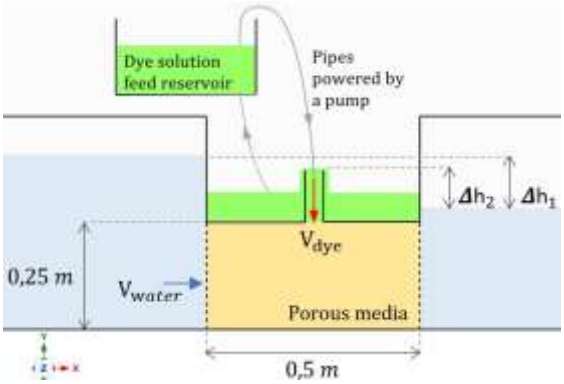

Figure 1. Physical model sketch.

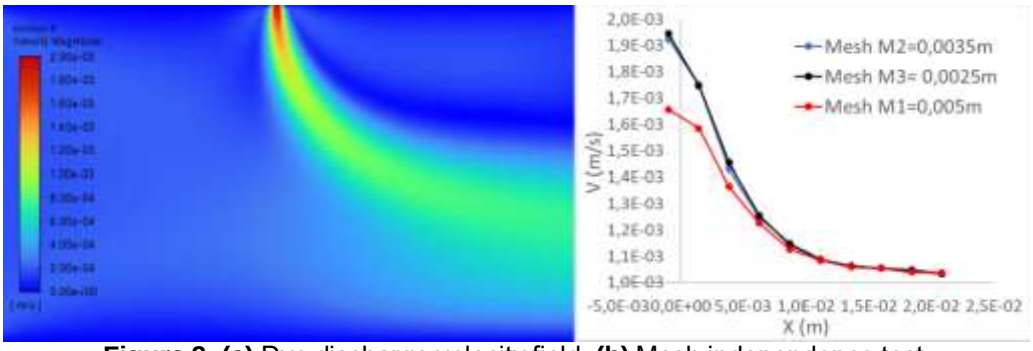

Figure 2: (a) Dye discharge velocity field. **(b)** Mesh independence test.

4 CONCLUSIONS

CFD based is a valid methodology to understand the process of transporting contaminants through subsurface porous media, with an appropriate computational mesh. As the dye discharge velocity increases, the reach of the contamination range expands in Y direction.

ACKNOWLEDGEMENTS
The authors would like to thank CAPES for the scholarship granted to the first author. The work had the support of the FCT (Portuguese Foundation for Science and Technology), through the Project UID/MAR/04292/2021, which was financed by MEC (Portuguese Ministry of Education and Science) and the FSE (European Social Fund), under the programs POPH/QREN (Human Potential Operational Programme from National Strategic Reference Framework) and POCH (Human Capital Operational Programme) from Portugal2020.

REFERENCES

Gharedaghloo, B., Price, J.S., Rezanezhad, F., Quinton, W.L. (2018). Evaluating the hydraulic and transport properties of peat soil using pore network modeling and X-Ray micro computed tomography, *Journal of Hydrology*. doi: https://doi.org/10.1016/j.jhydrol.2018.04.007.

Patil, S.B. & Chore, H. (2014). Contaminant transport through porous media: An overview of experimental and numerical studies. *Advances in environmental research*. 3. 10.12989/aer.2014.3.1.045.

Samadi, F., Shamshiri, S. (2019). *Numerical Modeling for Simulation of Contaminant Migration of Leachate in Soil Media.*

Seyedpour, S.M.; Janmaleki, M.; Henning, C.; Sanati-Nezhad, A.; Ricken, T. (2019). Contaminant transport in soil: A comparison of the Theory of Porous Media approach with the microfluidic visualization. *Science of the Total Environment.* doi: https://doi.org/10.1016/j.scitotenv.2019.05.095.

Wu, S.; Jeng, D. (2017). Numerical modeling of solute transport in deformable unsaturated layered soil. Water Science and Engineering. 10.10.1016/j.wse.2017.09.001.

IAHR YPN

Young Professionals Network

Hosted by
Spain Water and IWHR, China

IAHR AIRH

International Association for Hydro-Environment Engineering and Research

Hosted by
Spain Water and IWHR, China

Fluid Mechanics

Proceedings of the 2nd IAHR
Young Professionals Congress
30 Nov-2 Dec. 2021

Lock-exchange gravity currents propagating over roughness elements

Maria Rita Maggi [1], Claudia Adduce [2] and Maria Eletta Negretti [3]

[1,2] Roma Tre University, Rome, Italy,
mariarita.maggi@uniroma3.it, claudia.adduce@uniroma3.it
[3] Univ. Grenoble Alpes, CNRS, Grenoble INP, LEGI, 38000, Grenoble, France,
eletta.negretti@legi.cnrs.fr

ABSTRACT

Gravity currents flowing over rough surfaces are investigated by laboratory experiments and PIV is used to measure the instantaneous velocity field. Gravity currents are generated by the lock-exchange technique, by varying the height of the roughness elements and keeping constant their location. The bed roughness reduces the front and the streamwise velocity due to the introduction of an extra drag. Moreover a more homogeneous velocity distribution within the current is found.

Keywords: gravity currents; roughness; PIV; laboratory experiments.

1 INTRODUCTION

Gravity currents are buoyancy-driven flows generated by a density gradient due to a temperature or a salinity difference or solid particles in suspension. These currents occur spontaneously in nature for example as dense oceanic current or can be generated by anthropogenic causes as pollutant mass dispersing in a water body. The understanding of the mechanism involved in such flows is crucial for a proper modeling and for the development of risk mitigation measures. The lock-exchange technique and the use of particle image velocimetry (PIV) for the characterization of the velocity field have been widely used to investigate gravity currents in laboratory (Lombardi et al.,2015). Most of previous investigations deal with the currents flowing over flat surfaces (Ottolenghi et al.,2016). Few works studied the effect of bed roughness on the dynamics of gravity currents (Negretti et al.,2008; Tokyay et al.,2014), but despite all the research efforts, there is a lack of information of the bed roughness effect on the structure of gravity currents.
The contribution of this study is to characterize with PIV data the inner velocity of the lock released gravity currents and also to assess the effect of the bed roughness on them.

2 EXPERIMENTAL DETAILS

The laboratory experiments are conducted in 600 cm long Perspex tank, with horizontal bed and rectangular cross section of 25 x 30 cm^2 (Figure 1). A removable gate is placed at a distance x_0=50cm from the left wall dividing the tank into two volumes. The two reservoirs are filled up to the same water depth h_0=10cm. The left side of the tank is filled with salty water with initial density ρ_1, while the rest of the tank is filled with an ambient fluid of density $\rho_0<\rho_1$ ($\Delta\rho$=5±0.5 cm/s^2).

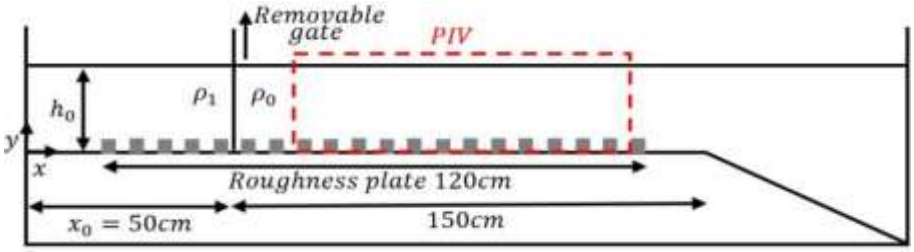

Figure 1. Sketch of the tank used to perform laboratory experiments.

ISBN: 978-90-824846-7-0

LEGO® Bricks are used as bottom roughness elements with a constant quadratic section of 0.78×0.78 cm^2 and a constant spacing of 5.2cm in x-z directions. Four series of experiments are performed: three with a constant height of the roughness elements (h_1=0.64cm, h_2=1.6cm, h_3=2.56cm) and one under smooth bed conditions without the use of the roughness elements.

The flow velocities are determined using the optical non-intrusive experimental technique PIV. Polyamide particles with a diameter of d_p =50μm and a specific density of ρ_p =1.016g/cm^{-3} are added in all tank. The generated laser sheet has a length of approximately 1m and a thickness of 5mm and it is positioned in the middle of the channel. Two fields of view are captured in the x-y directions, with a size of 64.7 x 11.3cm each one, located respectively at 8cm and 51.3cm from the gate. The images are captured with a CCD camera (FlowMaster3, 14 bit, 1600×1200 pixels) at a frame rate of 21.5Hz. With the Software package DaVis (LaVision) the velocity fields were computed using a cross-correlation PIV algorithm.

The laser starts firing, synchronized with the CCD camera, before removing the lock gate to ensure that measurements are being performed when the current enters the visualization window. The zero time reference is associated to the gate removal. Thereafter, the vertical column of heavier fluid collapses, forming a heavier gravity current developing along the tank bed, while a lighter density current formed by ambient fluid develops above the denser current in the opposite direction.

Figure 2 shows the instantaneous maps of the streamwise velocity u, for two of the runs performed when the current reaches almost the limit of the visualization window (1.6m). The frontal region of the current loses definition and the forward speed of the current decreases as the height of the roughness increases. By continuity the ambient fluid above the dense current decelerates too, and this deceleration seems to be related to the LEGO® Bricks height (h), the larger the h the larger the deceleration. Furthermore, Figure 2 shows some recirculation areas, with negative u values, near the bottom between the LEGO® structures, absent in the smooth case. The higher the height of the roughness elements, the stronger are the recirculation patterns between the elements that separate the main current from the bottom area. Indeed the high velocity regions within the dense flow are mostly positioned above the roughness level.

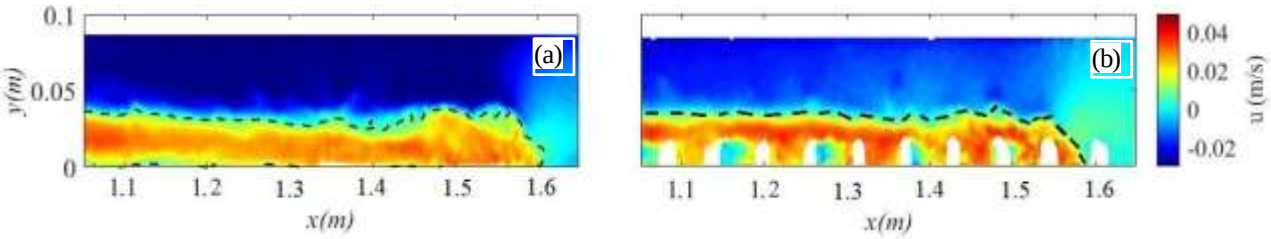

Figure 2. Streamwise velocity field, u, after the current has travelled $1.6m$ for the smooth run (a) and h_2 run (b) at $t = 23.07s$ end $t = 26.33s$, respectively.

REFERENCES

Lombardi, V., Adduce, C., Sciortino, G. and La Rocca, M. (2015). Gravity currents flowing upslope: Laboratory experiments and shallow-water simulations. *Phys. Fluids,* 27(1), 016602.

Negretti, M.E., Zhu, D.Z., and Jirka, G.H. (2008). The effect of bottom roughness in two-layer flows down a slope. *Dyn. Atmos. Oceans,* 45, 466-68.

Ottolenghi, L., Adduce, C., Inghilesi, R., Armenio, V., Roman, F. (2016). Entrainment and mixing in unsteady gravity currents. *J. Hydraul. Res,* 54, 541-557.

Tokyay, T., Constantinescu, G., and Meiburg, E. (2014). Lock-exchange gravity currents with a low volume of release propagating over an array of obstacles. *J. Geophys. Res. Oceans,* 119 (5), 2752-2768.

ISBN: 978-90-824846-7-0

Proceedings of the 2nd IAHR
Young Professionals Congress
30 Nov-2 Dec. 2021

Numerical simulation of droplets arrangement inside a pore using LBM

Stefano Miliani [1], Michele La Rocca[2], Andrea Montessori[3] and Pietro Prestininzi[4]

[1,2,4] Roma Tre University, Rome, Italy,
stefano.miliani@uniroma3.it, michele.larocca@uniroma3.it, pietro.prestininzi@uniroma3.it
[3] Istituto per le Applicazioni del Calcolo CNR, Rome, Italy,
and.montessori@gmail.com

ABSTRACT

Emulsions are ubiquitous in engineering applications. Their accurate modelling is required in fields like Enhanced Oil Recovery and Soil Washing. The employment of physical models may be difficult, hence the resort to numerical ones. In this study, a Lattice Boltzmann Method based multiphase model is employed and validated using previously published work as benchmark. The model proves to be able to reproduce complex patterns of emulsion flows in confined geometries, therefore opening to applications encompassing realistic conditions.

Keywords: CFD; LBM; numerical method; multiphase flow; flow in porous media.

1 INTRODUCTION

Enhanced Oil Recovery (EOR) and Soil Washing (SW) have recently drawn a consistent amount of attention; indeed, several studies have been carried out in order to improve their performance: in particular, it has been demonstrated that emulsions, created using surfactants, drastically increase their efficiency (Perrazzo et al., 2018). Nonetheless, the study of these phenomena using physical model may suffer of low repeatability and high cost. Hence, numerical models have been employed, among which the Lattice Boltzmann Method (LBM) (Wei et al., 2020), a mesoscopic approach where fluids are described in terms of the movement of particles in contrast to traditional method based on continuum models (Succi, 2001). In this study, a LBM based multiphase model, able to simulate near-contact interactions (NCIs) created by surfactants, is employed to simulate emulsion flows in a porous chamber. In particular, the model is validated against previously published data.

2 METHODS

For an exhaustive review on LBM, the reader is referred to Succi (2001). An in-house implementation of the LBM based model proposed by Montessori et al. (2019) is employed. The model is governed by the equations:

$$f_a^k(x + e_a\Delta t, t + \Delta t) = f_a^k(x,t) + \Omega_a^k[f_a^k(x,t)] \quad [1]$$

where f_a^k is the probability distribution function of the k^{th} ($k = 1, 2$) flow component and represents the probability of finding a particle at a position x and time t; a is an index spanning over the discrete lattice directions ($a = 0, \ldots, 26$), e_a is the lattice discrete velocity and Ω^k_a is the collision operator. Ω^k_a accounts for the fluid viscosity, the effect of the surface tension σ and the mutual diffusion of the two components.
NCIs are simulated adding to Eq. [1] a repulsive force only on the interface, defined as in Eq. [2].

$$F_{rep} = -A_h[d(x)]n\delta_i \quad [2]$$

where A_h the magnitude of the NCIs, $d(x)$ the distance between two interfaces, n the normal unit vector to the interfacial surface and δ_i a function which confines the effects of the force only on the interface.

3 RESULTS AND DISCUSSION

ISBN: 978-90-824846-7-0

The LBM model is validated using the work of Jose and Cubaud (2012) as benchmark. The experiment consists in the generation of droplets with viscosity μ_0 and diameter D_0 by means of a t-junction located at the beginning of an inlet channel of width h; droplets are carried by another fluid of viscosity μ_w inside a porous chamber and then through an outlet channel (see Figure 1). In the LBM model, the fluids viscosity ratio is set to *1.9*; droplets generation is performed by means of an internal periodic boundary condition located inside the inlet channel; the outflow is achieved by an open boundary.

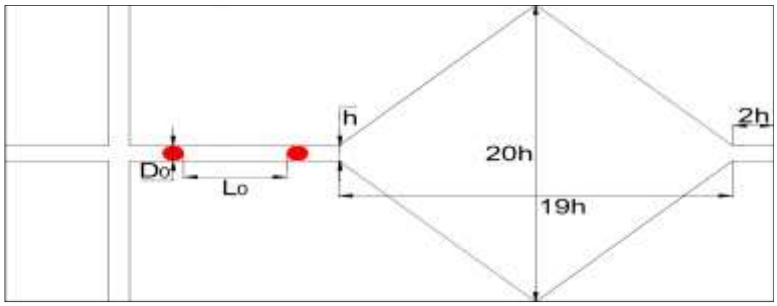

Figure 1. Sketch of the physical model in Jose and Cubaud (2012) [Adapted from Jose and Cubaud (2012)].

The phase diagram of the experiments carried out by Jose and Cubaud (2012) and the LBM simulations is shown in Figure 2a: the capillary number *Ca* ($Ca=U\mu_w/\sigma$ with U mean velocity in the inlet) appears on x-axis while the ratio L_0/D_0 (L_0 the distance between two droplets surfaces in the inlet), representing the droplets generation frequency, on the y-axis. With different combination of these two parameters, the droplets inside the pore assume particular arrangements (Jose and Cubaud, 2012). Figure 2b shows the results from the LBM: as shown, the numerical model can reproduce these geometrical patterns with ease.

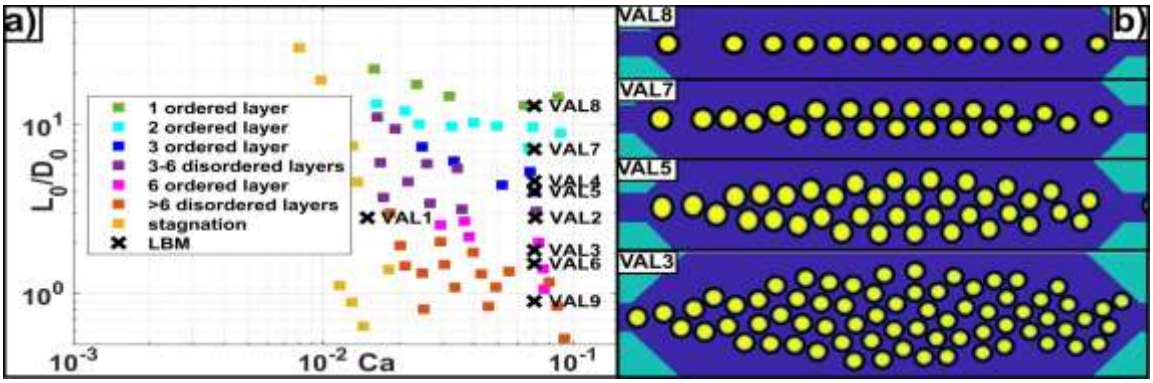

Figure 2. a) Phase diagram: colored squares represent the different droplet arrangements found in Jose and Cubaud (2012); crosses are the LBM simulations. b) Droplets arrangements simulated by the LBM model.

4 CONCLUSIONS

In conclusion, the present LBM model, explicitly accounting for NCIs through a minimal model, proves to be able to simulate these phenomena more than satisfactorily, allowing to explore parameters spaces relevant to technical scenarios (e.g. solid walls wettability, presence of surfactants) in order to improve both EOR and SW.

REFERENCES

Jose, B.M., Cubaud, T. (2012). Droplet arrangement and coalescence in diverging/converging microchannels. *Microfluid Nanofluid,* 12, 687-696.

Montessori, A., Lauricella, M., Tirelli, N. and Succi, S. (2019). Mesoscale modelling of near-contact interactions for complex flowing interfaces*. Journal of Fluid Mechanics*, 872, 327-347.

Perrazzo, A., Tomaiuolo, G., Preziosi, V. and Guido, S. (2018). Emulsions in porous media: From single droplet behavior to applications for oil recovery. *Advances in Colloid and Interface Science*, 256, 305-325.

Succi, S. (2001). *The Lattice Boltzmann Equation: For Fluid Dynamics and Beyond*. Oxford, Claredon Press.

Wei, B., Hou, J., Sukop, M.C., Du, Q. and Wang, H. (2020). Flow behaviors of emulsions in constricted capillaries: A lattice Boltzmann simulation study. *Chemical Engineering Science*, 227, 115925.

ISBN: 978-90-824846-7-0

Proceedings of the 2nd IAHR
Young Professionals Congress
30 Nov-2 Dec. 2021

A priori estimation of the performance of WENO and UWC schemes as iLES methods

Pablo Solán-Fustero[1], Adrián Navas-Montilla[1], Esteban Ferrer[2,3], Juan Manzanero[2,3] and Pilar García-Navarro[1]

[1] Fluid Mechanics Department-Aragon Institute of Engineering Research (I3A), Universidad de Zaragoza, Spain
psolfus@unizar.es

[2] ETSIAE-UPM - School of Aeronautics, Universidad Politécnica de Madrid

[3] Center for Computational Simulation, Universidad Politécnica de Madrid.

ABSTRACT

Implicit large eddy simulation (iLES) methods are able to resolve the large eddies in the flow, whereas the effect of the small-scale turbulent fluctuations is dissipated using the errors of the numerical discretization. This work aims at finding and evaluating a-priori guidelines for the computation of under-resolved turbulent flows by performing a thorough study of the numerical errors. In particular, we study the 3-rd, 5-th and 7-th order UWC and WENO reconstructions in space, and 3-rd and 4-th order Runge-Kutta time integrators. We use the approximate von Neumann analysis for non-linear schemes introduced by Pirozzoli, 2006. Moreover, we apply the "1% rule" proposed by Moura, Sherwin & Peiró, 2015, to the dispersion-diffusion curves to determine the range of wavenumbers that are accurately resolved. The cut-off wavenumbers defined by the "1% rule" are evidenced to serve as a good estimator of the beginning of the dissipation region of the energy cascade.

Keywords: dispersion-diffusion analysis; high-order schemes; Weighted Essentially Non-Oscillatory WENO; burgers' turbulence; implicit Large Eddy Simulation.

1 INTRODUCTION

Large eddy simulation (LES) methods have become over the last decade a valuable tool for the simulation of scientific and engineering problems of hydraulics. This eddy-resolving approach gives a high level of resolution in space and time when compared to other traditional methods (e.g. Reynolds-averaged Navier–Stokes equations), being key for the understanding of the underlying physical phenomena in the problems of interest in hydraulics. LES methods have been successfully applied to the resolution of free-surface flow in curved channels and meanders, sediment transport, flow around hydraulic structures, resonant flow in channels with lateral cavities, etc. (Stoesser, 2014).

The implicit LES method is a particular case of LES methods in which the numerical truncation errors of the discretization scheme play the role of the sub-grid model. High-order schemes can be used for this purpose due to their compromise between high accuracy and efficiency at all scales.

The von Neumann spectral analysis is a procedure used to check the validity of linear numerical schemes. In the non-linear case, an approximate version of this spectral analysis based on the fast Fourier transform is used. To test the spectral analysis on high-order schemes we use the Burgers' turbulence problem, which acts as a 1D version of the turbulent behavior. With this, we can obtain a-priori guidelines for the computation of under-resolved turbulent flows (Solán-Fustero et al., 2021).

2 METHODOLOGY

In this work we use high-order numerical schemes because they provide high accuracy at all scales. Furthermore, their discretization errors may help to dissipate turbulent fluctuations at the small scales, which would be useful in the framework of iLES methods.

The spatial extension to high order is carried out, on the one hand, by means of central upwind schemes (UWC), which are linear and use centered stencils. On the other hand, we have WENO schemes that are non-linear and use combinations of non-centered stencils to avoid oscillations in presence of shock waves. High-order temporal integration is carried out by means of third and fourth order Runge-Kutta method.

The spectral analysis allows the development of predictive tools, such as the "1% rule" proposed by Moura, Sherwin & Peiró, 2015. This rule estimates the effective resolution of the numerical scheme in terms of the largest wavenumber that can be resolved with error smaller than 1%. The 1% wavenumbers are good predictors of the start of the dissipation zone, as it can be seen in the results. For this reason, they are called cut-off

wavenumbers. They are computed using the 1D advection equation and stored to test the 1D Burgers' turbulence problem.

3 NUMERICAL RESULTS

In the results, we study the performance of the above mentioned numerical schemes on the 1D Burgers' turbulence problem. Their numerical energy cascades are compared with the ideal tendencies of the problem. In the plots we can also see the cut-off wavenumbers previously computed with the 1D linear equation.

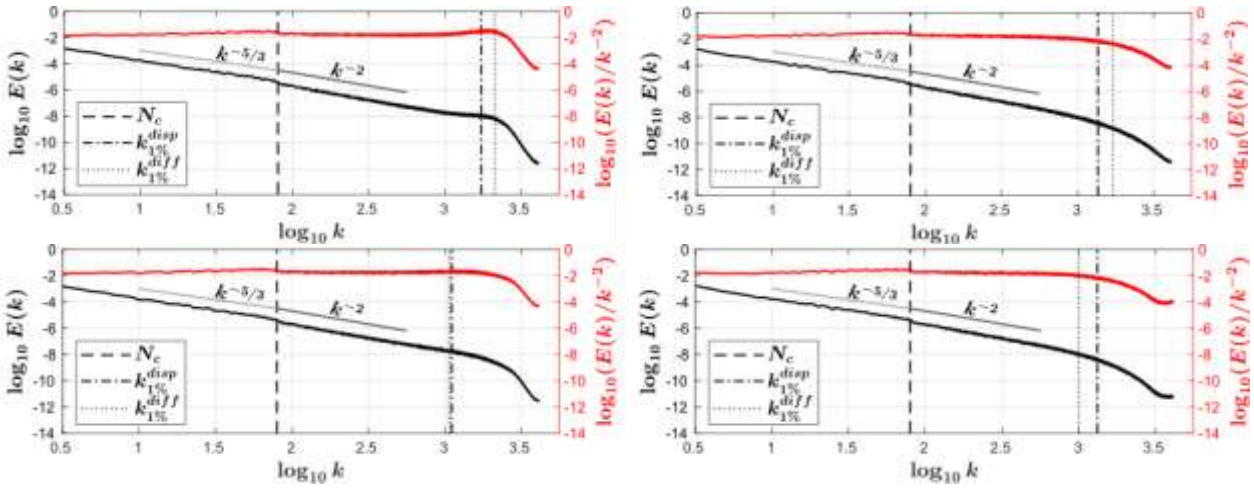

a. UWC7-RK3 (left) and WENO7-RK3 (right) schemes with CFL=0.1 (top) and CFL=0.9 (bottom).

4 CONCLUSIONS

We show that WENO schemes are more diffusive than UWC schemes, leading to stable simulations at the price of more dissipative results. However, it is concluded that both UWC and WENO schemes may be suitable schemes for iLES turbulence modelling, given their numerical dissipation level acting at the appropriate wavenumbers (Solán-Fustero et al, 2021).

ACKNOWLEDGEMENTS

This work was funded by the Spanish Ministry of Science and Innovation under the research project PGC2018-094341- B-I00 (Solán-Fustero, Navas-Montilla and García-Navarro). This work has also been partially funded by Gobierno de Aragón through Fondo Social Europeo (T32-20R, Feder 2014-2020 "Construyendo Europa desde Aragón") (Solán-Fustero, Navas-Montilla and García-Navarro).

REFERENCES

Maulik, R. and San, O. (2018). Explicit and implicit LES closures for Burgers' turbulence. *Journal of Computational and Applied Mathematics*, 327, 12–40.

Moura, R., Sherwin, S. and Peiró, J. (2015). Linear dispersion-diffusion analysis and its application to under-resolved turbulence simulations using discontinuous Galerkin spectral/hp methods. *J. Comput. Phys*., 298, 695–710.

Pirozzoli, S. (2006). On the spectral properties of shock-capturing schemes, *J. Comput. Phys*., 219, 489–497.

Shu, C.W. (2009). High Order Weighted Essentially Nonoscillatory Schemes for Convection Dominated problems. *SIAM Review*, vol. 51, n. 1, 82–126.

Solán-Fustero, S., Navas-Montilla, A., Ferrer, E., Manzanero, J. and García-Navarro, P. (2021). Application of approximate dispersion-diffusion analyses to under-resolved Burgers' turbulence using high resolution WENO and UWC schemes, *J. Comput. Phys*., 435, 489–497.

Stoesser, T. (2014). Large-eddy simulation in hydraulics: Quo Vadis? *Journal of Hydraulic Research*. 52. 441-452.

Proceedings of the 2nd IAHR
Young Professionals Congress
30 Nov-2 Dec. 2021

A cross-validation study of computational methods for droplet spreading

Juan Mairal[1] and Lennon Ó Náraigh[2]
[1] Universidad de Zaragoza, Zaragoza, Spain
mairalascaso@unizar.es
[2] School of Mathematics and Statistics, University College Dublin, Ireland
onaraigh@maths.ucd.ie

ABSTRACT

The impact of a droplet on a smooth surface is a problem that can be solved using different models, each of them having their own idiosyncrasies and particularities. These differences appear mainly on the treatment of the contact-line, the place where the droplet's interface meets the substrate. This work seeks to validate the Volume of Fluid method included in the popular CFD library OpenFOAM by comparing it with the Diffuse Interface method, which has undergone successful testing before and which is more "closed" in the sense that it does not need many parameters to be chosen. The validation is done in 2D and shows that behavior of the droplet is particularly similar in the initial spreading phase, and it diverges in later stages of the impact. Convergence tests show that coarser meshes can be used in Diffuse Interface but more resolution is needed in Volume of Fluid due to the unpredictability of the entrapped bubble dynamics. At the end, by comparing the methods, a set of parameters can be chosen in Volume of Fluid, looking towards using them in future 3D simulations.

Keywords: droplet; OpenFOAM; Diffuse interface; volume of fluid; contact-line.

1 INTRODUCTION

A droplet impacting on a smooth, hard, and chemically homogeneous surface spreads and contracts in a damped harmonic oscillator fashion until it reaches its static equilibrium configuration. This work is concerned with the dynamic phase of the impact (Figure to the right), for which several different models exist. The key difference between them is how they tackle the contact-line problem, since it was found that imposing the no-

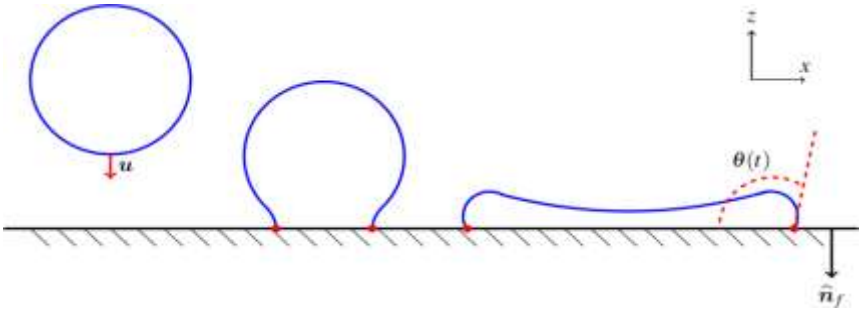

Figure 1: Schematic representation of droplet impact and spreading. The contact angle θ(t) plays a pivotal role in this discussion.

slip condition of no relative motion between the wall and the fluid leads to a stress singularity when applied at contact line (Davis, 1974). Some approaches introduce new physics. Slip-Length modeling allows for a little slip at the contact line proportional to the normal velocity to the substrate. Precursor Film modeling introduces an infinitely long, infinitely thin layer of fluid from the contact line beyond through the addition of a Van der Waals-like potential. Finally, the Diffuse Interface method introduces a certain width to the interface, allowing diffusion between the water and the air and thus the contact line moves naturally. In this work, the Diffuse Interface method is used as a baseline in a 2D validation of the available method in OpenFOAM, which is made up of the popular Volume of Fluid method to solve the two-phase flow and an imposed condition on the angle [1]. The

ISBN: 978-90-824846-7-0

conditions available in OpenFOAM are the constant angle condition in which θ(t) does not change, and the *tanh* model [2].

Imposed angle condition

$$\theta(t) = f(\theta_e, \theta_a, \theta_r, U_{CL}, \ldots) \quad [1]$$

OpenFOAM's dynamic contact angle
U_θ is a parameter velocity that needs finding

$$\theta = \theta_e + (\theta_a - \theta_r)\tanh\left(\frac{U_{wall}}{U_\theta}\right) \quad [2]$$

2 METHODOLOGY

The simulations have been carried out in a cluster of ICHEC (Irish Center for High-End Computing). First, a validation of the two methods with respect to established multiphase test cases is carried out, without any contact lines involved, following (Ding, 2007). The positive results of this validation awarded the confidence to go forward with the droplet impact tests. First, a set of simulations was done in Diffuse Interface with different equilibrium contact angles. Then, the mesh convergence was tested with excellent results: not a high spatial resolution is needed when using the Diffuse Interface method. Later, the same was done using the Volume of Fluid in two series of tests. The first used a contact contact angle condition and the second one used the dynamic contact angle condition [2].

3 CONCLUSIONS

Through comparing the results, it is found that the Volume of Fluid method in OpenFOAM with both the static and the dynamic contact angle [2] conditions are able to reproduce the behavior of the spreading droplet shown in Diffuse Interface simulations. The dynamic contact angle is preferred as it is believed that it has better potential to also model the receding phase correctly. In general, velocities of the receding phase seem to be underestimated in Volume of Fluid, probably because the imposition of a contact angle value restricts how small it would need to become to match recession in the Diffuse Interface method. A further complication is found in the form of an entrapped bubble whose dynamics are quite unpredictable and may even cause break up of the droplet. Moreover, its small size causes the Volume of Fluid simulation to require a much finer mesh for convergence, which increases computational costs. Nevertheless, having identified these problems opens the door to future research possibilities in tackling them. In addition, the parameters found through the validation can be transported to 3D simulations in which a richer phenomenology can be studied.

REFERENCES

References should appear together at the end of the extended abstract, listed alphabetically by last name of the first author. Please use Harvard APA 6 or 7 citation standard.

Davis, S. H. (1974). On the motion of a fluid-fluid interface along a solid surface. *Journal of Fluid Mechanics*, *65*(1), 71-95.

Ding, H., Spelt, P. D., & Shu, C. (2007). Diffuse interface model for incompressible two-phase flows with large density ratios. *Journal of Computational Physics*, *226*(2), 2078-2095.

Josserand, C., & Thoroddsen, S. T. (2016). Drop impact on a solid surface. *Annual review of fluid mechanics*, *48*, 365-391.

ISBN: 978-90-824846-7-0

Proceedings of the 2nd IAHR
Young Professionals Congress
30 Nov-2 Dec. 2021

Settling and rising patterns of microplastics in aquatic systems: a numerical study

Zihe Zhao [1], Shooka Karimpour [2]

[1,2] York University, Toronto, Canada,
[1] email: zihezhao@yorku.ca
[2] email: shooka.karimpour@lassonde.yorku.ca

ABSTRACT

The pollution of microplastics has become a growing concern in aquatic environments. Microplastics' dynamics in such environments deviates from natural particles and other contaminants, due to their size and shape variability. In the present study, the settling and rising dynamics of micro-sized plastic particles were simulated using a three-dimensional numerical model. For particles with regular shapes, the settling patterns obtained from the present numerical model match well with the previous theoretical models derived from the settling of natural sediments. Terminal settling velocities obtained from the present study are also compatible with previous experimental data for natural sediments. Further investigations are being conducted to model the settling and rising dynamics of microplastics with complex shapes, e.g. fibers, sheets, and fragments. The results from the present study will accurately parameterize irregularly shaped microplastics, which is essential in creating large-scale models which can accurately predict the fate and transport history of microplastics.

Keywords: microplastics; environmental hydrodynamics; numerical model; computational fluid dynamics; ANSYS Fluent.

1 INTRODUCTION

Ever since plastics have been introduced to the industry in the 1950s, their production has increased exponentially. Enhanced by increasing plastic production rates, the pollution of microplastics (MPs) in aquatic environments has become a growing concern in recent years. MPs are commonly defined as plastic particles with diameters smaller than 5 mm (Arthur et al., 2009). Because MPs can be transported over long distances by water currents, endangering the organisms over wide areas, the study of their hydrodynamics has become increasingly important (Shamkhany & Karimpour, 2021).

To describe the transport behaviors of MP particles in aquatic environments, it is essential to investigate their settling and rising patterns, which reveal their depositional tendency in a quasi-static fluid (Khatmullina & Isachenko, 2017; Hurley et al., 2018). This research direction will offer insights on the transport distance and destination of MP particles, providing knowledge in assessing the harm of MPs to certain aquatic organisms, devising the methods for its prevention, and predicting the outcome of its treatment.

MP particles, having a wide variety of densities, sizes, and shapes, are very difficult to characterize. So far, numerical models on the settling patterns of MPs are very limited. To date, all models (e.g., Kooi et al., 2017) fall short in accounting for MPs' complex shapes. A model that could parameterize the MP particles with complex shapes is crucial in predicting the hydrodynamics of MPs in natural aquatic environments.

2 METHODS

The present study employs a three-dimensional numerical scheme to simulate the particle settling and rising dynamics. The MP-sized particle is represented in the Finite Volume-based numerical model as a cavity with a predefined shape, density, and moment of inertia. The six-degree-of-freedom (6DOF) method is employed where the numerical cavity moves as it is subject to the gravitational and drag force. An overset mobile mesh method is employed to capture the particle shape and the fluid motion surrounding the MP-sized particle. The computational domain consists of one set of coarser background mesh with uniform mesh size and a finer refinement mesh surrounding the particle (Figure 1). The overset mesh is designed to contain the backflow behind the settling (or rising) particle. The flow evolution within the refinement zone is calculated according to the refinement mesh, whereas the flow evolution outside the refinement zone is computed through the

ISBN: 978-90-824846-7-0

background mesh. At every time step, flow data is exchanged at the refinement zone boundary over the two meshes.

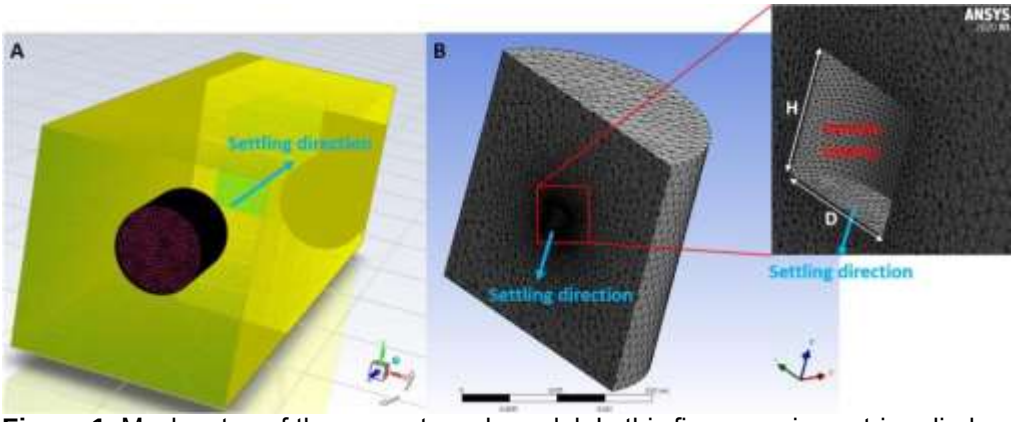

Figure 1. Mesh setup of the overset mesh model. In this figure, an isometric cylinder-shaped particle (diameter D = height H) is used as an example. (A) The whole domain consists of one background mesh (outlined in yellow) and one refinement mesh surrounding the particle (outlined in red). (B) In the refinement mesh zone, the mesh refines progressively towards the particle (cavity). The refinement zone has the same shape as the particle with 10 times the length of the particle.

3 DISCUSSIONS

The model in the present study numerically solves the flow velocity and particle position during the settling of a pre-defined MP particle. Through the present model, MP particles with complex shapes can be parameterized. Preliminary results suggest that the drag coefficients associated with settling velocities of negatively buoyant MPs of regular shapes, including spherical and cylindrical particles, are dependent on the particle's Reynolds number and are consistent with experimental data available for sediments. The present approach is also applied to MP particles with irregular shapes, e.g., thin cylinders which resemble MP films.

4 CONCLUSIONS

The computations in the present study are shown to be capable of simulating the settling dynamics of MP-sized particles near their upper size limit of 4 mm. This research will be extended to parameterize all MP particles with irregular shapes, which is essential to create an accurate large-scale model for the prediction of the fate and transport history of MPs in natural aquatic environments.

REFERENCES

Arthur, C., Baker, J. E., & Bamford, H. A. (2009). Proceedings of the International Research Workshop on the Occurrence, Effects, and Fate of Microplastic Marine Debris, September 9-11, 2008, University of Washington Tacoma, Tacoma, WA, USA.

Hurley, R., Woodward, J., & Rothwell, J. J. (2018). Microplastic contamination of river beds significantly reduced by catchment-wide flooding. *Nature Geoscience*, *11*(4), 251-257.

Khatmullina, L., & Isachenko, I. (2017). Settling velocity of microplastic particles of regular shapes. *Marine pollution bulletin*, *114*(2), 871-880.

Kooi, M., Nes, E.H.V., Scheffer, M. & Koelmans, A.A. (2017). Ups and downs in the ocean: effects of biofouling on vertical transport of microplastics. *Environmental science & technology*, *51*(14), 7963-7971.

Shamkhany, A. & Karimpour, S. (2021). The role of Microplastics' size and density on their vertical mixing and transport. *In the proceeding of the Canadian Society of Civil Engineering Annual Conference*.

ISBN: 978-90-824846-7-0

Proceedings of the 2nd IAHR
Young Professionals Congress
30 Nov-2 Dec. 2021

Hydrodynamics of floating vegetation in lateral cavities

Felipe Rezende da Costa [1], Luiz Eduardo Domingos de Oliveira [1] and Johannes Gérson Janzen [1]
[1] Universidade Federal de Mato Grosso do Sul, Campo Grande, Brasil
e-mail felipe.costa@ufms.br

ABSTRACT

This study evaluated the effect of floating vegetation inside lateral using Computational Fluid Dynamics (CFD). The resistance generated by the vegetation was represented by a porous zone. In all cases, the presence of floating vegetation reduced the velocity magnitude in the innermost part of the cavity compared to the non-vegetated areas. The increase of vegetation depth decreased flow velocity in the lateral cavity, reaching its maximum effect at an emergent case.

Keywords: lateral cavities; floating vegetation; computational fluid dynamics (CFD).

1 INTRODUCTION

Lateral cavities are an important structure of rivers and channels (Jackson et al. 2013). These structures promote the deceleration of the flow and the presence of gyres. From an environmental point of view, lateral cavities benefit the channel by: (1) storing sediments, (2) mitigating riverbank erosion, (3) favoring vegetation growth and (4) providing refuge for aquatic organisms Xiang et al. 2019). The presence of vegetation can significantly change the hydrodynamics and mass exchange in lateral cavities (Xiang et al. 2019). However, the effect of vegetation in lateral cavities is a recent topic and floating vegetation was still not studied. Therefore, the objective of this study is to analyze the impact of floating vegetation depths in the hydrodynamics of lateral cavities.

2 METHODOLOGY

The geometry consisted of a channel with a lateral cavity (Figure 1) based on the experiments of Xiang et al. (2019). The main channel was 1.25m long and 0.30m wide. The cavity was 0.25m long and 0.15m wide. The depth was 0.10m. The mean velocity in the channel was U = 0.101m/s, which resulted in a Reynolds number of 9000 and a Froude number of 0.102. The bottom (z=0 m) and the top of the channel (*z*=0.10 m) were defined as free-sliding walls. The channel inlet (x = 0 m) velocity profile was previously developed in a periodic simulation. The outlet plane at x = 1.25 m was considered as a zero-gradient surface. All other planes were considered as hydraulically smooth walls with velocity equal to zero.
The resistance caused by the vegetation was represented with an anisotropic porous medium, modelled with the Darcy-Forchheimer equation. The drag coefficients of the porous media, inertial (f) and viscous (d), were calculated with the Ergun equation in the x and y-axes. In the vertical direction, the vegetation diameter was equal to an equivalent hydraulic diameter (Oldham and Sturman 2001) that reduced the drag coefficient in the z-axes, The coefficients f and d were chosen to maintain a value of 0.1332% for the vegetation density (Table 1). The simulation was computed using OpenFOAM.

Table 1. Vegetation levels and the calculated Darcy-Forchheimer coefficients.

Case	z/H	Horizontal direction (x and y-axes)		Vertical direction (z-axes)		
		d (1/m2)	*f* (1/m)	d_h (m)	*d* (1/m2)	(1/m)
0	0	0	0	0	0	0
1	1	116.53	3.09	0.7624	0.00045	0.00608
2	0.8	74.52	2.47	0.7624	0.00029	0.00486
3	0.6	41.88	1.85	0.7624	0.00016	0.00364
4	0.4	18.60	1.23	0.7624	0.00007	0.00243
5	0.2	4.65	0.62	0.7624	0.00002	0.00121

ISBN: 978-90-824846-7-0

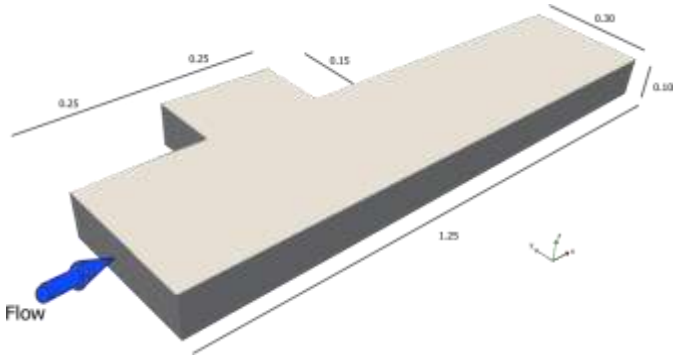

Figure 1. Computational domain. The direction of flow is indicated by the blue arrow. Dimensions are in meters. The origin of the coordinates (x, y, z = 0) comes from the lower left corner of the channel.

3 RESULTS

The presence of floating vegetation reduced the velocity in the innermost part of the cavity compared to the non-vegetated case. In cases where the ratio between vegetation height *(h)* and channel depth *(H)* was less than *0.6*, there was an increase in velocity in the region close to the cavity entrance in the vegetated region. Furthermore, in vegetated regions the center of the vortex moved along the y axes, towards the entrance of the cavity. Increasing the height of the cavity intensifies the effects of velocity reduction in the vegetated lateral cavity, reaching its maximum effect at *h = H.*

4 CONCLUSIONS

The effect of floating vegetation in the hydrodynamics of lateral cavity occurs in two phases: for h/H > 0.6, all vegetated part of the cavity decelerates faster than the regions close to the main channel; for h/H < 0.6, when the part closer to the cavity entrance has a greater velocity in the vegetated region, this part becomes larger as the vegetation becomes shallower, but in all when the depth is less than 0.4H, the region has the same size (y = 0.5H). Finally, as the depth of vegetation increased, more energy of the flow was absorbed, reaching the slowest flow when the cavity became fully filled with vegetation.

ACKNOWLEDGEMENTS

This work was carried out with the support of Conselho Nacional de Desenvolvimento Científico e Tecnológico (CNPq) and Lobo Carneiro at Núcleo de Atendimento em Computação de Alto Desempenho (NACAD).

REFERENCES

Jackson, Tracie R., Roy Haggerty, Sourabh V. Apte, and Ben L. O'Connor. 2013. "A Mean Residence Time Relationship for Lateral Cavities in Gravel-Bed Rivers and Streams: Incorporating Streambed Roughness and Cavity Shape." *Water Resources Research* 49 (6): 3642–50. https://doi.org/10.1002/wrcr.20272.

Oldham, C. E., and J. J. Sturman. 2001. "The Effect of Emergent Vegetation on Convective Flushing in Shallow Wetlands: Scaling and Experiments." *Limnology and Oceanography* 46 (6): 1486–93. https://doi.org/10.4319/lo.2001.46.6.1486.

Xiang, Ke, Zhonghua Yang, Wenxin Huai, and Ran Ding. 2019. "Large Eddy Simulation of Turbulent Flow Structure in a Rectangular Embayment Zone with Different Population Densities of Vegetation." *Environmental Science and Pollution Research* 26 (14): 14583–97. https://doi.org/10.1007/s11356-019-04709-x.

Proceedings of the 2nd IAHR
Young Professionals Congress
30 Nov-2 Dec. 2021

The numerical modelling of rock-ice avalanches in the hyperbolic range: first results

Stefania Sansone [1]

[1] Department of Civil, Environmental and Mechanical Engineering, University of Trento, Trento, Italy, stefania.sansone@unitn.it

ABSTRACT

This work aims to model numerically rock-ice avalanches, granular-liquid three-phase flows composed of rock, ice, and a liquid. The mathematical model considered corresponds to the one-dimensional depth-integrated version of a rock-ice avalanche model previously developed. Since this mathematical model loses the hyperbolicity for specific ranges of the liquid Froude number, we derive mathematical expressions that link the limits of the region where the hyperbolicity is lost to the other flow variables. Thanks to these mathematical expressions, the numerical solutions are computed in the hyperbolic case by applying a specific numerical scheme. The test case considered corresponds to the uniformly accelerated flow, whose analytical solution is derived and compared with the numerical solution. This comparison shows that the numerical solution approximates the analytical solution accurately, thus proving that the numerical scheme used is an accurate numerical method for the mathematical model considered.

Keywords: rock-ice avalanches; hyperbolic region; analytical solution; numerical solution.

1 INTRODUCTION

Rock-ice avalanches are granular-liquid free-surface flows that consist of three phases (rock, ice, and a liquid) and are affected by the ice melting, a physical process responsible for the continuous supply of water to the mixture. For a good hazard assessment and management in cold mountainous regions, it is necessary to provide mathematical and numerical models able to predict the flow of this type of phenomenon. However, only a few mathematical models for rock-ice avalanches exist in the literature (Pudasaini and Krautblatter 2014, Bartelt et al. 2018, Sansone et al. 2021). In this work, we consider the one-dimensional depth-integrated partially isokinetic rock-ice avalanche model proposed by Sansone et al. (2021). This model treats rock, ice and liquid as different phases characterized by their concentration and moving downslope with two distinct velocities, i.e., one referred to the liquid phase and the other to the overall solid phase (rock plus ice). As a result, the model is composed of three mass balances and two momentum balances, where the ice melting is taken into account in terms of mass and momentum transfers between ice and the liquid phase.

2 NATURE OF THE EQUATION SYSTEM

A preliminary step for the computation of numerical solutions for the mathematical model chosen consists in studying the nature of the equation system. As shown in Sansone et al. (2021), the 1D partially isokinetic rock-ice avalanche model is hyperbolic only for specific ranges of the liquid Froude number. More precisely, by defining $Fr_1^{\#}$ and $Fr_1^{\$\%}$ as the boundaries of the hyperbolic regions, hyperbolicity is guaranteed for liquid Froude numbers lying in the ranges $0 < Fr_1 < Fr_1^{\#}$ and $Fr_1 > Fr_1^{\$\%}$. Outside these ranges, a loss of hyperbolicity occurs because of two eigenvalues that become complex conjugate.

In order to compute numerical solutions in hyperbolic cases, it could be convenient to derive mathematical expressions that connect the boundaries $Fr_1^{\#}$ and $Fr_1^{\$\%}$ to the other flow variables, i.e., the phase concentrations and the ratio between the phase velocities. This goal can be achieved by analyzing the characteristic polynomial of the matrix that arises from the conservative and non-conservative terms of the equation system. Due to the complexity of the characteristic polynomial, no analytical expressions for $Fr_1^{\#}$ and $Fr_1^{\$\%}$ can be derived. However, approximated expressions for the boundaries of the hyperbolic ranges can be obtained by extending the procedure proposed for the two-phase debris-flow model of Pelanti et al. (2008) to the rock-ice avalanche model considered in this work.

To understand the degree of approximation of the approximated boundaries, “exact” limits of the hyperbolic ranges are computed numerically by analyzing how the eigenvalues change in terms of the liquid Froude

number, and by detecting the values of Fr_1 associated with a change in the nature of the equation system. The "exact" boundaries of the hyperbolic ranges are then compared with the approximated ones. As a result, the approximated boundaries can be considered good approximations of the "exact" ones.

3 ANALYTICAL AND NUMERICAL SOLUTIONS

In this work, we provide the analytical solution for the uniformly accelerated flow derived from the equation system by neglecting the mass and momentum transfers associated with the ice melting process. This analytical solution is characterized by flow depth and phase concentrations that are constant in time and by solid and liquid velocities that change over time exponentially until reaching a constant value.
Once the analytical solution has been derived, the equation system is integrated numerically in the hyperbolic region using numerical scheme proposed by Zugliani and Rosatti (2016), a finite volume method with Godunov fluxes of second order of accuracy in time and space. Figure 2 demonstrates that the chosen numerical scheme can detect the analytical solution with small relative errors.

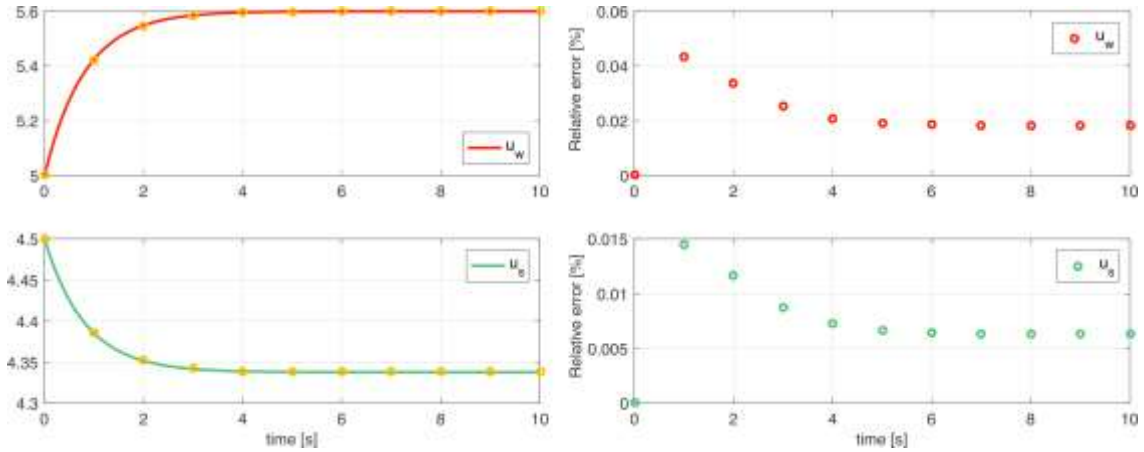

Figure 2. Analytical (solid lines) and numerical solutions (dots) related to the uniformly accelerated flow and relative error.

4 CONCLUSIONS

In this work, we provide analytical and numerical solutions of the uniformly accelerated flow derived starting from a rock-ice avalanche model existing in the literature. The comparison between the solutions shows that the chosen numerical scheme can solve accurately in the hyperbolic range the mathematical model considered.

REFERENCES

Bartelt, P., Christen, M., Buhler, Y., and Buser, O. (2018). Thermomechanical modelling of rock avalanches with debris, ice and snow entrainment. *In 9th European Conference on Numerical Methods in Geotechnical Engineering (NUMGE),* University of Porto, Porto, PORTUGAL.

Pelanti, M., Bouchut, F., and Mangeney, A. (2008). A Roe-type scheme for two-phase shallow granular flows over variable topography. *ESAIM: M2AN*, 42, 851-885.

Pudasaini, S., and Krautblatter, M. (2014). A two-phase mechanical model for rock-ice avalanches. *Journal of Geophysical Research: Earth Surface*, 119 (10), 2272-2290.

Sansone, S., Zugliani, D. and Rosatti, G. (2021). A mathematical framework for modelling rock-ice avalanche. *J. Fluid Mech.*, 919, A8.

Zugliani, D., and Rosatti, G. (2016). A new Osher Riemann solver for shallow water flow over fixed or mobile bed. *Proceedings of the 4th European Congress of the IAHR*, Liege, Belgium, 27-29 July, CRC Press/Balkema. pp. 707-713.

ISBN: 978-90-824846-7-0

Proceedings of the 2nd IAHR
Young Professionals Congress
30 Nov-2 Dec. 2021

Optimization of CFD numerical model for the analysis of a combined caisson

Claudio Iuppa [1], Lilia Carlo [1], Enrico Foti and Carla Faraci [1]
[1] Department of Engineering, University of Messina, Contrada Di Dio, Sant'Agata, 98166 Messina, Italy
claudio.iuppa@unime.it
lilia.carlo@unime.it
carla.faraci@unime.it
[2]Department of Civil Engineering and Architecture, University of Catania, Via Santa Sofia, 64-95123
Catania, Italy
enrico.foti@unict.it

ABSTRACT

The aim of the present research work is to provide a tool for predicting the attenuation of wave reflection due to a composite caisson, which is a port structure having an internal rubble mound to reduce residual wave energy within the port basin. The analyses were conducted through the OpenFOAM model using the *olaflow* toolbox. This toolbox allows the behavior of a composite caisson to be simulated using the Volume-Average Reynolds-Averaged Navier-Stokes (VARANS) equations which require however a calibration of some coefficients. By comparing the reflection coefficient of the numerical model with those obtained in the experimental campaign conducted at the Hydraulics Laboratory of the University of Messina, the present research work allowed the optimal combinations of such coefficients to be identified, such that the numerical model can provide an accurate estimate of the caisson performance.

Keywords: Reflection coefficient; porous media; VARANS equations; CFD; Physical model.

1 INTRODUCTION

Several studies have shown that the interaction between porous structures and waves are well reproduced through the Volume-Average Reynolds-Averaged Navier-Stokes (VARANS) equations (Higuera *et al.*, 2014; Jensen *et al.*, 2014). However, such equations require the introduction of closure terms that permit to consider the effects due to the interaction between the porous media and the water flow (i.e., frictional forces, pressure force, and added mass). Such terms are defined by the following relationship:

$$\Delta P = \rho \left(au + bu|u| + c \frac{\partial}{\partial t} u \right)$$

where ΔP [Pa/m] is the pressure drop per unit length due to porous media, ρ is the water density [kg m^{-3}], u [m s^{-1}] is the pore velocity and a [s^{-1}], b [m^{-1}] and c [-] are the pressure-drop coefficients. The coefficient c, according to previous works, can be kept constant. A suggested value is equal to 0.34 (Higuera *et al.*, 2014). As regards the coefficient a and b, they are function of the porosity and the median diameter of the porous media, the physical characteristics of the fluid and two coefficients, α [-] and β [-]. The value of these coefficients is not known a priori and therefore it is necessary to carry out a calibration process. In order to provide a tool for predicting the attenuation of wave reflection due to a composite caisson, in the present study the calibration process was performed using the reflection coefficients obtained during the experimental campaign conducted at the Hydraulic Laboratory of the University of Messina (see Faraci *et al.* (2015) for a detailed description of the experimental set up).

2 CALIBRATION OF THE DRAG TERMS

To individuate the best configuration of the coefficients of drag terms (i.e. α and β), several combinations of such coefficients through the OpenFOAM model were analyzed. In particular, the coefficient values were defined according to Van Gent (1996) and Jensen *et al.* (2014) (see Figure 1). For each combination, five regular

waves with different wave periods (0.57 – 1.67 s) and wave heights (0.01-0.06 m) were numerically simulated. The water depth was maintained constant at the value of 0.235 m. The median diameter and the porosity were set equal to 0.03 m and 0.3, respectively. The numerical simulations were carried out by means of the toolbox *olaflow* (Higuera, 2017) which implements the VARANS equations and offers a set of boundary conditions for generating and absorbing waves at the boundaries. To estimate the amplitude of the incident and reflected waves, the water elevation was measured at three different positions and then the collected data was processed by the method proposed by Mansard & Funke (1980). Figure 1 shows the comparison between reflection coefficients (k_r) obtained by: the experimental campaign, the relationship proposed for the combined caisson by Faraci *et al.* (2015) and the numerical simulations. As can be seen from Figure 1, the method proposed by Faraci *et al.* (2015) provided a more accurate estimate of the reflection coefficient for the dimensionless wave number (kd, where k is the wave number and d is the water depth) smaller than 1.15. For kd greater than 1.15, an underestimation of the experimental values is observed. The root mean square error (*rmse*) of such an empirical method is 0.14. As regards the numerical model, the behavior of the structure is reproduced quite well for almost all tested configurations. The greatest value of *rmse,* equal to 0.08, was estimated for the configuration of with α = 200 and β = 1.1.

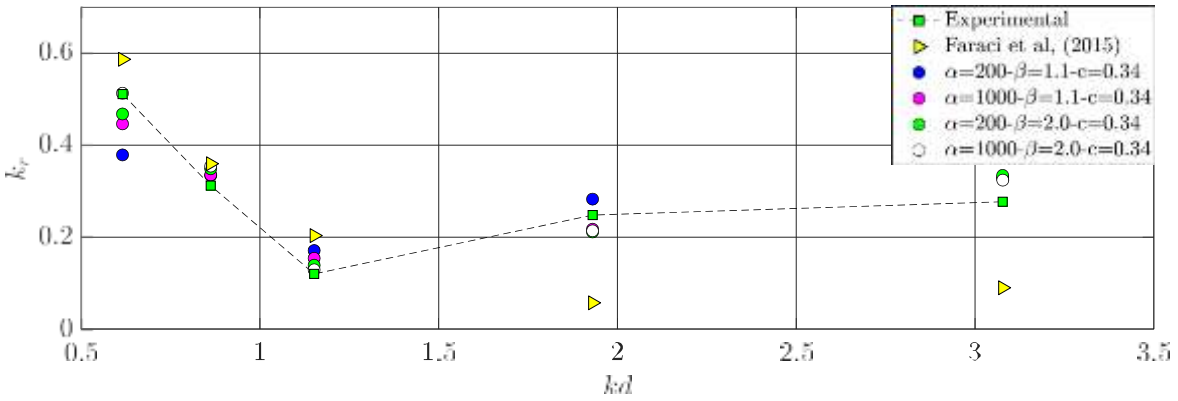

Figure 1. Comparison between the reflection coefficient obtained from the experimental campaign, that estimated by means of the empirical relationship proposed by Faraci *et al.* (2015) and the numerical model.

3 CONCLUSIONS

The study showed that adopting appropriate combination of the closure terms, the VARANS equations permit a reliable estimation of the reflection coefficient also for those wave conditions for which the currently available empirical method provide an underestimation.

ACKNOWLEDGEMENTS

This work has been partly supported by the project TETI - TEcnologie innovative per il controllo, il monitoraggio e la sicurezza in mare (code ARS01_00333) and by the project ISYPORT - Integrated SYstem for navigation risk mitigation in PORTs (code ARS01_01202).

REFERENCES

Faraci, C., Scandura, P. and Foti, E., 2015. Reflection of sea waves by combined caissons. Journal of Waterway, Port, Coastal, and Ocean Engineering, 141(2).

Higuera, P., 2017. olaFlow: CFD for waves. URL https://doi. org/10.5281/zenodo, 1297013.

Higuera, P., Lara, J.L. and Losada, I.J., 2014. Three-dimensional interaction of waves and porous coastal structures using OpenFOAM®. Part II: Application. Coastal Engineering, 83, pp.259-270.

Jensen, B., Jacobsen, N.G. and Christensen, E.D., 2014. Investigations on the porous media equations and resistance coefficients for coastal structures. Coastal Engineering, 84, pp.56-72.

Mansard, E.P. and Funke, E.R., 1980. The measurement of incident and reflected spectra using a least squares method. In *Coastal Engineering 1980* (pp. 154-172).

Van Gent, M.R.A., 1996. Wave interaction with permeable coastal structures. In *International Journal of Rock Mechanics and Mining Sciences and Geomechanics Abstracts* (Vol. 6, No. 33, p. 277A).

Proceedings of the 2nd IAHR
Young Professionals Congress
30 Nov-2 Dec. 2021

Numerical analysis of erosion rate around a cylinder surface

Bandi Surender[1], Anuj Kumar[2] and Anant Kumar Rai[3]

[1,3]National Institute of Technology Warangal, India
[2]Vellore Institute of Technology, Vellore
[1]email: bsme20118@student.nitw.ac.in
[2]email: anujkumar@vit.ac.in
[3]email: anant@nitw.ac.in

ABSTRACT

Bridge Scour around the bridge pier plays a critical role in the failure of bridge pier. Flow behavior of river water having silt particles around bridge pier helps to understand scour and erosion occurred. The aim of this paper is to study numerically flow of silt-laden water in a duct around a vertical cylinder to understand the flow behaviour around bridge pier. Discrete Phase Model (DPM) is used to model solid particle along with water as continuous medium in a duct using ANSYS 19.2. Realizable k-□ Turbulence model is used to solve turbulence intensity and turbulence dissipation rate. The initial results from the DPM velocity magnitude and erosion rate around the cylinder surface are presented here.

Keywords: sediment, CFD, erosion model, k-□ Turbulence model, Discrete Phase Model (DPM)

1. INTRODUCTION

Bridge piers are a type of substructure that supports the main structure of a bridge. One of main reason for bridge failure is Bridge Scour which means removal of sand from around piers or bridge abutments (Pandey et al. 2017, Chavan et al. 2019). Water normally flows faster around piers and abutments making them susceptible to local scour. Stream channel instability is causing river erosion. Due to scour and erosion, the pier begins to loss its strength (Pandey et al. 2017). Scour can also cause problems with the stability of a bridge. To study the flow behaviour around the bridge pier a geometry with cylinder wall which acts as an obstruction to the flow in a duct is modelled and the simulation study is carried out using ANSYS FLUENT 19.2. The initial results are presented.

2. METHODOLOGY

Water is made to flow continuously with inlet velocity 1 m s^{-1} and outlet is taken as zero-gauge pressure with no-slip boundary wall condition is applied to duct walls and cylinder surface and a flow geometry available in the literature is considered (Pandey et al. 2017) as shown in Figure 1 (a). To solve the Navier Strokes equation, a structured mesh with 2.08 million elements has been developed. Moreover, inflation layers are also added around the cylinder surface to study the boundary wall effects as shown in Figure 1 (b). Discrete Phase Model (DPM) is used to model solid particles suspended in the fluid flow with velocity 0 m s^{-1} and total mass flow rate 0.35 kg s^{-1} for DPM at inlet and outlet escape type boundary condition is applied and for duct and cylinder walls trap type boundary condition is applied. Realizable k-□ Turbulence model with enhanced wall treatment is used to solve turbulence intensity and turbulence dissipation rate. The SIMPLE algorithm is used to solve pressure and velocity values in segregated manner.

3. RESULTS

The particles velocity flow behaviour around the cylinder is shown in Figure 1 (c). The swirl flow around the cylinder is captured similar to the reported studies in literature (Devi et al. 2016). The magnitude of erosion rate on the cylinder surface is more on the inlet facing surface compared to the outlet facing

ISBN: 978-90-824846-7-0

surface (rear side) as shown in Figure 1 (d). This is mainly because of the swirl flow and velocity reduction at the rear side of the cylinder as depicted in Figure 1 (c). The solid particle behaviour around the cylinder is shown in Figure 1 (e). This also confirms the higher erosion rate in the front side of the cylinder. More results on different sections of the cylinder at depths will be analysed and shape of the pier will be changed to optimize the shape for minimum erosion in future.

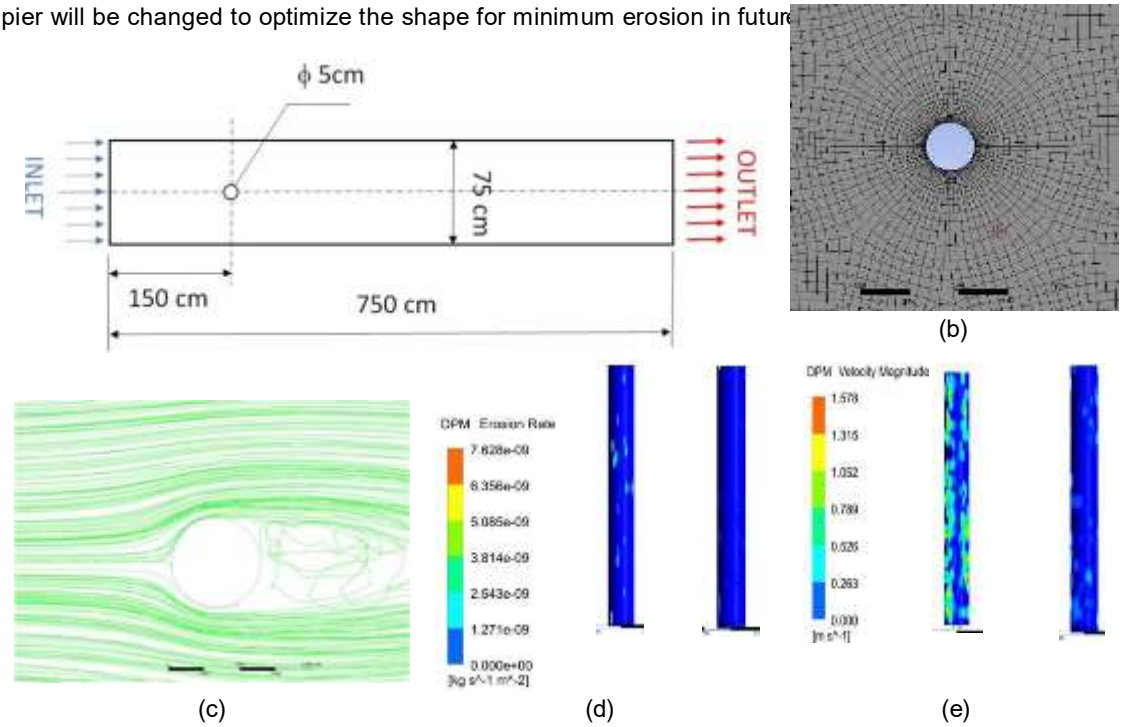

(b)

(c) (d) (e)

Figure 1: (a) Top view of duct geometry considered for simulation; (b) Inflation around cylinder; (c) Particle flow around cylinder; (d) Erosion rate viewed from Inlet and outlet sections; (e) DPM velocity viewed from Inlet and outlet sections.

4. CONCLUSION

In this paper a numerical scheme is developed to study the erosive flow around the cylinder surface in a duct. The initial results of the study have been presented here and found that the surface susceptible to be eroded the most has been the surface facing the inlet. These are initial results and the authors plan to explore the study further to optimize the shape of the cylinder to reduce the erosion around the bridge piers. Further, the open channel flow considerations will also be incorporated in future.

REFERENCES

Chavan, R., Gualtieri, P. and Kumar., B. (2019). Turbulent Flow Structures and Scour Hole Characteristics around Circular Bridge Piers over Non-Uniform Sand Bed Channels with Downward Seepage. *Water* 11, 1580.

Devi, T.B., Sharma, A., and Kumar, B. (2016). Turbulence Characteristics of Vegetated Channel with Downward Seepage. *Journal of Fluids Engineering*, 138, 121102.

Pandey, M., Sharma, P.K., Ahmad, Z., Singh, U.K. and Karna, N. (2017). Three-dimensional velocity measurements around bridge piers in gravel bed. *Marine Georesources & Geotechnology*, 663-676.

ISBN: 978-90-824846-7-0

IAHR YPN

Young Professionals Network

Hosted by
Spain Water and IWHR, China

IAHR AIRH

International Association for Hydro-Environment Engineering and Research

Hosted by
Spain Water and IWHR, China

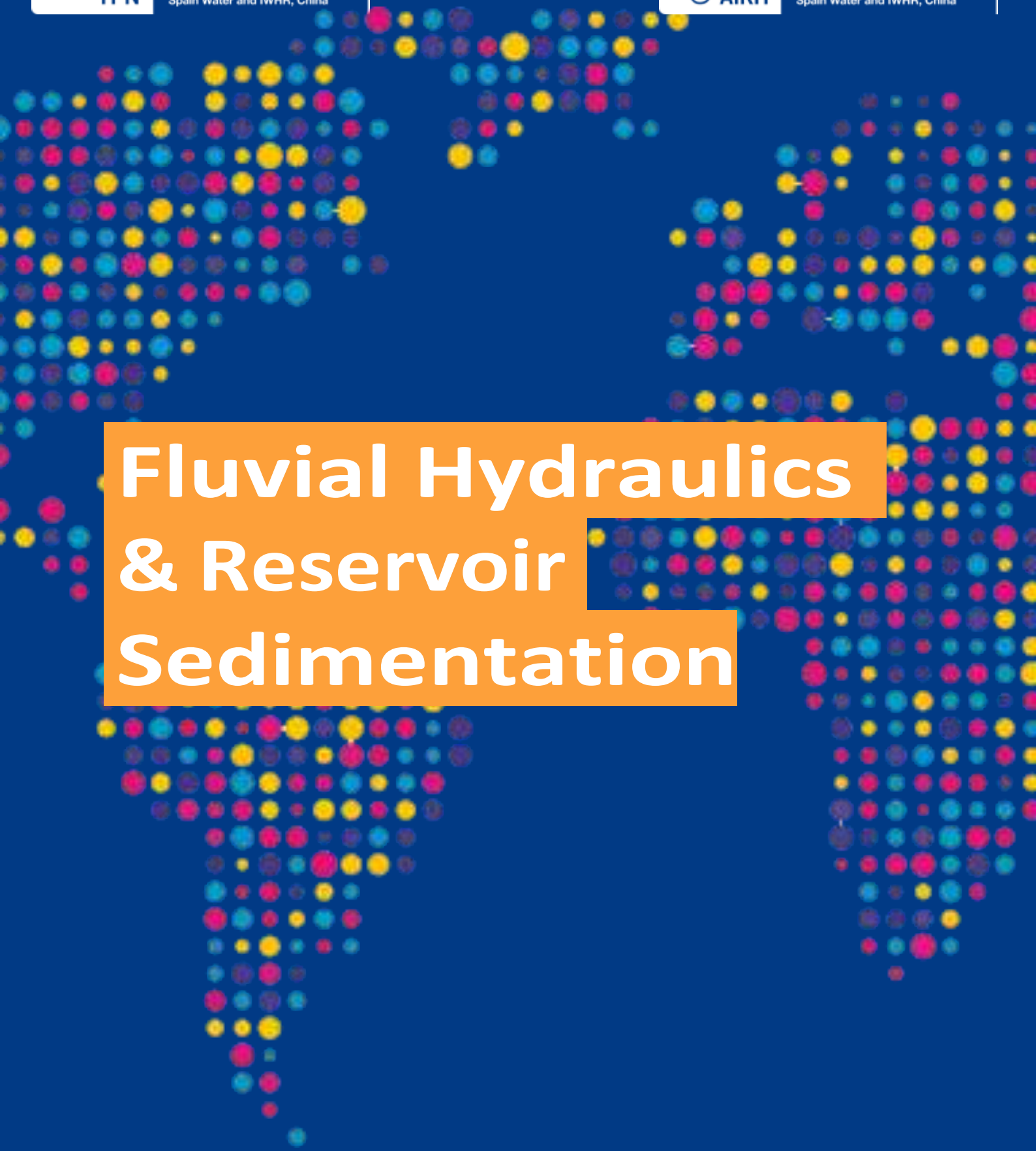

Fluvial Hydraulics & Reservoir Sedimentation

Proceedings of the 2nd IAHR
Young Professionals Congress
30 Nov-2 Dec. 2021

Sentinel2-derived hydro-morphological dynamics of a reach of the Vistula River in Poland

Michael Nones [1] and Carmela Cavallo [2]
[1] Institute of Geophysics, Polish Academy of Science, Warsaw, Poland; mnones@igf.edu.pl
[2] Salerno University, Salerno, Italy; ccavallo@unisa.it

ABSTRACT
The dynamics of sediments and outflows determines the morphology of rivers, as well as their ecological functionality. To evaluate the effects of human alterations on fluvial environments and infer future trajectories, continuous monitoring at the reach scale is needed. For this reason, using a reach of the Vistula River in Poland, we developed a Google Earth Engine script for tracking the water-sediment-vegetation dynamics during three years (2017-2020), as derived from Sentinel2 data. The preliminary results pointed out that moderate resolute images acquired remotely can be easily used for inferring past trends and eventually model future trajectories of fluvial dynamics.

Keywords: Google Earth Engine; river morphodynamics; Sentinel2; Vistula River.

1 INTRODUCTION

Even if already characterized by a rather long history, geospatial techniques are now common tools used also by non-experts in monitoring river hydrology and sediment dynamics at different spatiotemporal scales, because of their capability to cover multiple aspects and efficiently integrate them. Compared to more traditional methods, which are time-consuming and require cumbersome work for collecting and processing field data, geospatial tools are faster and more reliable in processing spatial data. They can be combined to infer qualitative and quantitative information on river morphology, pinpointing large scale and medium/long-term processes.
Google Earth Engine (GEE), a cloud-based computing platform for planetary-scale geospatial analyses, offers free access to remotely sensed Earth observation data (Gorelick et al., 2017), enabling geomorphological analyses at higher spatio-temporal resolution (Boothroyd et al., 2021). In this work, we applied GEE for monitoring the dynamics of a reach of the Vistula River, in Poland, as derived from the Sentinel2 (S2) constellation (spatial resolution 10 m, revisit time 5-10 days).

2 STUDY AREA

The Vistula River is the longest in Poland, rising in the south of Poland in the Carpathian Mountains, and then flowing towards the north, emptying into the Baltic Sea with a delta and several branches. The study area covers a reach of around 80 km from the confluence of the Vistula and the Narew rivers, just downstream of the city of Warsaw (Modlin), to the city of Plock, where the backwater effect of the Wloclawek Dam arrives (Figure 1).
The actual bankfull width has been narrowed to 300-500 m, starting from an original width of 1000-1600 m, while the construction of the Wloclawek Dam in 1968-1969 established a backwater area of about 60 km upstream of the reservoir till Plock. Because of the combined effect of backwater and channelization, this reach is characterized by a relatively fast aggradation rate (Lajczak et al., 2006; Nones, 2020).

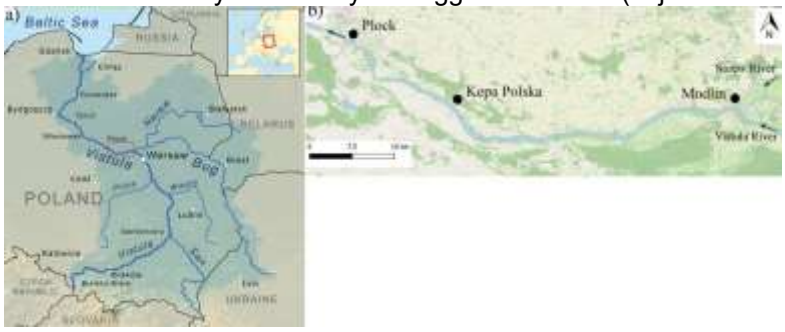

Figure 1. Study area: a) Vistula River; b) aerial image of the study area between Warsaw (Modlin) and Plock.

3 REMOTE SENSING INDEXES

The data analyzed here cover the period from May 18, 2017, to October 6, 2020, and were pre-processed to avoid cloud coverage. In total, 84 images were considered.
To derive insights on the river evolution during the last three years, four multispectral indexes were considered (Table 1). Such indexes evaluate the trend of vegetation (NDVI), presence of water (NDWI) and turbidity (NDTI), therefore allowing for a comprehensive analysis of the river dynamics.

ISBN: 978-90-824846-7-0

Table 1. Remote sensing indexes.

	MEANING	EQUATION
NDVI	Normalized Difference Vegetation Index	$NDVI = \frac{NIR - R}{NIR + R}$
NDWI	Normalized Difference Water Index	$NDWI = \frac{G - NIR}{G + NIR}$
NDTI	Normalized Difference Turbidity Index	$NDTI = \frac{R - G}{R + G}$

where the S2 bands are R=red, G=green, B=blue, NIR=near infrared.

4 PRELIMINARY RESULTS AND FUTURE STEPS

Figure 2 shows the temporal variation of the four indexes described above. As one can notice, NDVI is minimum during the winter months, as vegetation is not favoured by the season, and reaches the maximum values during the summer. As one can expect, the lower the influence of vegetation and the higher the area available for water (NDWI), the higher the turbidity (NDTI). During the study period, all these three indexes have a rather coherent trend, with annual oscillations.

Comparing the indexes with the monthly discharge measured at the upstream end of the reach (Modlin), a time lag between high-flow conditions and peaks in turbidity (NDTI) and water content (NDWI) is evident.

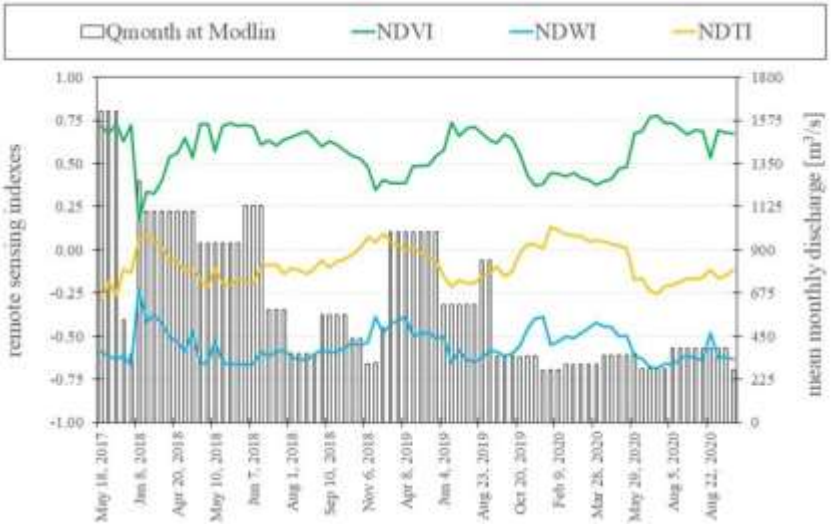

Figure 2. Temporal variation of the four indexes derived from satellite imagery.

The present application pointed out the capability of satellite images and GEE in monitoring river dynamics at a relatively high spatio-temporal resolution. However, the obtained data should be validated with ground truth information or images having an even higher spatial resolution (e.g., WorldView or Planet data), and this will constitute the next step of this research. Once validated, the images and the GEE algorithm will be further developed, also considering additional indexes, for inferring a relationship between the river hydrology and the satellite-derived indexes, aiming to provide water managers with additional evidence on past trends and potential future evolutive trajectories.

DATA AVAILABILITY

The source code is available at https://code.earthengine.google.com/1419e96230295d6d19aa80ec572597b0.

REFERENCES

Boothroyd, R. J., Nones, M., & Guerrero, M. (2021). Deriving planform morphology and vegetation coverage from remote sensing to support river management applications. *Frontiers in Environmental Science*, 9, 146.

Gorelick, N., Hancher, M., Dixon, M., Ilyushchenko, S., Thau, D., & Moore, R. (2017). Google Earth Engine: Planetary-Scale Geospatial Analysis for Everyone. *Remote Sensing Environ.*, 202, 18–27.

Lajczak, A., Plit, J., Soja, R., Starkel, L., & Warowna, J. (2006). Changes of the Vistula river channel and floodplain in the last 200 years. *Geographia Polonica*, 79(2), 65–87

Nones, M. (2021). Remote sensing and GIS techniques to monitor morphological changes along the middle-lower Vistula river, Poland. *Int. Journal of River Basin Management*, 19(3), 345-357.

Proceedings of the 2nd IAHR
Young Professionals Congress
30 Nov-2 Dec. 2021

A review for the piano key weir's hydraulic characteristics between modeling and modified based main and auxiliary geometric parameters

MAJED SHAKER[1], BADRONNISA YUSUF[2], SALEH KHASSAF[3], BALQIS MOHAMED[4], NOR AZLINA[5]
[1] Southern Technical University (STU), Nasiriyah, Iraq,
e-mail (majedsh.hussain@stu.edu.iq / gs58482@student.upm.edu.my)
[2,4,5] Universiti Putra Malaysia (UPM), Kuala Lumpur, Malaysia
ASSC.PROF.DR., e-mail (nisa@upm.edu.my , DR., balqis@upm.edu.my , DR., a_norazlina@upm.edu.my)
[3] University of Basrah, Basrah, Iraq
PROF.DR., e-mail (saleh.khassaf@uobasrah.edu.iq)

ABSTRACT

The novel technique of hydraulic structures (PKWs), piano key weir, is primarily confined and dispersed. The available gaps must be comprehended in this field of research to provide significant insights into experts and assist researchers in getting them. As a result, a review is done to map the research landscape into a consistent taxonomy. In four main databases: Web of Science, ScienceDirect, IEEE Explore, and Scopus, be conducted a concentrated search for every publication related to (1) Nonlinear weirs, (2) Performance of weirs, and (3) Geometry parameters of PKWs. The classification strategy yielded 82 articles separated into four categories. Then, identify the basic hydraulic characteristics in terms of motivation for utilizing PKW, and recommendations to increase acceptance and use of PKW therefore, the development of the piano key weir still requires modifications to Main (different plan shapes) and secondary (nonlinear parapet wall) parameters to enhance the performance of PK weir.

Keywords: piano key weir, parapet wall, Plan shapes, sischarge coefficient, performance efficiency.

1 INTRODUCTION

Water is essential for life on Earth. As a result, humans have attempted to safeguard and enhance water resources as best they can, such as by constructing dams and sluices on rivers. (Li, Li and Jiang, 2020). In addition, as a result of climate change, high-intensity rainfalls, floods, and droughts have grown more common and severe in many parts of the world. Furthermore, with increasing demands for more reservoir water storage and the ongoing need to improve dam safety, many existing spillways' capacities are already insufficient and in need of upgrading or replacement. Still, weirs, either gated or non-gated, are commonly used as flow control structures in reservoir spillways. (Olyaie, Banejad and Heydari, 2019). But, the low discharge capacity of linear weirs is one of their drawbacks. Besides that, If an increase in reservoir water level is not possible, there are three options for increasing discharge capacity: (1) increasing the weir length (L) up to a specific footprint size by replacing the linear weir with a nonlinear (labyrinth) one, (2) lowering the spillway crest elevation, and (3) increasing the weir width (W) up to a specific footprint size by replacing the linear weir with a nonlinear (labyrinth) one. At those points, Firstly, due to dam geometry or economic constraints, increasing L of a linear weir, and hence W, is typically unfeasible. Then, lowering the spillway crest reduces base-flow reservoir storage volumes, lowering the quantity of stored water available for the reservoir's specific function (e.g., municipal, agriculture, commercial, hydropower). However, where L > W, the use of nonlinear weirs is a realistic and increasingly popular alternative for boosting discharge capacity while ensuring the long-term viability of existing spillway equipment (e.g., spillway channel) (Anderson and Tullis, 2013). Because, vertical walls are used to construct labyrinth weirs, which are more efficient than linear spillways. Therefore, the design of labyrinth weirs is straightforward because of their basic geometry, but they require large footprint sizes, which limits their use when erecting concrete dams. Also, the bottom-approaching flows are subjected to considerable constriction after entering the span between the two vertical sidewalls in this form of the weir, and the upstream and downstream crests are rendered useless. To address the above the piano key weir (PKW) had been developed is a novel labyrinth weir with piano key-shaped openings that slant one by one upstream and downstream. (Akbari Kheir-Abadi *et al.*, 2020). As well as, Piano Key Weirs (PKWs) is considered an excellent technique to increase the discharge capacity of spillway systems (Sangsefidi *et al.*, 2021). It can also, a PKW can be utilized with embankment dams, on the abutment or crest of a gravity dam, or as a run-of-river construction in natural channels. So that, Labyrinth and PK weirs have been utilized to replace physically weak spillways and gated systems and improve operations and maintenance due to their hydraulic performance. (Crookston, Anderson and Tullis, 2018). Consequently,

PKWs are categorized in general based on whether or not they have overhangs. In addition, the upstream and downstream overhangs have caused the sidewalls to incline inwards, resulting in a significant reduction in weir foot length. (Belzner *et al.*, 2017). So that, increased spillway height is often necessary to increase reservoir water storage capacity in dams while redirecting flow in dam upstream channels. Moreover, PKWs have also been used in reservoirs and rivers in conjunction with low-head hydropower or to control and maintain waterways that meet navigational standards in recent years. Lastly, these requirements necessitate the use of different plane shapes and nonlinear parapet walls.

Fig.1. 3D view of the PKW (Belzner *et al.*, 2017))

Fig.2. Type of piano key weir VS. numbers (2006-2020)

2 CONCLUSIONS

A recent disruptive global warm trend has emerged important in the use of piano key weir and its applications in dams and rivers rehabilitation and projects. This trend is still being researched. It is critical to gain insight into this new trend. By surveying and taxonomizing linked works, this article intends to contribute such insights. The many works on PKW can be used to draw certain patterns. Reviews or surveys, research studies on PKW and their application as hydraulic structures, development attempts, and broad design suggestions are essentially divided into four areas. An in-depth examination of the publications aids in identifying and describing the PKW-related issues, benefits, and recommendations. The findings show that based on prior studies, And the addressing of the decreasing discharge in the shape of the rectangle due to flow interference at the opposite sides walls by changing it to a trapezoid despite the efficiency of the rectangle was increasing than the trapezoidal and it is hypothesized that parapet walls may aid in the enhancement of the PKW function. Most of the prior research has focused on PKWs of type A (Fig. 2). Furthermore, studies have paid little attention to the impact of the parapet walls' nonlinearity and, the flow condition (both free and submerged flow), the effects of different plane shapes of PKWs to assessment the optimum performance. Therefore, development of the piano key weir is based on make the modification of the main and secondary geometric parameters, also make improvements to the shape of the inlet and outlet keys. Furthermore, investment the new techniques for modeling the physical model of PKW in lab. instead of used to in past. In addition, for modeling using package software to make the modified on the cross-section PK weir however complicated. These suggestions can help overcome the obstacles that PKW applications face in dams and rivers.

REFERENCES

B. M. Crookston, R. M. Anderson, and B. P. Tullis, “Free-flow discharge estimation method for Piano Key weir geometries,” *J. Hydro-Environment Res.*, vol. 19, no. xxxx, pp. 160–167, 2018, doi: 10.1016/j.jher.2017.10.003.

E. Olyaie, H. Banejad, and M. Heydari, “Estimating Discharge Coefficient of PK-Weir Under Subcritical Conditions Based on High-Accuracy Machine Learning Approaches,” *Iran. J. Sci. Technol. - Trans. Civ. Eng.*, vol. 43, pp. 89–101, 2019, doi: 10.1007/s40996-018-0150-z.

F. Belzner, J. Merkel, M. Gebhardt, and C. Thorenz, “Piano Key and Labyrinth Weirs at German waterways: Recent and future research of the BAW,” Labyrinth Piano Key Weirs III – PKW 2017, pp. 167–174, 2017, doi: 10.1201/9781315169064-24.

M. Akbari Kheir-Abadi, M. Karami Moghadam, T. Sabzevari, and Z. Ghadampour, “An experimental study of the effects of the parapet walls geometry on the discharge coefficient of trapezoidal piano key weirs,” *Flow Meas. Instrum.*, vol. 73, no. March, p. 101742, 2020, doi: 10.1016/j.flowmeasinst.2020.101742.

R. M. Anderson and B. P. Tullis, “Piano Key Weir Hydraulics and Labyrinth Weir Comparison,” *J. Irrig. Drain. Eng.*, vol. 139, no. 3, pp. 246–253, 2013, doi: 10.1061/(asce)ir.1943-4774.0000530.

S. Li, G. Li, and D. Jiang, “Physical and Numerical Modeling of the Hydraulic Characteristics of Type-A Piano Key Weirs,” *J. Hydraul. Eng.*, vol. 146, no. 5, p. 06020004, 2020, doi: 10.1061/(asce)hy.1943-7900.0001716.

Y. Sangsefidi, H. Tavakol-Davani, M. Ghodsian, M. Mehraein, and R. Zarei, “Hydrodynamics and Free-Flow Characteristics of Piano Key Weirs with Different Plan Shapes,” *Water*, vol. 13, no. 15, p. 2108, 2021, doi: 10.3390/w13152108.

ISBN: 978-90-824846-7-0

Proceedings of the 2nd IAHR
Young Professionals Congress
30 Nov-2 Dec. 2021

Study on the hydraulic geometry in different hydrological periods based on one-dimensional hydrodynamic model

Chang Li
State Key Laboratory of Hydrology-Water Resources and Hydraulic Engineering, Nanjing, China, email (ecnulic@163.com)

ABSTRACT

There is a certain relationship between the dynamic and the riverbed morphology of navigable river. A one-dimensional hydrodynamic model was established to study the hydraulic geometry in different hydrological periods and its influence on the stability of riverbed in Guiping-Wuzhou reach of the Xijiang River, China. The results showed that the model has a good performance on hydrodynamic simulation and the coefficients of hydraulic geometry in the low-water period near the Guiping channel station can reach 4 times the medium-water period. Moreover, the river slope stability coefficients were relatively large, and the river banks were easy to scour in three reaches (Guiping, Jiyutan and Pingnan). The channel conditions of the other sections were suitable for navigation. This study has established hydraulic geometry in different hydrological periods, which can be used in waterway regulation planning.

Keywords: hydraulic geometry; hydrodynamic model; waterway regulation; Xijiang River.

1 INTRODUCTION

Hydraulic geometry is one of the main ways to research riverbed evolution. Its application in waterway of the Xijiang River could make predictions about the evolution and developing trend of the reach. Moreover, it also provides a reference basis for systematic management and development in waterway regulation planning. However, there are relatively few studies on hydraulic geometry and riverbed stability during different hydrological periods when there is a lack of scouring and silting data for such a fine reach as Guiping-Wuzhou (GW) of the Xijiang River. Theoretically, the fine reaches are in a dynamic water and sediment dynamic balance for a long time, and should have a stable hydraulic geometry. There have been some empirical hydraulic geometries in plain rivers (Leopold et al., 1953; Rich et al., 2013), while there are few studies and applications of alluvial rivers in mountainous areas. In this study, a one-dimensional hydrodynamic model was established for GW reach of Xijiang River, and the method of selecting fine reach and establishing hydraulic geometry was analyzed and discussed, which provides a reference for waterway regulation planning.

2 MATERIAL AND METHODS

2.1 Study area and datasets

The Guiping-Wuzhou (GW) reach located in the lower reaches of the Xijiang River, China. The total length of GW is about 186 km and an average channel slope of 0.10‰ in low-water period. Sediment in the GW reach mainly comes from the upstream of the Hongshui River. The river bank is composed of clay, limestone, sandstone, etc. The riverbed is mostly bedrock or pebbles, and some areas are covered by sand. The annual sediment content is only 0.385 kg/m^3 at Wuzhou hydrological station. However, due to the abundant water discharge of the Xijiang River and the large amount of suspended sediment transport, it has become the river with the largest sediment load in Guangxi Province, China.

2.2 Model and methods

In this study, the hydrodynamic model is based on the Saint-Venant equation (Wang et al., 2019). The continuous equation and boundary conditions are shown as follows:

$$\frac{\partial A}{\partial t}+\frac{\partial Q}{\partial x}=q \quad [1]$$

$$Q=Q(t) \qquad L=L(t) \qquad Q=Q(L) \quad [2]$$

where, A is the section area, m^2; t is time, s; q is river lateral flow, m^3; Q is the section discharge, m^3; L is water level, m.

ISBN: 978-90-824846-7-0

For the waterway regulation project, the most widely studied and applied is the hydraulic geometry (ζ) along the cross sections, mainly on the statistical analysis results of river width (B) and average water depth (H). The former Soviet Union Institute of Hydrology obtained the relationship between the average width of plain rivers and the average water depth based on a large number of hydrological data (Ni and Zhang, 1992). Hydraulic geometry (ζ) and stable width-depth ratio (λ_{u_c}) for bed flow were calculated as follows:

$$\sqrt{B} / H = \varsigma \quad [3]$$

$$\frac{\sqrt{B}}{H} = 4\lambda_{u_c}^{2.5} \quad [4]$$

The stable slope coefficient (m) can be used as a bank stability index. The more unstable the bank is, the smaller the slope angle and the larger the slope coefficient are.

$$\frac{\sqrt{B}}{H} = 10.5\left(\frac{m}{\sqrt{D_{50}}}\right)^{0.40} \quad [5]$$

3 Results And Discussion

The river width and average water depth of each section were simulated by using the established one-dimensional hydrodynamic model, and the hydraulic geometry of each section was counted. During the low-water and mid-water periods, the hydraulic geometry generally showed a downward trend from upstream to downstream, but the locations of the maximum value of ζ in different hydrological periods were different. According to the fitting results, the hydraulic geometry of the river reach in the low-water and mid-water periods were respectively:

$$\frac{\sqrt{B}}{H} = 20.979H^{-0.913} \quad [6]$$

$$\frac{\sqrt{B}}{H} = 33.75H^{-1.057} \quad [7]$$

In the low-water period, the λ_{u_c} of the most sections were less than 1.20, except the sections near the Guiping Hydro Project upstream. It shows that the river section was generally narrow and deep, and was not easy to scour. In the mid-water period, the λ_{u_c} of each section was between 0.35 and 1.01, indicating that the section tends to be narrow and deep. Besides, the river section was not easy to scour and the river bank material was more difficult to be disturbed than the riverbed material. In addition, the m of the downstream near the Changzhou Hydro Project was less than 3.00, indicating that the river was relatively stable and the navigation conditions of the channel were better than those of other reaches.

4 CONCLUSIONS

The one-dimensional hydrodynamic model established in this study can better simulate the basic river data such as river width and average water depth. At the same time, hydraulic geometry with power function significance under different hydrological periods in the GW reach of the Xijiang River were also established. From the results of the stable slope coefficient calculated based on the hydraulic geometry, the m of the three sections (Guiping, Jiyutan and Pingnan) in the low-water and mid-water periods were relatively large, and the river banks were relatively unstable and easy to scour. The water flow conditions in the remaining sections of the reach were better.

REFERENCES

Leopold, L., and Maddock, B. T., (1953). The hydraulic geometry of stream channels and some physiographic implications. *U. S. Geol. Survey, Prof. Paper*, 1953, 252: 56.

Ni, J. R., and Zhang, R., (1992). The relationship and various methods of Morphological relationships research. *Act, Geogra, Sini*, 4: 368-375. (in Chinese)

Rich. A., Keller, E. A., (2013). A hydrologic and geomorphic model of estuary breaching and closure. *Geomorphology*, 191: 64-74.

Wang, Z. L., Geng, Y. F., Lu, Y. J., Mo, S. P., Ji, R. Y., (2019). A generalized vertical coordinate three-dimensional unstructured mesh model with application to Pearl River Estuaries. *Adv.Water Resour*, 30(06): 882-891.

ISBN: 978-90-824846-7-0

Proceedings of the 2nd IAHR
Young Professionals Congress
30 Nov-2 Dec. 2021

Selection of the optimal alternative for Toma Grande Dam applying the Hierarchical Analysis Method AHP

Hulinho Yordy Arbaiza Ocrospoma[1], Samuel Ismael Quisca Astocahuana[2]
[1]Bach. Civil Engineer, EPIC-FIGMMG, National University of San Marcos, Perú, hulinho.arbaiza@gmail.com
[2] Principal Professor, School of Civil Engineering, National University of San Marcos, Perú, squiscaa@unmsm.edu.pe

ABSTRACT

In this research work, the analysis and selection of the optimal dam type for the Toma Grande dam was performed by applying the analytical hierarchical process (AHP) for the analysis of four dam alternatives (CFRD, CCR, concrete gravity, earth and rockfil), and selecting the optimal alternative. For the application of the method, all the factors that influence the selection of the optimum type of dam were identified, called Subcriteria, which were grouped into eight most representative groups, by means of a hierarchical tree called Criteria (topography and structural geology, availability of materials, related works, dam safety, diversion system, construction procedure, construction time and construction cost). Based on the basic engineering studies, the Criteria data were obtained, which were used to construct the paired comparison matrix and the weightings were obtained by comparing each of the Criteria with each other. The results of the hierarchical analysis indicate that the concrete gravity dam as the optimum dam alternative, with a weighting of 40%, which is the most suitable for the construction of the Toma Grande dam.

Keywords: multi-criteria decision making; decision making criteria; AHP; optimal dam type selection.

1 INTRODUCTION

The process of selecting the optimal dam alternative is influenced by numerous factors such as: topography, geological and geotechnical conditions of the site, climatic and hydrological conditions, availability of materials for dam construction, height of the dam, size and location of the crest spillway, cost of the works, construction time, environmental and social aspects of the region and country where the project is located, and seismicity of the area, among others. Usually, the different types of dams are favorable for some of these factors, and unfavorable for others, being necessary to balance the advantages and disadvantages in each one of them to be able to justify in a suitable way the optimal dam alternative. One of the most widely used methodologies in various fields to support multi-criteria decision making is the Analytical Hierarchical Process (AHP).

2 PROCEDURE AND RESULTS

the most representative factors were selected to proceed with the analysis using the AHP method; we will call these factors criteria.

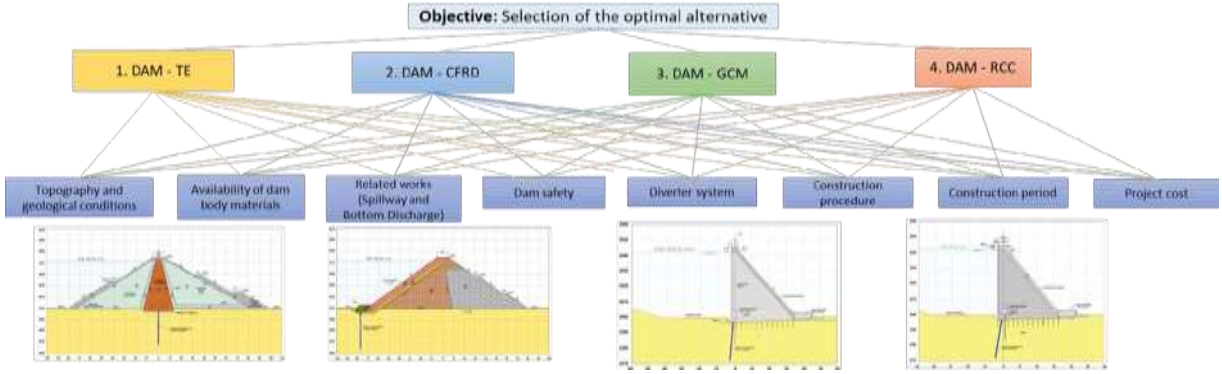

Figure 1 Hierarchy tree of the AHP Method (Source: Own elaboration).
Note: TE is defined as Soil and Rock Fill; CFRD, Concrete Faced Rock Fill Dam; GCM, Mass Concrete Gravity; and RCC, Roller Compacted Concrete.

Once the hierarchical tree is obtained, in the next step, we compare the criteria two by two. For this comparison, we attribute a value from 1 to 9, according to Saatyen's scale based on the degree of importance of criterion 1 over criterion 2; inverse values will be used when the second element is higher in the criterion to be compared. (Saaty 2008).

ISBN: 978-90-824846-7-0

Figure 2 Matrix of paired comparisons of criteria (Source: Own elaboration).

Once the weights of the sub-criteria (average vector) depending on each alternative are obtained, the priority matrix is assembled, which is composed of the alternatives. From this matrix the global weights of the alternatives in relation to the criteria are obtained. Finally, this matrix is multiplied with the relative weights of the criteria being evaluated and the prioritization percentages of each alternative are obtained.

CRITERION/ ALTERNATIVE	Topography and geological conditions	Availability of dam body materials	Spillway and Bot	Dam safety	Diverter system	Construction procedure	Constructio n period	Project cost	PRIORITIZATION
DAM TE	0,06	0.36	0,06	0.04	0.06	0.54	0.05	0.07	10%
DAM CFRD	0.13	0.36	0.06	0.12	0.09	0.29	0.12	0.12	14%
DAM GCM	0.40	0.17	0.51	0.49	0.43	0.12	0.29	0.34	40%
DAM CCR	0.40	0.10	0.36	0.35	0.43	0.06	0.55	0.48	35%
WEIGHTING	0.26	0.06	0.12	0.53	0.04	0.07	0.03	0.10	100%

Figure 3 Prioritization matrix and percentages (Source: Own elaboration).

The results of the hierarchical analysis indicate the concrete gravity dam as the optimal dam alternative, with a weighting of 40%, which is the most suitable for the construction of the dam Toma Grande.

3 CONCLUSIONS

Of the four proposed alternatives; according to the criteria considered for the analysis, the GCM dam has the highest priority (40%), followed by the RCC dam (35%); which is logical, since these types of dams present better performance in terms of the need to be able to cope with extreme flood or earthquake conditions; it allows the construction of the stepped spillway (efficient energy dissipation) in the body of the dam and the diversion conduit can be conditioned through the body of the dam, which considerably reduces the cost of the dam. The other two alternatives require expensive diversion systems during dam construction, and related works such as the spillway and bottom discharge must be located outside the dam body and require expensive structures.

This work demonstrates that the AHP method is suitable for solving complex problems with a large number of criteria, as presented in the problems of selecting the optimal dam alternative. Due to its methodological ease, and having a graphical component, the complex decision-making process is divided into manageable sections and allows a better understanding of the elements by integrating the decision criteria through paired comparisons.

REFERENCES

Al Khalil MI. 2012. Selecting the appropriate project delivery method using AHP. International Journal of Project Management, 20: 469-474.

F. Martinez (2019), "The Problem of Dam Type Selection in a Project: Criteria and Methods to Support Decision Making", Polytechnic University of Cartagena.

Razifar H (2013)., “Selection optimal type of dam using AHP method”, Journal of Novel Applied Sciences, Iran.

Xingi Day (2016). Dam site selection using an integrated method of AHP an Gis for decision making support in Bartola, Northwest, China.

ISBN: 978-90-824846-7-0

Proceedings of the 2nd IAHR
Young Professionals Congress
30 Nov-2 Dec. 2021

Velocity fields around tandem piers on mobile bed

Laxmi Narayana Pasupuleti [1], Prafulkumar Vasharambhai Timbadiya [2] and Prem Lal Patel [3]
[1]Kakinada Institute of Technological Sciences, Ramachandrapuram, India
[2,3] Sardar Vallabhbhai National Institute of Technology, Surat, India,
e-mail (laxmiraagini@gmail.com)

ABSTRACT

Present study investigated the velocity fields, viz., streamline patterns, velocity vectors and velocity power spectra around the tandem piers which are separated by centre-to-centre longitudinal distance, 2*d* (*d* is the diameter of pier). The outcomes of tandem arrangements are compared with single pier having same diameter under identical flow in the clear water condition. The approaching mean flow velocity was decreases to 20% at rear pier of tandem arrangement. The streamlines and velocity vectors revealed, there was a substantial upward flow created in between the piers of tandem arrangement. A clear re-circulating zone was formed at just upstream of rear pier. Velocity power spectra revealed, the strengths of wake vortex are significantly decreased upstream of rear pier in tandem arrangement vis-à-vis single pier.

Keywords: streamlines; velocity vectors; velocity power spectra; tandem arrangement; wake vortex.

1 INTRODUCTION

Flow measurements around bridge piers plays vital role and useful to hydraulic engineers for proper position, alignment, numbers on the river bed (Kothyari et al. 1992). Due to rapid growth in population and urbanization, the quantification of proposed bridge pier is required for proper placement, either upstream or downstream to exiting one. In past, few studies were focused on local scour around tandem piers (Wang et al. 2016; Khaple et al. 2017; Keshavarzi et al. 2018). However, the characterization of velocity fields around the tandem piers on mobile beds are scarce in the literature. The limited availability of studies on flow characterization in terms of velocity fields are motivated the authors to carry the present study with following objectives:

a) identification of downflow, adverse pressure gradient and vortex created upstream and around the piers for tandem arrangement.
b) The strengths of wake vortex at front and rear piers of tandem arrangements, are compared with the findings of single pier under identical flow conditions.

To fulfil the objectives, authors were performed the experimentations in the sediment transport flume having dimensions (15 m x 0.89m x 0.60 m) (Laxmi Narayana et al. 2021). The flow discharge 0.022 m^3/s was released through Supervisory control and data acquisition (SCADA) system, calibrated by flow meter, inserted into inlet pipe. A flow depth of 10.5 cm was maintained uniformly over the 6.0 m working section using tail gate provided at the end of the channel. Instantaneous three dimensional velocities are measured using Acoustic Doppler Velocimeter (ADV) at different grids around the piers. The flow Reynolds number and Densimetric Froude numbers are 24.7×10^{-3} and 2.43 respectively. Further, the flow and sediment characteristics are listed in Table-1.

Table 1 Sediment characteristics in the present study

	SEDIMENT SIZE D_{50} (MM)	STANDARD DEVIATION σ_g	COAFICIENT OF UNIFORMTY C_U	ANGLE OF REPOSE	APPROACHING MEAN FLOW VELOCITY (M/S)
UNIFORM SAND	0.75	1.29	1.6	31.5°	0.235

2 RESULTS AND DISCUSSIONS

The results of the current study reveals, the formation of downflow and horseshoe vortex at upstream of single and front pier of tandem arrangement, shown in Figure 1(a, b). The streamline patterns and velocity vectors revealed, formation of a strong horseshoe vortex at the foot of front pier in tandem arrangement as compare to single pier. On other hand, the strength of horseshoe vortex was significantly reduced around rear pier, wherein, the downflow and associated primary vortex are brought down by recirculation zone

ISBN: 978-90-824846-7-0

formed upstream to rear pier at near the bed. In past, Laxmi Narayana et al. (2020) identified larger scour hole around front piers of tandem arrangement. It is observed that, the wake vortex strengths are decreased by 30% at rear pier vis-à-vis single pier.

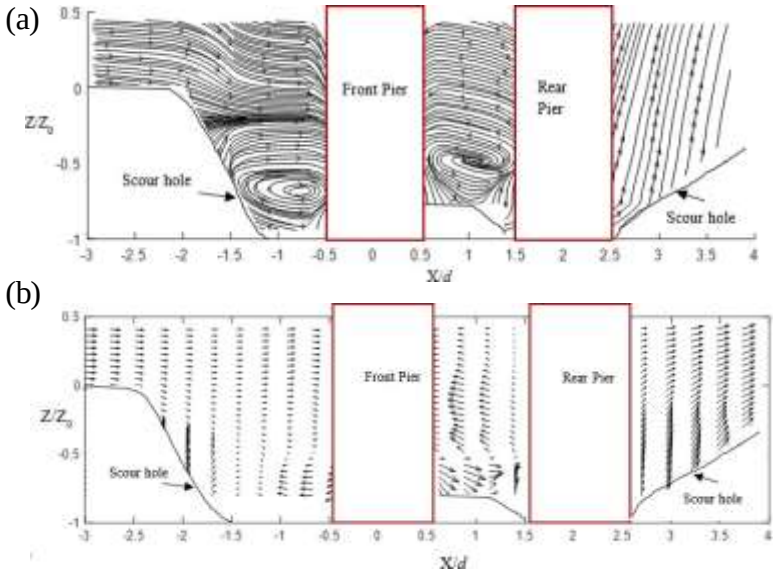

Fig.1 (a) streamline patterns around tandem piers, (b) velocity vectors around the tandem pier.

3 CONCLUSIONS

The investigations of velocity fields around the single and tandem pier configurations are presented in the current study. The following are key conclusions are listed:

a) From streamline and velocity vector patterns, at front pier in tandem arrangement, the size of horseshoe vortex is larger vis-à-vis single pier. It results in formation of more scour depth around front piers in tandem arrangement.
b) The velocity power spectra revealed, 30% decrease in the strength of wake vortex behind the front piers and in front of rear pier, resulted in formation of lesser scour depths around rear pier as compared to single pier.

REFERENCES

Keshavarzi, A., Shrestha, C. K., Melville, B., Khabbaz, H., Ranjbar-Zahedani, M., Ball, J. (2018). Estimation of maximum scour depths at upstream of front and rear piers for two in-line circular columns. *Environmental Fluid Mechanics,* 18(2), 537-550.

Khaple, S., Hanmaiahgari, P. R., Gaudio, R., Dey, S. (2017). Interference of an upstream pier on local scour at downstream piers. *Acta Geophysica, 65*(1), 29-46.

Kothyari, U. C., Garde, R. C. J., Ranga Raju, K. G. (1992). Temporal variation of scour around circular bridge piers. *Journal of Hydraulic Engineering, 118*(8), 1091-1106.

Pasupuleti, L. N., Timbadiya, P. V., Patel, P. L. (2020). Bed level variations around submerged tandem piers in sand beds. *ISH Journal of Hydraulic Engineering*,1-9.

Pasupuleti, L. N., Timbadiya, P. V., Patel, P. L. (2021). Vorticity fields around a pier in rigid and mobile bed channels. *ISH Journal of Hydraulic Engineering*,1-10.

Wang, H., Tang, H., Liu, Q., Wang, Y, (2016). Local scouring around twin bridge piers in open-channel flows. *Journal of Hydraulic Engineering, 142*(9), 06016008-8.

ISBN: 978-90-824846-7-0

Proceedings of the 2nd IAHR
Young Professionals Congress
30 Nov-2 Dec. 2021

Suspended sand load in lower Uruguay River

Alejandro Nardin[1], Ricardo Szupiany[2] and Alejandro Arcelus[1]
[1] Comisión Administradora del Río Uruguay, Paysandú, República Oriental del Uruguay
e-mail anardin@caru.org.uy
[2] International Center for Large Rivers Research,
Universidad Nacional del Litoral, Santa Fe, Argentina
e-mail rszupian@fich.unl.edu.ar

ABSTRACT

In spite of its size and importance, lower Uruguay River has been very little studied regarding sediment transport. A new methodology for estimating suspended sand concentration from ADCP data was used to estimate suspended sand concentration for several field measurements. From this data solid and liquid discharge rating curves were constructed. Historical limnimetric data was used to obtain liquid discharge and suspended sand load time series. Results presented here not only constitutes one of the few publications attending the matter but helped prove the existence of a suspended sand mode threshold that is associated with the 10% chance of occurrence discharge (10000 m^3/s).

Keywords: suspended sediment; Uruguay River; ADCP; rating curve.

1 INTRODUCTION

Uruguay River is the second fluvial system in de la Plata River Basin. Its flows through Brazil, then it becomes the international limit between Argentina and Brazil, and in the last 500 km it is the limit between Argentina and Uruguay. It has a mean discharge of 5500 m^3/s which is roughly one third of the Parana River. Its lower reach comprises from de la Plata River to 350 km upstream, where Salto Grande Dam is located. Despite of the river importance to the region, there is a big gap in hydrosedimentological knowledge comparing with the Parana and other great rivers. During the last five years the Comisión Administradora del Río Uruguay (Uruguay River Administrative Board) has funded a project dealing with this aspect in order to start correcting this asymmetry. One of the main topics of this project focuses on the relation between Acoustic Doppler Current Profiler (ADCP) data and suspended sand concentration (M_s) (Nardin et al. 2021). Results of this relation are used in this paper to build liquid discharge and suspended sand rating curves. This paper aims to produce a data series of suspended sand load that can be used to evaluate geomorphological changes in lower Uruguay River.

2 METHODOLOGY

A series of 29 measurements made with an ADCP Sontek M9® was used for this paper. This measurements were taken in the cross section of the General Artigas International Bridge, located between Colón (Argentina) and Paysandú (República Oriental del Uruguay), and were conducted between 2014 and 2018. Water discharge (Q) ranged between 190 and 23893 m^3/s. This data was used to fit Equation [1] as a water discharge rating curve. In Equation [1] h is a limnimetric value, obtained by interpolation of the corrected (for difference in the reference plane) limnimetric value between Colón (Argentina, 7 km upstream) and Paysandú (Uruguay, 5 km downstream). a_1, b_1 and h_0 are a fitting parameters where the latter represents the limnimetric value were no liquid discharge is present.

$$Q = a_1(h - h_0)^{b1} \quad [1]$$

Nardin et al. (2021) presented a fair description of the procedure to use data from ADCP Sontek M9® in order to obtain suspended sand (grain size > 62µm) concentration (m_s) via inversion of the radar equation. The cross section where the methodology is applied is discretized in cells as the ADCP measurement. Then, m_s value is calculated for each cell. The product between measured velocity and the sand concentration in each cell results in the local suspended sand load (g_{ss}). If the latter is integrated across the cross section the suspended sand load (G_{ss}) is obtained. Then, mean cross section suspended sand concentration (M_s) is calculated as the relation between G_{ss} and Q. The data pairs (h,M_s) were used to fit the power equation [2].

ISBN: 978-90-824846-7-0

$$M_s = a_2 h^{b2} + c_2 \quad [2]$$

a_2, b_2 and c_2 are fitting parameters.
With both curves fitted, the G_{ss} and Q data series were calculated from the water limnimetric data series between 1980 and 2020. G_{ss} data was then annually aggregated.

3 RESULTS

In spite of the simple methodology applied, Figure 1 shows for the first time an approximation of a G_{ss} time series in lower Uruguay River. Calculated values are in agreement with previous unpublished modeling and field efforts but never scientifically tested. It is also visible a threshold-like behavior in the sand load, which implies that there is a given liquid discharge that starts the suspension transport mode with enough significance to generate noticeable morphological changes. For the presented data this value was estimated around 10000 m^3/s, which is a hydrodynamic scenario of less than 10% chance of occurrence.
Annual data aggregation for suspended sand load yields 0.9 Mton/year, with a maximum of an order of magnitude above and a minimum of an order of magnitude below.

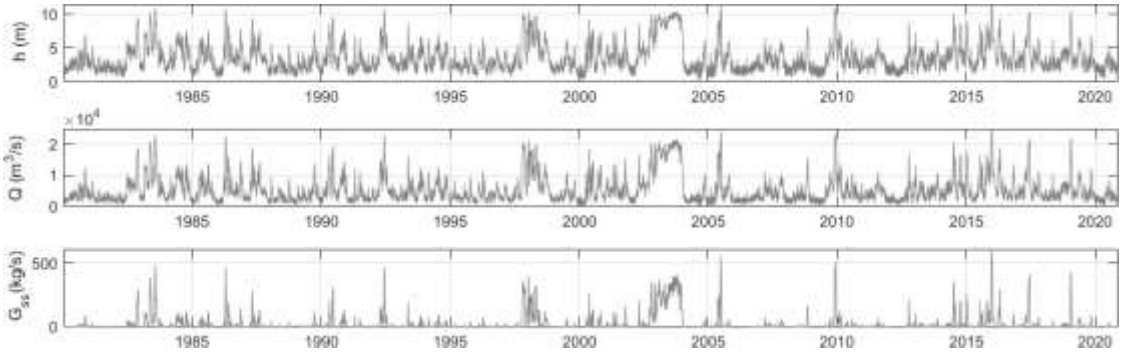

Figure 1. Time series for water head, liquid and suspended sediment discharge.

4 CONCLUSIONS

A newly developed methodology was used to estimate the bed material suspended sediment load in lower Uruguay River from Sontek M9® ADCP data. Liquid and solid discharge rating curves were fitted to obtained data. Time series of suspended sand load and liquid discharge were created. This information allowed for the first time to have results on sediment load in the study area, making a big step as reported information. Suspended load time series first analysis allowed to find a threshold for significant suspended sand load to occur, and provided information to compare, in future steps, with dredging volumes for example.

ACKNOWLEDGMENTS
This project was funded by the Comisión Administradora del Río Uruguay.

REFERENCES
Nardin, A., Szupiany, R., Lopez Weibel, C., Dominguez Ruben, L., Latosinski, F. and Arcelus, A. (2021). Procedimiento para la estimación de la concentración de sedimento en suspensión en un curso fluvial con un ADCP Sontek M9®. *Xxix Congreso Latinoamericano De Hidráulica.* 15 Al 19 de Noviembre de 2021. Virtual format.

Proceedings of the 2nd IAHR
Young Professionals Congress
30 Nov-2 Dec. 2021

Modelling the effects of vane on hydraulics and sediment transport

Syafiq Razali [1] and Badronnisa Yusuf [2]

[1] Universiti Putra Malaysia, Serdang, Malaysia,
gs62248@student.upm.edu.my

[2] Universiti Putra Malaysia, Serdang, Malaysia, ,
nisa@upm.edu.my

ABSTRACT

Operational problems associated with branching channel's water intake increase over time due to sediment accumulations. The success of branching channel projects depends on the design that can correctly maximize the water discharge and optimize the percentage of sediment discharge reduction. This study's main objective is to investigate the water and sediment flow in a branching channel system to compare the hydraulic performance of differently angled branching channels (30° and 60°) with submerged vanes to maximize the water discharge and optimize the percentage of sediment discharge reduction. Two types of vanes were tested that are a flat vane and a L-shaped vane with different vanes arrangements. This study implies that, the optimum vane arrangements and branching angle that will maximize the water discharge and optimize the percentage sediment discharge reduction is the 60° branching angle with one row flat vane because it managed to maximize the discharge by 34% resulting in the most optimized amount of sediment discharge reduction equivalent to 91.20%.

Keywords: branching channel; branching angle; vane arrangement; water discharge; sediment discharge.

1 INTRODUCTION

Civil engineers define water discharge in open channels as gravity-driven free surface flow, which often encounters flow patterns. Such a flow can be considered an inviscid and irrotational potential flow, provided that the flow velocity is relatively high and there is no severe separation between flow and definite boundaries (Batchelor, 2000). There have been many studies about water discharge in the branching channels in recent years. Primarily, they help by discovering how the bifurcation's flow characteristics are affected by its branching angle (Al Omari et al., 2012). One of the crucial problems that occurred at the entrance of the river intake is sediment deposition. The most common way to control the sediment load entering the branching channel is by vanes (Odgaard and Wang, 1991). Furthermore, with regards to vanes, the arrangements, and types of vanes to prevent deposition of sediment in the branching channel were proposed by Emamgholizadeh & Torabi, (2008). Nevertheless, there is still lack of studies pertaining to the optimum arrangements and types of vanes at the intake of the branching channel that can correctly maximize discharge and minimize the percentage of sediment discharge reduction. Furthermore, the water discharge in the branching channel was measured using a volumetric method by collecting water from the branching channel drainpipe for a period of one second. As a result, the water discharge at the downstream of the main channel can be calculated from the mass conservation equation, Equation 1 (Al Omari et al., 2020). For measuring the sediment discharge, a sediment basket with 75 µm mesh size was used to collect the sediment from the branching channel outlets. This basket was positioned below the drainpipe of the branching channel outlets to collect the sediment. By collecting the sediment from the branching channel outlets, the sediment discharge can be measured. Thus, the wet sediment was weighted and oven-dried (24 hours under 110℃), and the dried sediment was then weighted again. Furthermore, the percentage sediment discharge reduction was further calculated using Equations 2. A sand bed physical model comprised of two main channel channels that measured 12.25 m long, 0.313 m wide and 0.6 m deep and a branching channel that measured 2.75 m long and 0.6 m deep (Figure 1) was used to achieve this study's objectives.

$$QQ_{mm}(uuuuuuuuuuuuuuu\ uuuummmm\ ddmmuddh_{uuuuaauu}) = QQ_{bb}\ (bbuuuummddh_{mmmaa}\ ddmmuddh_{uuuuaauu}) + QQ_{dd}(ddddddmmuuuuuuuuuuuu\ uuuummmm\ ddh_{uummmmuuuu}\ ddmmuddh_{uuuuaauu}) \quad [1]$$

$$PPuuuudduummuuuuaauu\ ddoo\ uuuuddmmuuuummuu\ ddmmuddh_{uuuuaauu}\ uuuudduudduummddmm = \frac{DDDDDD\ mmaassss\ wwwwwh\ nnnn\ vvaannvv - DDDDDD\ mmaassss\ wwwwwh\ vvaannvv}{DDDDDD\ mmaassss\ nnnn\ vvaannvv} \times 100 \quad [2]$$

ISBN: 978-90-824846-7-0

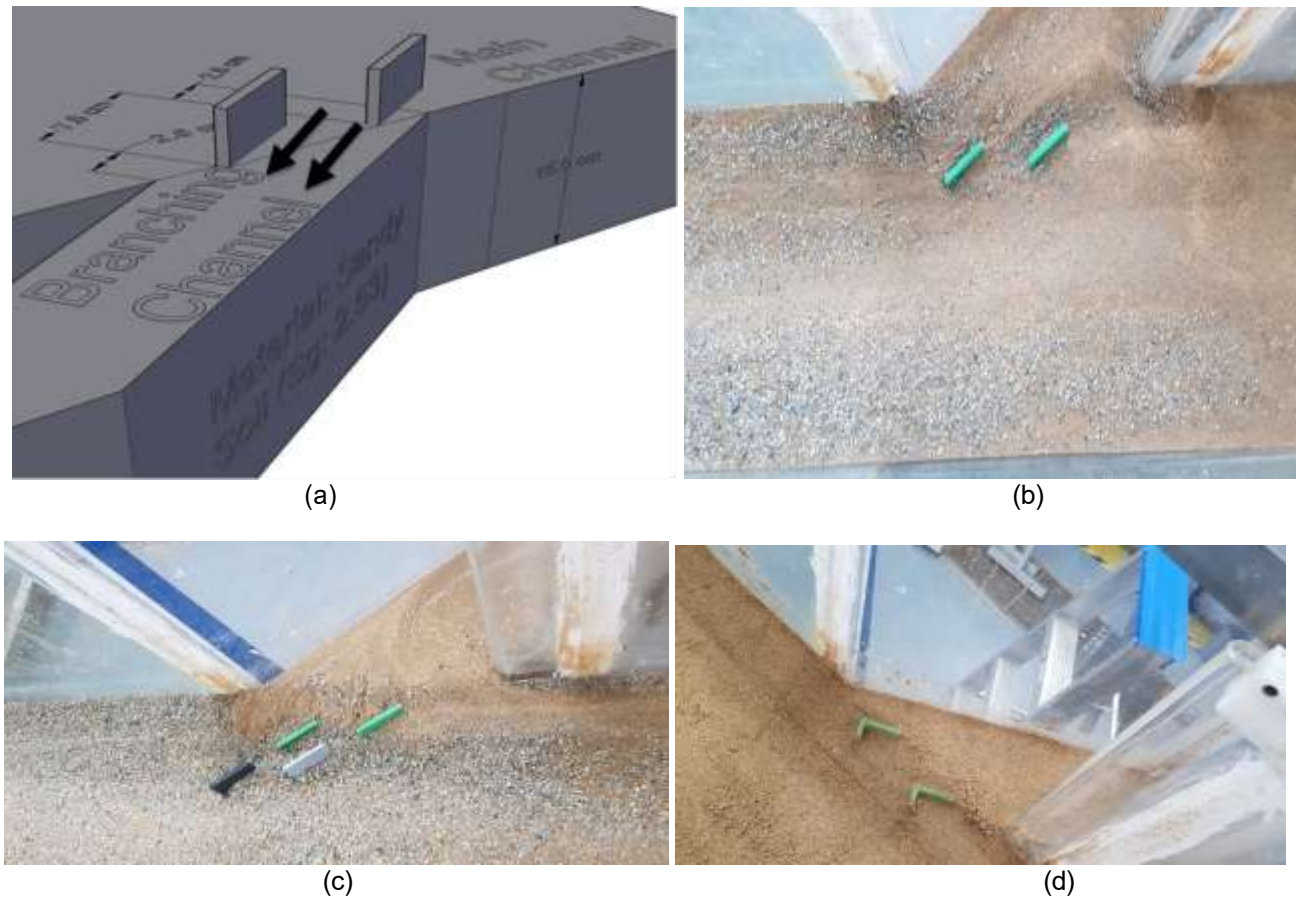

Figure 1: Vane arrangement (a) schematic of one row flat vane (b) lab work of one row flat vane (c) lab work of two rows flat vane (d) lab work of one row L-shaped vane.

2 CONCLUSIONS

The optimum vane arrangements and branching angle that will maximize the water discharge and optimize the percentage of sediment discharge reduction at the intake of the branching channel is the 60-degree branching angle with one row flat vane. It managed to maximize the discharge by 34% resulting in the most optimized amount of sediment discharge reduction that is 6.387 gram of sediment compared to 72.598 gram of sediment without a vane which equivalent to 91.20%.

REFERENCES

Al Omari, N. K., & Khaleel, M. S. (2012). Laboratory study of the effect of the branching angle and the branching channel slope on flow. Al-Rafadain Engineering Journal, 20(5), 33-41.Dong, N.C.,Araki, H., Yamanishi, H., and Koga, K. (2005). Simulation of groundwater flow and environmental effects resulting from pumping. *Environmental Geology,* 47 (3), 361-374.

Al Omari, N. K., Yusuf, B., Mohammad, T., Ghazali, A. (2020). Influence of diversion angle on water and sediment flow into diversion channel, International Journal of SedimentResearch,35(6),600-608.Retrieved from https://doi.org/10.1016/j.ijsrc.2020.06.006.

Batchelor, G. K. (2000). An introduction to fluid dynamics, Cambridge University Press. Cambridge, NY.

Emamgholizadeh, S., & Torabi, H. (2008). Experimental investigation of the effects of submerged vanes for sediment diversion in the veis (ahwaz) pump station. Journal of Applied Sciences, 8(13), 2396-2403.

Odgaard, A. J., & Wang, Y. (1991). Sediment management with submerged vanes. I Theory. Journal of Hydraulic Engineering, 117, 267-283.

ISBN: 978-90-824846-7-0

IAHR YPN

Young Professionals Network

Hosted by
Spain Water and IWHR, China

IAHR AIRH

International Association for Hydro-Environment Engineering and Research

Hosted by
Spain Water and IWHR, China

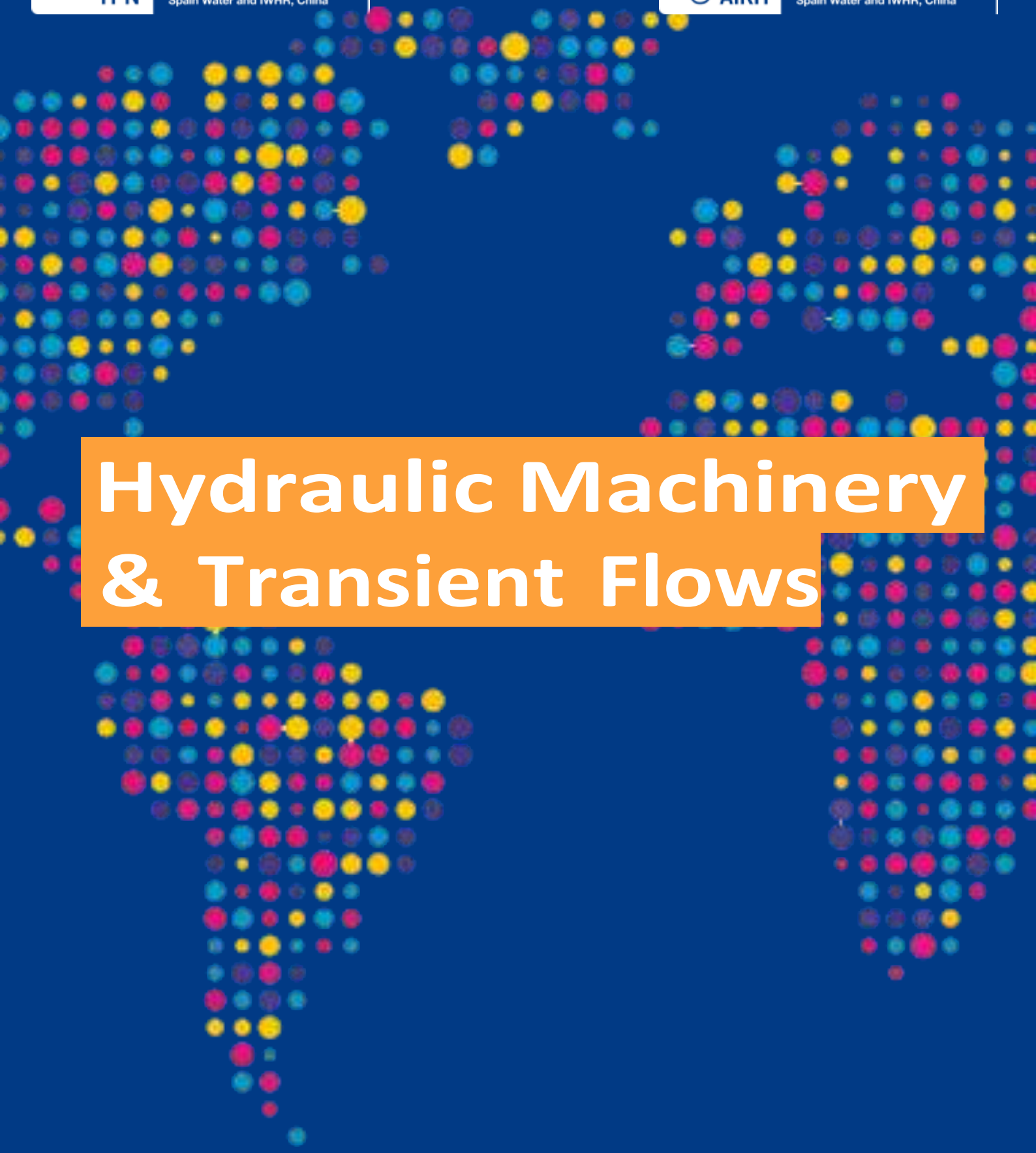

Hydraulic Machinery & Transient Flows

Proceedings of the 2nd IAHR
Young Professionals Congress
30 Nov-2 Dec. 2021

Power decay of a low head Kaplan turbine due to common vegetal bodies ingestion and accumulation

Emanuele Quaranta [1], Maurizio Previati [2]
[1] European Commission Joint Research Centre, Ispra, Italy
emanuele.quaranta@ec.europa.eu / quarantaemanuele@yahoo.it
[2] Interuniversity Department of Regional and Urban Studies and Planning (DIST), Politecnico di Torino and Università di Torino, Italy
maurizio.previati@unito.it

ABSTRACT

The problem of ingested bodies and sediments in hydropower plants is one of the current research trends in the hydropower sector, since sediments can generate several problems such as abrasion, increased maintenance costs, reduction of storage capacity. However, most researches focus on the effects of fine sediments rather than on the effects of common organic vegetal material that may enter the turbine and get stuck inside it. In this study, preliminary results on the power decay generated by the progressive accumulation of leaves and small wood branches in a micro Kaplan turbine are discussed, showing that the power output reduces by 15% over a time period of 3 days.

Keywords: ingested bodies; Kaplan turbine; micro hydropower; sediments.

1 INTRODUCTION

Hydropower is the largest renewable energy source, with slightly more than 1300 GW of installed capacity worldwide (IHA, 2020) and it is expected to grow in the future, especially thank to its flexibility in power control (IEA, 2021). However, some issues occur during hydropower operations, such as the problem of sediments and the impact on fish (Botelho et al., 2017). The problem of sediments is of interest both for the civil structures and for the electro-mechanical equipment. Reservoirs may suffer of sedimentation and reduction of storage capacity (Schleiss et al., 2016), while turbines may suffer of abrasion, with consequent efficiency and lifespan reduction, increased of maintenance costs and failures (Neopane et al., 2011). New materials can help in reducing the abrasion effects (Quaranta and Davies, 2021).
One of the less studied topics related to sediment is the problem of the ingested bodies, including leaves and small branches (e.g. Egusquiza et al., 2011) that are frequently abundant in most watercourses and are difficult to retain. The ingestion and accumulation of bodies in turbines can generate unbalanced forces up to blockages. Blockage in the distributor can change the amplitude and uniformity of the pressure pulsations, reducing the flow passing through the turbine and the power output, as well as the efficiency. Mechanical damages may also be generated (Egusquiza et al., 2011). If the ingested bodies are large enough, they can stick to the guide vanes of the distributor or to the runner channels, especially in micro turbines, due to the reduced spaces within the turbine unit. To shed more light on this, preliminary results of the power decay of a micro Kaplan turbine due to ingested bodies are discussed in this study.

2 CASE STUDY

A micro Kaplan turbine installed in North Italy was here examined. It is double regulated and designed for a head difference of 4.85 m, a design flow of about 0.65 m^3/s and a nominal power of 30 kW. The external runner diameter at the blade tip is 450 mm. The number of guide vanes is 13, while the runner blades are 4. The power take-off is composed by a pulley and a generator. During operation, a power decay of 2.7 kW was observed (from 17.2 kW to 14.5 kW) over a period of 3 days, as shown in Fig.1. The flow rate is almost constant during the power decay period, since it reduces from 590 l/s to 585 l/s. This means that the power decay is mostly due to a reduction of the turbine efficiency.
Since the flow rates Q (m^3/s) and power P (kW) are known, the head is constant at H=4.85 m and $P = 9.81\ \eta\ H\ Q$, where η is the unit efficiency, it is possible to deduce that the overall plant efficiency reduces from 61.2% to 52.1%, thus it reduces by 15%. In order to better understand this phenomenon, and considering that the literature review was not successful to help on this, visual inspections were carried out (Fig.2). It was found that the problems lied in the accumulation of large organic vegetal bodies within the guide vanes. They got stuck in the gap (< 0.5 mm) between the guide vanes and the shroud. The original condition (P=17.5 kW) could be

ISBN: 978-90-824846-7-0

restored through a start and stop cycle, that, anyway, is not a recommendable practice due to the high stresses undergone by the turbine, with a consequent reduction of the life span (Trivedi et al., 2013).

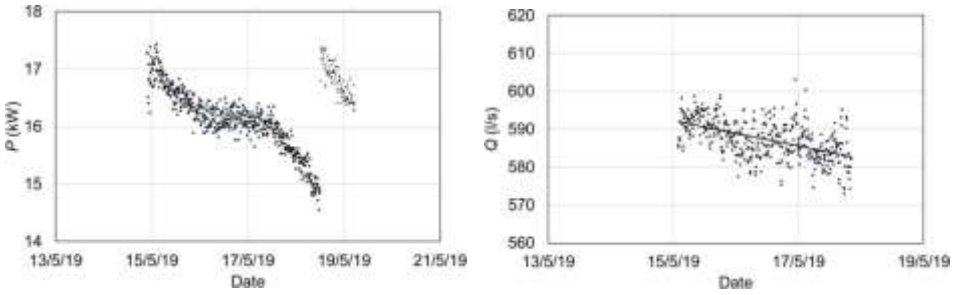

Figure 1. Power decay (left) and observed flow rate reduction (right). The flow rate was monitored every 10 minutes and the figure shows the mobile average every 30 minutes.

Figure 2. Visual inspections and accumulation of organic vegetal bodies: immediately after operation (left) and after few minutes of inactivity (right).

3 CONCLUSIONS

In this work it was shown as micro turbines may suffer of occlusions due to ingestion and accumulation of vegetal material difficult to retain. The scientific literature on this phenomenon is rather limited, thus with our results we aimed at shedding more light on this problem and at stimulating future researches. We showed that the main effect of this phenomenon is the rapid decrease in the turbine efficiency (e.g. 15% in few days) rather than a decrease in the flow rate. This effect may become even worse in autumn, with a larger and faster decay, in relation to the increased availability of suspended material into the water.

REFERENCES

Botelho, A., Ferreira, P., Lima, F., Pinto, L. M. C., & Sousa, S. (2017). Assessment of the environmental impacts associated with hydropower. *Renewable and Sustainable Energy Reviews*, 70, 896-904.

Egusquiza, E., Valero, C., Estévez, A., Guardo, A., & Coussirat, M. (2011). Failures due to ingested bodies in hydraulic turbines*. Engineering failure analysis*, 18(1), 464-473.

International Energy Agency (IEA) (2021). Hydropower Special Market Report. Analysis and forecast to 2030.

International Hydropower Association (IHA), (2020). Hydropower Status Report Sector trends and insights, IHA Central Office, United Kingdom.

Neopane, H. P., & Cervantes, M. (2011). Sediment erosion in hydraulic turbines. *Global Journal of Research Engineering*, 11(6).

Quaranta, E. & Davies, P. (2021). Emerging and innovative materials for hydropower engineering applications: turbines, bearings, sealing, dams and waterways, and ocean power. *Engineering, in press.*

Schleiss, A. J., Franca, M. J., Juez, C., & De Cesare, G. (2016). Reservoir sedimentation. *Journal of Hydraulic Research*, 54(6), 595-614.

Trivedi, C., Gandhi, B., & Michel, C. J. (2013). Effect of transients on Francis turbine runner life: a review. Journal of Hydraulic Research, 51(2), 121-132.

ISBN: 978-90-824846-7-0

Proceedings of the 2nd IAHR
Young Professionals Congress
30 Nov-2 Dec. 2021

Performance monitoring of two Pico-Hydropower Pumps as turbines over time

Daniele Novara [1], Aonghus McNabola [1]

[1] Department of Civil, Structural & Environmental Engineering, Trinity College Dublin, Ireland
novarad@tcd.ie

ABSTRACT

While a substantial literature has been produced on hydraulic energy recovery from water supply pipelines, only a limited number of such applications exist with nominal power less than 100 kW. A hydro turbine technology particularly suitable to such context is that of Pumps As Turbines (PAT), which can offer a lower cost when compared to conventional machines. However, the application and performance over time of this kind of devices has not been extensively investigated. In the present research, two PAT installations which were built and commissioned in Ireland and Wales in late 2019, have since been monitored in order to assess their performance in terms of power generation. The results show that both PATs have proved themselves to work in a satisfactory way initially, although after a few months their production was limited by external phenomena.

Keywords: Pump as Turbine (PAT); energy recovery; technology demonstration

1 INTRODUCTION

Energy recovery from water pipelines through Micro-Hydropower (MHP), i.e. hydro power with installed capacity <100 kW, is a widely investigated practice which has found limited practical application to date due to several factors such as the large acquisition cost of miniaturized conventional hydro turbines and the lack of records of practical installations (Novara, Carravetta, McNabola, & Ramos, 2019). Indeed, this is also true when considering Pico-Hydropower (PHP) applications in water pipelines, i.e. with capacity <5 kW, where the acquisition costs present an even greater challenge, yet the number of potential PHP opportunities is large.

In order to reduce installation costs, the use of a Pump As Turbine (PAT) has been suggested (Williams, 1996; Novara, Carravetta, McNabola, & Ramos, 2019). Such devices are generally inexpensive, easy to source, repair and adapt for installation within wholly pressurized conduits (Williams, 1996; Lahimer & al., 2012; McNabola, et al., 2014). In order to demonstrate the technical and economical applicability of PAT technology at the PHP scale, two energy recovery pilot plants have been designed and built in 2019.

The first scheme is located in Ireland at the raw water inlet of the Blackstairs Water Treatment Plant (WTP). Before the installation of the PAT, water was being collected from a stream on the side of the mountain and from there it was conveyed by gravity to the WTP. After the MHP installation, a 3.3 kW PAT working at 17 l/s and 36 m of head has been placed on the terminal portion of the water supply pipe in order to recover the potential energy which was otherwise being dissipated as friction and turbulence losses. The turbine was commissioned in October 2019 and its performances have been tracked via a remote monitoring sensor suite. The recorded monthly energy generation over 22 months is displayed in Figure 1.

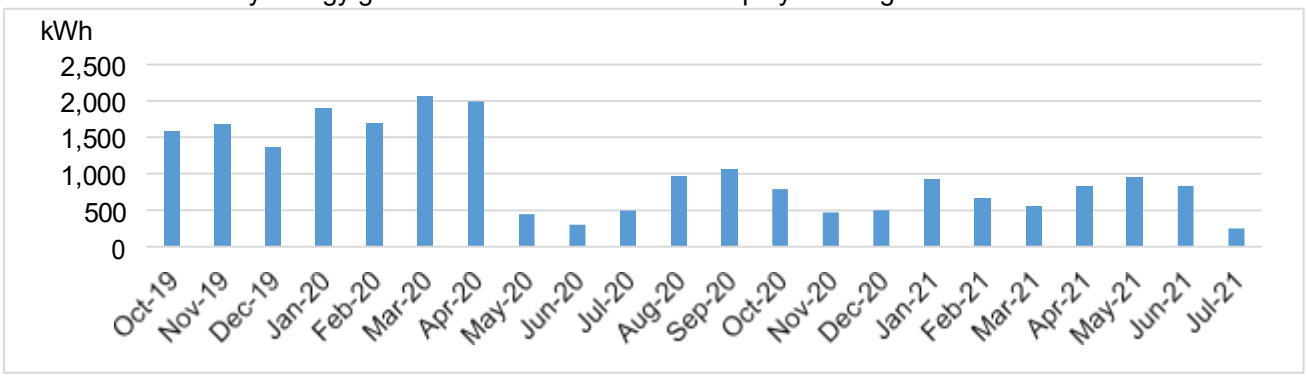

Figure 1. Monthly electricity output from the PAT installed at the Blackstairs WTP.

During the first 12 months the scheme generated 15,600 kWh which was entirely self-consumed within the premises of the WTP allowing the saving of €2,037 and avoiding the emission of 3.6 tons of CO_{2eq}. In the first seven months of operations the monthly energy output was between 1,500-2,000 kWh while it dropped below 500 kWh during the summer season as the river source dried up. During the months between October 2020

ISBN: 978-90-824846-7-0

and April 2021 the power generation remained low and equivalent to 1/4th of the values recorded between October 2019 and April 2020 due to a recurring air lock phenomenon which have since been solved.
The second PAT installation is located on a river in Northern Wales, next to the historical farmhouse of Ty Mawr Wybrnant. Here, a river diversion intake has been built on the Wybrnant stream in order to convey up to 25 l/s of water to the downstream turbine site located 300 m away. At the powerhouse, a 3.7 kW PAT has been installed to generate electricity for self-consumption within the property. The monthly energy generation as recorded by the telemetry system is displayed in Figure 2.

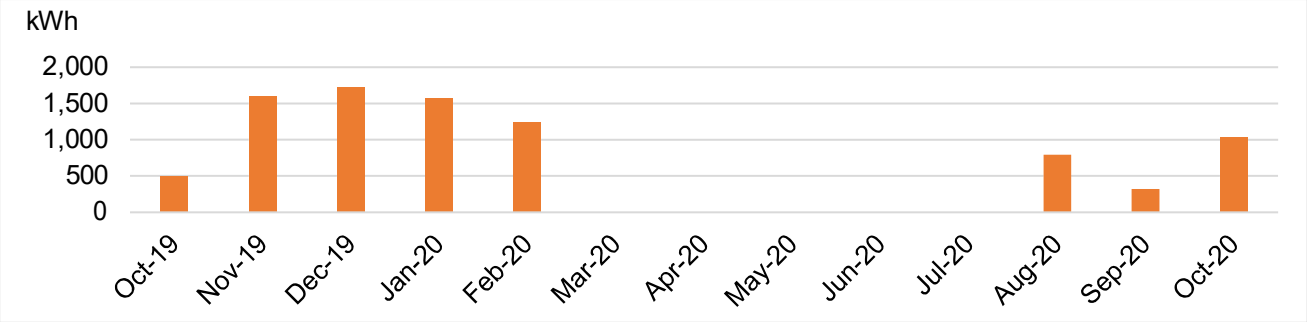

Figure 2. Monthly electricity output from the PAT installed at the Ty Mawr Wybrnant.

Since its commissioning in late October 2019 the turbine has generated a satisfactory amount of monthly electricity. However, during the course of 2020 the installation suffered flood damages in two separate storms and is currently awaiting repairs.

2 CONCLUSIONS

The applicability of PAT technology from both man-made and natural water streams has been demonstrated via two pilot schemes located in Ireland and Wales respectively. Thanks to the continuous remote monitoring of the two installations, it was determined that the Blackstairs turbine in Ireland has been operating in a satisfactorily way for most of the 22 months since commissioning. Instead, the PAT installed at Ty Mawr Wybrnant in Wales although proved to generate the expected power output in the first five months of operations was repeatedly damaged by natural events during the course of 2020.

ACKNOWLEDGEMENTS

This research was part funded by the ERDF Interreg Ireland Wales Programme 2014-2020, through the Dŵr Uisce Project (80910).

REFERENCES

Lahimer, A. A., & al. (2012). Research and development aspects of pico-hydro power. *Renewable and Sustainable Energy Reviews, 16.8*, 5861-5878.

McNabola, A., Coughlan, P., Corcoran, L., Power, C., Williams, A. P., Harris, I., . . . Styles, D. (2014). Energy recovery in the water industry using micro-hydropower: an opportunity to improve sustainability. *Water Policy, I*(16), 168-183.

Novara, D., Carravetta, A., McNabola, A., & Ramos, H. M. (2019). Cost Model for Pumps as Turbines in Run-of-River and In-Pipe Microhydropower Applications. *J. of Water Resources Planning and Management, 145*, pp. 1-9. https://doi.org/10.1061/(ASCE)WR.1943-5452.0001063

Williams, A. (1996). Pumps as turbines for low cost micro hydro power. *Renewable Energy, I*(9), 1227-1234

ISBN: 978-90-824846-7-0

Proceedings of the 2nd IAHR
Young Professionals Congress
30 Nov-2 Dec. 2021

Numerical simulation of vavitation in Pelton turbine injector

Navam Shrivastava[1], Chetan Mali[2] and Anant Kumar Rai[3]

[1,2,3]National Institute of Technology Warangal, India
[1]email: ns720040@student.nitw.ac.in
[2]email: meetchetanmali@gmail.com
[3]email: anant@nitw.ac.in

ABSTRACT

The wear of turbines components from hydro-abrasive erosion and cavitation is one of the major concerns in hydropower plants especially in Himalayan Mountains. In this work, the cavitation prone regions of a Pelton turbine injector are studied numerically. A Discrete Phase Model (DPM) along with Volume of Fluid (VOF) method was used to simulate the multiphase flow in Pelton turbine injector and thelocations prone to cavitation were determined. The initially obtained results were validated with the measured values from a hydropower plant in the Indian Himalayas. The measured values showed traces of cavitation in addition to hydro-abrasive erosion.

Keywords: Cavitation, Erosion, Pelton turbine Injector, CFD, Volume of Fluid

1. INTRODUCTION

In geologically young mountains like Himalayas, the presence of sediment particles causes cavitation of the turbine surfaces which leads to significant losses in energy production. Messa et al. (2019) tried to analyze hydro-abrasive characteristics in terms of single variable, i.e. effective nozzle opening area. Guo et al. (2020) reported asymmetrical pattern of erosion in Pelton turbine injector where more weight loss takes place at upstream of nozzle outlet and reduces further towards the needle tip region due to decrease in momentum of sediment particles. Rossetti et al. (2014) used Eulerian-Eulerian multiphase model with assumption of homogeneous flow to study cavitation dynamics on Pelton turbine buckets. In present study, initial numerical results of cavitation prone regions in Pelton injector are compared with the field readings of volume wear reported by Din and Harmain (2020).

2. METHODOLOGY

Discrete Phase Model (DPM) is used to model sediment particles suspended in the fluid flow. Volume of fluid (VOF) multiphase model is used in ANSYS workbench for simulations of air-water mixture. K-omega SST turbulence model is used to solve two equations for turbulence intensity and turbulence dissipation rate since it provides more accurate results in case of adverse pressure gradient and y+ value less than 5.Sum of static pressure and dynamic pressure i.e. total gauge pressure of 40 bars is used as boundary condition at water inlet as per field conditions. The pressure outlet is set to zero static gauge pressure. The SIMPLE algorithm is used to compute pressure and velocity values in segregated manner. Further, a transient approach and mixture multiphase model is used to study the formation of bubble growth of water vapour.

3. RESULTS

The basic geometric details of Pelton turbine injector with its different parts is shown in Figure 1. It can be observed from contour plot of velocity (Figure 2) that there is an increase in velocity of localized region near nozzle ring where negative pressure is observed (Figure 4). The increased velocity leads to higher

ISBN: 978-90-824846-7-0

hydro-abrasive erosion. The deformed profile gives rise to local cavitation on the needle surface and the synergic effects of erosion and cavitation accelerates the wear processes significantly (Figure 3).It was found that bubble growth of wa er vapour near the nozzle seat sustained for 100 to 150 microseconds. Figure 5 shows the bubble of water vapour generated near the nozzle ring. Eroded parts of Pelton turbine, i.e. needle and nozzle ring of the Chennai hydropower plant, which is located in Indian Himalayas and was used for validation purpose, are shown in Figure 3 and Figure 6, respectively. The eroded regions of the injector components, i.e. nozzle and needle are classified into various zones as per its severity.

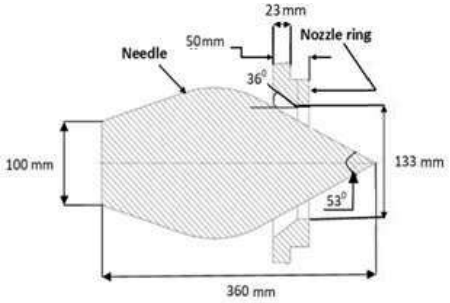

Figure 1.Pelton Injector modified from Din and Harmain (2020)

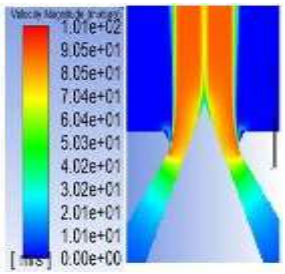

Figure 2. Velocity contour plot

Figure 3. Blunt needle tip subjected to high pressure (Din and Harmain 2020)

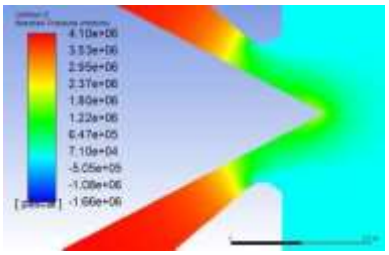

Figure 4. Absolute pressure plot near the nozzle seat

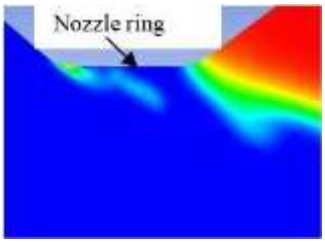

Figure 5.Bubble formation in transient modelling approach

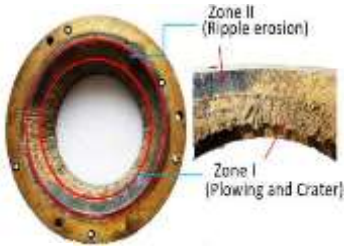

Figure 6. Wear on nozzle ring (Din and Harmain 2020)

4. CONCLUSIONS

The cavitation in a Pelton turbine injector has been studied in the present work and initial results are provided. As the cavitation phenomenon magnifies at the part load conditions, the authors plan to extend the work for various load conditions by varying the opening of the injector. Most widely used transient modelling approach along with Schnerr-Sauer cavitation model will be used further to study cavitation in Pelton turbine injector. Time step size in order of microseconds is sufficient to capture the bubble growth.

REFERENCES

Guo,B., Xiao, Y.X., Rai, A.K., Zhang, J. and Liang, Q.(2020). Sediment-laden flow and erosion modeling in a Pelton turbine injector. *Renewable energy* 162 30-42.

Messa, G.V., Mandelli, S. and Malavasi, S. (2019). Hydro-abrasive erosion in Pelton turbine injectors: a numerical study. *Renewable Energy* 130 474–488.

Rossetti, A., Pavesi, G., Ardizzon, G. and Santolin, A.(2014).Numerical analyses of cavitating flow in a Pelton turbine. *Journal of Fluids Engineering*136 (8)81304.

Din, M.Z.U. and Harmain, G.A.(2020).Assessment of erosive wear of Pelton turbine injector: Nozzle and spear combination – A study of Chenani hydro-power plant. *Engineering Failure Analysis* 116 104695.

ISBN: 978-90-824846-7-0

Proceedings of the 2nd IAHR
Young Professionals Congress
30 Nov-2 Dec. 2021

Pumps as turbine regulation study through a Decision-Support Algorithm

Maël Le Marre [1,2], Philippe Mandin [1,2], Jean-Louis Lanoisellé [1], Erik Zilliox[2], Farah Rammal[2]
[1] *Univ. Bretagne Sud, UMR CNRS 6027, IRDL, F-56300 Lorient, France*,
e-mail: mlemarre.esli@campus-redon-industries.com
[2] *GIP Campus ESPRIT Industries, Redon, F-35600, France*

ABSTRACT

Today, a major aspect of sustainability in our society is energy efficiency. Regarding the water distribution network (WDN), pressure reducing valves (PRV) are implemented to reduce water leakages, which leads to energy losses. To recover some of the wasted energy for electricity, and make the area more efficient, the pumps as turbine (PAT) are adequate devices to replace the PRV, in particular for their low investment cost compared to conventional turbines. In the WDN, the flow conditions are variable; furthermore, the efficiency of the PATs decreases sharply at partial load, hence, it is necessary to use hydraulic regulation methods via valves or electrical regulation methods via frequency inverters. Two regulation methods are presented and analyzed in this study through 3 operating sites, and a decision-support algorithm is also described.

Keywords: energy efficiency; water distribution network; pumps as turbine; regulation; decision-support algorithm.

1 INTRODUCTION

The energy consumption of clean water treatment and distribution consumes between 2 and 3% of global energy [De Marchis et al. 2014]. Water transport and distribution pipes are subject to numerous breakages during their lifetime, resulting in leakage rate. This results in over-consumption of pumps that load the network. These leakage rates are directly related to the pressure within the pipes [Araujo et al. 2006]. One solution for reducing the pressure in the pipes and converting this pressure drop into electricity is micro-hydropower.
Micro-hydropower (MHP) is defined as small hydroelectric power plant for powers between 5 and 100kW. Implementing this type of solution in the water distribution network (WDN) can allow 25% recovery of the WDN energy consumption [De Marchis et al. 2014]. The use of conventional turbines is not economically viable for MHP due to a high investment cost. To resolve this economical issue, the pumps as turbine (PAT) are a good solution.
Indeed, the PAT are cost-effective elements and have a good efficiency at their best efficient point (BEP) [Chappalaz et al. 1992]. One of the main issues of using PATs is that manufacturers only provide the characteristics in pump mode. To estimate the BEP in turbine mode, it is necessary to use predicting methods. One possibility is to use numerical simulation, but it may be problematic to get the pumps geometry from the manufacturers. Another possibility is to use empirical correlations, which only use the characteristics given by the manufacturers [Yang et al. 2012]. However, nowadays, it remains an uncertainty up to 20% with those methods. In WDN, the flow rates and head are variables, therefore, knowing the BEP of a PAT is not enough. Hence, researchers have developed some dimensionless polynomial correlations to estimate the entire characteristic curves by recovering experimental data from the publications [Pérez-Sánchez et al. 2020].
The other main problem of the PAT is their bad behavior at part load conditions. It is therefore necessary to use regulation methods. Three regulation methods have already been studied. The first one, the hydraulic regulation (HR) consists in placing two PRVs, one in series which absorbs the overpressure, and one in parallel which by-passes the overflow. The second one, the electrical regulation (ER) consists in adding a frequency inverter between the electrical motor and the grid to adapt the rotational speed of the pump with the upstream conditions. The third one is the coupling of HR and ER (HER) [Stefanizzi et al. 2020].
The energy production calculation's methods remain unclear in the scientific literature. Therefore, a decision-support algorithm for energy production and economic calculation has been developed and will be explained in detail through the study of 3 sites located in Brittany (France). A comparison between the HR and HER regulation on these sites is analyzed in energetic and economical terms.

2. DECISION-SUPPORT ALGORITHM

In this part, a novel algorithm is presented. Also called a decision-support algorithm, it allows to rapidly calculate the energy production and the payback period of a PAT site with only in inlet a set of

measurements. One of the goals of the software is to allow the water companies to estimate their energy recovery potential by themselves, because it is often difficult for the researchers and private companies to recover the data of the water distribution network. The software is composed of two inlet files, the data set of measurement, and a data set of more than 700 PATs, with their characteristics in turbine mode estimated with the Yang's correlations [Yang et al. 2012]. The figure 1 shows the general scheme of the algorithm.

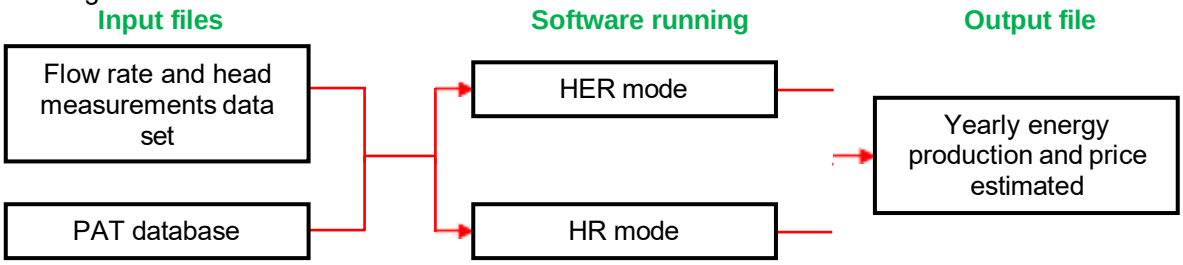

Figure 1: General scheme of the decision-support algorithm

3 RESULTS OF TWO REAL SITES WITH THE DECISION-SUPPORT ALGORITHM

The results of three real sites obtained with the decision-support algorithm are shown is table 1. For the three sites, the HER gives a better energy production but increase the payback period.

Table 1: Results of the decision-support algorithm

	Site	Herbignac	Rennes	St Malo de Phily
HR	Energy production (MWh/year)	74.41	69.62	49.63
	Payback period (years)	6.5	11.5	10
HER	Energy production (MWh/year)	75.81	76.53	53.56
	Payback period (years)	9	15	15

4 CONCLUSIONS

The study shows that in term of energy saving, the HER is more viable than the HR, but it increases the cost of investment, and the frequency inverter must be replaced every 8 years, by consequence, in economical term, the HR is more viable. Water companies can therefore focus on the energy saving and/or the economical side as well.

ACKNOWLEDGEMENTS

This project is co-financed by the European Regional Development Fund through the Interreg Atlantic Area program (EERES4WATER). The authors gratefully acknowledge the European financing.

REFERENCES

Araujo, L. S., Ribeiro, M. F. M., Enzveiler, A., Schenkel, P., Fernandes, T. R. G., Partata, W. A., Irigoyen, M. C., Llesuy, S. & Belló-Klein, A. (2006). Pressure Control for Leakage Minimisation in Water Distribution Systems Management. *Water Resources Management*, *249*(1–2), 133–149.

Chappalaz JM, Eichenberger P., Fischer G. (1992) Manual on pumps used as turbines. *MHPG*

De Marchis, M., Fontanazza, C. M., Freni, G., Messineo, A., Milici, B., Napoli, E., Notaro, V., Puleo, V. & Scopa, A. (2014). Energy recovery in water distribution networks. Implementation of pumps as turbine in a dynamic numerical model. *Procedia Engineering*, *70*, 2013.

Pérez-Sánchez, M., Sánchez-Romero, F. J., Ramos, H. M. & López-Jiménez, P. A. (2020). Improved planning of energy recovery in water systems using a new analytic approach to PAT performance curves. *Water (Switzerland)*, *12*(2).

Stefanizzi, M., Capurso, T., Balacco, G., Binetti, M., Camporeale, S. M. & Torresi, M. (2020). Selection, control and techno-economic feasibility of Pumps as Turbines in Water Distribution Networks. *Renewable Energy*, *162*, 1292–1306.

Yang, S. S., Derakhshan, S. & Kong, F. Y. (2012). Theoretical, numerical and experimental prediction of pump as turbine performance. *Renewable Energy*, *48*, 507–513.

Proceedings of the 2nd IAHR
Young Professionals Congress
30 Nov-2 Dec. 2021

Operation of a pumping station: Selecting the number of active pumps

Araceli Martín[1], Francisco Javier Martin-Carrasco[2], David Santillán Sánchez[3]

Universidad Politécnica de Madrid, Madrid, Spain,
araceli.martin@upm.es[1], f.martin@upm.es[2], david.santillan@upm.es[3]

ABSTRACT

The objective of this research is to determine how many hydraulic pumps must be running to provide the desired volume of water using the least possible amount of energy. This is typically done with complex iterative algorithms that require great computational efforts. In this work, the objective has been analyzed from an analytical perspective, resulting in the expression of curves that are easy to elaborate and of instantaneous use, they are the curves of Hyperbolic Convexity. Its immediate applicability and simplicity make it a method ready for practical use by professional engineers. These curves immediately indicate which is the best combination of pumps to minimize energy consumption, based on the desired volume of water.

Keywords: water supply systems; operation; pumping station; energy

1 INTRODUCTION

When the pumps are arranged in parallel, the consumed energy **E** varies as a function of the number of active pump groups. The specific energy **e** is defined as the amount of energy required to pump a cubic meter of water, that is $e = E/V$. Therefore, pumping a volume of water **V** using the least energy also implies using the least specific energy. When plotting the specific energy **e** versus the volume of water consumed **V**, as in Figure 1, if only one group $\mathbf{n_g=1}$ of pumps were pumping the whole time $\mathbf{t_t}$, the obtained volume of water would be $\mathbf{V_{1g}}$, whilst if there were two pumps working $\mathbf{n_g=2}$ the volume would be $\mathbf{V_{2g}}$. However, if we desired a different volume of water **V***, in between $\mathbf{V_{1g}}$ and $\mathbf{V_{2g}}$, the arrangement of the active pumps could be considered in the following different ways:

i. Solution 1: Use two groups $\mathbf{n_g=2}$ until you obtain **V***.
ii. Solution 2: Use one group $\mathbf{n_g=1}$ to pump part of the time, and two groups $\mathbf{n_g=2}$ the rest of the time.

These two options are represented in Figure 1. The key question is to determine which of the two options consumes less energy.

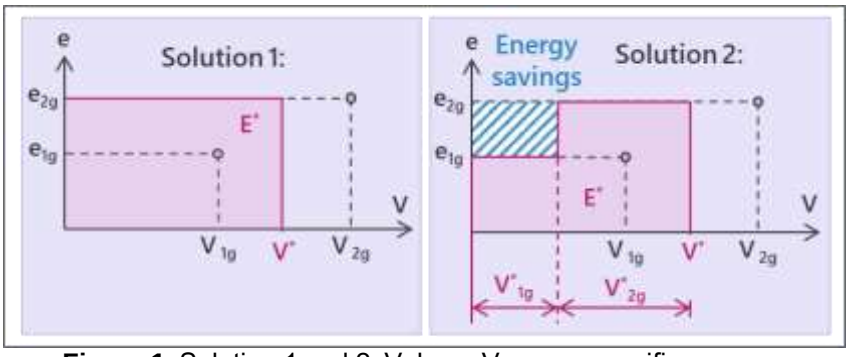

Figure 1. Solution 1 and 2. Volume V versus specific energy e.

As can be seen, Solution 2 represents an energy saving compared to Solution 1 represented by the rectangle lined in blue. Therefore, to the questions “How to pump a desired volume of water **V *** before a certain time $\mathbf{t_t}$ using the least amount of energy? How many groups should work?" the answer is "You have to combine the number of groups: pump one time with a number of groups, and the remaining time with another number of active groups."

ISBN: 978-90-824846-7-0

However, new questions now arise: Knowing that it is convenient to combine different pump groups, instead of alternating between $\mathbf{n_g=1}$ and $\mathbf{n_g=2}$, one could go from $\mathbf{n_g=1}$ to $\mathbf{n_g=3}$; or from $\mathbf{n_g=2}$ to $\mathbf{n_g=5}$? Ultimately, what is the best combination of $\mathbf{n_g=i}$ and $\mathbf{n_g=j}$?

2 THE THEORY BEHIND THE METHOD

The key to solving these questions is to draw the evolution of the specific energy e* consumed to pump any volume **V***. For this, it will be necessary to find the function **e*=f(V*)**. This function is obtained from the following fundamental equations:

$$t_t = t^*_{1g} + t^*_{2g} \quad [1]$$

$$V^* = V^*_{1g} + V^*_{2g} \quad [2]$$

$$E^* = E^*_{1g} + E^*_{2g} \rightarrow V^* \cdot e^* = V^*_{1g} \cdot e_{1g} + V^*_{2g} \cdot e_{2g} \quad [3]$$

Being $\mathbf{t^*_{1g}}$ and $\mathbf{t^*_{2g}}$ the time spent pumping respectively with $\mathbf{n_g=1}$ and $\mathbf{n_g=2}$; $\mathbf{V^*_{1g}}$ and $\mathbf{V^*_{2g}}$ are respectively the volume pumped using $\mathbf{n_g=1}$ and $\mathbf{n_g=2}$. By combining these three equations, after a mathematical development the following Equation 4 is reached. It is expressed in its general form, without particularization, for any $\mathbf{n_g=i}$ and $\mathbf{n_g=j}$. The specific energy is the result of the sum of a constant plus a convex hyperbola. Therefore, each combination of pumps $\mathbf{n_g=i}$ and $\mathbf{n_g=j}$ allows us to draw a convex hyperbola. This can best be seen in the following Figure 2.

$$e^* = e_{jg} - \frac{V_{ig} \cdot (V_{jg} - V^*)}{V^* \cdot (V_{jg} - V_{ig})} \cdot (e_{jg} - e_{ig}) = f(V^*) \rightarrow \mathbf{e^* = \propto - \frac{\beta}{V^*} = Constant - Hyperbola} \quad [4]$$

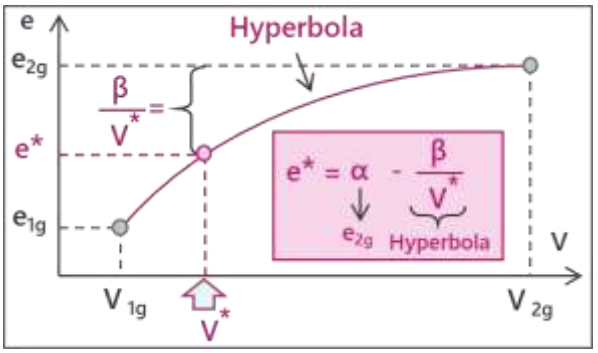

Figure 2. The convex hyperbola.

3 STRATEGY OF SELECTION OF THE PUMPS

The strategy to be applied therefore to use will be to draw the curves e*-V *, that is, the convex hyperbolas, for all the possible combinations of pumps within the station. Once drawn, the engineer should enter the graph with the volume V * to be pumped, and selects the lowest possible curve, since that will be the curve that indicates which is the combination that consumes the least energy. The following figure shows several examples of pumping stations, with theoretical cases of how the curves could be crossed. These curves only need to be elaborated once and are a permanent tool for the operation of pumping stations.

4 CONCLUSIONS

A method has been proposed to select the number of groups that should be combined to pump any desired volume of water. The method consists of drawing a collection of convex hyperbolas for all possible groups combinations. For each desired volume of water V*, the engineer should look in the charts which is the lowest of the curves. The lowest of the curves will indicate which is the least energy consuming combination of pumps.

REFERENCES

Martin-Candilejo, A., Martin-Carrasco, F.J., and Santillán, D. (2021). How to select the number of active pumps during the operation of a pumping station: The Convex Hyperbola Charts. *Water,* 13 (11), 1474.

ISBN: 978-90-824846-7-0

Proceedings of the 2nd IAHR
Young Professionals Congress
30 Nov-2 Dec. 2021

Analysis of flow characteristics of Pump-turbine in transient process

Xilong Yin[1], Shaozhen Zhang[1], Huili Bi[1], Xingxing Huang[2*] and Zhengwei Wang[1*]

[1] Department of Energy and Power Engineering, Tsinghua University, Beijing 100084, China
[2] InnoFuture GmbH, Binzstrasse 5, 8953, Z¨urich, Switzerland

Yinxl21@mails.tsinghua.edu.cn

ABSTRACT

In modern society, the demand for grid load regulation is increasing, and pumped storage power stations are very important in the power system, and the pump-turbine units need more start-stops per day. As an important component of the unit, the research of the steady-state flow phenomenon of the pump-turbine has been widely studied, while the unsteady flow characteristics in the transient process are more complicated and have not been explored in depth. Therefore, it is of great significance to study the unsteady flow characteristics of the pump-turbine in the start-up and shut-down transient process. In this study, the coupling calculation method of the one-dimensional pipeline model and the three-dimensional model of the unit was used to numerically simulate the start-up and shut-down process of the pump-turbine in turbine mode through the coupling calculation, and the flow characteristics of the unit during the start-up and shut-down process were analyzed.

Keywords: Pump-turbine; coupling simulation; transient process; Pumped storage power station; start-up and shut-down

1 INTRODUCTION

This paper researches a prototype reversible pump-turbine unit of a high head pumped storage power station and analyzes the pressure change of the unit under start-up and shut-down conditions. The three-dimensional calculation domain of the pump-turbine unit consists of five parts: spiral casing, stay vane, guide vane, runner, and draft tube, as shown in Figure 1. Among them, the spiral casing inlet centerline is parallel to the draft tube outlet centerline. The pump-turbine has a rated head of 545m and a rotational speed of 428.6r/min. At the rated head, the rated output power of the turbine is 357.1MW, and the number of runner blades is 11, the number of stay vanes and the number of guide vanes are both 20.

Figure 1. Three-dimensional computational domain of pump-turbine

When the turbine starts up, the guide vanes will gradually open, from the fully closed state to the no-load opening; when the turbine shuts down, the guide vanes will gradually close [1]. According to the the movement law of guide vanes during the turbine start-up and shut-down processes, the one-dimensional pipeline transient calculation can be carried out, and the pressure at the spiral casing inlet and the draft tube outlet can be obtained. Taking these pressure distributions as boundary conditions, the three-dimensional CFD calculation of the pump-turbine unit can be performed [2, 3].

2 START-UP PROCESS

Based on the time-varying data of the pressure, flow rate, and rotational speed during the turbine start-up process from one-dimensional pipeline calculation, a total of 11 key time points are selected in order to better describe the physical phenomenon. Steady-state calculations are performed for these 11 key moments. The spiral casing inlet is set to total pressure for these calculations, and the draft tube outlet is set to static

pressure. The pressure changes of the turbine runner during the start-up process are shown in Figure 2. It can be seen that in the initial stage of the start-up process of the pump-turbine (from 9.6s to 16.7s), the guide vanes open synchronously and gradually, so the flow rate, rotating speed and the pressure level of the guide vanes, and the runner also increases gradually and slowly. Then, at 18.4s the guide vane opening is reduced to prevent the speed from exceeding the rated speed, thus the flow rate is reduced, and the pressure level of the guide vanes and the runner is also significantly dropped down. After that, the rotating speed of the runner continues to increase but with a smaller increment ratio than before, and finally stabilizes near the rated rotating speed. Then, from 30.7s to 100.8s the guide vanes also open a little bit more gradually until the unit enters speed no-load operation condition. Meanwhile, the pressure distributions of the spiral casing, draft tube, guide vanes, and runner stabilize gradually. At 201.6s the start-up process is finalized, and the unit is ready to connect to the power grid.

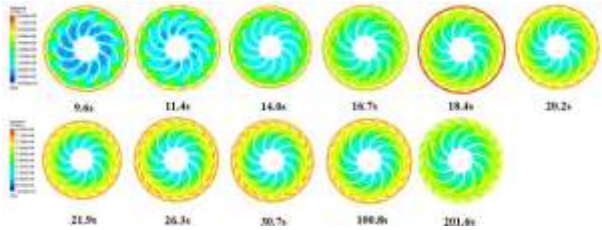

Figure 2. Pressure changes of guide vanes and runner during the start-up process (cross-section)

3 SHUT-DOWN PROCESS

Similarly, based on the time-varying data of the pressure, flow rate, and rotational speed during the turbine shut-down process from one-dimensional pipeline calculation, a total of 7 key time points are selected in order to describe the physical phenomenon in detail. Steady-state calculations are conducted of these 7 key moments. The spiral casing inlet is set to flow rate for these calculations, and the draft tube outlet is set to static pressure. The pressure change of the turbine during the shut-down process is shown in Figure 3. It is clear that in the initial stage of the shut-down process (from 0s to 10.52s), the flow in the runner is stable. The water flows smoothly along the curvature of the blades, and it is obvious that the pressure distribution of different blade channels shows a rotational symmetry periodicity. The pressure level gradually decreases from the inlet to the outlet of the runner. It is also clear that during the shut-down process, the overall pressure distribution of the runner gradually decreases in general.

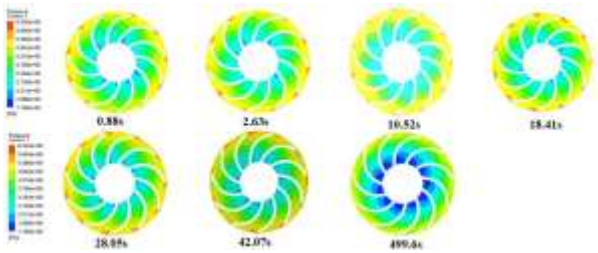

Figure 3. Pressure changes of runner during the shut-down process (cross-section)

4 CONCLUSION

During the beginning of start-up process, the guide vanes open and then close while the pressure of the runner increases and then decreases. Then the guide vanes gradually open, and the pressure of the runner stabilizes gradually. During the shut-down process, the pressure distribution of the runner gradually decreases.

REFERENCES

[1]J Nicolle and J F Morissette and A M Giroux. (2012). Transient CFD simulation of a Francis turbine startup. *IOP Conference Series: Earth and Environmental Science,* 15(6),

[2]Peter Mössinger and Roland Jester-Zürker and Alexander Jung. (2017). Francis-99: Transient CFD simulation of load changes and turbine shutdown in a model sized high-head Francis turbine. *Journal of Physics: Conference Series*, 782(1),

[3]M Gagnon et al. (2010). Impact of startup scheme on Francis runner life expectancy. IOP Conference Series: *Earth and Environmental Science*, 12(1), pp. 012107 (8pp).

ISBN: 978-90-824846-7-0

Proceedings of the 2nd IAHR
Young Professionals Congress
30 Nov-2 Dec. 2021

3D simulation of positive surge waves: turbulent structure, anisotropy, and aeration patterns

Zhuoran Li [1], Akash Venkateshwaran [2] and Shooka Karimpour [3]
[1,3] York University, Toronto, Canada,
[1] zli29@my.yorku.ca; [3] shooka.karimpour@lassonde.yorku.ca
[2] Vellore Institute of Technology, Chennai, India,
[2] akash.v2018@vitstudent.ac.in

ABSTRACT

In this study, positive surge waves are investigated numerically. Surge characteristics including air entrainment and depth profiles, as well as turbulent characteristics such as anisotropy tensors are investigated. The simulations are performed based on the OpenFOAM software along with the Volume of Fluid method for interface capture and Large Eddy Simulation using the *k*-equation model for turbulent modelling. 3D simulations are performed with a minimum mesh size of 0.005 m. The width of the domain is determined based on the isotropy of velocity perturbations. As a result, 40 mesh in z-dimension is selected. At surge Froude number of 1.71 and 2.13, analysis of water depth, phase fraction and eddy viscosity profiles showing the overlap of air entrainment and mixing cone boundaries. The air entrainment profiles obtained conform with profiles suggested in literature. Furthermore, our results suggest that the mixing cone reaches a lower level with a greater surge Froude number.

Keywords: positive surge waves; turbulent modelling; air entrainment; Large Eddy Simulation.

1 INTRODUCTION

A sudden change in the flow, such as a dam break, will lead to the formation of a surge wave. Positive surge waves refer to the waves with a discontinuity in the surge front that is higher than the normal water level. Positive surge waves such as tsunami waves exhibit flow discontinuity in terms of pressure and velocity profiles. Meanwhile, the surge waves present turbulent behavior. The chaotic and complex turbulence associated with the aeration within the surge waves, the environmental concerns of contaminant spread, and sediment gathering (Li and Chanson, 2018). The turbulent structures have been measured and studied experimentally by Koch and Chanson (2009). Numerical study becomes more common with the advantage of capturing the overall turbulent structures, such as Lubin et al. (2010) presented an early simulation of surge waves and their turbulent properties. For the air entrainment profiles, Chanson (2003) performed an experimental investigation with conductivity probes in dam break waves. Due to their transient nature, a few papers have investigated the detail of perturbation patterns in the surge front area. In this study, we examine turbulence and aeration patterns, including formation of mixing cone and anisotropy tensors, using a 3D 2-phase computational approach.

2 METHODOLOGY

For turbulent modelling, Large Eddy Simulation (LES) is used with the governing equation:

$$\rho \frac{\partial \overline{u}_i}{\partial t} + \rho \frac{\partial \overline{u_i}\overline{u_j}}{\partial x_j} = -\frac{\partial \overline{p}}{\partial x_i} + \mu \left(\frac{\overline{\partial^2 u_i}}{\partial x_j \partial x_j} \right) + \frac{\partial \tau_{ij}^{SGS}}{\partial x_j} \qquad [1]$$

where $\overline{u_i}$ and $\overline{p}$ are the filtered velocity and pressure, respectively; τ_{ij}^{SGS} represents sub-grid scale turbulent shear stress which is modelled with the sub-grid scale *k*-equation Large Eddy Simulation (LES) model. The simulation is conducted in OpenFOAM, using the two-phase solver "interFoam" based on the Volume of Fluid method (Hirt and Nichols, 1981) for different surge Froude numbers. A periodic boundary condition is applied in the z-direction.

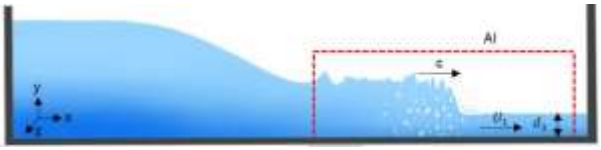

Figure 1. Illustration of the positive surge wave, where AI indicates local refinement zone. Surge Froude number is $Fr_1 = \frac{c+U_1}{\sqrt{gd_1}}$, where U_1 is the velocity downstream of the wave and c is the celerity.

ISBN: 978-90-824846-7-0

3 RESULTS

As shown in Figure 2, for instantaneous time steps of $t = 4.0\ s$ and $t = 4.5\ s$, eddy viscosity of water (ν_t) profiles coincide well with the air entrainment distribution. This indicates turbulence related eddies movement contributes to the air entrainment especially near the surge front. Furthermore, the area between the water surface (green line) and ν_t profile (orange line) is known as the mixing cone which originates from the surge toe due to the shear layer. We have identified two mixing regions 1) originated from wave discontinuity and 2) from instability point at the surge toe. Our previous observations in 2D cases and comparison of $Fr_1 = 1.60$ and 2.49 indicates that the mixing cone tends to reach deeper with a higher Fr_1 (Li and Karimpour, 2021).

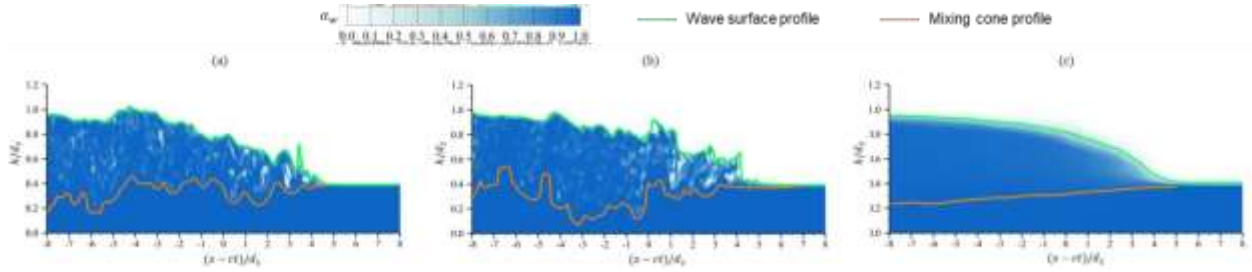

Figure 2. Wave surface and mixing cone profiles at (a) $t = 4.0\ s$, $z = 0.2\ m$ (b) $t = 4.5\ s$, $z = 0.2\ m$ and (c) averaged, where $\alpha_w = 1.0$ or 0.0 represent solely water or air, respectively; $z_{total} = 0.4\ m$, $Fr_1 = 2.13$.

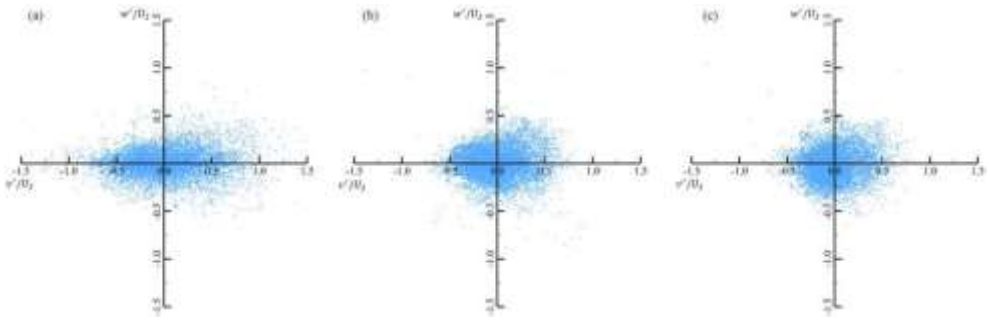

Figure 3. Quadrant plot of v' in y-direction vs w' for z-direction, normalized by U_2 (velocity behind the surge) for (a) 10 z-grids (b) 20 z-grids and (c) 40 z-grids at $z = 0.01\ m$, $Fr = 2.13$.

From Figure 3, v' and w' manifest isotropic behavior for 40 z-grids with a circular distribution compared to that of 10 and 20 z-grids. The phenomenon indicates 40 z-grids is suitable for the simulation as the domain limitation does not limit the growth of w' and hence u' and v' do not contribute to the false magnification of air entrainment.

4 CONCLUSIONS

Dam break wave is simulated in 3D at $Fr_1 = 1.71$ and 2.13. Our study also investigated the air entrainment. Turbulent eddies contribute to the air entrainment as the mixing cone matches the aeration area. The depth of mixing cone will increase with larger Fr_1 according to our previous 2D study. The width in z-dimension needs to satisfy the isotropic requirement between v' and w' and 40 mesh is desirable based on the perturbation cloud between v' and w'.

REFERENCES

Chanson, H. (2003). Two-phase flow characteristics of an unsteady dam break wave flow.

Hirt, C. W., & Nichols, B. D. (1981). Volume of fluid (VOF) method for the dynamics of free boundaries. *Journal of computational physics*, *39*(1), 201-225.

Koch, C., & Chanson, H. (2009). Turbulence measurements in positive surges and bores. *Journal of Hydraulic Research*, *47*(1), 29-40.

Li, Y., & Chanson, H. (2018). Sediment motion beneath surges and bores.

Li, Z., & Karimpour, S. (2021). Numerical investigation of turbulent structures and air entrainment in positive surge waves. In *CSCE Virtual Conference 2021*.

Lubin, P., Chanson, H., & Glockner, S. (2010). Large eddy simulation of turbulence generated by a weak breaking tidal bore. *Environmental Fluid Mechanics*, *10*(5), 587-602.

ISBN: 978-90-824846-7-0

IAHR YPN

Young Professionals Network

Hosted by
Spain Water and IWHR, China

IAHR AIRH

International Association for Hydro-Environment Engineering and Research

Hosted by
Spain Water and IWHR, China

Hydraulic Structures

Proceedings of the 2nd IAHR
Young Professionals Congress
30 Nov-2 Dec. 2021

Modeling the structural response of a dam to earthquake induced dynamic stresses

Biniyam Sishah [1] and Hua-Dong Yao [2]

[1]Department of Civil, Chemical and Environmental Engineering, University of Genoa, Genoa, Italy,
biniyam.birhan@edu.unige.it
[2]Department of Mechanics and Maritime Sciences, Chalmers University of Technology, Gothenburg, Sweden,
huadong.yao@chalmers.se

ABSTRACT

The structural response of a dam to an earthquake with a dominant horizontal ground acceleration was modeled using three techniques: static structural analysis, one- and two-way coupled Fluid-Structure Interaction (FSI) modeling approaches. The aim was to investigate how the choice of method affects the peak total deformation, the principal stresses, and the maximum shear stresses within the dam body. Overall, the two-way FSI model predicted large deformations that linearly increased with time, while the other models predicted minor deformations. This may be due to the two-way FSI model accurately representing the FSI in the vicinity of the dam. The peak stresses predicted by all models had different magnitudes, but were all within the allowable compressive and tensile stress limits of the Roller Compacted Concrete (RCC) structure.

Keywords: dam; earthquake; fluid-structure interaction; static analysis.

1 INTRODUCTION

Dams are essential structures for navigation, hydroelectricity, and flood mitigation. However, they may pose a significant threat to downstream settlements in the event of a catastrophic failure. One reason for the dam failure is earthquakes. Earthquakes increase the hydrodynamic pressure and inertial forces acting against the stability of the dam. As a result, predicting the expected deformations and stresses due to a probable earthquake is an integral part of dam design. The response of a dam to forces of uplift, weight of dam and hydrostatic pressure can be computed with a static model. However, when earthquake-induced hydrodynamic stresses and inertial forces are present, the use of Fluid-Structure Interaction (FSI) simulations is vital to gain accurate understanding of the system. In accordance with the type of solution that is transferred at the interfaces of the fluid and the structure, FSI models can be classified into two groups. In one-way FSI coupling, only the fluid pressure acting at the structure fluid interface is transferred to the structure solver. On the other hand, in two-way coupled simulations, the displacement of the structure is additionally transferred to the fluid solver which increases the accuracy. In this study, a 2D model was setup to investigate how the peak total deformation, principal and maximum shear stresses within a dam body depend on the choice of method when an earthquake event (Ersin,2019) is considered. Both static structural analysis and FSI (one- and two-way coupled) approaches were used.

2 METHOD

2.1 Study area

Gilgel Gibe III gravity dam is located in Ethiopia. It was constructed with RCC material (Pietrangeli et al., 2013). The dam lays in an earthquake zone with a 20 % risk of an earthquake with 7 to 8 Richter scale magnitude occurring within the next 50 years (Carr, 2017). The dam geometry is depicted in figure 1a.

2.2 Model

The commercial software ANSYS (2020) was used in this investigation. The computational domain of the fluid and solid co-joined is presented in figure 1b. Note that, in the static model only the dam section (in red) was used and the hydrodynamic loads were not considered. The fluid part stretched 750 m and 300 m upstream and downstream with height of 350 m, respectively. The dam has a base width of 214 m, a height of 228 m and its elements were sized as 2 m, whereas grid cells in the fluid domain has sizes between 1 - 5 m, see figure 1b.

ISBN: 978-90-824846-7-0

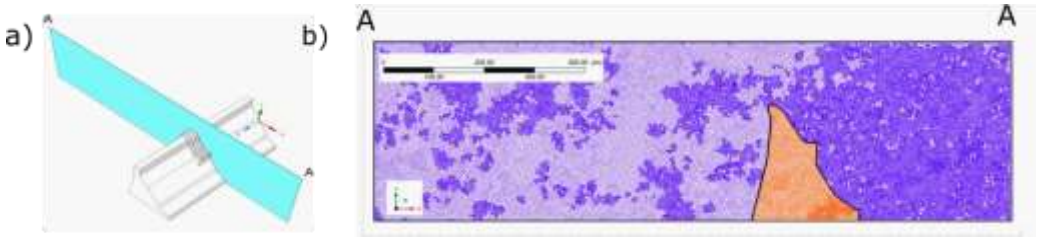

Figure 1: a) The dam geometry with the computational plane (colored in blue), and b) the mesh – blue (the fluid part) and red (the dam section).

3 RESULT AND DISCUSSION

The time solution of the maximum deformation within the dam body is reported in figure 2a. The values obtained from the static and one-way coupled FSI models were comparatively close. However, the two-way coupled FSI model predicted a linear increase in the deformation from the peak ground acceleration event onwards. This may be due to the accurate representation of FSI by the method. Similarly, the peak maximum shear stress and principal stresses were reported by the two-way coupled FSI model, see figure 2b and 2d. In figure 2c and 2d, values predicted by the static model were close to the averaged values of the one-way coupled FSI model. Overall, the peak stresses predicted with the different approaches were within the allowable compressive and tensile stress limits of the RCC structure. This was not the case for the deformation predicted with the two-way coupled FSI model. This needs to be investigated further.

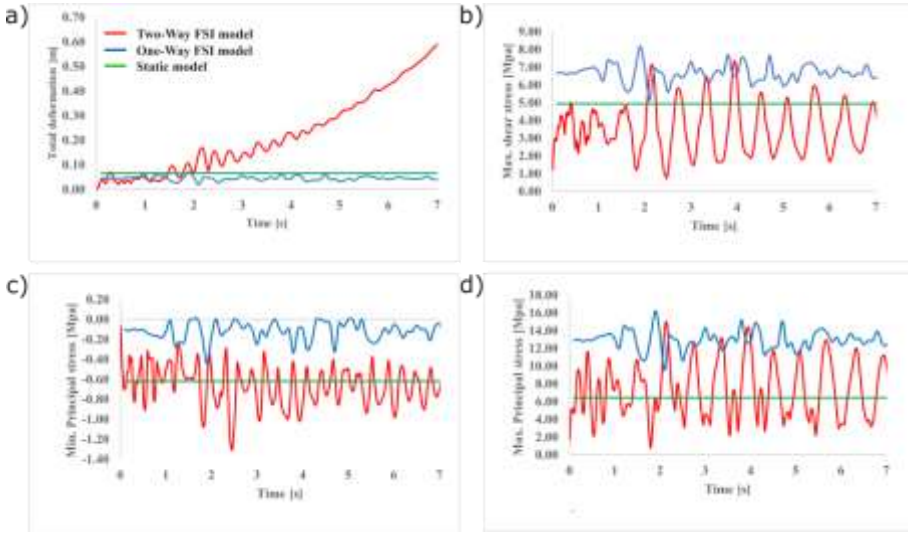

Figure 2: The time history of the peak values of a) the total displacement, b) the maximum shear stress, c) and d) the minimum and maximum principal stresses, respectively.

4 CONCLUSIONS

The structural response of a dam to earthquake-induced stresses was investigated using different modeling approaches. The results suggest that the predicted stresses were within the allowable compressive and tensile stress limits of the RCC dam. The higher deformation predicted by the two-way coupled FSI model was attributed to its accuracy, but further investigation is recommended.

REFERENCES

Carr, C. J. (2017). The Seismic Threat to the Gibe III Dam: A Disaster in Waiting. In River Basin Development and Human Rights in Eastern Africa — A Policy Crossroads (pp. 43–52).

Ersin Dinçer(2019). Investigation of the sloshing behavior due to seismic excitations considering two-way coupling of the fluid and the structure. *Water* 11.12 (2019): 2664.

Pietrangeli, A., Cagiano De Azevedo, A., Pittalis, G., & Rossini, C. (2013). Gibe III dam, design of RCC zoning

ANSYS (2020), user guide, ANSYS Inc. version 15.

ISBN: 978-90-824846-7-0

Proceedings of the 2nd IAHR
Young Professionals Congress
30 Nov-2 Dec. 2021

3D computational hydraulic modeling of stepped spillways variable section for gravity and RCC concrete dams

Gideael Quislón Cántaro Fabián[1] y Samuel Ismael Quisca Astocahuana[2]

[1] Bach. Civil Engineer, EPIC-FIGMMG, National University of San Marcos, Lima, Peru
gideael.cantaro@unmsm.edu.pe

[2] Principal Professor, School of Civil Engineering, National University of San Marcos, Lima, Peru

squiscaa@unmsm.edu.pe

ABSTRACT

An advance of the 3D computational hydraulic modeling of stepped spillways of constant and variable section is presented, with the purpose of finding the optimal sections of the stepped spillway, expressed in the minimum residual energy of the water flow at the end of the spillway. 6 types of stepped spillway geometries are analyzed, of which 3 types of geometry are of constant section and the other 3 of variable section, for a CCR dam. The modeling and numerical simulations were performed with OpenFoam 3D software. The results of the numerical simulations show that the stepped spillways of constant geometry allow efficient dissipation of energy through the vorticity cores that form between the steps. In the case of spillways with variable contraction sections from the crown of the dam to its foot, it requires a readjustment of the dimensioning of the vertical and horizontal steps to achieve effective hydraulic energy dissipation. The contraction of the spillway section on the downstream slope of the dam makes it possible to have space in the body of the dam for the location of the bottom discharge, optimizing the sizing of the energy dissipation structures at the foot of the dam. dam and thus reducing the construction costs of the bottom discharge valve house and its dissipative pools.

Keywords: Stepped spillway; gravity concrete dam; RCC dam; residual energy in spillways; Variable section

1 INTRODUCTION

In tall dams, stepped spillways dissipate hydraulic energy efficiently compared to conventional spillways. Since the 1990s, theoretical and experimental studies of stepped spillways of constant section have been intensified, applied to gravity concrete (CG) and roller compacted concrete (RCC) dams. The steps of a stepped spillway significantly increase the rate of energy dissipation in the spillway section, reaching the dissipation pool with low residual energy, which requires a dissipative pool of reduced dimensions compared to conventional spillways, which arrive with high speeds to the dissipating pool, which is why larger pools are required. This type of exceedance spillway is very convenient to place in the body of concrete gravity dams, RCC dams or in other types of dams, but external to the body mainly due to the constructive, operational and hydraulic and structural efficiency advantages. This research analyzes stepped spillways of constant and variable section looking for the most efficient way to dissipate hydraulic energy.

Model SC1: Cst. Sec. spillway, H dam = 48.5 m; Slope 0.75H: 1V, Cst. width = 4 m. with steps 0.3V: 0.225H	**Model SC2:** Cst. Sec. spillway, H dam = 48.5 m; Slope 0.75H: 1V, Cst. width = 4 m. with steps 0.5V: 0.375H	**Model SC3:** Cst. Sec. spillway, H dam = 48.5 m; Slope 0.75H: 1V, Cst. width = 10 m. with steps 0.5V: 0.375H	**Model SVL1:** Sec. Cst. spillway, H dam = 48.5 m; Slope 0.75H: 1V, top. width = 15 m, bot. width = 8 m.	**Model SC-SVL1-SC:** Sec. Cst. spillway, H dam = 48.5 m; Slope 0.75H: 1V, top. width = 15 m, bot. width = 8 m.	**Model SC-SVP1-SC:** Sec. Cst. spillway, H dam = 48.5 m; Slope 0.75H: 1V, top. width = 15 m, bot. width = 8 m.

Source: the autor

2 MODELING AND NUMERICAL SIMULATION

The three-dimensional numerical modeling was carried out in the CFD OpenFoam 3D software, for which the three-dimensional geometry of the different types of spillways was constructed; The mesh of the computational model was defined with the cell size 0.045 m (x and z axes) and 0.10 m (y axis); As an initial condition, a water height of 0.25 m was established on the steps; the boundary conditions upstream of the spillway (Xmin) a flow-type boundary condition (1.25 m2 / s) was defined, downstream of the

ISBN: 978-90-824846-7-0

spillway (Xmax) an outflow-type boundary condition was specified, on both sides of the spillway (Ymin and Ymax) a symmetry condition was established, at the base (Zmin) a wall-type boundary condition was considered, and finally a pressure-type boundary condition at the top (Zmáx); and the turbulence model used is k-ε / RNG.

3 SIMULATION RESULTS

Stepped spillway 0.75H: 1V, with steps 0.3V: 0.225H. Hydraulic energy dissipative vortices are not formed within the steps. No skimming flow is formed, forming an undamped shoulder in the pool. The flow reaches the dissipating pool with a velocity of 12 m / s, which is not cushioned by the pool, and delivers to the river with 5 m / s. The flow braces in the steps are less than 1 m, and in the dissipating pool it reaches braces of 5 m.

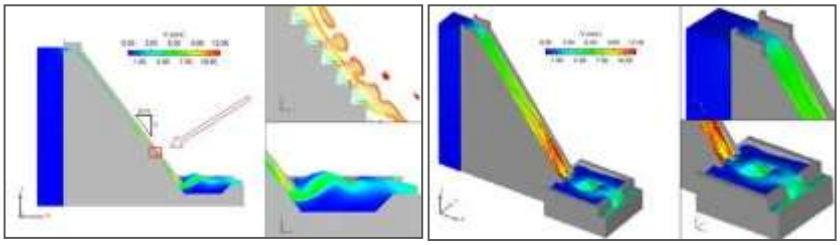

Source: the author

Stepped spillway 0.75H: 1V, with steps 0.5V: 0.375H. Hydraulic energy dissipating vortices are formed within the steps. The skimming flow is dampened by the energy dissipating pool, the flow reaches the dissipating pool with a velocity of 9 m / s, which is cushioned by the pool and delivered to the river with 3 m / s. The flow braces in the steps are less than 1 m, and in the dissipating pool it reaches braces of 4 m.

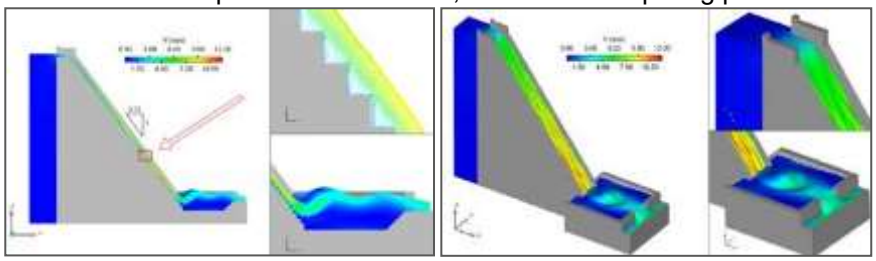

Source: the author

4 CONCLUSIONS

Advances made to date in stepped spillway alternatives of constant and variable section are presented, and their efficiency in reducing energy through the formation of energy dissipation vortex cores between passages is examined. For a stepped spillway, the dimensions of the vertical step and the horizontal length of the step depend exclusively on the slope of the dam on the downstream slope, thus conditioning the macro roughness (Ks). Between the SC1 and SC2 models where the difference is only in the size of the step height, it is observed that the second model is more efficient in dissipating energy, requiring a smaller size of the dissipating pool and delivering the flow of water with a slower speed towards the riverbed.

REFERENCES

Matos, J. (2020). Hydraulic design of stepped spillways on RCC dams. In Stepped Spillway Hydraulics (pp. 187-194). CRC Press.

Chanson, H. & Toombes, L. (2002). Air- Water Flows down Stepped chutes: Turbulence and Flow Structures Observation. International of Multiphase Flow, volume 27, N°11, pp. 1737-1761.

Boes, R. M. (2000). Zweiphasenströmung und Energieumsetzung an Grosskaskaden (Doctoral dissertation, ETH Zurich).

Amador, A., Sánchez Juny, M., and Dolz Ripolles, J. (2006). Hydraulic design of stepped spillways in HCR dams. Water Engineering, 13(4), 289-302.

Chatila, J. G., & Jurdi, B. R. (2004). Stepped spillway as an energy dissipater. Canadian Water Resources Journal/Revue canadienne des ressources hydriques, 29(3), 147-158.

Quisca, S. I. (2018). Technical report of Quisco Dam. Plan MERISS INKA. Cusco, Peru.

ISBN: 978-90-824846-7-0

Proceedings of the 2nd IAHR
Young Professionals Congress
30 Nov-2 Dec. 2021

Discharge capacity of labyrinth weirs by physical modeling: Influence of weir orientation

Alicia Ros-Bernal[1], José M. Carrillo[1], Antonio Vigueras-Rodríguez[1] & Jorge Matos[2]

[1]Civil Engineering and Mining Engineering School, Universidad Politécnica de Cartagena, Cartagena, Spain.
[2]CERIS, Instituto Superior Técnico, Universidade de Lisboa, Lisbon, Portugal
alicia.ros@edu.upct.es, jose.carrillo@upct.es, avigueras.rodriguez@upct.es, jorge.matos@tecnico.ulisboa.pt

ABSTRACT

The labyrinth weir is an interesting solution to increase the release flood capacity from dams and weirs, eventually mitigating negative effects triggered by climate change. The readjustment in the configuration of the discharge line allows to regulate the water levels and increase the discharge capacity. Despite their advantages, these are complex structures that require experimental studies for their hydraulic design. The main focus of this research was to evaluate the influence of the labyrinth weir orientation on the discharge coefficient. For this purpose, two steel plate labyrinth weirs of different angles (15° and 35°), in normal and inverse orientations, were tested in a hydrodynamic channel. The results of the discharge coefficient compared well with those obtained in other studies, and indicated a small influence of the weir orientation.

Keywords: labyrinth weir, weir orientation, discharge coefficient, physical modeling.

1 INTRODUCTION

In recent decades, the adaptation of existing spillways to increase their discharge capacity has promoted the use of labyrinth weirs. The morphology of these weirs leads to an increase of the length crest, therefore, of the discharge capacity, compared to that of a conventional straight weir arranged on the same channel width.
The hydraulic behavior of labyrinth-type weirs is markedly three-dimensional, which is why most of the design procedures for these structures have been experimental (Carrillo et al., 2019). One of the most common ways to describe the performance of labyrinth weirs is by the discharge coefficient, C_d. This coefficient is affected by geometric factors (e.g., weir height P, wall thickness t_w, sidewall angle between the labyrinth wall and the centerline of the approach channel α, crest shape), by flow conditions (e.g., total energy head HT, flow approach angle, local submergence), and, consequently, by nappe aeration conditions. Regarding the labyrinth weir orientation, some studies were reported on the effect of the normal (outside apexes connected to channel sidewalls as upstream apexes) or the inverse (outside apexes connected as downstream apexes) orientation of the weir on the discharge capacity. In Houston (1983), labyrinths with a magnification ratio of five in the normal orientation were found to yield higher discharges (up to 9%) compared to those of identical geometry, on the inverse orientation. In turn, Crookston and Tullis (2013a) evaluated the discharge in normal and inverse orientations with a sidewall angle of 6°, and no measurable deviation was obtained. Lopes (2011) also observed relatively similar values of C_d in normal and inverse orientations with sidewall angles of 12° and 30°, with relative differences being lower than 5%. In line with these investigations, this study is focused on the influence of the weir orientation on the discharge coefficient, for different sidewall angles (15° and 35°).

2 MATERIALS AND METHODS

The experimental campaign was carried out in a hydrodynamic channel assembled at the University of Cartagena (UPCT), with an effective length of 12.5 m and a cross section of 0.31 x 0.45 m^2 (width versus height). The channel operates on a recirculation system with a maximum flow rate of 40 l/s and incorporates an electromagnetic flowmeter. The longitudinal slope of the channel is variable between -1/200 and +1/40. A digital readout limnimeter installed on a trolley that slides along the channel was used to measure the head above the crest (resolution: 0.01 mm).The geometry of the tested weirs consists of a single cycle steel plate labyrinth with a thickness t_w = 5 mm and a width w = 0.309 m. The height of the weir is P = 0.103 m, following the recommendations of Crookston and Tullis (2013a,b) with respect to w / P (*normally* $2 \leq w/P \leq 4$). The shape of the crest is half-round with a radius R = 2.5 mm. The total crest length is approximately 1.098 m and 0.472 m for a sidewall angle of 15 and 35 degrees, respectively. These weir geometries were tested in both normal and

ISBN: 978-90-824846-7-0

inverse orientations, with the channel in the horizontal position, and were installed on a raised platform to avoid submergence conditions in the weir, due to the limitation in the channel outlet capacity (Figure 1).

Figure 1. Left) Scheme of the top view of the labyrinth weir assembled at UPCT; Center) labyrinth weir with α =15° in normal orientation; Right) labyrinth weir with α =15° in inverse orientation.

3 RESULTS AND CONCLUSIONS

In Figure 2, the discharge coefficient (C_d) is plotted in function of the relative head (H_T/P). For both 15° and 35° labyrinth weirs, the influence of the weir orientation is not significant, which concurs with findings of other studies. The results for both weirs are similar to those obtained from Crookston and Tullis (2013a,b), for large heads (e.g., H_T/P > 0.35 to 0.50, on quarter-round and half-round labyrinth weirs, respectively), and even for smaller heads (H_T/P > 0.20, for the 15° labyrinth weir). The larger differences obtained for small to moderate heads may be explained by distinct weir geometry and scale effects, including the aeration condition.

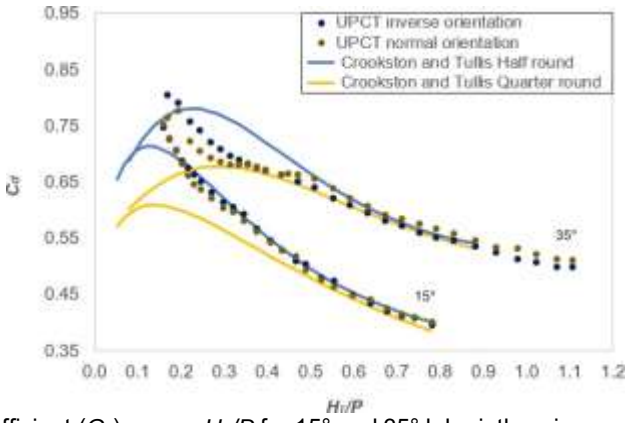

Figure 2. Discharge coefficient (C_d) versus H_T/P for 15° and 35° labyrinth weirs assembled at UPCT, along with the results from Crookston and Tullis (2013a,b) with their weirs in normal orientation.

The determination of the discharge coefficient of labyrinth weirs continues to be a challenging topic of research. In this preliminary study, the influence of weir orientation for 15° and 35° sidewall angles was found to be small, in line with findings from other studies. In future research, the experiments will include additional sidewall angles.

ACKNOWLEDGEMENTS

The authors thank the support given by the Fundación Séneca-Agencia de Ciencia y Tecnología de la Región de Murcia (Spain), Project 20879/PI/18.

REFERENCES

Carrillo, J.M., Matos, J., and Lopes, R. (2019). Numerical modeling of free and submerged labyrinth weir flow for a large sidewall angle. *Environ Fluid Mech*, 20, 357–374 (2020).

Crookston, B.M., and Tullis, B.P. (2013a). Hydraulic Design and Analysis of Labyrinth Weirs. I: Discharge Relationships. *J.Irrig.Drain.Eng*., 139 (5), 363-370.

Crookston, B.M., and Tullis, B.P. (2013b). Hydraulic Design and Analysis of Labyrinth Weirs. II: Nappe Aeration, Instability, and Vibration. *J.Irrig.Drain.Eng.*, 139 (5), 371-377.

Houston KL (1983). Hydraulic model study of Hyrum Dam auxiliary labyrinth spillway. Report No. GR 82-13, U.S. Bureau of Reclamations, Denver, Colorado.

Lopes R (2011). Capacidade de vazão, energia específica residual e caracterização do escoamento de emulsão ar-água em soleiras descarregadoras em labirinto. Ph.D. thesis, IST, Lisbon, Portugal (in Portuguese).

Proceedings of the 2nd IAHR
Young Professionals Congress
30 Nov-2 Dec. 2021

Influence of crest shapes on trapezoidal piano key weir hydraulic performance

Xiaoyang Shen [1], Mario Oertel [2]
[1] Research Assistant, Helmut-Schmidt-University, Hamburg, Germany,
xiaoyang.shen@hsu-hh.de
[2] Full Professor, Helmut-Schmidt-University, Hamburg, Germany,
mario.oertel@hsu-hh.de

ABSTRACT

This study investigates the influence of various crest shapes on the hydraulic performance of a symmetrical trapezoidal piano key weir. Four different crest configurations were fabricated via 3D printing technique and examined with focus on discharge efficiency and nappe behavior. Results indicate that significant efficiency gain could be achieved by replacing regular flat crests with half-round or quarter-round crests, especially at small heads. Depending on the crest shape and upstream head, different nappe behaviors were generated that could affect the hydraulic performance of the structure under certain conditions. Related nappe instability and sensitivity to surface tension were also documented and discussed based on experimental data and laboratory observations within the study.

Keywords: piano key weir, discharge efficiency, crest shapes, nappe behavior

1 INTRODUCTION

Piano key weirs (PKW) have been gaining growing attention in the past fifteen years due to their efficient hydraulic performance. Extensive experimental and numerical studies have been carried out to investigate the geometric parameters influencing its hydraulic performance, such as the magnification ratio (L/W), weir height (P), in- and outlet key width ratio (W_i/W_o) and more. However, most of the studies were conducted with models with flat crests. The present study evaluates the influence of four different crest shapes on the hydraulic performance of a trapezoidal piano key weir – which has been proven to offer a higher discharge efficiency per unit crest length than PKWs with traditional rectangular plan form (Shen and Oertel, 2021).

2 METHODS AND RESULTS

Within the present study a symmetrical trapezoidal PKW model (P = 300 mm, B = 480 mm, L/W = 3.68, $W_{i,u}/W_{o,d}$ = 1, B_i/B_o = 1,B_b = 240 mm) was fabricated via 3D printing technique and tested with four different crest shapes: (1) flat-top, (2) half-round and quarter-round in (3) up- and (4) downstream direction (see Fig.1). Experiments were conducted in a horizontal rectangular flume (width W = 0.3 m, depth H_f = 0.5 m, length L_f = 10 m). Discharges were measured via Magnetic Inductive Flow Meter (MID) and flow depths were determined at a distance of 5P upstream the weir, using a point gauge and an ultrasonic sensor. All model runs were reproduced twice in order to minimize human errors in measurement. Final results present mean values of collected data.

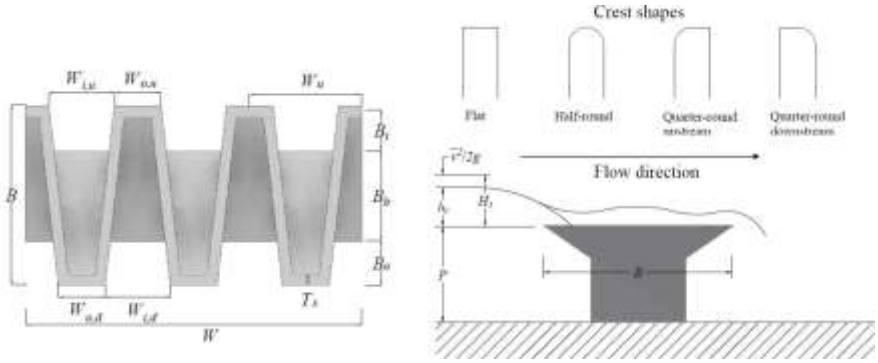

Figure 1. Geometric parameters of tested trapezoidal piano key weir model

Figure 2(a) compares the discharge efficiency of the tested models in terms of discharge coefficients C_{dw}, which can be calculated using the classical weir flow formula: $CC_{dddd} = 3QQ/(2WW\sqrt{2}\sqrt{gg}HH_{tt}^{1.5})$, where: Q = discharge,

W = flume width, g = acceleration due to gravity, H_t = upstream head = $h_t + v_m^2/(2g)$, with h_t = upstream flow depth, v_m = mean upstream velocity. As suggested by several authors, only results with a minimum upstream total head of 3 cm were considered for quantitative data analysis to avoid size scale effects related to surface tension. The flat crest configuration was found to provide the lowest discharge efficiency among the tested models and the curve of C_{dw}-values is flatter than the other, which means it has a smaller disparity of discharge capacity within the tested head range. Significant improvement in discharge capacity could be achieved by replacing the flat crest with half-round or quarter-round configurations, especially for low heads (H_t/P < 0.2). Compared with the flat crest configuration, PKWs with half-round crests offer up to 30% increase in discharge capacity. Although this efficiency gain decreases with increasing heads, an overall improvement of more than 10% can be expected as long as the relative head does not exceed 0.5. A minimum efficiency gain of 6% was measured. Similar results were also reported in Cicero (2016) based on experimental data from regular rectangular PKW configurations. For H_t/P < 0.4, both quarter-round configurations (quarter round up- and downstream) generally show identical trend and offer up to 15% improvement of discharge efficiency relative to the flat crest configuration. Only minor differences can be observed for very low heads (H_t/P < 0.1) where results were possibly affected by surface tension (scale effects). Still, this minor deviation indicates that quarter round crests in downstream direction might be more sensitive to surface tension relative to another models. Furthermore, within the range of 0.4 <H_t/P < 0.6, PKWs with quarter-round crests in downstream direction (○) deviates unexpectedly from discharge coefficients of the quarter-round upstream configuration (□), while a nearly perfect alignment can be observed for the rest H_t/P regions. The possible reason could be the different nappe behavior generated by the crest (see Fig. 2(b)). For 0.4 <H_t/P < 0.6, the outlet section of the model with a quarter-round crest in upstream direction was almost completely submerged due to nappe interferences. Another configuration, however, has a rectangular edge in the upstream direction where the flow is approaching. This rectangular edge guides the nappe trajectory into vertical direction and generates air cavity formation downstream of the crest, which increases the flow depth and makes the outflow less efficient. As upstream heads grow, this effect becomes less significant due to increased turbulent mixing and the air cavity formation gradually diminishes. This explains why the C_{dw}-curve of these two quarter-round configurations approach each other again at high heads (H_t/P > 0.5).

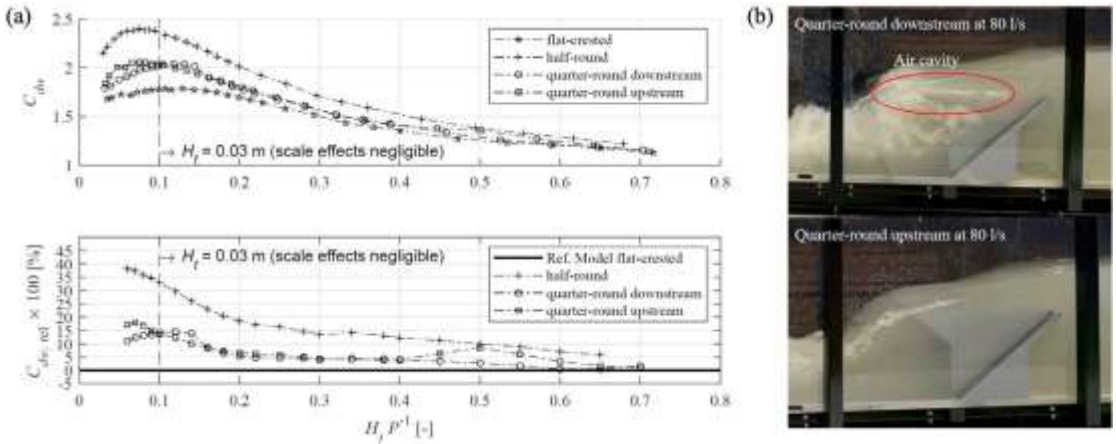

Figure 2. (a) Comparison between tested models in terms of C_{dw}-values (b) Air cavity formation

3 CONCLUSIONS

The present study compares the hydraulic performance of a symmetrical trapezoidal piano key weir model with different crest shapes. Results show that the nappe behavior over the weir crest can be optimized through rounding the rectangular edge and significant efficiency gain up to 30% could be achieved by replacing regular flat crest to half-round or quarter-round crest.

REFERENCES

Cicero, G. (2016). Influence of some geometrical parameters on Piano Key Weir discharge efficiency. *In B. Crookston & B. Tullis (Eds.), Hydraulic Structures and Water System Management. 6th IAHR International Symposium on Hydraulic Structures*, Portland, OR, (pp. 367-377).

Shen, X. and Oertel, M. (2021). Comparative study of nonsymmetrical trapezoidal and rectangular piano key weirs with varying key width ratios. *Journal of Hydraulic Engineering*, 147 (11), https://doi.org/10.1061/(ASCE)HY.1943-7900.0001942

ISBN: 978-90-824846-7-0

Proceedings of the 2nd IAHR
Young Professionals Congress
30 Nov-2 Dec. 2021

Microscale hydrodynamic analysis of flow in circular piles with shallow spherical cavities using CFDM

A. Lizbeth Alvarez M. [1], Humberto Salinas T. [2], Boris M. Lopez R. [2], Carlos Díaz D. [2] Juan A. García A. [2]
[1] Master's student, Instituto Interamericano de Tecnología y Ciencias del Agua, Toluca, México.
e-mail: aalvarezm388@alumno.uaemex.mx
[2] Teacher-Researcher, Instituto Interamericano de Tecnología y Ciencias del Agua, Toluca, México.
e-mail: hsalinast@uaemex.mx

ABSTRACT

Rough surfaces on bridge piers as scour depth reduction mechanisms require a thorough study of the flow behavior. The application of CFD techniques is ideal for analyzing the hydrodynamics of highly turbulent flows. In this work, CFD was used to evaluate the hydrodynamic behavior of the flow around a pile with a surface finish based on spherical micro-cavities. The results were validated with the physical model analyzed experimentally with PIV (Salinas et al., 2017). The simulations were under a transient (VOF) scheme. Spherical cavities decrease the turbulence energy.
Keywords: local scour, bridge piers, CFD, rough surfaces, VOF.

1 INTRODUCTION

The development of flow around a circular cylinder is encountered in numerous engineering applications, hence the special interest in understanding the physics of the flow characteristics around it such as flow separation point, pressure distribution and vortex shedding. (Islam and Mohany, 2020). This phenomenon is encountered when a current impinges on the pier of a bridge, causing a highly turbulent flow field whose vortex structures, trigger the migration of material from the bottom to the foot of the structure, a phenomenon called local scour, and which is one of the main causes of bridge collapse worldwide. The modification of the flow field is mainly associated with the change in the drag that decreases the resistance to flow, interrupting the process of vortex shedding and consequently reducing the scour depth. The present study analyzes the hydrodynamic flow behavior of the surface finish of bridge piers based on spherical caps, a pattern that has been previously evaluated experimentally by other authors by means of physical models, showing that it reduces the scour depth, compared to a smooth finish pier. However, there are questions about the use, size and distribution of the finish, which need to be analyzed three-dimensionally with computational fluid dynamics (CFD).

2 BACKGROUND

The pressure differential that the flow produces around the circular section pillar leads to an increase in velocity at the front and braking at the rear, where the fluid experiences a pressure gradient opposite to the direction of motion. If the kinetic momentum is not high enough to overcome the pressure increase, a reversal in the direction of flow may occur, separating from the cylinder wall and forming a turbulent wake.The incorporation of patterned surface finishes on the pile surface as a control mechanism modifies this separation. Authors such as Jiménez et al. (2006), evaluated the separation of the boundary layer around a circular pile using 7 types of artificial roughness, highlighting the "V" and "inverted V" patterns, the most favorable being a configuration of conical caps of 8 mm in diameter separated by 12 mm. Gris (2010) combined the roughness of spherical caps similar to the texture of golf balls with the "V" directional roughness. Likewise, Salinas et al. (2017) presents an experimental analysis with the PIV technique taking the theoretical support exposed by Jiménez et al. (2006) and Gris (2010) obtaining the velocity and turbulence fields around a circular pillar. For their part Butt & Egbers (2016) studied the structure of the vortices generated in a cylinder with concave hexagonal cavities concluding that they reduce by 35% the values of the drag coefficient compared to a smooth cylinder. Shahsavari (2017) proposed a spiral-shaped finish through an experimental model that reduces the local scour depth of a circular pile by 47%. All of them showed a drastic modification in the flow development by incorporating a different finish than the smooth one.The objective of the present work is to analyze with CFD the three-dimensional flow field around a circular section pile with a surface finish based on spherical caps, with a high level of detail in the spatial scale, identifying parameters that affect the hydrodynamics such as cap size, separation and/or depth. This will allow orienting an effective design as a measure to control the detachment of vortices that produce the scour pit. The purpose of this study is to consider different flow conditions and identify the ideal arrangement to reduce scour.

3 METHODS

For the analysis of the hydrodynamic behavior around the pile, two types of piles were selected, one smooth and the other with a spherical cap type pattern of 6 mm diameter, 2 mm depth, and 3 mm separation. The piles used were those presented in Salinas et al. (2017) using particle image velocimetry (PIV), which served as the basis for model calibration. The stacks are 6 cm in diameter and 20 cm in height. The intersection of the piles at the origin with a channel of rectangular section of 0.40 m wide, 8.0 m long and 0.2 m high was considered as the flow domain. The inlet condition was a mass flow rate of 0.007 m3/s, the flow depth was a 0.07 m, the outlet condition was an "outflow" type, and the side walls, bottom and wall of the pile were wall type conditions. The tool used was Ansys Fluent, and the geometry of the fluid domain was created using the Ansys Design Modeler tool. Regarding the calculation mesh, sensitivity analysis of type, size and quality were performed by monitoring the velocity variation within the domain. The type of mesh proposed is based on tetrahedrons with an overall element size of 5 mm with refinement of up to 0.2 mm in the cylinder wall scenarios with different Reynolds number ranges were proposed to cover the threshold domains of interest Re = (3,30,250,5x10^4 y 1x10^6) for to analyze the behavior in the two types of pile finishes. Pressure-velocity coupling was used, which is based on pressure, absolute velocity, in steady state and transient, using the Volume of Fluid (VOF) models in free surface channels and Shear Stress Transport (SST).

4 RESULTS

The experimental data allowed validating the results of the numerical model and deepening in the behavior of other variables of interest. It is shown that the presence of the spherical cavities decreases the turbulence energy around the elements, crossing the high turbulence zone by up to 3 times the diameter of the pile, which helps to reduce the scour process near the pile. The flow characterization corresponds to the detachment of vortex structures established in the literature and in previous studies, verifying the relevance of the assumed parameters, models and conditions.

5 CONCLUSIONS

The presence of spherical cavities in the wall of bridge supports constitutes a potential application of rough surfaces in engineering, which can guide design parameters as a control measure to guarantee the integrity of structures in the face of hydrodynamic causes of local scour.

The results obtained allow us to propose different configurations of the caps, seeking to optimize the arrangement for different flow conditions. (Re).

REFERENCES

Butt, U., & Egbers, C. (2016). Flow structure due to hexagonal cavities and bumps on a plate surface. *Thermophysics and Aeromechanics*, 23(6), 839–847. https://doi.org/10.1134/S0869864316060068

Salinas, T., H., Diaz, G., E. V. Garcia A.,J.A. (2017). “Análisis de la profundidad de socavación de pilas de puente con diferente acabado superficial, con Particle Image Velocimetry (PIV)”. XXII *Congreso nacional de hidráulica*, Acapulco, Guerrero, México.

Gris, R. B. (2010). Sheath for reducing local scour in bridge piers. *Geotechnical Special Publication*, 210 GSP, 987–996. https://doi.org/10.1061/41147(392)99

Islam, M. R., & Mohany, A. (2020). On the three-dimensional flow development around circular finned cylinders. *Physics of Fluids*, 32(11). https://doi.org/10.1063/5.0026603

Jimenez-Pérez, F.G., Roldan-Herrera, M.D. y Uribe Chávez, D.Y. (2006). *Reducción de la Socavación en pilas circulares mediante el uso de rugosidades artificiales*. [Tesis de Licenciatura] Instituto Politecnico Nacional de México.

Shahsavari, H., Heidarpour, M., & Mohammadalizadeh, M. (2017). Simultaneous effect of collar and roughness on reducing and controlling the local scour around bridge abutment. *Acta Universitatis Agriculturae et Silviculturae Mendelianae Brunensis*, 65(2), 491–499. https://doi.org/10.11118/actaun201765020491

ISBN: 978-90-824846-7-0

Proceedings of the 2nd IAHR
Young Professionals Congress
30 Nov-2 Dec. 2021

Impact of surge wave Froude number on the transport of macro-plastics

Preet Patel [1], Magdalena Krol [2] and Shooka Karimpour [3]

[1,2,3] Department of Civil Engineering, Lassonde School of Engineering, York University, Toronto, Canada,
[1] Preet26@my.yorku.ca
[2] Magdalena.krol@lassonde.yorku.ca
[3] Shooka.karimpour@lassonde.yorku.ca

ABSTRACT

There is no viable solution to cope with increasing plastic pollution, eventually forcing plastics into landfills and natural environment. Rivers and coastal activities play a critical role in transporting plastic debris from inland sources to marine environment. Highly turbulent breaking bores have the potential to washoff mismanaged plastics and transport plastic debris offshore. The motive behind this research is to explore the role of surge wave and its Froude number, Fr_s, on the transport of plastic debris. To do this, solid macrosized polypropylene (PP) and acrylic (ACR) balls were introduced in a surge wave, generated in a hydraulic flume. Based on initial observations, buoyant PP balls were considerably entrained in the surge wave, while negatively buoyant ACR balls sank. Horizontal transport of both PP and ACR balls increased with higher Fr_s, and this was more evident as ball size decreased. Additionally, settled ACR balls were re-suspended at higher Froude numbers.

Keywords: surge waves; coastal plastic pollution; Froude number; macroplastics; turbulence.

1 INTRODUCTION

The world has produced more than 6.3 billion tonnes of plastic waste, of which 9% has been recycled and 12% has been incinerated, while the rest (79%) accumulates in the natural environment and landfills (Geyer et al., 2017). In 2019, around 368 million tonnes of plastics was produced globally (Plastics Europe, 2020), and the plastic production is expected to increase significantly in the near future. This means that plastic pollution will continue to pose a concern to the natural environment, marine wildlife, and possibly to the human food chain. Among all polymer types, polyethylene and polypropylene accounts for the nearly 50% of global plastics market (Plastics Europe, 2020), and these two polymers are predominant in the marine environment (Erni-Cassola et al., 2019; Schwarz et al., 2019). Every year, an estimated 12.7 million tonnes of plastics infiltrate marine environment (Jambeck et al., 2015) by being carried to oceanic waters through various pathways, namely rivers and coastal events (e.g., flood events, coastal waves such as bores, surge waves, and tsunamis). Accumulation and transport of plastic waste is considerably influenced by the density, size, and surface area of plastic debris. The turbulent front of surge waves is often associated with entrainment of sediment and debris. This turbulent front also induces air entrainment which is linked to the surge wave's Froude number (Fr_s) (Chanson, 2010). In coastal areas, this phenomenon can lead to the washoff and entrainment of mismanaged plastics. Additionally, in a breaking bore, there is roller on top of the incoming flow that propagates against the flow of the channel (Chanson, 2010) and at higher Fr_s, which can transport low-density material. Strong turbulent surge front is induced by the breaking of discontinuous wave front at high Froude numbers, as well as the shear layer formation, identified as the advective diffusion region. Transport of debris and natural sediments are influenced by this transient highly turbulent wave front (Patel et al., 2021). Adverse effect of plastics waste, predominant polymer type in marine environment, and surge wave dynamics have been well documented, however the transport of plastic debris in surge waves have commonly been overlooked. Therefore, the motivation behind this research is to comprehend the impact surge wave Froude number has on the transport of plastic debris.

2 METHODOLOGY

A hydraulic flume was used to generate a desirable breaking bore with a Fr_s of between 1.4 and 2.3. Solid macrosized (1.1 cm to 2.5 cm) polypropylene (PP) and acrylic (ACR) plastic balls were introduced into the surge wave. To capture the rapid transport of plastics in a generated surge wave, a high frame rate camera was used,

ISBN: 978-90-824846-7-0

along with acoustic water displacement sensors to record upstream and downstream water depth. The data obtained from the experiments were analyzed using an open-source particle tracking velocimetry (PTV) program, Tracker, developed by the Multiphase Flow Science Group at US Department of Energy, National Energy Technology Laboratory (2018).

3 INITIAL FINDINGS AND ANTICIPATED OUTCOMES

The negatively buoyant ACR balls sank to the flume bed, while the buoyant PP balls were mainly afloat and entrained in the surge wave. In addition, PP balls were transported vertically and were engaged at the bore front, while the ACR balls had no vertical transport in surge wave at low Fr_s, as shown in Figure 1 (a) & (c). However, it was observed that the ACR ball's horizontal transport, due to entrainment with surge front, was considerably influenced by the transient recirculation zone even at low Fr_s. This behaviour was dependent on the ball size and Fr_s. Entrainment of PP balls increased, and the balls were transported further upstream as the Fr_s increased, see Figure 1 (b). Similarly, ACR ball's horizontal transport was also influenced as the Fr_s increased. In addition, at greater Fr_s, the wave motion resulted in minor vertical transport of negatively buoyant ACR balls, as illustrated in Figure 1 (d).

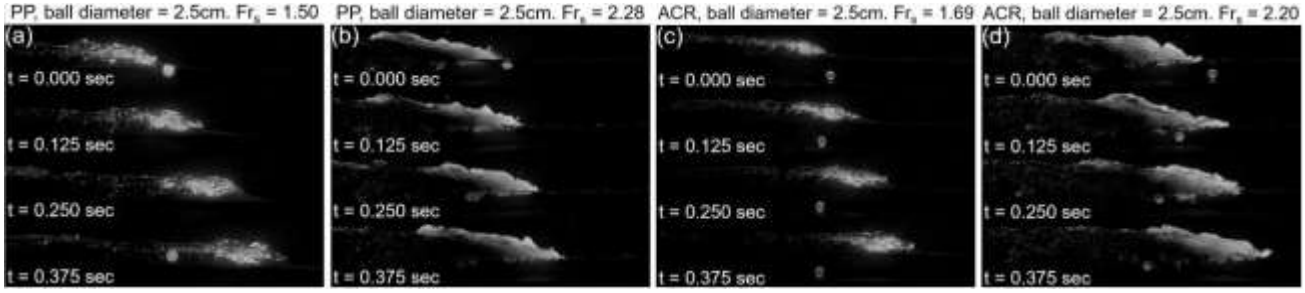

Figure 1. Sequence of images showing the transport mechanism of: (a) PP ball at a Fr_s of 1.50, (b) PP ball at a Fr_s of 2.28, (c) ACR ball at a Fr_s of 1.69, and (d) ACR ball at a Fr_s of 2.20. Breaking bore propagating upstream (left to right).

Exploratory findings may yield new insights and initiate enhanced mitigation plans to combat the ever-growing plastic pollution in marine environments. In addition, this study may also motivate further research to examine the role of turbulent flow in mobilization and transport of plastic debris.

REFERENCES

Chanson, H. (2010). Unsteady turbulence in tidal bores: Effects of bed roughness. *Journal of Waterway, Port, Coastal and Ocean Engineering*, *136*(5), 247–256. https://doi.org/10.1061/(ASCE)WW.1943-5460.0000048

Erni-Cassola, G., Zadjelovic, V., Gibson, M. I., & Christie-Oleza, J. A. (2019). Distribution of plastic polymer types in the marine environment; A meta-analysis. *Journal of Hazardous Materials*, *369*, 691–698. https://doi.org/10.1016/j.jhazmat.2019.02.067

Geyer, R., Jambeck, J. R., & Law, K. L. (2017). Production, use, and fate of all plastics ever made. *Science Advances*, *3*(7), 25–29. https://doi.org/10.1126/sciadv.1700782

Jambeck, J. R., Geyer, R., Wilcox, C., Siegler, T. R., Perryman, M., Andrady, A., Narayan, R., & Law, K. L. (2015). Plastic waste inputs from land into the ocean. *Science*, *347*(6223), 768–771. https://doi.org/10.1126/science.1260352

Patel, P., Krol, M., & Karimpour, S. (2021). INFLUENCE OF SURGE WAVES ON THE TRANSPORT OF MACROPLASTICS. *Canadian Society of Civil Engineering Annual Conference 2021*, *May*, 1–10.

Plastics Europe. (2020). Plastics – the Facts 2020. In *PlasticsEurope*. https://www.plasticseurope.org/en/resources/publications/4312-plastics-facts-2020

Schwarz, A. E., Ligthart, T. N., Boukris, E., & van Harmelen, T. (2019). Sources, transport, and accumulation of different types of plastic litter in aquatic environments: A review study. *Marine Pollution Bulletin*, *143*(March), 92–100. https://doi.org/10.1016/j.marpolbul.2019.04.029

US Department of Energy National Energy Technology Laboratory. (2018). *Tracker*. National Energy Technology Laboratory. https://mfix.netl.doe.gov/tracker/

ISBN: 978-90-824846-7-0

Proceedings of the 2nd IAHR
Young Professionals Congress
30 Nov-2 Dec. 2021

Large-eddy simulation of the free-surface impact on the wake of a circular cylinder

Fawaz Alzabari [1], Pablo Ouro[2], Catherine Wilson[1]

[1]Hydro-environmental Research Centre, School of Engineering, Cardiff University, Cardiff, UK
Alzabarif@cardiff.ac.uk

[2]Department of Mechanical, Aerospace and Civil Engineering, The University of Manchester, Manchester, UK,
pablo.ouro@manchester.ac.uk

ABSTRACT

The instantaneous flow around a submerged circular cylinder located near to the free-surface is studied using Large-Eddy Simulation (LES) with a level-set method to represent the air-water interface. Four submergence ratios are modelled with Froude number in the range of 0.53-0.26 and a constant Reynolds number of 13,333 based on the cylinder's diameter. As Froude number increases, free-surface effects start to appear for values above Fr = 0.31, and the cylinder hydrodynamic forces also increased. For all cases, the instantaneous wake develop a von-Karman vortex street but in the shallowest submergence this is highly constrained by the proximity of the free-surface that leads to a quick loss of coherence of the vertical structures. Our study shows that adopting a free-surface capture method, e.g. level-set method, is required to accurately account for the free-surface effects in submerged cylinder flows for Froude numbers larger than 0.3.

Keywords: level-set method; large-eddy simulation; circular cylinder; hydrodynamic force; free-surface deformation.

1 INTRODUCTION

Despite being one of the most classic cases studied in fluid mechanics, ongoing research is currently being conducted experimentally and numerically in the field of the flow around circular cylinders due to its relevance to engineering applications such as submerged marine pipelines for offshore structures, bridge piers for scour protection and woody debris structures in natural flood management (Muller et al., 2021, Muhawenimana et al. 2019). To date, most research has considered cylinder flows in unbounded conditions or in the presence of a bottom wall in a boundary layer flow (Yang et al., 2018). The flow around cylinders located underneath a free-surface layer and a bottom wall has been less extensively studied. These hydraulic structures are relevant for constructing Woody Debris Dams (WDDs) across river channels for natural flood management practices. WDDs structures can be artificially built by comprising several horizontal cylinders perpendicular to the flow direction, akin to tree branches. The WDDs are commonly introduced in the natural watercourse with the aim to minimise the flow so that flood peaks are reduced, minimising the extension of downstream areas likely to experience flooding. Recent efforts have shed new light into the hydrodynamics of WDDs and its dependence on the structure's porosity, void ratio, length or layout (Muller et al., 2021). These experimental studies provided mean flow results whilst the instantaneous flow has not yet been unveiled and thus well understood. This study aims to quantify the effect of the free surface in proximity of a circular cylinder by varying the water depth. The cylinder is located close to the bottom surface with a gap-to-diameter ratio of 0.5, small enough to also lead to changes in the wake dynamics. Large-eddy simulation (LES) is employed due to its practicability to simulate turbulent flows allowing to resolve the large flow structures that dominate the cylinder's wake and forces.

2 NUMERICAL FRAMWORK AND SETUP

The in-house code Hydro3D is used to perform large-eddy simulations, which has been well validated in hydraulic and environmental flows (Stoesser et al., 2010; Ouro et al. 2019). Hydro3D adopts a staggered-storage scheme for the velocity and pressure variables and the fractional step method to advance the simulation in time using a three-step low-storage Runge-Kutta scheme. A 5^{th}–order weighted essentially non-oscillatory (WENO) is adopted to compute velocity fluxes and to resolve the advection equation from the level-set method (Ouro et al. 2021). The numerical setup reproduces that of the laboratory experiments performed in Muhawenimana et al., 2019 and are similar to previous LES studies (Ouro et al. 2019).

ISBN: 978-90-824846-7-0

3 RESULTS AND DISCUSION

The results of the free surface elevation obtained during an experimental campaign and from the LES are presented in Figure 1. For the case with Fr=0.31, the experiments and LES agree relatively well, with the free-surface drop behind the cylinder being slightly underestimated by the LES. As the Fr increases, the water level upstream of the cylinder increases and the amplitude of the surface drop immediately downstream of the cylinder is also enhanced, being almost negligible for the smallest Froude number (Fr = 0.26). Spanwise vorticity contours presented in Figure 2 for the four cases analysed shows that the vortical structures developed behind the cylinder are impacted by the submergence level. At Fr = 0.31, the cylinder wake causes a small spilling breaker to form at the free surface at a distance of five diameters downstream. The instabilities generated by that breaking interacts with the von-Karman vortices from the cylinder wake changing the wake dynamics. With Fr over 0.31, hydraulic jumps appear at different downstream locations and well captured by the LES. These results evidence the need for resolving the free-surface layer to fully capture the wake dynamics.

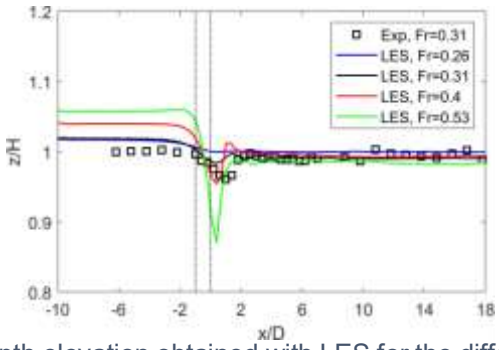

Figure 1. Profiles of water depth elevation obtained with LES for the different submergence values and experimental value for the case with Fr = 0.31.

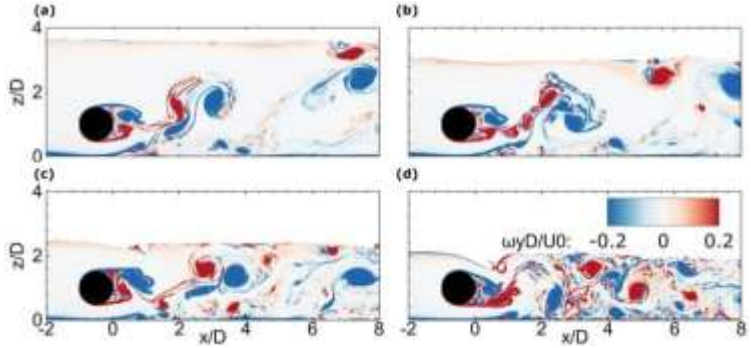

Figure 2. Contours of normalised instantaneous spanwise vorticity obtained from LES for the four submergences studied: (a) Fr = 0.26, (b) Fr = 0.31, (c) Fr = 0.4, and (d) Fr = 0.53.

REFERENCES

Muhawenimana, V., Wilson, C. A. M. E., Ouro, P., & Cable, J. (2019). Spanwise Cylinder wake hydrodynamics and fish behavior. Water Resour. Res., 55(11): 8569-8582.

Müller, S., Wilson, C. A., Ouro, P., & Cable, J. (2021). Leaky barriers: leaky enough for fish to pass?. R. Soc. Open Sci., 8(3): 201843.

Ouro, P., Lopez-Novoa, U., & Guest, M. F. (2021). On the performance of a highly-scalable Computational Fluid Dynamics code on AMD, ARM and Intel processor-based HPC systems. Comput. Phys. Commun., 269: 108105.

Ouro, P., Muhawenimana, V., & Wilson, C. A. (2019). Asymmetric wake of a horizontal cylinder in close proximity to a solid boundary for Reynolds numbers in the subcritical turbulence regime. Phys. Rev. Fluids, 4: 104604.

Stoesser, T., Kim, S. J., & Diplas, P. (2010). Turbulent flow through idealized emergent vegetation. J. Hydraul Eng, 136(12): 1003-1017.

Yang, F., An, H., & Cheng, L. (2018). Drag crisis of a circular cylinder near a plane boundary. Ocean Engineering, 154, 133-142.

ISBN: 978-90-824846-7-0

Proceedings of the 2nd IAHR
Young Professionals Congress
30 Nov-2 Dec. 2021

Failure of a penstock as an example of an extreme load case and countermeasure to reduce the impact of such load case

[1]Christian Kröner, [1]Jakob Seibl and [2]Roman Gabl
[1]University Innsbruck, Innsbruck, Austria
c.kroener@icloud.com
jakob.seibl@gmx.de
[2]The University of Edinburgh, Edinburgh, United Kingdom
Roman.Gabl@ed.ac.uk

ABSTRACT
A comprehensive methodological approach is presented in order to investigate a penstock failure as an extreme load case of a high-head hydropower plant and a countermeasure in order to reduce the impact of such a catastrophic event. The approach is ranging from numerical 1D and 3D modelling to small scaled experimental investigations and measurements on an implemented system. First, different modelling strategies for simulating the load case were conducted. Then, an innovative concept as a countermeasure to reduce the impact of such load case is presented. Finally, a proof of concept is conducted based on a real implementation of the concept and specific testing at a hydropower plant. As a conclusion it could be shown how to realistically simulate the extreme load case and impacts thereof. It has also been shown that the concept is capable of reducing impacts and can be efficiently implemented in an active plant.

Keywords: high-head hydropower plant; penstock failure; 1D and 3D numerical simulation; nature measurement

1 INTRODUCTION

Normally, during the planning phase of a hydro power plant, hydraulic and construction optimizations are required, among other things, whereby the most diverse tools and procedures can also be combined with additional added value [1]. The subsequent operation and potential emergencies must also be considered early in the planning process in order to optimally design the individual plants [2]. Extreme load cases could cause great damage in the very unlikely event that they occur. Such catastrophic load cases include the failure of the penstock aboveground pipes. Despite the very low probability of recurrence of such an event, the consequences are not only a total failure of the hydropower plant but also endanger everybody downstream of it. Knowledge and investigation of the possible impact of such an extreme load case and potential counter measures is required in order to meet the social and economic responsibility placed on the (future) operator.

2 BREAKAGE OF THE PENSTOCK AS LOAD CASE

Generally, a hydropower plant has an upper reservoir and a lower reservoir into which the water is discharged via turbines. The connection between the two reservoirs is formed by a hydraulic system divided into two sections. In the first section, with a relatively low gradient and a long flow distance, e.g. a pipe gallery (conduit) or pressure tunnel and in a second section, with a greater gradient and a shorter flow distance, usually designed as a penstock. In the following, a pipe failure will be presented which takes place in the in the penstock because a higher pressure inside the system makes it more likely that a failure occurs and also at this position the impact is greatest due to the massive water volume within the hydraulic systems upstream of the position of failure.

3 MODELLING OF THE LOAD CASE

First, a model using the commercial 1-D numerical software WANDA Liquid V. 4.2 from Deltares was built for simulating the extreme load case. Accordingly, boundary conditions of WANDA were adapted so as to simulate a break of the penstock, wherein cavitation was not considered at this stage. Parallel to this, a simplified approach based on Bernoulli's formula were conducted to evaluate the results of the 1D model. As a result, it could be shown that the load case could be simulated using the 1D model. Subsequently, cavitation was taken into account by implementing a controllable boundary condition in the 1D model. As a conclusion it could be shown that the cavitation provokes a significantly lower value for the discharge as compared to the scenario where cavitation was not considered.

4 ALTERNATIVE HYDRAULIC PROTECTION OF PENSTOCKS

Normally, in order to reduce the impact of such load case, a pipe rupture valve is installed within the hydraulic system. As an alternative to this, a submerged wall can be added in the penstock so as to represent a local high point within the hydraulic system, as a fixed installation. In case of an emergency this local high point allows

holding back the water upstream thereof after closing the inlet gate at the upstream reservoir. To evaluate this concept, different experimental model tests were conducted to study steady and unsteady behavior of this installation. In addition, these results are also used to validate 1D- and 3D-numerical calculations [3].

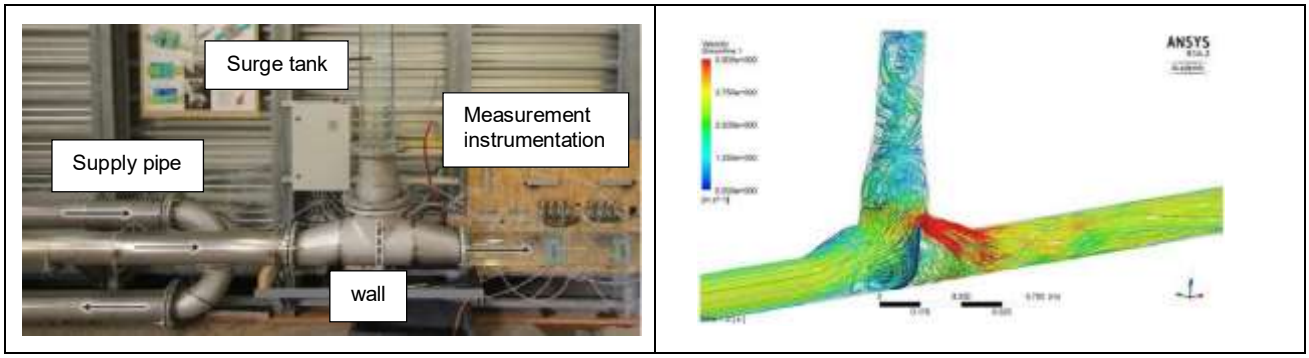

Figure 1 small-scale model in the laboratory at the University of Innsbruck and 3D-numerical simulation using ANSYS-CFX [3]

In *Figure 1* the small scale model and the 3D numerical model using ANSYS-CFX is shown which are used to examine and verify the behavior of the wall in the event of a penstock failure. In ANSYS-CFX the SST model is used as the turbulence model. It could be determined that the main task of the wall, the retention of the water, can be fully fulfilled. In addition, the total outflowing water volume for the entire rupture scenario is reduced by the additional loss through the wall compared to the system without a wall and with a rapid closure device, but this is accompanied by a loss that also acts during regular operation.

5 IMPLEMENTATION IN PRACTICE

The concept of the submerged wall as a local high point in the headrace tunnel, which can—in combination with the intake gates—replace existing penstock shutoff valves was implemented in the hydropower plant Schneiderau in Austria (see *Figure 2*). The realization of the concept allowed to prove the concept based on measurements including a simulated penstock failure. The penstock failure was simulated by keeping the turbines running and closing the gates at the inlet of the upper reservoir. It could be proven that the water level behind the wall remains very close to the top edge of the normally submerged structure. The presented solution can help to reduce investment costs and also minimize maintenance efforts and therefore is an attractive option for classic penstock shutoff valves for comparable projects [4].

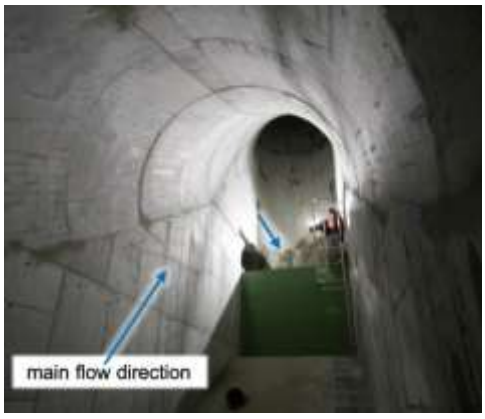

Figure 2 realized concept of the high point

6 CONCLUSIONS

The poster and the presentation show a methodical approach based on numerical simulations, which could be validated by experimental investigations and real measurements. It could be shown how a rupture of the penstock can be realistically simulated as an extreme load case. Furthermore, the effectiveness of an underwater wall in the penstock of a hydropower plant could be shown to reduce the effects of the extreme load case.

REFERENCES

[1] Gabl, R.; Achleitner, S.; Sendlhofer, A.; Höckner, T.; Schmitter, M.; Aufleger, M. (2013). Optimierter Einsatz und Kombination von 3-D-Numerik und physikalischer Modellierung. *WasserWirtschaft* 103, Magazine 5, P.128-131.

[2] Giesecke, J.; Heimerl, S. (2014). Wasserkraftanlagen - *Planung, Bau und Betrieb*, 6. Auflage, Springer-Verlag, DOI: 10.1007/978-3-642-53871-1.

[3] Seibl, J. (2016) Numerische und physikalische Untersuchung des hydraulischen Verhaltens von wandartigen Strukturen am Übergang von Druckstollen zu Druckschacht (PhD Thesis) University of Innsbruck

[4] Gabl, R.; Wippersberger, M.; Seibl, J.; Kröner, C.; Gems, B. (2021). Submerged Wall Instead of a Penstock Shutoff Valve—Alternative Protection as Part of a Refurbishment, *Water*, DOI: 10.3390/w13162247.

ISBN: 978-90-824846-7-0

Proceedings of the 2nd IAHR
Young Professionals Congress
30 Nov-2 Dec. 2021

Integrated hydrological and sediment modelling of an Irish River catchment

Rodhraí Crowley[1], Joe Harrington[1], Leonard O' Driscoll[1], Juan T. Garcia[2], Juan M. Garcia-Guerrero[2]

[1]Sustainable Infrastructure Research and Innovation Group, Munster Technological University, Cork, Ireland.
[2]Department of Mining and Civil Engineering, Universidad Politécnica de Cartagena, Cartagena 30203, Spain.
Corresponding Author Email Address: rodhrai.crowley@mycit.ie

ABSTRACT

Fine sediment can have deleterious effects on waterbodies, and is a major pressure on water quality in Ireland today. Hydrological models are a useful tool for catchment sediment management when integrated with soil erosion and sediment transport models. However, publications of this application in an Irish context are limited. In this paper, the HEC-HMS model is applied for continuous simulation of river discharge and suspended sediment in the River Owenabue catchment in County Cork, Ireland. The model was calibrated and validated against observed discharge at the Upper Ballea Bridge hydrometric station for the 2018-19 and 2019-20 hydrologic years, respectively. The HEC-HMS model showed good performance for daily simulation of river discharge. This has provided a basis for soil erosion and sediment modelling to predict suspended sediment load, which will be validated against turbidity-based measurements. This application will be a valuable contribution to catchment sediment modelling and management.

Keywords: hydrological modelling; water quality; HEC-HMS; discharge; sediment.

1 INTRODUCTION

Fine sediment can have negative impacts on the aquatic environment (Bilotta and Brazier, 2008). 43% of Ireland's rivers currently have 'unsatisfactory' water quality (Trodd and O'Boyle, 2021),with fine sediment among the main pressures on water quality in Ireland today (O'Boyle *et al.,* 2019). Integrated hydrological, soil erosion and sediment transport models are an important tool for catchment fine sediment management (Walling and Collins, 2016). However, this application in an Irish context has been limited to date, and while providing valuable insights has shown bias in sediment load prediction (Zi *et al.,* 2016). HEC-HMS is a semi-distributed hydrological model (US Army Corps of Engineers, 2021) that can simulate catchment hydrological processes, soil erosion based on the Modified Universal Soil Loss Equation (**MUSLE**) (Williams and Berndt, 1977) [A] and in-stream sediment transport, generating a sediment load. In this paper, the HEC-HMS model is applied to an Irish river catchment for continuous, daily simulation of river discharge and suspended sediment.

$$Y = 11.8(Q\ x\ q_p)^{0.56}.K.L.S.C.P \qquad [A]$$

Where Y is the event sediment load in megatonnes (MT), Q is the runoff volume (m^3), q_p is the peak runoff rate (m^3/s), K is the soil erodibility factor, L is the slope-length factor, S is the slope-gradient factor, C is the land cover and management factor, and P is the erosion-control practice factor.

2 ANY OTHER POINT YOU WISH TO ADD

2.1 Study area: This study focuses on the River Owenabue Catchment in County Cork, Ireland. The River Owenabue drains a total area of approximately 117km^2. There are long-term, continuous (15-minute resolution) records of river flow and turbidity (owned and managed by the Office of Public Works and Munster Technological University, respectively) at the Upper Ballea Bridge. The Cork Airport Weather Station is located approximately 5km north-west of the Upper Ballea Bridge providing a continuous, long-term record of meteorological data.
2.2 Methodology: 1) Geospatial analysis of the catchment using GIS; 2) Import catchment model and input data into HEC-HMS and select appropriate methods for representing catchment hydrological processes; 3) Model calibration for the 2018-19 hydrologic year and 4) Model validation for the 2019-20 hydrologic year. Model performance was evaluated with the Nash-Sutcliffe Efficiency (**NSE**) (Nash and Sutcliffe, 1970), percent bias (**PBIAS**) (Gupta *et al.,* 1999), and coefficient of determination ($\mathbf{R^2}$), as recommended by Moriasi *et al.* (2015).

ISBN: 978-90-824846-7-0

2.3 Results and Discussion

(A) Model Calibration: 2018-19

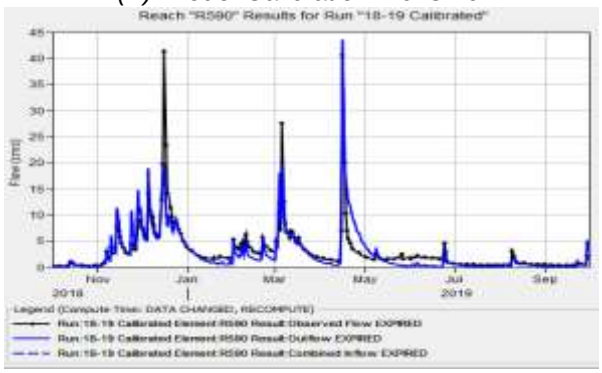

(B) Model Validation: 2019-20

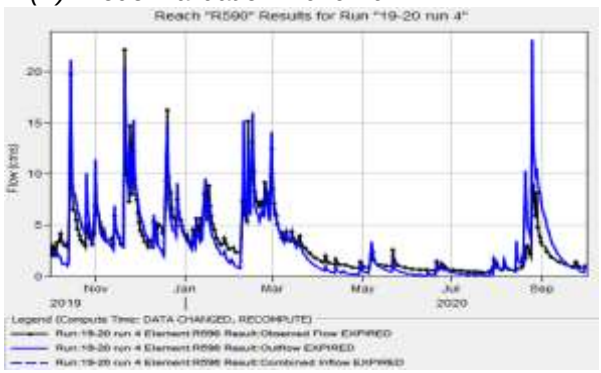

Figure 1. Simulated hydrograph (blue) versus the observed hydrograph (black) for (A) the 2018-19 hydrologic year, and (B) the 2019-20 hydrologic year, generated in HEC-HMS version 4.8.

The model captured the timing of all flow events, but underpredicted or overpredicted the magnitude of high flow events in isolated cases, while also showing some tendency to underpredict flow during dry periods (Figure 1 (A) and (B)). Nonetheless, the model accurately captures the timing and magnitude of flow events for most of the simulation period. Model performance was 'good' (Moriasi *et al.,* 2015). Calibration period: NSE = 0.77, PBIAS = -9.8%, R^2 = 0.78. Validation period: NSE = 0.74, PBIAS = -1.6%, R^2 = 0.81. Good hydrologic model performance has provided a strong foundation for soil erosion and sediment modelling in the catchment.

3 CONCLUSIONS

Overall, the HEC-HMS model demonstrated good performance for continuous daily simulation of river discharge, with biased prediction limited to isolated events. Accurate flow prediction has provided a reliable basis for soil erosion and suspended sediment transport modelling. This will be validated with turbidity-based suspended sediment load data. When completed, this application will be a valuable contribution to fine sediment modelling and management in river catchments; in both an Irish and international context.

REFERENCES

Bilotta, G.S., Brazier, R.E., 2008. Understanding the influence of suspended solids on water quality and aquatic biota. Water Research 42, 2849–2861.

Gupta, H., Sorooshian, S., Yapo, P., 1999. Status of Automatic Calibration for Hydrologic Models: Comparison With Multilevel Expert Calibration. Journal of Hydrologic Engineering, 4, 135-143.

Moriasi, D.N., Pai, N., Gitau, N.W. and Daggupati, P., 2015. Hydrologic and Water Quality Models: Performance Measures and Evaluation Criteria. Trans. ASABE 58, 1763–1785.

Nash, J.E., Sutcliffe, J.V., 1970. River flow forecasting through conceptual models part I - A discussion of principles. Journal of Hydrology 10, 282–290.

O'Boyle, S., Trodd, W., Bradley, C., Tierney, D., Wilkes, R., Ní Longphuirt, S., Smith, J., Stephens, A., Barry, J., Maher, P., McGinn, R., Mockler, E., Deakin, J., Craig, M., Gurrie, M., 2019. Water Quality in Ireland 2013-2018. EPA, Co. Wexford, Ireland. 26-27.

Trodd, W., O'Boyle, S., 2021. Water Quality in 2020: An Indicators Report. EPA, Co. Wexford, Ireland. 2-3.

US Army Corps of Engineers, 2021. HEC-HMS User's Manual, Version 4.8.

Walling, D.E., Collins, A.L., 2016. Fine sediment transport and management, in: Gilvear, D.J., Greenwood, M.T., Thoms, M.C., Wood, P.J. (Eds.), River Science. John Wiley & Sons, Ltd, Chichester, UK, 37–60.

Williams, J. R. and Berndt, H. D., 1977. Sediment Yield Prediction Based on Watershed Hydrology. Transactions of the ASAE 20, 1100–1104.

Zi, T., Kumar, M., Kiely, G., Lewis, C., Albertson, J., 2016. Simulating the spatio-temporal dynamics of soil erosion, deposition, and yield using a coupled sediment dynamics and 3D distributed hydrologic model. Environmental Modelling & Software 83, 310–325.

ISBN: 978-90-824846-7-0

Proceedings of the 2nd IAHR
Young Professionals Congress
30 Nov-2 Dec. 2021

Numerical investigation of the impact of roughness and infiltration in rainfall-runoff experiments

Yangwei Zhang[1], Franziska Tügel[1], Hao Han[2] and Reinhard Hinkelmann[1]

[1] Chair of Water Resources Management and Modeling of Hydrosystems, Technische Universität Berlin, Berlin, Germany, yangwei.zhang@wahyd.tu-berlin.de
[2] State Key Laboratory of Eco-hydraulics in Northwest Arid Region of China, Xi'an University of Technology, Xi'an, China, haohan@stu.xaut.edu.cn

ABSTRACT

Rainfall-runoff experiments carried out in Xi'an University of Technology, China with different rainfall intensities and slopes, were used to calibrate and validate the robust shallow water model hms and to investigate differences between traditional and LID surface conditions. Depth-dependent roughness and depth-dependent infiltration methods were implemented and lead to the best agreements of computations and measurements with Nash-Sutcliffe efficiencies higher than 0.92. LID conditions are more efficient with regard to infiltration when compared to traditional conditions.

Keywords: depth-dependent roughness; depth-dependent infiltration; robust shallow water model; rainfall runoff simulation; LID measures.

1 INTRODUCTION

Rainfall-runoff simulation with robust shallow water model has becoming very important in recent years for flood protection, urban drainage and the implementation of LID (low impact development) measures and Sponge City concepts. The past two decades have seen many generations of robust shallow water models, among them there is one-Hydroinformatics Modelling System (hms) (Özgen-Xian et al., 2014). And it is essential to calibrate and validate such models with experiments. In hms rainfall, depth-dependent roughness (Jain et al., 2004) and depth-dependent infiltration (Langhans et al., 2013) were implemented. The equations of the latter two are as follows:

$$n = \begin{cases} n_0 \left(\frac{h}{d_0}\right)^{-\varepsilon}, & h \le d_0 \\ n_0, & h > d_0 \end{cases} \qquad i = \begin{cases} i_0 \left(\frac{h}{h_0}\right)^{t}, & h \le h_0 \\ i_0, & h > h_0 \end{cases} \qquad [1]\ [2]$$

Where n represents the depth-dependent Manning's value, while n_0 is the originally chosen Manning's value, [s/m$^{1/3}$]; i represents the depth-dependent infiltration, while i_0 is the basic infiltration, [mm/min]; h is the water depth, d_0 and h_0 denote the threshold of water depth for depth-dependent roughness and depth-dependent infiltration method respectively, [m]; t and ε are calibration parameters, [-].

2 EXPERIMENT AND MODEL RESULTS

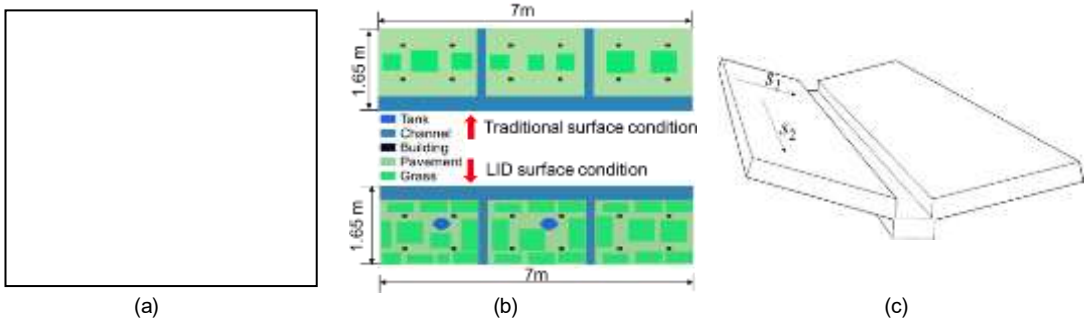

Figure 1. Experimental setup: a) platform; b) surface setup; c) V-catchment

ISBN: 978-90-824846-7-0

The experiments carried out at Xi'an University of Technology, China have the design of a V-catchment (Fig. 1) and apply a 7m long and 1.65m wide platform with varying longitudinal slope s_2 from 1° , 5° to 10° along the flow direction (Hou et al., 2019). In the experiments, three rainfall intensities are investigated, however here only results of the calibration using the rainfall intensity of 0.47mm/min are shown considering traditional and LID surface conditions.

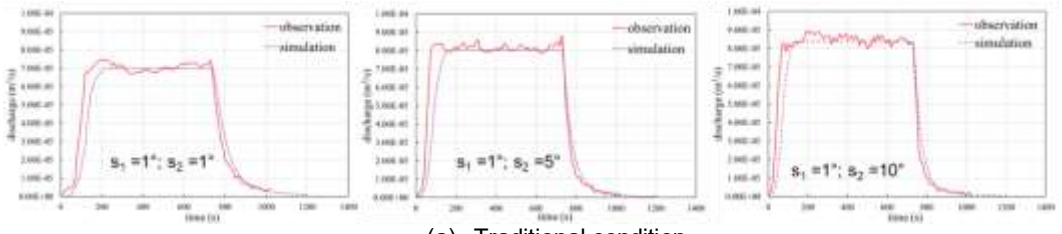

(a) Traditional condition

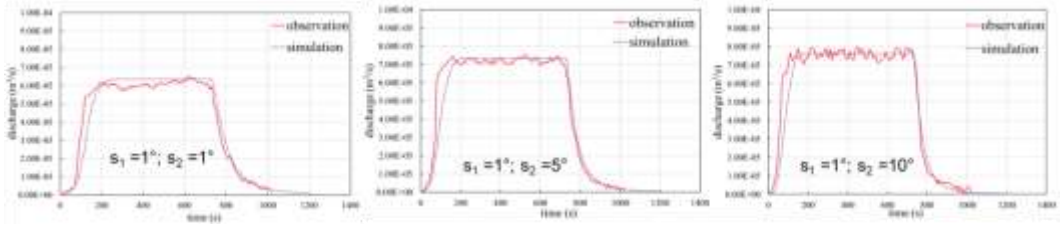

(b) LID condition

Figure 2. Computational and experimental results for calibration

The graphs above (Fig. 2) demonstrate that the computational processes are consistent with the experimental processes. The calibration parameters and results are listed in Table 1 below. After calibration, the same parameters are used for validation using rainfall intensities of 0.84mm/min and 0.67mm/min separately. The surface conditions differ for LID and traditional conditions, however they were simulated with the same parameters (Tab. 1). As there is more grass and two water tanks in LID condition, more water infiltrates compared to traditional condition.

Table 1. Calibration parameters obtained for the rainfall intensity of 0.47mm/min

	0.47 [mm/min]	d_0 [m]	ε [-]	h_0 [m]	t [-]	NSE [-]	
						TRADITIONAL	LID
s_2=1°; s_1=1°	√	0.035	0.45	0.001	0.30	0.96	0.94
s_2=5°; s_1=1°	√	0.035	0.45	0.001	0.30	0.92	0.95
s_2=10°; s_1=1°	√	0.035	0.45	0.001	0.30	0.94	0.95

3 CONCLUSIONS

The results of the calibration show good agreement with observation data expressed by Nash-Sutcliffe efficiencies higher than 0.92. Similar good results were also obtained for the validation. We found out that Manning's n becomes greater with smaller water depth, while infiltration shows totally reverse direction, i.e. infiltration gets smaller along with decreasing water depth. LID is more efficient with regard to infiltration when compared to traditional condition.

REFERENCES

Hou J.M., Han H., Qi W.C., Guo K.H., Li Z.B. and Hinkelmann R. (2019). Experimental investigation for impacts of rain storms and terrain slopes on low impact development effect in an idealized urban catchment. Journal of Hydrology,124176.

Jain M.K., Kothyari U.C. and Ranga Raju K.G. (2004). A GIS based distributed rainfall–runoff model. Journal of Hydrology, 107-135.

Langhans C., Govers G. and Diels J. (2013). Development and parameterization of an infiltration model accounting for water depth and rainfall intensity. Hydrol. Process., 3777-3790.

Özgen-Xian I., Simons F., Zhao J. H. and Hinkelmann R. (2014). Modeling shallow water flow and transport processes with small water depths using the Hydroinformatics Modelling System. 11th International Conference on Hydroinformatics. New York: City University of New York (CUNY) 2.

Proceedings of the 2nd IAHR
Young Professionals Congress
30 Nov-2 Dec. 2021

Long-term urban river flow water quality and hydrological responses in subtropical climates

Xuan Pang [1], Mingfu Guan [2]

[1] PhD Candidate, Department of Civil Engineering, University of Hong Kong, Hong Kong SAR, xuan.pang@connect.hku.hk
[2] Assistant Professor, Department of Civil Engineering, University of Hong Kong, Hong Kong SAR, mfguan@hku.hk

ABSTRACT

For keeping sustainable water resources, two essential parts including providing sustainable supply of water quantity and protecting and restoring water quality are important evaluation factors on urban hydrology. This study aims to explore the urban river flow and water quality trends at both long-term and seasonal scales. Taking the study site at subtropical climates, the potential drivers of trends in urban river flow and water quality will also be investigated. Seasonal trend decomposition using loess (STL) will be used for revealing the seasonal trends for river flow and water quality. We found obvious differences in ranges and spatial distributions of monthly river flow for the four chosen periods (i.e., 1989, 1999, 2009 and 2019). An alkalinity trend from 1989 to 2019 is also found. Monthly total solids may have strong correlations with conductivity.

Keywords: water quality; hydrological response; long-term and seasonal trends; subtropical climates; river and creek.

1 INTRODUCTION

As a crucial component of hydrological processes, river flow is key for sustainable water use (Cheng et al., 2018). Water quality is also a vital role in urban water resources management which is related to non-source pollution. In this study, three research questions are typically explored: (1) What are the long-term and seasonal trends of river flow? (2) what are the long-term and seasonal trends of river flow water quality? (3) what are the potential drivers of trends in river flow and water quality?
We chose Hong Kong city as our study site on behalf of urban area in subtropical climates. Eight water control zones (i.e., Western Buffer, Deep Bay, Junk Bay, Victoria Harbour, Tolo Harbour And Channel, Southern, Port Shelter, North Western) were included. Each water control zone contains individual rivers and stations. The period of 1988-2019 was chosen as the study period.

2 PRELIMINARY RESULTS

In this study, seasonal trend decomposition using loess (STL) will be used to reveal the long-term and seasonal trends for river flow and water quality. This method has been previously used to analyze long-term water quality and river discharge data (Cheng et al., 2018; Stow et al., 2015). Median polish method will be used for reckoning missing values of monthly data (especially for river flow data).
In terms of river flow, we found obvious differences in ranges for the four chosen periods (Figure 1). For example, the magnitudes of flow in 1989 varies from zero to over 175 m^3/s; however, in 1999, the upper limit of river flow is no more than 3.5 m^3/s. Despite from the temporal distinction, spatial differences are also found. Overall, for the four periods with equal time intervals, Deep Bay contains more outliers compared with other seven water control zones, which indicates that the monthly river flow in Deep Bay displays the most fluctuations over all water control zones. In contrast, there are rare fluctuations for monthly river flow in Junk Bay and Western Buffer during the four periods. Additionally, in 2009, Victoria Harbour shows entirely different distribution pattern with other zones, with the most median values and prominent interquartile-range (Figure 1).
We chose seven physicochemical parameters for water quality analysis (i.e., Conductivity (μS/cm), Dissolved Oxygen (%saturation), Dissolved Oxygen (mg/L), pH, Total Solids (mg/L), Turbidity (NTU), Water Temperature (°C)). We found that the water control zone with the highest conductivity shifts from North Western to Victoria

ISBN: 978-90-824846-7-0

Harbour after two decades within our chosen periods (not shown in the figure). However, Tolo Harbour And Channel displays the most considerable outliers out of its interquartile-range consistently, which can be related to its discrete dissolved ion contents among three decades (Angrill et al., 2017). A slight increase trend in pH is found for the four given year. Thus, there is an alkalinity trend from 1989 to 2019. For the Total Solids, we found an identical shift from North Western to Victoria Harbour with the shift of conductivity. Regarding all rivers and creeks, monthly total solids may have strong correlation with conductivity. Water temperature has the most intensive values which shows that all most all the values are within their interquartile-ranges.

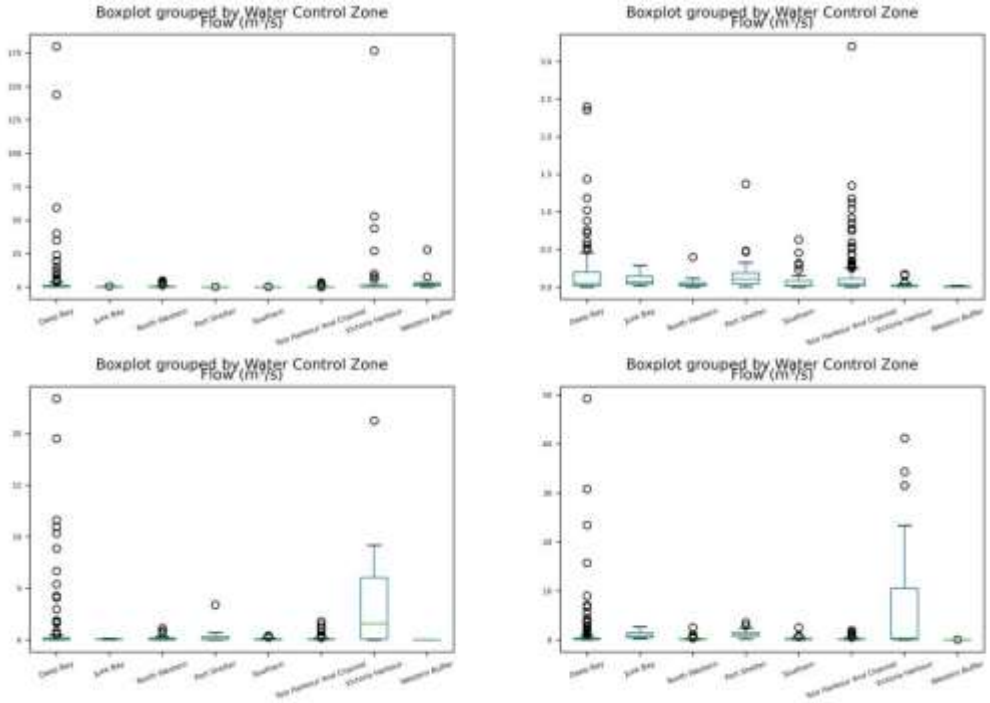

Figure 1. Boxplot diagram of river flow (m^3/s) for each water control zone in 1989, 1999, 2009 and 2019, respectively.

3 CONCLUSIONS

We found obvious differences in ranges and spatial distributions of monthly river flow for the four chosen periods (i.e., 1989, 1999, 2009 and 2019). A slight increase trend in pH indicating an alkalinity trend from 1989 to 2019 is also found. Monthly total solids may have strong correlations with conductivity.

ACKNOWLEDGEMENTS
The work is supported by the Environment and Conservation Fund, Hong Kong (grant number: 108/2019) and the General Research Fund of Hong Kong RGC (grant number: 17202020).

REFERENCES

Angrill, S., Petit-Boix, A., Morales-Pinzón, T., Josa, A., Rieradevall, J., & Gabarrell, X. (2017). Urban rainwater runoff quantity and quality–A potential endogenous resource in cities? *Journal of environmental management*, *189*, 14-21.

Cheng, P., Li, X., Su, J., & Hao, S. (2018). Recent water quality trends in a typical semi-arid river with a sharp decrease in streamflow and construction of sewage treatment plants. *Environmental Research Letters*, *13*(1), 014026.

Stow, C. A., Cha, Y., Johnson, L. T., Confesor, R., & Richards, R. P. (2015). Long-term and seasonal trend decomposition of Maumee River nutrient inputs to western Lake Erie. *Environmental Science & Technology*, *49*(6), 3392-3400.

Proceedings of the 2nd IAHR
Young Professionals Congress
30 Nov-2 Dec. 2021

Assessment and guidelines for the selection of the input data for the numerical modelling of suspended sediment transport in a subtropical reservoir.

Gonzalez Wendy [1], Seidel Frank [1], Klassen Irina [2] and Franz Nestmann[1]
[1] Karlsruhe Institute of Technology, Karlsruhe, Germany,
wendy.otero@kit.edu
[2] Federal Waterways Engineering and Research Institute, Karlsruhe, Germany.

ABSTRACT

The prediction of the suspended sediment transport through numerical modelling is a useful tool for the management of storage reservoirs. The quality and quantity of input data to set up a robust model can be challenging, especially for developing countries, where measurement campaigns are not often performed. The present study deals with the analysis of sediment related input data such as the sediment rating curve, particle size distribution, dry bed density, critical bed shear stresses for erosion and deposition and their impact on the results of a 3D-numerical model of a reservoir set up with the software Delft3D. It was observed that the temporal resolution of the data to construct a sediment rating curve has a notorious influence for the modelling results. The spatial and temporal variation of input parameters should be considered in the modeling, since it may have an impact on the predictions of the sedimentation processes.

Keywords: reservoir sedimentation; reservoir management; numerical modelling; suspended sediments.

1 INTRODUCTION

The deposition of fine sediments not only contributes to the reduction of the storage capacity of reservoirs, but also to the pollution of the storaged water due to their turbidity and adsorption capacity for substances such as heavy metals and polycyclic aromatic hydrocarbons. The numerical modelling of suspended sediments transport can be used as a tool to predict the suspended solid concentrations (SSC), the sedimentation patterns and deposition volume within a reservoir. For any numerical model, the amount of incoming sediments into the reservoir is required which is often defined as a function of the discharge (Q), i.e. a rating curve (RC). For the application of the threshold formulations of Partheniades-Krone to calculate the fine sediment fluxes at the bed/water column, the critical bed shear stresses for erosion ($\tau_{ero,crit}$) and deposition ($\tau_{dep,crit}$) are required. The transformation of the sediment mass at the bed into a layer thickness occurs through the use of the dry bed density (DBD). Further, the particle size distribution (PSD) of the incoming sediment is also a requirement. To set up a robust model, the input data should originate from measurements. Nevertheless, this is rarely the case in many countries and the modelers are forced to use literature/default values. Table 1 aims to show the dependency of the mentioned parameters on several factors.

Table 1. Typical ranges and factors affecting the studied parameters.

PARAMETER	RANGE	UNITS	DEPENDECY
RC	N.A.	Q [$m^3 s^{-1}$]; SSC [$mg l^{-1}$]	Catchment's hydrology and erosion processes.
$\tau_{ero,crit}$	0.04-20	Pa	DBD, grain size, consolidation, mineral composition.
$\tau_{dep,crit}$	0.04-0.1	Pa	Gran size, SSC, mineral composition.
DBD	500-1500	Kg m^{-3}	Consolidation, mineral composition.
PSD	N.A.	μm	Catchment soil materials, flocculation processes.

2 MATERIALS AND METHODS

Within the framework of the MuDak-WRM-Project (MuDak-WRM, 2019) studies were performed to analyze the possibilities how to reduce the complexity of the input data for 3D-numerical modelling of the hydrodynamics and sediment transport. This document directs the focus to the sediment related parameters listed in Table 1. A numerical model of the Passaúna Reservoir in southern Brazil was set up with the software Delft3D as a case study and calibrated according to available measured water profiles of temperatures, horizontal flow velocity, suspended sediment concentrations and sedimentation rates. Figure 1 describes the sediment-input parameters for the present study. For each data set one reference simulation (Ref) of a 2 months period (11.12.2018-12.02.2019) was started. The SSC and sedimentation rates at "PARK" (Figure 2a) as well as the deposition volume from the sensitivity studies (see Figure 1) were compared to the reference simulation.

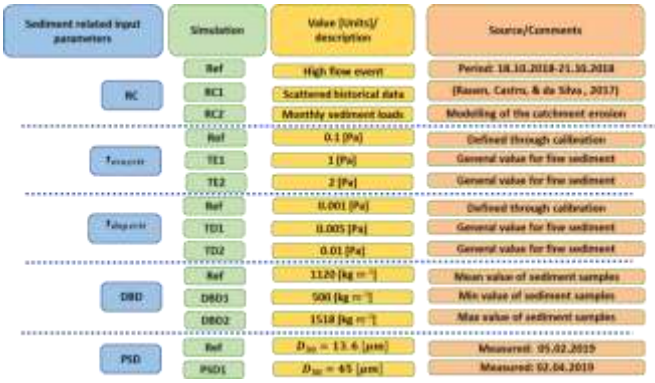

Figure 1. Description and variation range of the studied parameters.

3 RESULTS AND CONCLUSIONS

Figure. 2b displays the sedimentation pattern for the reference simulation for the studied period. Figures 2c to 2e show the resulting SSC and sedimentation rate at the location PARK and the erosion/deposition in the reservoir. As expected, the use of a determined RC influences the sedimentation volume. It is important to highlight how different approaches to build a rating curve can affect the amount of solids entering the reservoir due to the variation of the temporal resolution of the data on which they are based. The bed shear stresses for erosion and deposition are crucial for the resulting sedimentation pattern (reflected on the variation of the sedimentation rate at PARK). For a reservoir, the critical value for erosion should be measured, especially for zones with the highest flow velocities. It is advised to determine the threshold for shear stress for sedimentation through model calibration, due to its high variability or even due to the discussion about its existence. The PSD of the incoming sediment, should be measured for different flow conditions, since it may variate for different time instants, as it was the case in this study. The different PSDs will directly affect the deposition patterns and the SSC. The selection of a non-suitable dry bed density value will lead to misprediction of the deposited sediment volume. As shown in this study, the range of this value can be wide even for the same reservoir.

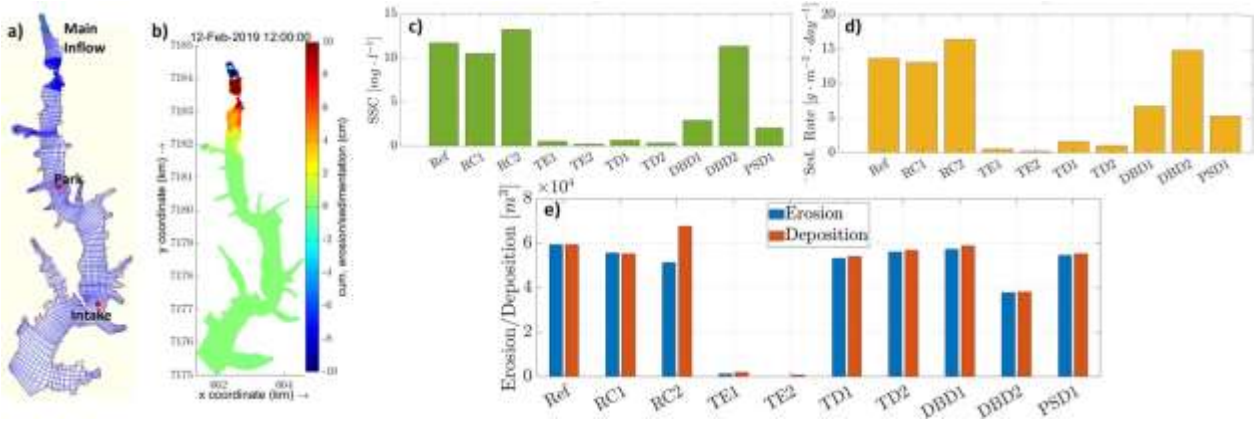

Figure 2. a) numerical grid b) Erosion/deposition simulation Ref, c) SSC at Park, d) Sedimentation rate at PARK and e) Total Erosion/Deposition for the model area.

ACKNOWLEDGEMENTS

The present study was funded by the German Federal Ministry of Education and Research (Grant number: 02WGR1431A). The authors thank all partners, who provided measurements and data for the model.

REFERENCES

MuDak-WRM. (2019). Multidisciplinary data acquisition as the key for a globally applicable water resource management. Online: https://www.mudak-wrm.kit.edu/.

Rauen, W., Castro, C., & da Silva, M. (2017). Caracterização Hidrossedimentológica do Rio Passauna, PR, Brasil, a partir de Dados Históricos. XX Simpósio Brasileiro de Recursos Hídricos,Associação Brasileira De Recursos Hídrico

Proceedings of the 2nd IAHR
Young Professionals Congress
30 Nov-2 Dec. 2021

Simulating roughness heights impact on secondary circulations in ice covered flow

Samaneh Ebrahimi [1], Majid Mohammadian [1] and Colin Rennie [1]
[1] University of Ottawa, Ottawa, Canada,
sebra017@uottawa.ca

ABSTRACT

The influence of different roughness heights on secondary flow circulations is simulated in a closed curved flume to represent the behavior of transverse flow in an ice covered river bend channel in the natural environment. OpenFOAM is used to model the effects of different roughness heights, K_s, using RANS model, with a uniform size and distribution assumption. The results of the realizable k-epsilon model for three sand grain sizes are presented here to account for different degrees of ice cover roughness. The different simulations have shown a clear increasing influence of rough ice on the flow as the roughness height increased. The asymmetric cells produced in the rough ice simulations are associated with an increase in the wall shear stress. Additionally, the position of maximum velocity was lowered as the ice cover surface roughness was increased.

Keywords: roughness height simulation, OpenFOAM, secondary cells, closed curved channel.

1 INTRODUCTION

To understand the effect of surface roughness on fluid flow, this study presents the results of a simulated ice covered river with different wall boundary conditions for the channel's top surface. Previous studies have shown that for a wall without roughness, the velocity profile between the wall and adjacent cell follows the logarithmic law of the wall. This means the dimensionless velocity, U+, is logarithmically related to the distance normal to the wall, y+, presented in Equations 1 to 4, where K is von karman constant, E is constant, y is distance from the wall, u_* is friction (or shear) velocity, τ_w is the wall shear stress, and ρ is the density of fluid (here water).

$$U^+ = 1/K \log(Ey^+) \quad [1]$$

$$y^+ = y\, u_*/\nu \quad [2]$$

$$u_* = \sqrt{\tau_w/\rho} \quad [3]$$

$$U^+ = u/u_* \quad [4]$$

The roughness of the wall calls for a modification to the equation by adding the function ΔB to the right hand side of Equation 1 (Shockling et al, 2006). Thus U^+ is calculated from the standard log-law with, and ΔB, which is generally a function of the size and shape of the roughness elements.

$$U^+ = 1/K \log(Ey^+) - \Delta B \quad [5]$$

Here ΔB is characterized by two parameters: Ks which is a representative roughness height and Cs which is the roughness constant (Shockling et al, 2006).

2 RESULTS

The effect of different roughness values of ice cover on the two cell pattern in a 135° bend closed channel is modeled using different RANS turbulence models and the LES. Here the result from the realizable k-epsilon turbulence model is presented showing the transverse velocity for an aspect ratio of 2, corresponding to the water depth of 10 cm. In these simulations the roughness constant, C_s, is set to 0.5 and the effect of varying

ISBN: 978-90-824846-7-0

sand-grain size, k_s, for three different degrees of under-ice-cover roughness of 0 (smooth), 1, and 2 mm are examined (Figure below). The streamlines in the middle of the two cells go from the inner bank (right side of figures) to the outer bank (left side of figures) and the streamlines on the top and bottom go from the outer to inner bank. The shapes of the main cells are closed and elliptical (not seen in this figure due to axis scale setting) in all cases, consistent with the previous studies (e.g. Yanase et al. 2002). The two cells in smooth wall channel (left sub-figure) are symmetrical as expected from the same boundary conditions for both the top and bottom walls. To model the rough ice's effect, the roughness height was modified for the upper wall, while the other three walls are assumed smooth. The smaller roughness, 1 mm (middle sub-plot), showed a clear change in the previous symmetric shape of the two main cells. Increasing the size of roughness height to 2 mm, a greater influence on the flow is visible with the top cell moving further down. The figure clearly demonstrates the rougher ice surface enlarged the top cell's extension. As a result the bottom cell has been further pushed down as the top wall roughens more.

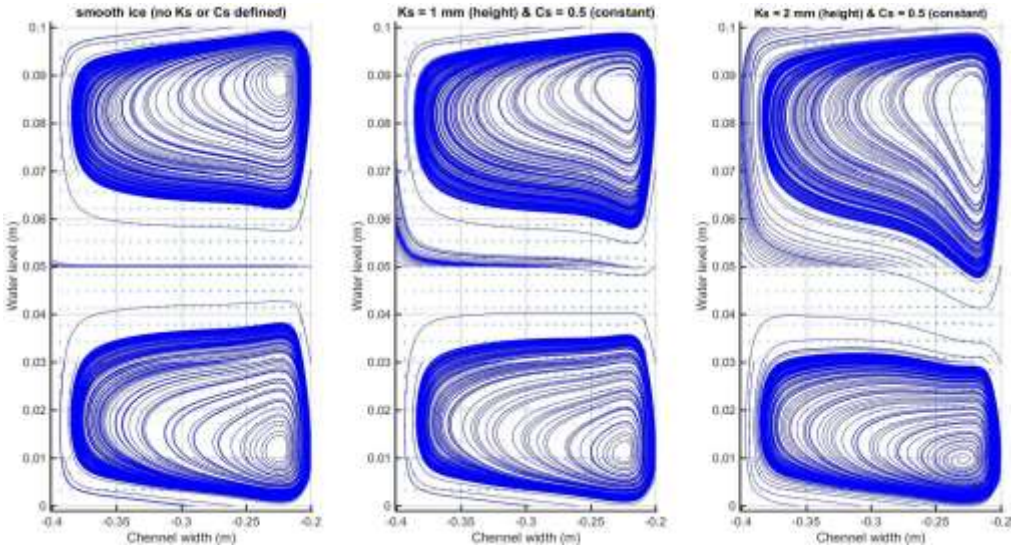

Additionally, all models with the rough upper wall have demonstrated the roughness will push the point of maximum streamwise velocity lower in the flow. The elevation of the maximum velocity was at 0.5 of the flow depth from the bed in the smooth walls, however when the ice cover was roughened, it was pushed further down towards the bed. Consequently, a downward shift in mean velocity profile below the smooth wall is a major effect of wall roughness (Hama 1954).

3 CONCLUSIONS

The comparison of different cases here showed the two counter rotating cells are not behaving the same when the roughness factor is added. All roughness heights tested have captured the asymmetric circulation of the secondary cells and increasing the size of roughness height increased the influence on the flow by enlarging the top cell as the ice cover gets rougher. The increase in the roughness height has resulted in further lowering the point of maximum velocity. Additional experiments are required for evaluating the degree of agreement between the laboratory and numerical flow dynamics.

REFERENCES

Hama, Francis R. "Boundary layer characteristics for smooth and rough surfaces." Trans. Soc. Nav. Arch. Marine Engrs. 62 (1954): 333-358.

Shockling, M. A., J. J. Allen, and A. J. Smits. "Roughness effects in turbulent pipe flow." Journal of Fluid Mechanics 564 (2006): 267-285.

Yanase, S., Kaga, Y. and Daikai, R. 2002. Laminar flows through a curved rectangular duct over a wide range of the aspect ratio. Fluid Dynamics Research, 31(3), p.151.

ISBN: 978-90-824846-7-0

Proceedings of the 2nd IAHR
Young Professionals Congress
30 Nov-2 Dec. 2021

Clustering and Machine Learning algorithms as tools to support groundwater management in water-stressed areas. Application in the agricultural region of Campo de Dalías (Almería, Spain)

Miguel Ángel Diaz[1], Lupicinio García[1], Francisco Núñez[1], Manuel Argamasilla[1], José Manuel Nieto[1], Damián Sánchez[1]
[1]Fundación Centro Andaluz de Investigaciones del Agua – Cetaqua Andalucía, Málaga (Spain)
miguelangel.diaz@cetaqua.com

ABSTRACT

The semi-arid regions of the Mediterranean coast, such as Campo de Dalías and Sierra de Gádor aquifer (SE Spain), are characterized by frequent and longtime dry periods, high temperatures and a strong dependence on groundwater. Campo de Dalías Groundwater body consist of a complex aquifer system, with 8 aquifers, some of them interconnected. The intense exploitation of groundwater (> 100 hm3/yr.) has caused a decrease in piezometric levels and water availability which affects water quantity and quality, with eventually episodes of marine intrusion. Clustering and different Machine Learning techniques can be very helpful for groundwater management and water table prediction.

Keywords: Clustering; water table prediction; water-stressed areas; Machine Learning.

1 INTRODUCTION

The semi-arid regions of the Mediterranean coast, such as Campo de Dalías and Sierra de Gádor aquifer (SE Spain), are characterized by frequent and long time periods of low rainfall, high temperatures and a strong dependence of groundwater. In the 80's, Campo de Dalías became one of the most intensive and productive agricultural areas in the world. Otherwise, the greenhouse's irrigation activity has progressively been increased totalizing nowadays more than 20.000 ha of greenhouses.

2 HYDROLOGICAL AND CLIMATE CONTEXT

A climate assessment has been carried out with data from 10 weather stations. The average rainfall for the period 1996/97-2018/19 is 301 mm/yr, with a predominance of dry and medium-dry years.
The most important water resource in Campo de Dalías area is groundwater, which is stored in detritic and karstic materials of Triassic, Miocene and Pliocene ages. The geological structure has a complex geometry, involving eight different aquifers, some of them interconnected. From an administrative point of view, they are all included in the Campo de Dalías and Sierra de Gádor Groundwater body (060.013). These aquifers can be divided in two classes: upper (unconfined) and lower (confined) aquifers.
From the 80's to the 90's of the last century the total groundwater demand has been increasing in all aquifers, upper and lower. Because of this intense groundwater exploitation for agriculture and the use of fertilizers, the shallow aquifer became to a bad chemical status. The groundwater resources were therefore substituted with surface water resources coming from the Benínar reservoir. From this moment on, most of the groundwater started to come from the deep aquifers (IGME, 2014).
According to the most recent Water Management Plan (DHCMA, 2020), the main water demand in groundwater body 060.013 is for agricultural use (146 hm3/yr.), followed by urban supply (47 hm3/yr.). From the total of irrigation demand, more than 60% correspond to groundwater resources and 20% correspond to surface water. Currently, new alternative water sources have been introduced to meet the water demand, like treated wastewater (8%) and desalinated water (5%).

3 RESULTS

ISBN: 978-90-824846-7-0

In this study, funded by the European PRIMA call (**GOTHAM** on-going project), the impact of water availability on groundwater quantitative status at Campo de Dalías and Sierra de Gádor Groundwater Body has been assessed using Machine Learning techniques. Firstly, the missing values of the historical series have been completed using different methods, such as linear regression, mice forests, etc. Also, the values ±10% of variation between near values have been removed because they are considered outliers.
Then, Clustering techniques have been carried out to identify representative points of water table time series in each aquifer sector. The clustering method applied has been K-means using Dynamic Time Warping Matching metric. As a result of the 14 points available, 3 groups have been obtained (Figure 1) and 4 points have been left out due to the lack of continuity of the series. Also, 3 synthetic series have been developed as representative series of each group, that will be used for the water scarcity index estimation.
The input data used for the groundwater availability forecasting have been piezometric time series as the target variable (univariate approach). Moreover, to improve the goodness of fit of the predicted results, different Machine Learning algorithms (Linear Regression, XGBoost, SVR…) have been tested and the target variable (groundwater table) has been iterated with other explanatory variables (natural recharge in the aquifer and rainfall and temperature). The best results have been obtained using the target variable (accuracy ≈90% in one step prediction while maintaining a good bias-variance ratio), while the explanatory variables do not significantly increase the accuracy. The results have been verified by analyzing the metrics (MAE, RMSE, etc.) in both the training and test sets, to avoid overfitting the models.

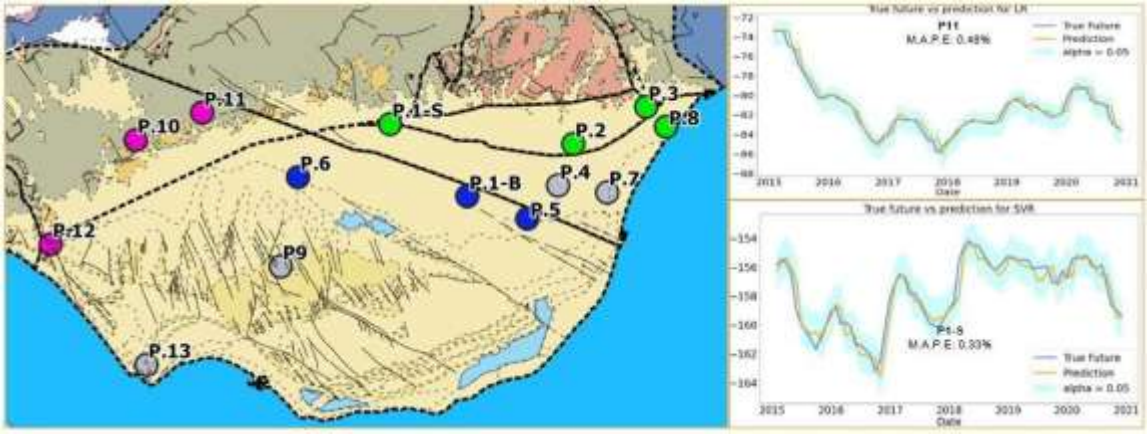

Figure 1.(*left)*Clustering map. *(Right)* Predictions using LR and SVR algorithms.

4 CONCLUSIONS

In conclusion, from the results obtained, the classification by clusters has allowed us to classify piezometers according to their hydrodynamic behaviour where there is no hydrogeological information and to optimize the monitoring points. In addition, the accuracy of the results obtained for short-term prediction has been 90% and quite good for long-term predictions. However, for clusters 1 and 3 it will be necessary to add the explanatory variable of the season of the year. It also serves to anticipate possible future events and to cope with climate change. It has been demonstrated that the use of Machine Learning models is a very useful tool for efficient management of water resources in scenarios such as the one studied, where socio-economic activities are highly dependent on the availability of groundwater.

5 REFERENCES

DHCMA (2020). *Plan hidrológico de la Demarcación Hidrográfica de las Cuencas Mediterráneas Andaluzas 2021-2027*. Documento para la consulta pública. Junta de Andalucía, 1127 pp.

IGME (2014). *Memoria Final de los trabajos realizados durante la Fase I del Programa de actividades científico – técnicas de apoyo a la protección – Regeneración de los Acuíferos del Sur de Sierra de Gádor–Campo de Dalías (Almería)*. Convenio de colaboración Agencia Andaluza del Agua – IGME – ACUAMED – JCUAPA. Informe técnico, Almería, 295 pp.

ISBN: 978-90-824846-7-0

Proceedings of the 2nd IAHR
Young Professionals Congress
30 Nov-2 Dec. 2021

Estimation and mapping soil erosion caused by maximum daily rainfall using GIS and remote sensing techniques in the Tumbaro river basin - San Martin region

Jhon Walter Gómez Lora [1], Victor Hugo Gallo Ramos [2] and Katherine Camacho Zorogastúa [3]

[1,2 y 3] Instituto Especializado de Investigación y Gestión del Agua INEIGA, Lima, Peru,
e-mail jgomez@unfv.edu.pe
[2] Young Professional Network YPN, Lima, Peru,
e-mail 2012000392@unfv.edu.pe
[3]Environmental and Hydrologic Engineering ENHYDRO, Lima, Peru
2016313001@unfv.edu.pe

ABSTRACT

The Tumbaro River Basin is an important river that carries its waters to the Mayo River in the San Martín region. It is challenged by an increase in its socio-economic development due to agricultural activity. In addition, factors such as heavy rainfall, slope, vegetation cover and soil properties affect and are susceptible to erosion. This study aimed to estimate and map average soil erosion in terms of spatial distribution by using the revised universal soil loss equation (RUSLE) and GIS techniques. This study also applied remote sensing and available data sources for this analysis. Annual erosion varies from 1 t/km^2/year to 2532 t/km^2/year. Approximately 60% of the area has low to moderate erosion. The northern part of the Tumbaro River and the upper middle part of the sub-basin are the most vulnerable to increased erosion rates.

Keywords: soil erosion, maximum daily rainfall, RUSLE, Tumbaro basin.

1 INTRODUCTION

Soil is very important natural resources in the perpetuation of human life as the natural environment upon which agriculture, but it's exposed in many regions of the world to the problem of erosion (Buringh, 1960). There is a closed relationship between rainfall an erosion in terms of increases and decreases of rate erosion through rain data. The water erosion is caused by surface water runoff or collision of rain drops of the soil (Helmut & Anson, 1984). The rain is the main cause of water erosion (Elaheh et al., 2011). The average soil erosion by water is estimated to exceed 2000 t/km^2/y with this type of erosion mainly occurring on croplands in tropical areas (Fod and Agriculture Organization of the United Nations, 2015). In Peru, erosion problems are present in the forest region mainly due to heavy rainfall and scarce soil conservation practices. Therefore, this work proposes to estimate the loss of soil due to maximum rainfall in the sub-basin of the Tumbaro River to know the rates of erosion and contribute to the sustainable management of the sub-basin and its natural resources.

2 MATERIALS AND METHODS

We used cartographic information from the National Geographic Institute, a digital SRTM elevation model at 30m resolution and 12 available images from Sentinel 2A of the year 2019. The soil component was obtained from Soilgrids at 250m resolution. Information on maximum rainfall in 24 hours (1980 – 2007) was used from Rioja, Naranjillo, Moyobamba and Jepelacio stations. The sub-basin of the Tumbaro River is located in the San Martín region, in the province of Rioja and comprises the districts of Awajun and Miguel Pardo. It has an area of 140 km2. Its altitudinal range varies between 848 to 1762 m.a.s.l.m. with an average altitude of 982 m.a.s.l.m. Its lands in the lower part are agricultural. The equation of the RUSLE model was used, which is expressed with equation 1:

$$\mathbf{A = R \times K \times LS \times C \times P} \qquad [1]$$

Where: A is the average annual soil loss (t/ha · y); R is the erosivity factor of rainfall (MJ · mm / ha · hr · year); K is the soil erodability factor (t ·hr/MJ·mm); LS is the topographic (dimensionless) factor; C is the crop management factor (dimensionless); and P is the supporting (dimensionless) practice factor. The maximum rainfall in different return periods (RP) was estimated using the Gumbel distribution and regional hydrological modelling. The erosivity factor was calculated using the equation proposed by Arnoldus (1980) and Foster G.R., Wischmeier W.H. (1974). The factor C was determined from the NDVI of the sentinel images. The LS factor by Moore and Nieber (1991). The K factor using soildgrid data, as conservation practices were not identified, was considered 1. The processing was carried out in Google Earth Engine and QGIS. The reduction of scale to 30 meters of pixel was carried out in SAGA GIS.

3 RESULTS

The erosivity factor (5years RP) varied between 65.58 to 261.90 MJ.mm/ha.h.año and mean of 200.67 (MJ.mm/ha.h.año) for RP 10, 15 and 20 years were 222.23, 265.46 and 298.18 MJ.mm/ha.h.año respectively.

ISBN: 978-90-824846-7-0

K factor varied between 0.015 to 0.017. Factor C ranged from 0.07 to 0.46. LS factor varied between 0.03 to 159.05. Figure 1 shows the loss of soil due to maximum rainfall for 5 years of return time in the sub-basin of the Tumbaro River. In that sense the values vary between 1 t/km^2/y to 2532 t/km^2/y. The average erosion in the sub-basin was 56 t/km^2/y. For RP 10, 15 and 20 years the average annual erosion in the basin was 0.62, 0.75 and 0.90 t/ha/year equivalent to 62, 75 and 90 t/km^2/year.

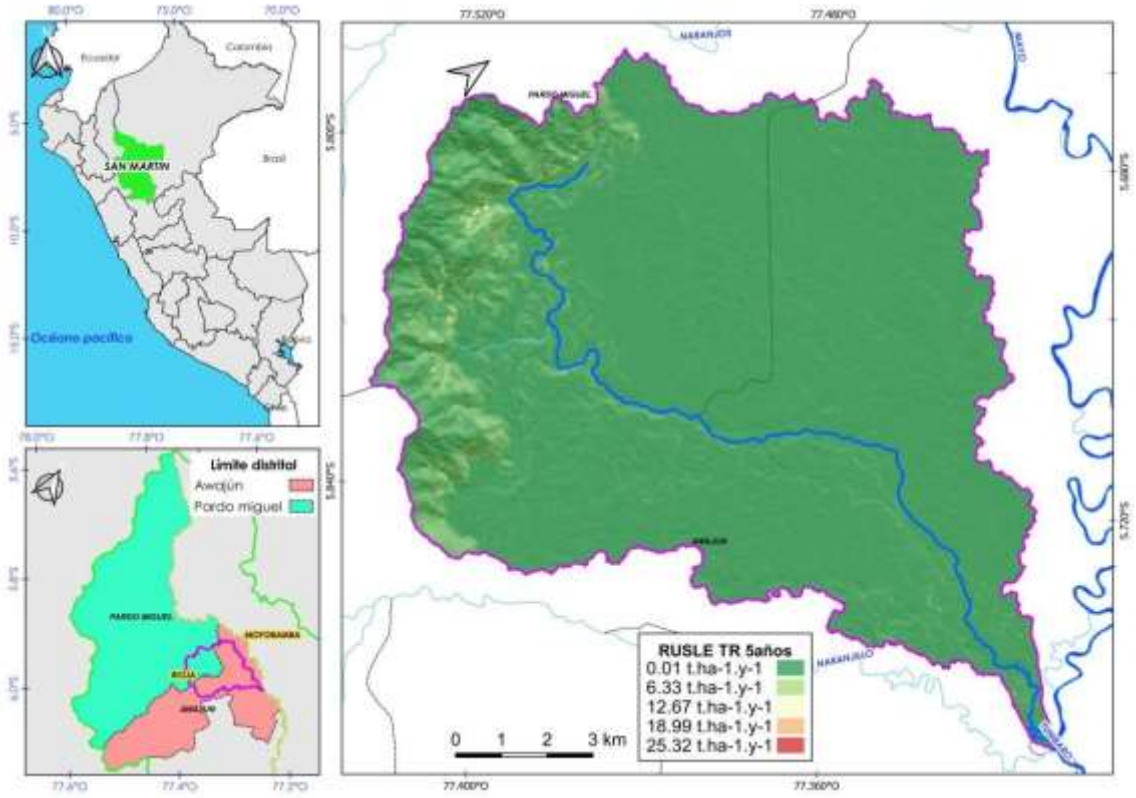

Figure 1 Soil erosion by 5 years return period of Tumbaro basin.

According to (Rosas & Guitierrez, 2020) there is an urgency and challenges to quantify soil erosion rates in developing countries. In this sense, this work adds to the efforts to quantify erosion in different regions of Peru.

4 CONCLUSIONS

The RUSLE model was successfully applied in the estimation and mapping of water erosion in the Tumbaro sub-basin. Finally, the authors mentioned that this work can contribute to local governments and organizations to improve their decision-making on the sustainable management of the sub-basin and its natural resources and with water resources management.

REFERENCES

Arnoldus, H. (1980). Una Aproximación del Factor de Lluvias en la Ecuación Universal de Pérdida de Suelo.

Buringh, P. (1960). Soils and Soil Condition in Iraq. Baghdad: Ministry of Agriculture.

Elaheh, M., Davood, N., Hossein, M., & Ebrahim, P. (2011). Investigating Rainfall Erosivity Indices in Arid and Emiarid Climates of Iran. *Journal of Hydrology*, 30-48.

Fod and Agriculture Organization of the United Nations (2015). Soil Change: Impacts and Responses. Rome, Italy: FAO.

Foster G.R; Wischmeier W.H. (1974) Evaluating irregular slopes for soil loss prediction. Transactions of the ASAE, 17: 305 – 309.

Helmut, K., & Anson, B. (1984). Soil Conservation. Mosul: Faculty of Agriculture and Forestry, Mosul University.

Moore, I., & Nieber, J. (1991). Landscape assessment of soil erosion and nonpoint source pollution. Minnesota Acad, 18-25.

Rosas, M., & Gutierrez, R. (2020). Assessing soil erosion risk at national scale in developing countries: The technical challenges, a proposed methodology, and a case history. Science of Total Enviroment, 703, 135474. doi:10.1016/j.scitotenv.2019.135474

ISBN: 978-90-824846-7-0

Proceedings of the 2nd IAHR
Young Professionals Congress
30 Nov-2 Dec. 2021

Adaptation strategies for rice cultivation under climate change in the Northern Malaysia

Y.W. Mok[1], Z. Zulkafli[1] and N. Raffar[1]

[1]Department of Civil Engineering, Faculty of Engineering, Universiti Putra Malaysia, 43400 UPM Serdang, Malaysia
e-mail: gs58415@student.upm.edu.my; zeddiyana@upm.edu.my; anaraffar@gmail.com

ABSTRACT

This study assessed the potential impacts of climate change from the baseline period (1986-2005) to the future period (2015-2095) in the Muda Irrigation Scheme area, Malaysia. The Soil and Water Assessment Tool (SWAT) was used to project streamflow and rice yield production in response to the MPI-ESM REMO15 RCP 8.5 future climate scenario. Our results indicated 5.6% (off season) and 10.2% (main season) decreases in yield. Nevertheless, the yield reduction in yield could be mitigated by delayed planting in the off-season and early planting in the main season. In contrast, increased irrigation only slightly improved yield.

Keywords: climate change adaptation; SWAT; planting dates; irrigation; rice production.

1 INTRODUCTION

Rice is the primary staple food in Malaysia, with 70% of the nation's requirements produced locally (Che Omar et al., 2019). Climate change could pose a severe threat to national food security by aggravating the problems of insufficient supply and higher costs (IPCC, 2014). Regional climate modelling projected warming and a decrease of mean rainfall in the northern region of Peninsular Malaysia (Tangang et al., 2020). Potential adaptation strategies like shifting planting dates could mitigate the negative impact of climate change, by securing suitable temperatures during critical growth stages of the rice crop. A modelling study (Azdawiyah et al., 2014) using Decision Support System for Agrotechnology Transfer (DSSAT 4.5) revealed that shifting planting dates could increase rice production in the MADA area. Besides, temperature increase with a reduction in precipitation could affect irrigation supply (Ismail et al., 2020). Irrigation water requirement at Pedu-Muda reservoir for paddy cultivation has been projected to decrease slightly from 2010 to 2099 due to the increased rainfall in the future (Tukimat & Harun, 2012). Neither of the above studies has comparatively evaluated the impact of these possible adaptation measures in improving rice yield under climate change. This study will investigate shifting planting dates in conjunction with adjusting irrigation schedules to improve rice production. The objectives of this study are (1) to calibrate and validate SWAT model based on streamflow and rice yield data; (2) to quantify the changes in rice production under climate change scenario; and (3) to evaluate shifting planting dates and adjusting irrigation schedules to offset the climate change impact on rice production.

2 MATERIALS AND METHODS

2.1 Study area and climate data

The Muda Irrigation Scheme area is located in the northwest region of Peninsular Malaysia with a total land area of 1006.85 km^2 (Figure 1). About 77% of the scheme is utilized as the rice cultivation area with a double-cropping system, also known as the largest rice cultivation area in Malaysia. The climate of the region is tropical with a mean annual precipitation of 2,072 mm. The main water resources for paddy cultivation depend on direct rainfall, river flows, and irrigation supply from Muda and Pedu dam. Baseline (1986-2005) and future projections (2015-2095) were analyzed by temporal periods of 20 years. The projection data were extracted from the outputs of MPI-ESM REMO15 RCP 8.5 scenario. These were bias-corrected using linear scaling at ground based observations. Dam daily outflow data, streamflow data, historical data of rice phenology, yields and management practices are collected from MADA.

ISBN: 978-90-824846-7-0

Figure 1: Calibration of SWAT over the study area

2.2 Model setup and adaptation strategies

SWAT model is calibrated, validated, and evaluated to simulate rice yield in Region 2 with and without adaptation. Three different planting dates: (1) actual planting dates on Season 1 and Season 2 – baseline, (2) advanced planting by two weeks; and (3) delaying the planting date by two weeks. Three scenarios will be proposed to adjust the supplemental irrigation: (1) current practices of irrigation - baseline (2) irrigation supplementary increased by 20%; and (3) irrigation supplementary increased by 40%. The methodological flowchart of the study is shown in Figure 2.

Figure 2: Schematic description of a modelling approach

3 RESULT AND DISCUSSIONS

The projection of rice yield with the future periods suggest that rice cultivated in main season (Season 2) are expected to decrease in the range of 2.35 to 10.23%. Projected rice yield in the off-season (Season 1) shows a minor increase from early century to mid century, and a substantial decrease in the late century. Under the baseline climate, rice yield increases by 5.5 to 12.2% by shifting the transplanting date by + 14 days. This suggests that a late transplanting strategy can mitigate the effects of climate change on yield. The results also suggest that supplementary irrigation up to 40% can increase the rice yield; however the effects are limited (0.03-4.73%).

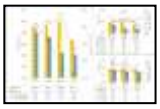

Figure 3: Projected change in rice yield

4 CONCLUSIONS

This study examines the rice yield production along with an evaluation of adaptation measures to overcome the projected impact of climate change in the Muda irrigation scheme. Future works can investigate the effects of maximizing irrigation supply, while maintaining environmental flow in the river.

REFERENCES

Azdawiyah, A. T. S., Zabawi, A. G. M., Hariz, A. R. M., Fairuz, M. S. M., Fauzi, J., Faisal, M. S. M. S., Azdawiyah, S., Zabawi, M., Hariz, M., Fairuz, M. S. M., & Faisal, M. S. M. S. (2014). Simulating Climate Change Impact on Rice Yield in Malaysia Using DSSAT 4.5: Shifting Planting Date as an Adaptation Strategy. *Nahrim*, *August*, 115–126. journalarticle.ukm.my/7292/1/43_1_09.pd

Che Omar, S., Shaharudin, A., & Tumin, S. A. (2019). The Status of the Paddy and Rice Industry in Malaysia. In *Khazanah Research Institute*. http://www.krinstitute.org/assets/contentMS/img/template/editor/20190409_RiceReport_Full Report_Final.pdf

IPCC. (2014). Intergovernmental Panel on Climate Change working group II. Climate Change 2014: Impacts, Adaptation, and Vulnerability. Part B: Regional Aspects, Polar regions. *Cambridge University Press, New York*.

Ismail, H., Kamal, M. R., Abdullah, A. F. b., Jada, D. T., & Hin, L. S. (2020). Modeling Future Streamflow for Adaptive Water Allocation under Climate Change for the Tanjung Karang Rice Irrigation Scheme Malaysia. *Applied Sciences 2020, Vol. 10, Page 4885*, *10*(14), 4885. https://doi.org/10.3390/APP10144885

Tangang, F., Chung, J. X., Juneng, L., Supari, Salimun, E., Ngai, S. T., Jamaluddin, A. F., Mohd, M. S. F., Cruz, F., Narisma, G., Santisirisomboon, J., Ngo-Duc, T., Van Tan, P., Singhruck, P., Gunawan, D., Aldrian, E., Sopaheluwakan, A., Grigory, N., Remedio, A. R. C., … Kumar, P. (2020). Projected future changes in rainfall in Southeast Asia based on CORDEX–SEA multi-model simulations. *Climate Dynamics*, *55*(5–6), 1247–1267. https://doi.org/10.1007/s00382-020-05322-2

Tukimat, N. N. A., & Harun, S. (2012). Comparative Methods in Measuring the Irrigation Water Needs at Muda Irrigation Scheme, Kedah. *Undefined*.

ISBN: 978-90-824846-7-0

IAHR YPN

Young Professionals Network

Hosted by
Spain Water and IWHR, China

IAHR AIRH

International Association for Hydro-Environment Engineering and Research

Hosted by
Spain Water and IWHR, China

Flood Risk Management

Proceedings of the 2nd IAHR
Young Professionals Congress
30 Nov-2 Dec. 2021

Effectiveness assessment of a flood retention lake in response to various floods

Haochen Yan [1] and Mingfu Guan [2]

[1] PhD Candidate, Department of Civil Engineering, The University of Hong Kong, Hong Kong, China,
Email: yanhch@connect.hku.hk
[2] Assistant Professor, Department of Civil Engineering, The University of Hong Kong, Hong Kong, China,
Email: mfguan@hku.hk

ABSTRACT

The recently constructed flood retention lake (RL) in the upper Shenzhen River is a typical application of Blue-Green Infrastructure in a subtropical rural-urban catchment. Yet, the performance of an RL of such kind in response to various flood frequencies has not been investigated systematically. In this study, the effectiveness of the RL during different flood events is assessed by (i) performing frequency analysis for event design and (ii) conducting hydrodynamic modeling for contrastive analysis. Preliminary results show that the RL effectively damps the peak discharge and delays the peak time particularly for small to moderate flood events (return period < 20 years). Contrary to the effect of RL, the contribution of floodplain to the damping of flood peak increases steadily with flood frequency.

Keywords: Blue-Green Infrastructure; flood retention lake; frequency analysis; hydrodynamic modeling.

1 INTRODUCTION

With growing urbanization and intensifying weather extremes in recent years, many rural-urban catchments are placed in the face of low flood protection standards and high flood risk. Numerous Blue-Green Infrastructures (BGIs) for stormwater regulation are emerging around the world, which are designed to improve social resilience by moderating the potential climate impact while keeping environmental sustainability. One type of BGIs, flood retention lakes/ponds (RL), are widely applied due to their effects in improving water quality as well as flood mitigation (Ayalew et al., 2015). In small rural-urban catchments under subtropical coastal environments, heavy rainfalls associated with typhoons may generate flash floods in the steep headwaters, whose peaks converge to the downstream river within few hours and result in significant flood risk. RLs thus can attenuate the flow magnitude and disperse the peaks downstream, and a typical application recently can be found in one of the upstream reaches of the Shenzhen River, the boundary river between Shenzhen and Hong Kong (ERM Hong Kong, 2010). The current study aims to carry out a systematic assessment of the effectiveness of the RL in response to various flood frequencies by numerical experiments.

2 MATERIALS AND METHODOLOGY

2.1 Study site and Data

The upstream section of Shenzhen River near Liantang / Heung Yuen Wai Boundary Control Point is concerned in this study, which was initially narrow and winding with some collapsed embankment. To upgrade the flood protection standard, the Stage 4 regulation project has been conducted recently, including river modification (a total of about 4.5 km) and an RL in the midstream (ERM Hong Kong, 2010). The hydrologic and topologic data are provided by the Shenzhen River Regulation Office of the Shenzhen Municipal Government. Water stage and runoff data in 2018-2020 are obtained from the Liantang station (Lat 22°33'30.88"N, Long 114°9'29.05"E); the digital elevation model is transferred from point survey with a 1 m resolution.

2.2 Frequency analysis

Frequency analysis is first conducted for the design of input flood events. The Peak-Over-Threshold method is applied to the processed runoff data and 40 events are identified to have peak flow rates above 97% percentile (corresponding 7.1 m^3/s). Various probability distribution models are fitted against peak flow rates of the events; goodness-of-fit is inspected by the Anderson-Darling test and also the Chi-Square test.

ISBN: 978-90-824846-7-0

2.3 Hydrodynamic modeling

Full 2D shallow water equations driven by HEC-RAS 6.0 are applied to model the hydrodynamic process of flood events in the studied basin. The computational meshes have a 2 m resolution in the main channel and the RL and 5 m in the floodplain. In each simulation scenario, sufficient time with a base flow input to reach a steady wetted condition is guaranteed before the flood.

3 PRELIMINARY RESULTS AND FUTURE WORK

The approximation of extreme event size beyond data coverage varies considerably among different probability models. Although both well represent smaller events, in the extrapolation range, the Weibull curve tends to underestimate while the Log P-3 curve tends to overestimate the event size. Results show that the RL is able to take effect as long as the runoff exceeds 51 m^3/s, corresponding to a 1.3-year event. The sizes of larger events are determined jointly by both models to reduce bias, specifically, 5-year, 10-year, and 20-year flood events with peak flow rates of 108 m^3/s, 140 m^3/s, and 184 m^3/s, respectively, are used. It is clear from Fig.1 that the RL effectively damps the peak flow rate and can also delay the peak time. Albeit not fully presented in the figure, the area of maximum inundation in the cases without the RL is also larger than the cases with the RL particularly for the Hong Kong side (right-hand side). However, the effectiveness of the RL decreases with increasing event size. From 5-year to 20-year return periods, the flood peak at the downstream boundary is reduced by 14.2%, 6.3%, and 2.3%, respectively. In contrast, the damping induced by the floodplain sees a slight and steady increase (4.6%, 5%, 5.5%, respectively). In addition, while the flood wave celerity is observed to be insensitive to the event size concerned, the RL retard the flood peak by about 15 min, 6 min, and 1 min for the 3 cases. Further studies will be extended to consecutive events and events with various durations.

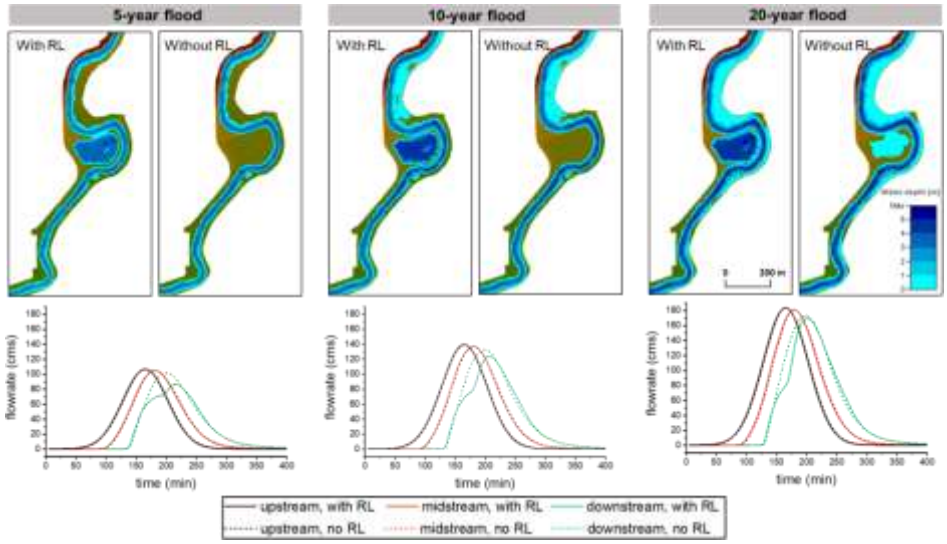

Figure 1. Inundation map and hydrograph of cases with/without the RL given different event sizes

ACKNOWLEDGEMENT

The study is financially supported by the Environment and Conservation Fund, Hong Kong (project number:108/2019).

REFERENCES

Ayalew, T. B., Krajewski, W. F., & Mantilla, R. (2015). Insights into Expected Changes in Regulated Flood Frequencies due to the Spatial Configuration of Flood Retention Ponds. *Journal of Hydrologic Engineering*, *20*(10), 04015010.

ERM Hong Kong. (2010). *Regulation of Shenzhen River Stage 4 EIA Study: Executive Summary Report (Hong Kong Side)* (p. 13).

Proceedings of the 2nd IAHR
Young Professionals Congress
30 Nov-2 Dec. 2021

Effects of anthropic changes on the propagation of the Gleno dam break wave in the Valle Camonica Floodplain

Riccardo Bonomelli[1], Gabriele Farina[2] and Marco Pilotti[3]

[1]University of Brescia, Brescia, Italy, r.bonomelli@unibs.it
[2]University of Brescia, Brescia, Italy, gabriele.farina@unibs.it
[3]University of Brescia, Brescia, Italy, marco.pilotti@unibs.it

ABSTRACT

The catastrophic flood following the Gleno dam break, which occurred in 1923, claimed the lives of about 500 people. The event has been investigated in the literature considering the 20 km long steep alpine valley separating the dam location from the hamlet of Corna. In this contribution, we investigate the propagation of the flood wave from Corna, where the computed hydrograph from previous investigation provides the upstream boundary condition, as far as the Lake Iseo outlet in Sarnico. In the middle, the flood crossed 10 km of a wide pre-alpine floodplain that has been deeply modified over the last century and 23 km of a deep lake.

Keywords: dam break wave propagation; case study; HEC RAS; shallow water; numerical simulation.

1 INTRODUCTION

A previous work on the Gleno event located in Valle di Scalve (Italy) performed by Pilotti et al. (2011) focused on the reconstruction of the dynamics and timing of the failure of the dam, as well as the propagation of the dam break wave as far as the alluvial fan of Corna. In a later work Milanesi and Pilotti (2021) investigated the dynamic interaction between the flood wave and the buildings present in the highly populated area around Corna. After devastating Corna, the flood wave with a peak higher than 2200 m^3/s (1.6 times the T_{500} discharge in the same location) and a volume of about $4*10^6$ m^3 swept a 10 km long stretch of floodplain in Valle Camonica before entering Lake Iseo at Costa Volpino. Although strongly laminated, the wave caused a swift increase of the lake level that was recorded at the lake outlet, in Sarnico, 23 km from the tributary entrance. Accordingly, a suitable modeling of the propagation of the flood in the lake provides a way to reconstruct the unknown hydrograph entering at Costa Volpino. This hydrograph can be used to crosscheck the accuracy of the simulation of the floodplain flooding of Valle Camonica, an area where very little documents attest the extent of the flood. This study highlights some interesting features of extreme floods in a mountaing region: first, it completes the historical reconstruction of the Gleno dam break, computing the extent of the flooded areas on a modified bathymetric reconstruction of 1923 Valle Camonica. Second, the same flood is propagated on the bathymetry of present time Valle Camonica. The comparison highlights the difference in terms of hazard and of risk following 100 years of anthropic pressure and river training works in this valley.

2 METHODS

The simulation has been accomplished by coupling two different 2D solver of the Shallow Water Equations: the well known HEC-RAS 2D software was used to cover the floodplain from Corna up to lake Iseo inlet, while a shock-capturing finite volume scheme was used to compute the propagation throughout the lake. As a first step, the simulation was performed on the topography derived from the LIDAR DTM surveyed in 2008-2009. A computational mesh was built with average grid size of 10 m aligned in correspondence of levees and other singularities. This first simulation dramatically showed how the propagation of the flood wave was affected by the presence of linear structures such as levees and embankments, absent in 1923 as shown by historical maps. For this purpose, the linear structures that affect the flow was removed from the 2008-2009 DTM and a second simulation was performed in order to compare the different flow hydrograph into the lake. An important fallout of the modelling effort is the reconstruction of the 1923 original bathymetry of the river in Valle Camonica, compared with the present one, affected by 100 years or river training works. The numerical scheme used to model the lake is based on the Weighted Averaged Flux (WAF) solver developed by Toro (Toro, 2001) and further adapted to account for the geometry of lake Iseo using an unstructured mesh. The scheme used retains

ISBN: 978-90-824846-7-0

shock-capturing capabilities and well-balanced properties crucial to withstand the constanly changing bathymetry of the lake as well as the unsteadiness of the hydrodynamics modelled. As an upstream boundary condition the hydrograph computed with HEC-RAS is used to impose the discharge flowing into the lake. The computed lake level variation was valided against an historical measurement of the water level change due to the Gleno event located in Sarnico.

3 RESULTS

The maximum extent of the flooding for 1923 and 2009 is shown in Figure 1. The computed map for the 1923 event well matches the only documented water mark in the flooded area. 100 years of river training has strongly reduced the extent of the flooding in the upper part of the domain; however the overall risk has soared due to the increase of exposure.

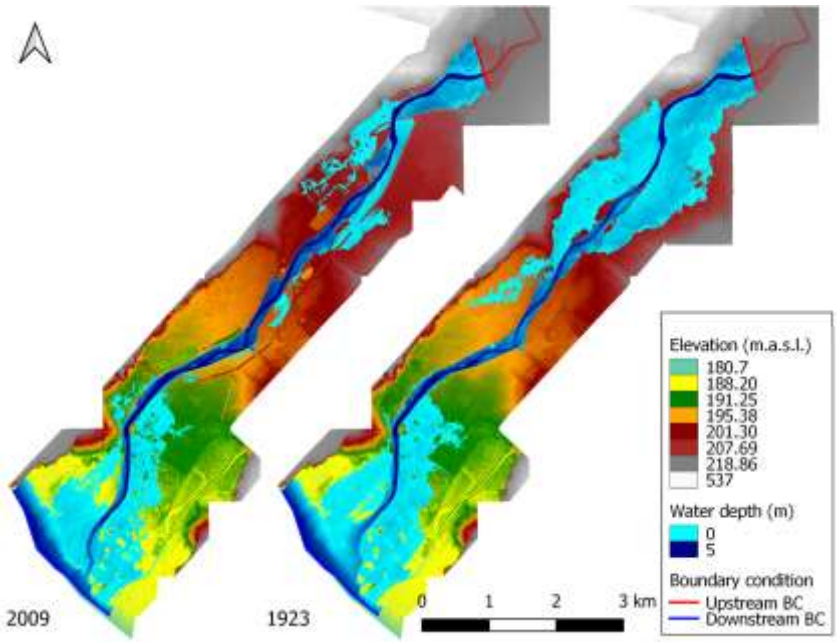

Figure 1 HEC-RAS inundation maps, 2009 bathymetry (left) 1923 bathymetry (right).

4 CONCLUSIONS

The comparison of the flood propagation using the two bathymetries highlights the consequences of systematic hydraulic works on the hazard distribution for the same event. Paradoxically the residual risk is now much higher than 100 years ago. Moreover, the simulations show that a claim of a 50 cm high bore at the inlet of the Oglio river near Sarnico is unsubstantiated by the model results and that the corresponding request of damages was based on a false statement.

REFERENCES

Milanesi, L., and Pilotti, M., (2021). Coupling Flood Propagation Modeling and Building Collapse in Flash Flood Studies, *J. Hydraulic Engrg., ASCE*, DOI: 10.1061/(ASCE)HY.1943-7900.0001941.

Pilotti, M., Maranzoni, A., Tomirotti, M., and Valerio, G. (2011). The 1923 Gleno dam-break: case study and numerical modelling, *J. Hydraulic Engrg., ASCE*, 137, 480.

Toro, E.F., (2001). *Shock-capturing methods for free surface shallow flows*, Wiley, Chicester, UK.

ISBN: 978-90-824846-7-0

Proceedings of the 2nd IAHR
Young Professionals Congress
30 Nov-2 Dec. 2021

Shallow water model with heat transfer and variable density for non-Newtonian simulations

Isabel Echeverribar [1,2], Sergio Martínez-Aranda[1], Javier Fernández-Pato[1,2], Reinaldo García[2] and Pilar García-Navarro [1]
[1] Universidad de Zaragoza, Zaragoza, Spain,
e-mail: echeverribar@unizar.es
[2] Hydronia Europe S.L., Madrid, Spain,

ABSTRACT
Non-Newtonian behavior of fluids can be assumed in many flows such as petroleum, mud flows or slurries of mining. Additionally, when considering non-homogeneous spatial distributions of the variables that directly affect the fluid density, such as particle concentration or temperature, density turns into an important variable that must be coupled with the rest of variables within the system. This work presents a 2D free surface flow model to solve the shallow water equations considering density and temperature variations, with heat transfer mechanisms for oil spill overland simulations. Results show the importance of including density within the system for oil spill simulation.

Keywords: oil flow, hear transfer, variable density, shallow water, finite volume

1 INTRODUCTION TO MODEL AND EQUATIONS

The dynamics of the system can be expressed by a continuity equation, two x- and y-momentum equations, the temperature transport equation -derived from energy equation-, and a closure equation to relate temperature with density:

$$\begin{aligned}
&(\rho h)_t + (\rho hu)_x + (\rho hu)_y = 0 \\
&(\rho hu)_t + \left(\rho hu^2 + \frac{1}{2}\rho g h^2\right)_x + (\rho huv)_y = -g\rho h(z_b)_x - \tau_{bx} \\
&(\rho hv)_t + (\rho huv)_x + \left(\rho hv^2 + \frac{1}{2}\rho g h^2\right)_y = -g\rho h(z_b)_y - \tau_{by} \\
&(hT)_t + (huT)_x + (huT)_y = S_T
\end{aligned} \qquad [1]$$

the temperature source term , $S_T = Q/(\rho C_p)$, takes into account the heat transfer with the environment, Q, and the specific heat of the fluid, C_p, as in Gordillo *et al.* 2020. The closure equation relates density and temperature, and updates also viscosity and yield stress as

$$\rho(T) = \rho_0 + K\,(T - T_0); \qquad YS(T) = 10^{(Ays\,T^2 + Bys\,T + Cys)}; \quad \mu(T) = A_\mu + \frac{B_\mu}{T} \qquad [2]$$

where parameters of the expressions come from experimental works to characterize oils. Finally, it is important to note that both, viscosity and yield stress, affect directly to friction stresses in momentum equations following a particular formulation. To compute stresses in equation [1] as a function of yield stress and viscosity of equation [2] a Simplified Bingham Model has been chosen in this case.

The system is solved by means of a finite volume first order method following the same wet/dry treatments as in Echeverribar *et al.* 2019, including the density into the solver.

2 RESULTS OF THE SIMULATIONS

Dambreak simulation

The model has been applied to a dam break test case. It has been simulated with the variable density model (DF1) and with a shallow water model that only considers temperature as a transported scalar, without including variable density inside the equations (DF2). The initial condition consists of a discontinuity on the

water depth, which can be seen on Figure 1(a). Additionally, a shifted discontinuity on temperature is also present (see also Figure 1(b)), provoking differences on water depths when variable density is considered.

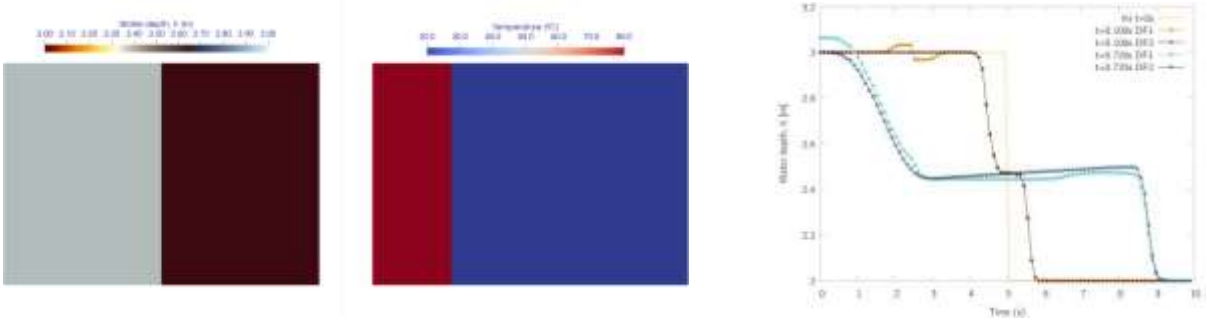

(a) (b) (c)

Figure 1: Initial condition of water depth (a) and temperature (b); and results along the longitudinal profile of water depth for different times and different models (DF1 and DF2) (c).

Figure 1(c) shows the longitudinal profiles of water depth for both models at different times. It is seen the discontinuity on *h* provoked by a discontinuity on temperature and how the dam break evolves differently for both models.

Overland oil spill

The model has been prepared to deal with wet/dry fronts to simulate overland oil spills. Arrival times of the front wave and progress speed of the flooded area can be estimated. The necessity of considering the spatial distribution of temperature, density and heat transfer is clearly demonstrated on the results. Figure 2 shows the different temperature distribution provoked by two oil sources at the same temperature (85ºC) spilled on two different environments: environment A, with no wind, normal air temperature and solar radiation; and environment B, with high wind speed, low air temperature and no solar radiation.

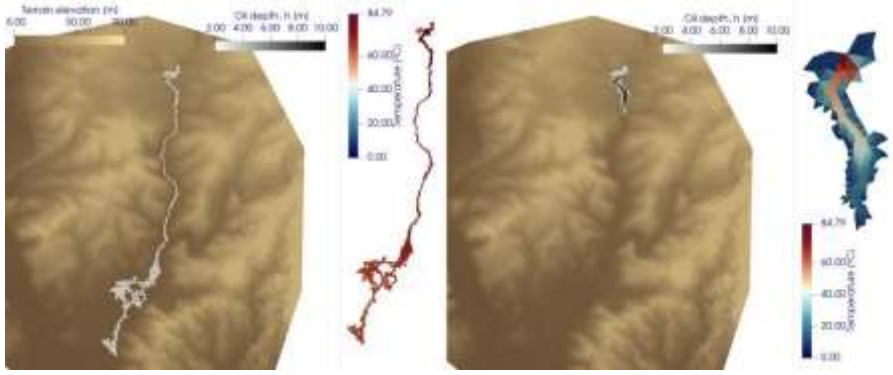

Figure 2: Flooded area and temperature at t=20 h of an overland oil spill for the same oil into environment A (left) and B (right).

In this case, the differences on the flooded area are provoked by differences on yield stress and viscosity –both influenced by temperature, which changes depending on the environment-. Colder environments provoking important heat transferences lead to high yield stress, cold oil and reduced flooded areas.

3 CONCLUSIONS

When dealing with high temperature non-newtonian flows, the treatment of density entails a difference on the results. When density is included on the numerical solver, temperature gradients provoke water depth discontinuities, leading to different results when solving realistic cases as overland oil spills.

REFERENCES

Gordillo, B.G., Morales-Hernández, M. and García-Navarro, P. (2020). Finite volume model for the simulation of 1D unsteady river flow and water quality based on the WASP. *Journal of Hydroinformatics,* 22 (2), 327-345.

Echeverribar, I., Morales-Hernández, M., Brufau, P., and García-Navarro, P. (2019). 2D numerical simulation of unsteady flows for large scale floods prediction in real time. *Advances in Water Resources,* 134, p.103444.

ISBN: 978-90-824846-7-0

Proceedings of the 2nd IAHR
Young Professionals Congress
30 Nov-2 Dec. 2021

Calibrating saturated conductivity and soil cohesion in rainfall-triggered landslides in the Langhe area (1994)

Giulia Evangelista [1], Monica Barbero [2], Ilaria Butera[3], Marta Castelli[4], Pierluigi Claps[5] and Stefania Tamea[6]
[1,3,5,6] Politecnico di Torino, Department of Environment, Land and Infrastructure Engineering, Torino, Italy,
giulia.evangelista@polito.it
[2,4] Politecnico di Torino, Department of Structural, Geotechnical and Building Engineering, Torino, Italy,
monica.barbero@polito.it

ABSTRACT

In this work we have analyzed a “cold case”, i.e., the prolonged rainfall and flood event occurred in the Piedmont region (Northern Italy) in November 1994, causing several hundred of shallow landslides. The research aim is to put some focus on the possibility to calibrate soil parameters by means of the combined use of a simple hydrological model (Rosso et al. 2006) and post-event geotechnical surveys. For this purpose, a database of geometries and soil characteristics for 238 observed landslides has been used. To address the calibration of the cohesion and hydraulic conductivity parameters, the safety factor expression from the Limit Equilibrium Analysis has been targeted to assume a maximum value of 1 for all the slopes made unstable by the actual (measured) rainfall. Significant reduction of the cohesion parameter was observed after calibration, suggesting caution in the use of literature values, typically obtained on mechanically undisturbed soil samples**.**

Keywords: shallow landslides; rainfall; calibration.

1 INTRODUCTION

Landslides are crucial contributors to sediment production, which is a key topic as part of river systems management strategies. Knowing the mechanical and hydraulic triggering conditions is therefore a fundamental target.
In this context, the hundreds of shallow landslides which occurred in the Piedmont Langhe area in November 1994 were investigated, still identified among the most sever events in the last 30 years in Italy, both in terms of economic damages and human lives.
The aim of this work is to put some focus on the possibility to obtain calibrated parameters (i.e., the saturated permeability and cohesion values), in order to overcome the uncertainty in the determination of soil parameters generally linked to the use of physically based models.

2 METHODS

To achieve the above-mentioned goals, a simple model was preferred (Rosso et al., 2006), since it allowed a better check on the sensitivity of soil parameter values to the instability condition, under the assumption that these were the main sources of uncertainty.
On the one hand, the saturated permeability value calibration was carried out by

$$h = \frac{a\,p}{b\,k\,sin\theta}\ [1 - \exp\,(-\frac{k\,bsin\theta}{a}\ t)] \qquad [1]$$

with h denoting the water table depth, a/b the specific drainage area, p the rainfall intensity, k the saturated permeability, θ the slope angle and t the rainfall duration.
An interval of variation of *k* values was obtained, the upper limit of which referred to the so-called *bucket model.* Under the assumption that only an aliquot of the precipitation infiltered during the event, by means of the proportional flow method ψ, a lower permeability value was derived, consistently with the real dynamics of the processes.
Soil cohesion *c*, on the other hand, was calibrated by mechanical analysis based on the infinite slope theory, by targeting SF to assume the value 1, according to Eq. 2.

ISBN: 978-90-824846-7-0

$$SF = \frac{c + [(1 - \frac{h}{z})\gamma + \frac{h}{z}\gamma'] z \cos^2\theta \tan\varphi}{[(1 - \frac{h}{z})\gamma + \frac{h}{z}\gamma_{sat}] z \, sen\theta \cos\theta} \quad [2]$$

where z is the soil depth, φ is the internal friction angle, γ is the average bulk unit weight of soil above the groundwater level, γsat is the saturated unit weight of soil under the groundwater level and γ' is the submerged unit weight of soil.
The analysis was conducted on a small number of cases carefully selected from regional database of 238 observed landslides, for which well-documented geometries and geotechnical parameters are available (Figure 1). The comparison between locally calibrated cohesion and permeability and the reference ones found in the database shows some differences; in particular, in several cases, safety factors quite lower than 1 have been derived, compared to those obtained using the published parameter values.

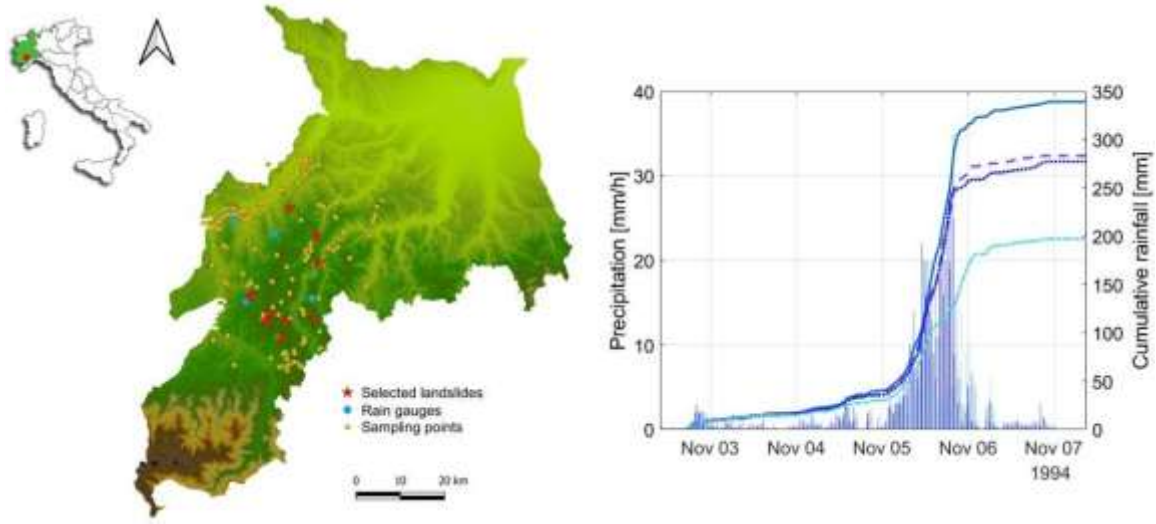

Figure 1. Overview of the area of interest (left panel) and actual rainfall measured during the November 1994 event (right panel).

3 CONCLUSIONS

The possibility of getting reliable soil parameters to be used in physically based modelling of shallow landslides is a complex task. Here we use a calibration method for obtaining meaningful saturated hydraulic conductivity and cohesion values, compatible with the observed instabilities. A simple hydrological framework and starting values from a geotechnical database were combined.
The procedure was applied in the Langhe Area (Northern Italy) where, with reference to the 1994 event, 238 landslides have been characterized, with the attribution of standard values for the variables of interest.
Analysing a limited (5%) number of carefully examined landslides, we targeted safety factors equal or less than 1, obtained recalibrated values for *c* and *k*. Coherent values of cohesion demonstrate to be lower than the published ones. In this regard, it should be pointed out that the calibration procedure allowed us to characterize shallow soils, made up of remolded and often vegetated soil, while the regional dataset provided information on undisturbed soil samples, typically collected at depths greater than those of interest.
The implications of these differences will lay the foundations for subsequent investigations.

REFERENCES

Rosso, R., Rulli, M.C., Vannucchi, G. (2006). A physically based model for the hydrologic control on shallow landsliding. *Water Resour. Res*., 42, W06410.

ISBN: 978-90-824846-7-0

Proceedings of the 2nd IAHR
Young Professionals Congress
30 Nov-2 Dec. 2021

Susceptibility assessment of Debris Flow in Southwest of the Rimac River Basin using Artificial Neural Networks

Cesar Sanchez [1], Jeancarlo Escalante [2] and David Gonzalez [3]
[1,2] National University of Engineering, Lima, Peru,
email: csanchezo@uni.pe [1], jescalantep@uni.pe [2]
[1,2,3] Institute for the Mitigation of the Effects of El Niño Phenomenon (IMEFEN), Lima, Peru,
[3] Technological University of Peru, Lima, Peru, email
email: 1625678@utp.edu.pe

ABSTRACT

Debris flows represent one of the most catastrophic natural hazards in Peru, leading to great consequences on the economy and human life. In this research to establish a suitable risk assessment and prevent the effects of this phenomena, a debris flow susceptibility map (DBS) has been developed using an artificial neural network (ANN) model based on seven causative factors: elevation, slope, slope aspect, NDVI, precipitation, and land cover. Moreover, the debris flow inventory map was compiled between 1986-2018 from previous episodes, as a result, a total of 127 events were identified and randomly divided into a training dataset of 70% and 30% for validation dataset. Finally, the DBS has been validated by the area under the receiver operatic characteristic curve (AUC) with a prediction accuracy of 82.3 %. The ANN model employed in this study proves to be effective and agile criteria for future hazard assessment of debris flow.

Keywords: Debris flows, susceptibility mapping, artificial neural network, GIS.

1 INTRODUCTION

Debris flows are one of the most frequent natural hazards in mountain regions of Peru, usually involves a mixture between solid particles, organic matter, and water that travels down gullies by the action of gravity (Wang et al., 2013). These events are responsible for the significant destruction of properties, casualties, and extensive economic losses. Therefore, the zoning of debris flow susceptibility is essential to reduce the impact of disasters and allow strategies to create preventive measures. The assessment of debris flow susceptibility refers to the uncertainty of the spatial occurrence of debris flows in a certain area, which is based on the relation between conditioning factors and the identification of debris flow-prone areas. This study aims to model the susceptibility of debris flows by applying an ANN based on previous work (Chen et al., 2020).

2 METHODS AND RESULTS

The ANN is a quantitative method thar makes use of nonlinear and complex learning and prediction algorithms to extract the complex relationships among the various independent variables (Youssef & Pourghasemi, 2021). The predicted $Cell_i$ in the ANN indicates the expected degree of for each terrain pixel, and higher cell values represent more susceptibility. In ANNs, the input (x_i), hidden (y_j), and output (Z_k) layers can be expressed as

$$y_j = f(X_j) = f\left(w_{oj} + \sum_{i=1}^{I} w_{ij} x_i\right) \quad [1]$$

$$Z_k = f(Y_k) = f\left(w_{ok} + \sum_{j=1}^{J} w_{jk} y_j\right) \quad [2]$$

$$\text{For layer } l \text{ in the } y^{(l)}: \quad y_j^{(l)} = \sum_{i=0}^{p} \left(y_i^{l-1}(t) w_{ji}^{l}(t)\right) \quad [3]$$

where, w_{oj} and w_{ok} are the bias weights for setting the threshold values. X_j and Y_k represent temporary results before using the activation function, f, which should be applied in the hidden and output layers. To adjust the weight, the error between the input-hidden and hidden-output layers is derived by applying the stochastic gradient descent and the cross-entropy error.
Besides, geographic information system (GIS) was applied to create maps of impact factors (slope gradient, slope aspect, precipitation, NDVI, geology, and land cover) and debris-flow inventory map, then the debris-flow susceptibility assessment was performed using the artificial neural network model with neuralnet (nn) package from R (Figure 1.b).

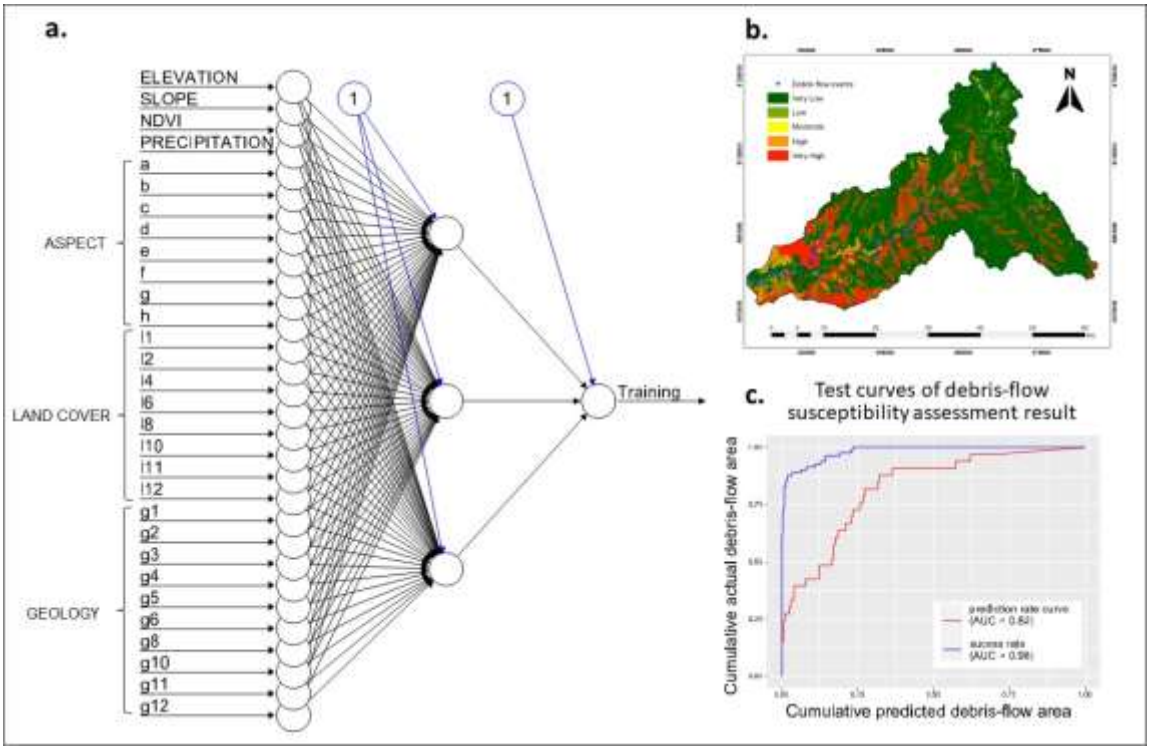

Figure 1. (a) The structure of the optimized model, (b) Debris-flow susceptibility map and (c) ROC curves of the model.

Finally, the area under the curve (AUC), which assesses the goodness of fit between the actual debris flow and the prediction model, worked out at 0.82 with the test dataset.

3 CONCLUSIONS

It is found that the most important components in debris flow susceptibility modeling using the artificial neural network model are elevation, precipitation, and land cover. The performance of the model was evaluated by the ROC curve, results indicated that the model performance is high with AUC value of 82.27% in debris flow prediction. The susceptibility map shows that more than 50% of the population centers in the Rimac river basin are in a very high susceptibility zone.

REFERENCES

Chen, Y., Qin, S., Qiao, S., Dou, Q., Che, W., Su, G., Yao, J., & Nnanwuba, U. E. (2020). Spatial predictions of debris flow susceptibility mapping using convolutional neural networks in Jilin province, China. *Water (Switzerland)*, *12*(8). https://doi.org/10.3390/W12082079

Wang, Z.-Y., Lee, J. H., & Melching, C. S. (2013). River Dynamics and Integrated River Management. En *Journal of Chemical Information and Modeling* (Vol. 53, Número 9).

Youssef, A. M., & Pourghasemi, H. R. (2021). Landslide susceptibility mapping using machine learning algorithms and comparison of their performance at Abha Basin, Asir Region, Saudi Arabia. *Geoscience Frontiers*, *12*(2), 639–655. https://doi.org/10.1016/j.gsf.2020.05.010

ISBN: 978-90-824846-7-0

Proceedings of the 2nd IAHR
Young Professionals Congress
30 Nov-2 Dec. 2021

River driftwood as a resource for batteries material production

Julie Michel [1,2], Abdullah F. Qatarneh [1], Capucine Dupont [1], Loïc Simonin [2], Hervé Piégeay [3], Virginia Ruiz-Villanueva [4] and Mario Franca [5]
[1] IHE Delft, Delft, Netherlands
[2] CEA/LITEN/DEHT, Université Grenoble Alpes, Grenoble, France
[3] University of Lyon, Lyon, France
[4] University of Lausanne, Lausanne, Switzerland
[5] Delft University of Technology, Delft, Netherlands
e-mail: julie.michel@cea.fr

ABSTRACT

Driftwood is removed from dams and rivers for safety reasons, most of the time it is just seen as waste. A promising alternative to replace fossil graphite in batteries is hard carbon that can be obtained from biomass. An interesting valorization is to use driftwood as starting material for electrode. Hydrothermal carbonization is a thermal treatment that avoids drying the material before use, which is very interesting for wet materials. This study works on the influence of the driftwood genera as starting material for electrode on electrochemical performances of a Na-ion cell. The batteries obtained have very good performances, similar to graphite. It was reported that only one material, the bark, has lower performances due to its higher ash content. Driftwood is a very promising material, and there is no need to separate the genera.

Keywords: river driftwood, energy storage, Na-ion battery, hydrothermal carbonization, circular economy

1 INTRODUCTION

Driftwood is accumulating in dams and rivers and affects geomorphology and ecology of the river positively. They impact the dynamics of particulate organic matter storage, aquatic life and bedload transport in rivers (Gurnell et al., 2002), at the same time it increases flood destructive effect and structure damages (Lagasse et al., 2010; Parola et al., 2000). For safety reasons, they are removed and stored, and often combusted or landfilled (Bartocci et al., 2017).
Sodium batteries are a promising technology to replace Li-ion batteries in energy storage applications. The most suitable material for negative electrode is hard carbon, which can be obtained from wet biomass, such as driftwood. Hydrothermal carbonisation (HTC) is an autogenous pressure thermic treatment in which the sample is immersed in water. With this method, there is no need to dry the biomass before processing. Furthermore, during the process, inorganics, which are an obstacle to electrochemical properties in hard-carbon (Saavedra Rios, 2020), tend to leach in the liquid phase.
The objective of this work is to evaluate the potential of driftwood as raw material for Na-ion batteries. This study focuses on the influence of the driftwood genera first on the HTC product, and then on the electrochemical properties of the final electrode.

2 MATERIAL & METHOD

The research is focused on the case of the Génissiat dam located on the Rhône River in France 50 km downstream from Geneva (Switzerland) and 160 km upstream from Lyon. The driftwood at Génissiat is supplied mainly during floods. It consists of wood stored within the fluvial corridor and wood recruited from bank erosion along the Rhône River and its two main tributaries; the Arve and Valserine Rivers. The woods coming from upstream of Génissiat dam from the Arve and Valserine Rivers are is blocked since the river has no overflow pathway (Benacchio et al., 2017).
Five genera were identified and studied: *conifer*, *salix*, *fraxinus*, *populus*, *alnus* and *anlus bark*. All driftwood samples were milled to 1mm and dried at 105°C.
HTC are performed in a 2 L high-pressure reactor (Parr series 4530 floor stand reactor), at 200°C during 12hrs. solid and liquid are separated by sieving (100, 45 and 20µm). Pyrolysis were performed on the hydrochars at 1400°C for 1h. Coin cells were performed adapted from Saavedra Rios (2020).
CHNS were carried out following UNI 15104:2011 standard. Ash content were determined by the remaining mass after calcination at 550°C. Inorganic composition were identified by ICP-OES (Avio 200, Perkin Elmer). The cycling tests were performed using an Arbin Instruments battery cycler adapted from Saavedra Rios (2020).

ISBN: 978-90-824846-7-0

3 RESULTS & DISCUSSION

The study shows that after the same conditions of 200°C, 12hrs, hydrochars from driftwood of *conifer*, *fraxinus*, *populus*, *salix* and *alnus* have similar properties in C content (55.4 to 57.4 %) and ash content (0.2 to 1.4 %wt dry). Only the bark-derivate hydrochar presented a higher ash content after HTC (8%wt dry) with an initial content largely superior (7.4%wt dry) to the other raw biomasses (0.7 to 2.2%wt dry).
After pyrolysis and formulation in an electrode, two parameters are analysed: the cyclability and capacity, reported in Figure 1. We can see the curves very stable among 100 cycles, with a specific capacity from 280 $mAh.g^{-1}$ (*salix*) to 290 $mAh.g^{-1}$ (*populous*), which is superior to commercial hard-carbon reference with $260mAh.g^{-1}$. It is higher than commercial hard-carbon. An exception is for *alnus bark*, with only 170 $mAh.g^{-1}$ reported, as much as a lower reversibility of 63%. This different behavior was attributed to the initial composition of the bark, with a higher ash content, rich in Si and Ca, both known to decrease electrochemical performances of a biomass-based hard carbon (Saavedra Rios, 2020). Also, the bark and the wood tend to be separated during the time spent in water, so the driftwood doesn't need debarking. Therefore, it makes driftwood a very promising material for negative electrode in sodium batteries.

4 CONCLUSION

The good cyclability, high specific capacity and high initial reversibility of these cells make driftwood a very promising precursor for negative electrode in Na-ion batteries. The similarity of the results highlights that there is no necessity to separate driftwood depending on their genera, as long as their ash contents are close. Furthermore, the bark is separated from the wood during the time spent in the water, which reduces the number of process steps.

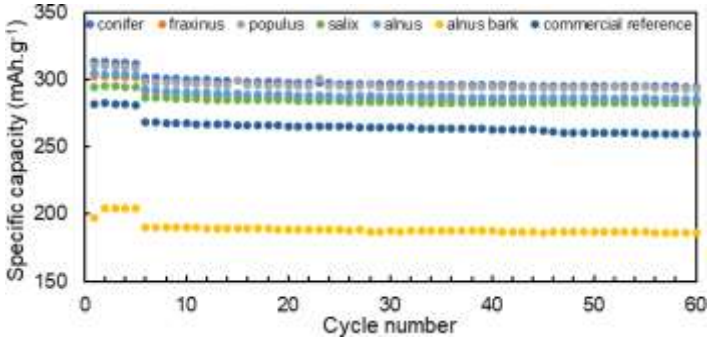

Figure 1: Stability of cycling for the different driftwood genera hard-carbon

REFERENCES

Bartocci, P., Barbanera, M., D'Amico, M., Laranci, P., Cavalaglio, G., Gelosia, M., Ingles, D., Bidini, G., Buratti, C., Cotana, F., & Fantozzi, F. (2017). Thermal degradation of driftwood: Determination of the concentration of sodium, calcium, magnesium, chlorine and sulfur containing compounds. *Waste Management (New York, N.Y.)*, *60*, 151–157. https://doi.org/10.1016/J.WASMAN.2016.08.035

Benacchio, V., Piégay, H., Buffin-Bélanger, T., & Vaudor, L. (2017). A new methodology for monitoring wood fluxes in rivers using a ground camera: Potential and limits. *Geomorphology*, *279*, 44–58. https://doi.org/10.1016/J.GEOMORPH.2016.07.019

Gurnell, A. M., Piégay, H., Swanson, F. J., & Gregory, S. V. (2002). Large wood and fluvial processes. *Freshwater Biology*, *47*(4), 601–619. https://doi.org/10.1046/J.1365-2427.2002.00916.X

Lagasse, P. F., Zevenbergen, L. W., & Clopper, P. E. (2010). *Impacts of Debris on Bridge Pier Scour*. 854–863. https://doi.org/10.1061/41147(392)85

Parola, A. C., Apelt, C. J., & Jempson, M. A. (2000). Debris Forces on Highway Bridges. *NCHRP Report*, *445*. http://trid.trb.org/view.aspx?id=674405

Saavedra Rios, C. del M. (2020). *Study of biomass-derived hard carbons for Sodium-ion battery application*. Université Grenoble-Alpes.

ISBN: 978-90-824846-7-0

Proceedings of the 2nd IAHR
Young Professionals Congress
30 Nov-2 Dec. 2021

Learnings from an observational campaign for data scarce regions

Elanchezhiyan Duraisekaran [1], Krushil Modi [2] and Balaji Narasimhan [3]
[1] Junior Research Fellow, Indian Institute of Technology - Madras, India,
ce20d088@smail.iitm.ac.in
[2] Junior Research Fellow, Indian Institute of Technology - Madras, India,
krushilmodi1996@gmail.com
[3] Professor, Indian Institute of Technology - Madras, India,
nbalaji@civil.iitm.ac.in

ABSTRACT

The decision-making process for the operation of reservoirs in data scarce regions is mostly based on heuristic judgment rather than on a scientific basis. This may lead to improper operation of the reservoir which can either lead to floods or water shortage during the lean period. To alleviate this problem, an observational campaign was undertaken to collect data on a short, flashy and ephemeral river in south India with numerous small reservoirs (tanks) in the upstream which need to be operated to avoid floods and augment the water supply for Chennai city. The campaign for field data collection during the Nivar cyclone of 2020 was undertaken with an Acoustic Doppler Velocity Profiler (ADVP) to measure the flow in the river at strategic locations to improve the understanding of the response mechanism of the river. This paper discusses the learnings from an observational campaign in the context of reservoir operation.

Keywords: Acoustic Doppler Velocity Profiler; data scarce region; observational campaign.

1 INTRODUCTION

The improvement of science in understanding of the hydrology of any given area has increased significantly from empirical equations to more physically based approaches and finally the emergence of geospatial technology. But the data acquisition process for the same has not been able to keep pace with the same. Due to this shortcoming, the modelling in data scarce regions have uncertainty which also translates to the decision making process. However, with increasing importance given to field data collection in hydrology this is being slowly alleviated. As a result, knowledge sharing of the observational campaign will be useful for improving the data collection process.

The observational campaign was undertaken during the Nivar cyclone of 2020 in the south Indian city of Chennai, Tamil Nadu with a view of improving the understanding of the hydrological response mechanism of the Adyar River, prone to floods. The region is characterized by a short, flashy and ephemeral river with numerous water-harvesting structures (colloquially referred to as tanks) in the upstream, making it unique to this region in south India. In addition, the rainfall is highly dependent on the North East Monsoon (NEM) concentrated during the last three months of the year. The urbanized catchment in the downstream only compounds the problem. In this complex hydrologic setting, the response mechanism of the catchment has not been clearly understood mainly due to the lacunae of data. The lack of temporal observational data as well as monitoring stations does not help the cause.

The need for the observational campaign arose from the point of view of operation of the numerous tanks in the upstream which needs to be operated in a scientific manner unlike the rational approach based on heuristic judgment which is being carried out now. The necessity for the operation arises from the diabolic problem of meeting the municipal water supply needs during the rest of the year and flood regulation during the monsoon season especially when the reservoir does not have a dedicated flood control zone. The lack of monitoring stations and observational data makes it difficult to operate the reservoir in an optimized manner from the perspective of flood regulation and water supply.

This paper discusses the learnings from such an observational campaign in addition to the processing of the acquired raw data to be used for modelling purpose and the importance of such data in data scarce regions to help in modelling and finally decision making process.

2 METHODOLOGY

In this background, the observational campaign was undertaken with help of the Acoustic Doppler Velocity Profiler (ADVP) to discretely measure the flow for different water level stages in the river, along with continuous

ISBN: 978-90-824846-7-0

water level measurement, at strategic locations to improve the understanding of the hydrologic response of the catchment. In order to obtain continuous water level measurement, a pressure water level logger was used.

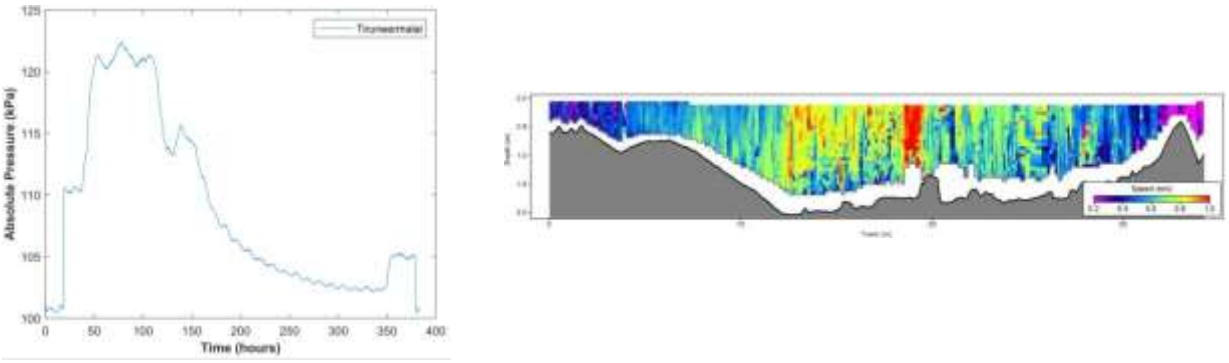

Figure 1. Absolute pressure graph (left) and the bathymetry along with velocity profile from ADVP (right)

Thus, a continuous graph of variation of pressure with respect to time is obtained (refer Fig 1.). In order to develop the rating curve, ADVP was used to measure the discharge. As the ADVP is moved from left bank to right bank along the downstream of the bridge, the depth and velocity are measured simultaneously and discharge is estimated using the velocity-area method. The values are also stored in the ADVP which can be retrieved after the completion of the campaign. Using the principle of superposition, the continuous pressure graph was matched with the measured discrete discharge values to arrive at the final hydrograph.

3 STUDY AREA

An ungauged subbasin with thickly populated city in the downstream in the south Indian state of Tamil Nadu was taken up for the study. The index map of the Adyar subbasin along with flow measurement locations is shown in Fig 2.

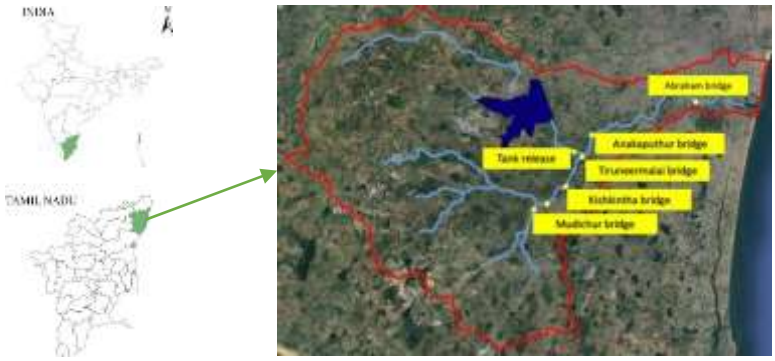

Figure 2. Index map showing Adyar subbasin with flow measurement locations

4 CONCLUSIONS

The deployment of two teams – one in the upstream and another in the downstream for data collection using ADVP during the Nivar cyclone demonstrated it is possible to temporarily change an ungauged Adyar River basin into a gauged one. In addition, when compared to the earlier scenario when calibration of the model was possible only for a reservoir, the uncontrolled catchment can now be calibrated due to the distributed hydrographs available at multiple locations. The event based intense observational campaign thus undertaken with an idea of improving the knowledge base proved to be highly effective for understanding the hydrologic response of the catchment. The critical flow data thus collected will be crucial for hydrologic and hydraulic modelling of the river basin for subsequent scenario analysis of different reservoir regulation and flood management options.

ISBN: 978-90-824846-7-0

IAHR YPN

Young Professionals Network

Hosted by
Spain Water and IWHR, China

IAHR AIRH

International Association for Hydro-Environment Engineering and Research

Hosted by
Spain Water and IWHR, China

Sustainable Development Goals & Global Water Security

Proceedings of the 2nd IAHR
Young Professionals Congress
30 Nov-2 Dec. 2021

Assessing catchment baseflow and streamflow responses to land cover dynamics using the SWAT model

Tesfaye Belay Senbeta [1] and Renata Julita Romanowicz [2]

[1,2] Institute of Geophysics Polish Academy of Sciences, Warsaw, Poland
e-mail tsenbeta@igf.edu.pl

ABSTRACT

The main objective of the study is to assess the impact of land cover dynamics (LCD) on the catchment baseflow and streamflow responses. We chose the Kamienna River, which is known for natural and man-made hazards. We studied the changes in LCD in the catchment over the last four decades from the 1980s to 2010s. The results reveal that built-up, forested area and water bodies showed an increase of 7.4%, 3.9% and 0.33% respectively, while agricultural land decreased by 11.3%. We also applied the SWAT model to assess the impact of LCD on baseflow and streamflow. The result showed that annual streamflow in the catchment decreased considerably, with the highest decreases in the 1983-1994. The responses of baseflow to LCD also showed a decrease during the study period with least decline in 2010s, indicating the existence of naturalization processes taking place in the catchment**.**

Keywords: baseflow; streamflow; land cover dynamics.

1 INTRODUCTION

The main driving factors that can have a significant impact on baseflow and streamflow are divided into two categories: natural and human activities such as land cover dynamics (LCD). These factors influence baseflow and streamflow mainly by changing the physical characteristics of the catchment and cause water problems and disturbances in the hydrological cycle by increasing or decreasing water resources in a catchment. Knowledge of the influences of the LCD on hydrological processes is used as an indicator to identify the initial determinants of change in baseflow and streamflow in response to these factors (Qiu et al., 2016). The Kamienna River in central Poland, which is known for natural and man-made hazards, including hydrological extremes, i.e., floods and droughts, was used as a case study. The specific objectives of the study include: (1) assessing historical land cover dynamics in the catchment of Kamienna River using satellite imagery and (2) assessing the response of baseflow and streamflow in the catchment to LCDs. We applied the Soil and Water Assessment Tool (SWAT), a physical catchment model based on long-term yields and processes, simulating runoff, sediment, and water transport, and using daily time steps (Arnold et al., 2012). The model was developed for the catchment using meteorological (precipitation, maximum and minimum temperature) and spatial input data (the DEM, land use map and soil map) and further used to assess scenarios concerning the LCDs impacts on baseflow and runoff processes.

2 DATA AND METHODS

The data used in this research are divided into two groups: (a) spatial data - topographic, soil and land cover types; (b) temporal data - hydrological and meteorological data. Land use maps were generated from CORINE Land Cover (CLC) and United States Geological Survey (USGS) Landsat 4 for the last four decades using QGIS and used as input for assessing the impact of LCDs on baseflow and streamflow in the catchment. Hydrometeorological variables used in the study include daily streamflow and daily meteorological variables. Hydrometeorological stations were selected considering the length of the period of record, number of missing data and quality; stations with missing data for a longer period were excluded from the analysis. In the SWAT model, the Hargreaves method was selected to estimate the potential evapotranspiration and the Soil Conservation Service (SCS) curve number to assess the catchment responses.

ISBN: 978-90-824846-7-0

3 RESULTS

The SWAT model was developed, calibrated, and validated and then used for scenario analysis to assess the impact of LCDs on baseflow and runoff response. The result showed that runoff and streamflow have changed significantly since the early 1980s, which could be due to climate variability and/or land cover dynamics within the catchment. The result from the LCD analysis showed that built-up, forested and water bodies showed an increase of 7.4%, 3.9% and 0.33%, respectively, while agricultural land decreased by 11.3% over the last four decades. The change in runoff due to climate variability is separated from land cover changes by naturalizing runoff through simulation with the SWAT model. Annual streamflow and baseflow in the catchment decreased, with the first and second highest decreases in 1983-1994 and 1994-2006, respectively (Fig. 1), compared to the baseline period (1971-2017). The decrease in runoff and baseflow compared to the increase in precipitation in recent years indicates the impact of human interventions such as reservoirs.

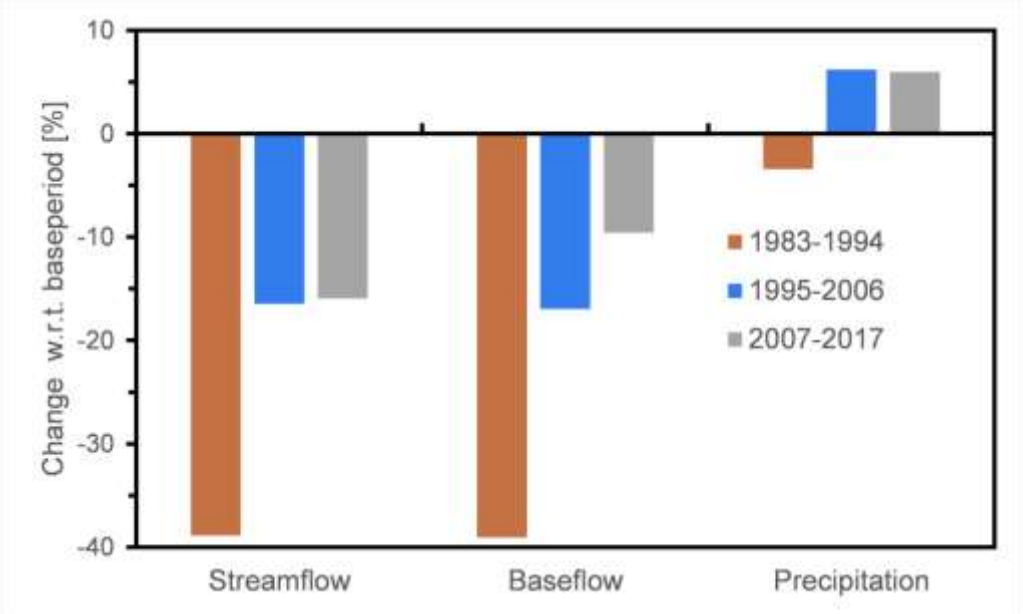

Figure 1. Change in streamflow, baseflow and precipitation in response to land cover dynamics with respect to (w.r.t) baseline period (1971-1982).

4 CONCLUSIONS

Land use and land cover change in the 1990s and 2000s is high, resulting in significant changes in baseflow and streamflow during this period. The influence of this change on baseflow is decreasing in the basin recently (2010s), which could be the long-term effects of reservoir management and afforestation.

ACKNOWLEDGEMENTS

This work was partially supported within statutory activities No 3841/E-41/S/2019 of the Ministry of Science and Higher Education of Poland and the project HUMDROUGHT (contract 2018/30/Q/ST10/00654). The hydro-meteorological data were provided by the Institute of Meteorology and Water Management (IMGW), Poland. We appreciate the cooperation and efforts of all authors in producing the proceedings.

REFERENCES

Arnold, J.G., Moriasi, D.N., Gassman, P.W., Abbaspour, K.C., White, M.J., Srinivasan, R., Santhi, C., Harmel, D., Griensven, A. van, Liew, M.W. Van, Kannan, N., & Jha, M.K. (2012). SWAT: Model Use, Calibration, and Validation. *American Society of Agricultural and Biological Engineers*, *55*(4), 1491–1508.

Qiu, L., Peng, D., Xu, Z., & Liu, W. (2016). Identification of the impacts of climate changes and human activities on runoff in the upper and middle reaches of the Heihe River basin, China. *Journal of Water and Climate Change*, *7*(1), 251–262. https://doi.org/10.2166/wcc.2015.115

Proceedings of the 2nd IAHR
Young Professionals Congress
30 Nov-2 Dec. 2021

Determination of the concentration of Total Suspended Solids in urban wastewater by means of spetrophotometry-based genetic algorithm models

Daniel Carreres-Prieto[1], Juan T.García[1], José M. Carrillo[1], Luis G. Castillo Elsitdié[1]

[1] Civil Engineering and Mining Engineering School. *Universidad Politécnica de Cartagena* (*Spain*)

daniel.carreres@upct.es, *juan.gbermejo@upct.es,* jose.carrillo@upct.es, luis.castillo@upct.es

ABSTRACT

The European Union legislation highlights the need to minimise the pollution emitted to the receiving environment due to overflows from sewer systems during rainfall episodes. Real-time information of the evolution of pollutants along the sewer system is essential to provide an early warning that helps in the operation of the wastewater treatment plants. To achieve that, the current research work has focused on the own-development of a low-cost, small-dimensions and low-consumption equipment based on a spectrophotometric analysis with LED technology in the range of 380 to 700 nm. Making use of a series of mathematical models based on genetic algorithms, the equipment is able to estimate pollutants, such as: Chemical Oxygen Demand (*COD*), Biological Oxygen Demand after 5 days (BOD_5) or Total Suspended Solids (*TSS*), among other. The equipment can analyse raw water with high concentration of *COD* and BOD_5 higher than 700mg/l and 450mg/l, respectively, and treated water.

Keywords: Total Suspended Solids (*TSS*), real time monitoring, genetic algorithms model, spectrophotometer.

1 INTRODUCTION

In this research work, a low-cost system has been developed which, by means of variable wavelength spectrophotometry, allows to carry out a characterization of water samples in a reduced time and without the need of using chemical reagents or subjecting the samples to pre-treatment. As presented in previous research works in the field of LED spectrophotometry (Carreres-Prieto et al. 2019, 2020), the system can generate a total of 81 wavelengths between 380nm and 700nm, using 33 LED diodes of fixed spectral width, without the use of diffraction gratings or monochromators, typical of equipment based on incandescent lamps. This has made it possible to develop a much smaller, more cost-effective and less energy-consuming device. Thanks to a sampling campaign carried out between June 2019 and April 2020, in the Cabezo Beaza WWTP, both at influent wastewater at the entrance of the WWTP (raw water) and at the effluent of the secondary settler, prior to the third treatment (treated water), it has been found that there is a correlation between the spectral response of the samples and the contaminant load, as shown in Figure 1, where the lower the solids concentration is, the higher the transmittance values are.

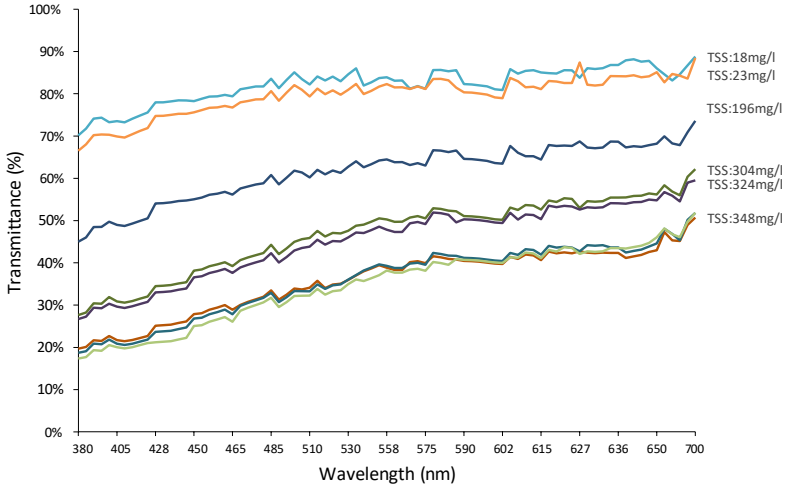

Figure 1. Relationship between spectral response and total suspended solids (TSS).

The correlation between the spectral response measured by the developed equipment and the analytical values measured in the WWTP laboratories has been achieved through the development of genetic algorithms. These learn to extract patterns from the input data, allowing better fits than other techniques such as linear regression.

ISBN: 978-90-824846-7-0

2 LOAD POLLUTION ESTIMATION MODELS

Equation (1) shows the model calculated for total suspended solids, which presents an average Pearson coefficient of 92.46% (94.70% with the training data and 90.21% with the test data), where A_x and T_x are the absorbance and transmittance values measured at x wavelength. This model was calculated from a total of 172 samples measured at the Cabezo Beaza treatment plant located in the city of Cartagena. Additional models can be seen in Carreres-Prieto et al. (2020).

$$TSS_{(mg/l)} = (((c_0 * T_{380} - c_1 * T_{521}) - \frac{c_2}{c_3 * T_{405}}) + \frac{c_4 * T_{574}}{c_5 * T_{380}} * c_6 * T_{580} \; \cancel{c_7 * T_{380}}) * c_8 + c_9 \quad [1]$$

$$c_0 = -0.1237,\ c_1 = 1.5555,\ c_2 = -6.5989,\ c_3 = -0.11876,\ c_4 = 1.4691,\ c_5 = -0.1237$$
$$c = 2.3003,\ c = -0.1237,\ c = 0.95604,\ c = -210.38$$

Although this work focuses on the estimation of total suspended solids, it is possible to extend it to other variables such as the 5-day Biochemical Oxygen Demand (BOD5), as shown in Equation (2), with an average Pearson coefficient of 94.18%.Thanks to this type of techniques, it is possible to model how the pollutant load evolves in basins and rivers in a quick and simple way, a key aspect to establish measures to control and/or mitigate its effect. Moreover, this demonstrates the suitability of the system to estimate parameters such as the presence of fecal matter in the water, from the spectral response, which makes it possible to implement measures to correct and/or mitigate the possible impacts that these waters may have on the natural environment.

$$BOD_{5\,(mg/l)} = (c_0 + c_1 * T_{585}) * (c_2 * T_{435} + c_3 * T_{585}) * \frac{c_4 + c_5 * T_{420}}{c_6 * A_{580} + c_7 * T_{585}} * c_8 + c_9 \quad [2]$$

$$c_0 = -4.8093,\ c_1 = 16.686,\ c_2 = -37.668,\ c_3 = 36.892,\ c_4 = -54.47,\ c_5 = 69.836$$
$$c_6 = -13.845,\ c_7 = 24.77,\ c_8 = -6.1496,\ c_9 = 1.754$$

The high accuracy of the model for estimating the amount of dissolved solids from the spectral response can be seen in Figure 2a, where almost all points are within ±1% of the interval of the standard deviation, both training (violet circles) and test (green triangle) data.

The model uses six variables (wavelengths): transmittance at 380, 405, 521, 560 and 574nm. However, the most relevant are 380 and 405nm, as shown in Figure 2b. Tests carried out have shown that as the wavelengths approach the infrared spectrum, the relative weight of these variables decreases significantly, as is the case at 574nm. This shows that suspended particles are much more sensitive to wavelengths closer to the violet than to others.

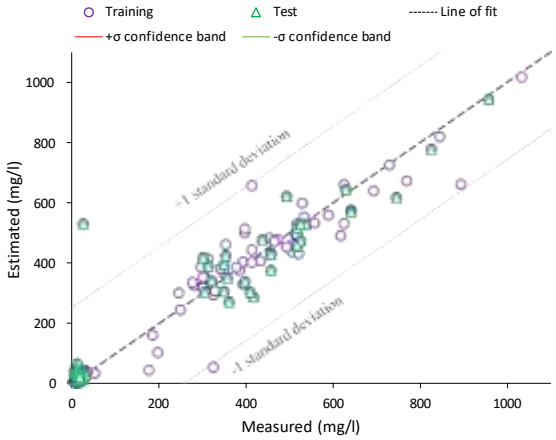

(a)

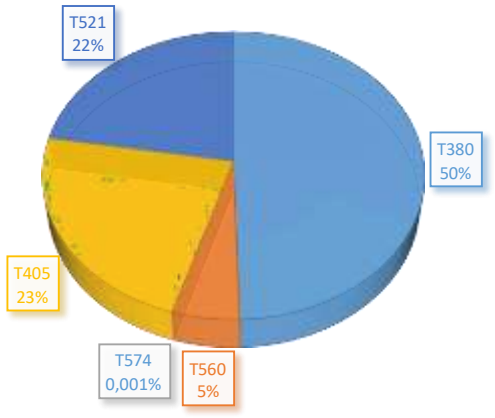

(b)

Figure 2. (a) Correlation chart between TSS values measured in the laboratory and those estimated using the model of Equation (1), based on the genetic algorithm. (b) Distribution of impact indexes of the variables used in the model of Equation (1).

REFERENCES

Carreres-Prieto, D., García, J. T., Cerdán-Cartagena, F., & Suardiaz-Muro, J. (2020). Wastewater Quality Estimation Through Spectrophotometry-Based Statistical Models. *Sensors*, *20*(19), 5631.

Carreres-Prieto, D., García, J. T., Cerdán-Cartagena, F., & Suardiaz-Muro, J. (2020). Performing Calibration of Transmittance by Single RGB-LED within the Visible Spectrum. *Sensors*, 20(12), 3492.

Carreres-Prieto, D., García, J. T., Cerdán-Cartagena, F., & Suardiaz-Muro, J. (2019). Spectroscopy Transmittance by LED Calibration. *Sensors*, 19(13), 2951.

ISBN: 978-90-824846-7-0

Proceedings of the 2nd IAHR
Young Professionals Congress
30 Nov-2 Dec. 2021

Exploratory analysis of planet data to identify HABs in Small Arizona Reservoirs

Vineeth Manthapuri [1], Rebecca L. Muenich [2] and Matthew Scholz [3]

[1] Indian Institute of Technology Madras, Chennai, India,
e-mail: ce18s006@smail.iitm.ac.in
[2,3] Arizona State University, Tempe, Arizona, United States,
e-mail: rebecca.muenich@asu.edu; Matthew.Scholz@asu.edu

ABSTRACT

Harmful algal blooms (HABs) in inland freshwaters have become ever-increasing in many parts of the world. In Saguaro Lake, a small reservoir in Central Arizona, they are becoming more intense in summer months especially. We investigated the dynamics of HABs by comparing the in-situ chlorophyll-A concentration from 2017 to 2020 and surface reflectance of the various bands and band ratios of Planetscope satellite data. The ratio of reflectance of NIR/RED bands produced a promising correlation of 62.2% to help with prediction of the presence of HABs within the lake. With the proposed algorithm, spatial maps were developed for the lake in 2020. The project outcomes provide a better understanding of algal dynamics in the lakes and the importance of Planetscope imagery in quantifying HABs, especially in small reservoirs. Results from this work can help environmental managers to control and warn the community about emergence of blooms**.**

Keywords: Harmful Algal Blooms (HABs); planet; chlorophyll-A;

1 INTRODUCTION

Harmful Algal Blooms (HABs) are the condition of uncontrolled algae growth in water bodies (Martin et al., 2021). Being a photosynthetic organism, HABs predominantly depend upon the availability of sunlight, but require nutrients like nitrogen and phosphorus. Additionally, optimum levels of temperature and water level will accelerate the growth metabolism of HABs (Huang et al., 2014) in any waterbody. The presence of HABs can alter the odour and taste for the water thereby making it unfit for portable purposes (Backer, 2002). An excessive amount of chlorine may be needed to remediate HABs from the surface water before becoming portable (Berardo et al., 2019). Additionally, excess HABs in water bodies are associated with eutrophic zones, eventually depleting the oxygen levels in the water body and causing dead zones (Stumpf et al., 2007). More importantly, dermal contact with HABs has shown detrimental health effects like skins allergies, gastrolienal disorders, etc. (Storming et al.,2020). Hence there is an immediate need to detect and remediate HABs as soon as possible.

Generally, the detection of HABs is carried out in two ways. One is through conventional in situ data collection, where samples are taken from the water bodies and laboratory analyses confirm the presence and species of algae and their toxins. Even though the accuracy of this detection method is very high, it is expensive, time consuming, labour intensive, and may take too long to make fast management decisions to prevent public harm (Shafique et al., 2001). Identifying the blooms through remote sensing techniques can be carried without such constraints and within a limited time frame, though its accuracy is decreased. Stroming et al. (2020) have shown that sensing the blooms through satellite data will have an economic benefit compared to conventional in-situ experiments. Thus, the goal of this work was to complete an explorative investigation to understand the effectiveness of Planetscope satellite data (which has a 3-5m resolution and 1-day return period) in detecting the blooms of Saguaro Lake (Arizaona, USA).

2 METHODOLOGY

The proposed framework of the methodology followed for sensing the HABs using Planetscope satellite data is shown in Figure 1. First, a preliminary inspection of satellite images is done. If HABs were undetected through visual inspection, a scientific algorithm is developed by correlating the in-situ chlorophyll-A data with the surface reflectance.The algorithm was developed by correlating the in-situ chlorophyll-A concentration with the maximum reflectance of NIR/RED bands of Planet data. The developed Algorithm with a R^2 of 62.2% is

ISBN: 978-90-824846-7-0

indicated as in Equation 1. The developed algorithm is integrated into the raster calculator of QGIS.3.20 to create the HABs spatial maps of Saguaro Lake for the year 2020.

$$Chlorophyll - A\ (\frac{\mu g}{L}) = 106.4 - 79.96\ (\frac{NIR}{Red}) \qquad [1]$$

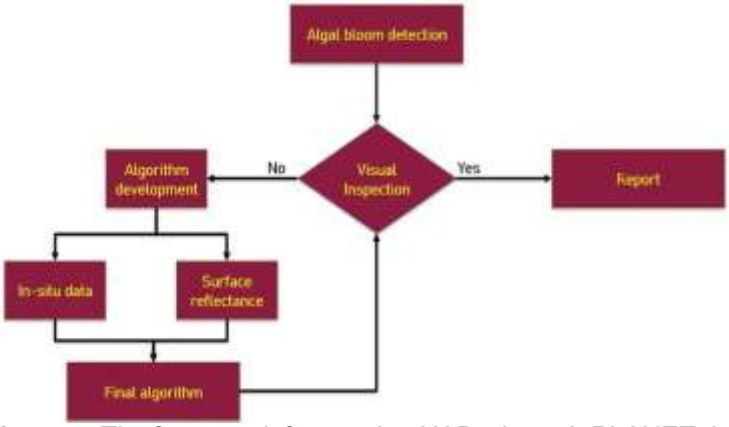

Figure.1. The framework for sensing HABs through PLANET data.

3 CONCLUSIONS

HABs that were undetected through False color composite (FCC) were identified through an algorithm developed by correlating the Planetscope data surface reflectance and in-situ chlorophyll-A concentration. The better spatial and temporal resolution of Planetscope data resulted with a good correlation of 62.2 % in sensing HABs. Nevertheless, HABs were difficult to distinguish at a chlorophyll-A concentration less than 20 µg/L, mainly because of similar water reflectance values. More complex scientific algorithms should be developed to overcome this shortcoming, and during sampling, the collection station of chlorophyll should be marked with accurate latitude and longitude to improve future algorithms.

REFERENCES

Backer, L. C. (2002). Cyanobacterial harmful algal blooms (CyanoHABs): Developing a public health response. *Lake and reservoir Management*, 18(1), 20-31.

Berardo, R., Turner, V. K., & Rice, S. (2019). Systemic coordination and the problem of seasonal harmful algal blooms in Lake Erie. *Ecology and Society*, 24(3).

Huang, C., Li, Y., Yang, H., Sun, D., Yu, Z., Zhang, Z., ... & Xu, L. (2014). Detection of algal bloom and factors influencing its formation in Taihu Lake from 2000 to 2011 by MODIS. *Environmental earth sciences*, 71(8), 3705-3714.

Martin, J. F., Kalcic, M. M., Aloysius, N., Apostel, A. M., Brooker, M. R., Evenson, G., ... & Wang, Y. C. (2021). Evaluating management options to reduce Lake Erie algal blooms using an ensemble of watershed models. *Journal of Environmental Management*, 280, 111710.

Shafique, N. A., Autrey, B. C., Fulk, F., Cormier, S. M., & Environmental, S. (2001). The selection of narrow wavebands for optimizing water quality monitoring on the Great Miami River, Ohio using hyperspectral remote sensor data. *Journal of Spatial Hydrology*, 1(1), 1-22.

Stroming, S., Robertson, M., Mabee, B., Kuwayama, Y., & Schaeffer, B. (2020). Quantifying the human health benefits of using satellite information to detect cyanobacterial harmful algal blooms and manage recreational advisories in US Lakes. *GeoHealth*, 4(9), e2020GH000254.

Stumpf, R. P., & Tomlinson, M. C. (2007). Remote sensing of harmful algal blooms. *In Remote sensing of coastal aquatic environments* (pp. 277-296). Springer, Dordrecht.

ISBN: 978-90-824846-7-0

Proceedings of the 2nd IAHR
Young Professionals Congress
30 Nov-2 Dec. 2021

Characterization of droughts in the Quilca-Chili Basin, Peru using the Standardized precipitation index (SPI)

Michell A. Fernández [1] and Ivana K. Escate [1]
[1,2] Young Professional Network Peru, Arequipa, Peru,
e-mail mafernandezv5@gmail.com
e-mail ing.escate05@gmail.com

ABSTRACT

The Quilca-Chili basin, located in southern Peru, is one of the main sources of water supply in Arequipa and the basis of its development. In its upper zone, there is a system of reservoirs that capture water resources from precipitation and provides water for human consumption and other productive uses. Nevertheless, the basin has been affected several occasions by droughts, due to its location and meteorological phenomenon such as El Niño-Southern Oscillation (ENSO). Using the Regional Vector Method (RVM), we divided the basin into three regions named Transfer Zone, Basin Head and Intermediate Basin covering the period 1970-2020. These regions showed an increase in their frequency, duration and intensity during the events of the ENSO that affected the availability of the water resources for Arequipa.

Keywords: drought, standardized precipitation index, Quilca - Chili basin, precipitation, ENSO.

1 INTRODUCTION

According to WMO, drought is an insidious natural hazard that results from lower levels of precipitation than what is considered normal. When this phenomenon extends over a season or a longer period of time, precipitation is insufficient to meet the demands of human activities and the environment. This problem is exacerbated by climate change in southern Peru according to the National Meteorology and Hydrology Service of Peru (SENAMHI).

Due to its geography and location, the Quilca-Chili basin is frequently affected by drought events, especially during the ENSO periods which affect the precipitation in the region. The SPI will allow the establishment of areas in the Quilca Chili basin where the impact of droughts has eventually increased in intensity and frequency. It is necessary to know these parameters to be able to carry out an adequate plan to mitigate the effects of droughts. These zones mentioned have not yet been analyzed in light of the continuous changes in climate variability in the Quilca Chili basin. Therefore, the objectives of this research were i) to identify in which areas the values of the characteristics occur with greater intensity, duration and frequency in the Quilca-Chili basin from the point of view of meteorological droughts and ii) to analyze the change in the characteristics of droughts during ENSO events. The results can serve as a basis for developing risk management strategies for future droughts in the basin.

2 DATA AND METHODS

We selected monthly series of precipitations (P) from 19 rainfall stations along the three regions of the basin, during the period 1970-2020 proposed for the analysis. We did not use precipitation in the lower basin because it is almost null throughout the year. To start with, the homogenization of the stations in these three regions was calculated with the Vector Regional Method using the software Hydraccess. Secondly, the SPI was calculated on each station according to Mckee (1993) in 3 – scales: 3-, 6- and 12- months. Then, we evaluated the results considering droughts as SPI lower than -1 for at least 3, 6 and 12 months respectively to the time scales. Finally, in each region of the analysis period, the frequency of occurrence of droughts and the characteristics of duration, intensity and severity were based on the “run theory” and were mapped to facilitate spatial analysis.

3 RESULTS

The SPI series in each region were averaged and the characteristics of the droughts were analyzed for each time scale. The SPI time series revealed that drought events were generally more intense (maximum intensity) and severe (negative index accumulation within a long drought duration) during ENSO events. The periods of

82-83, 91-92 and 97-98 coincide with ENSO events. In addition, in most of the stations of the three regions, it is evident that the year 1983 presents the highest intensity with respect to the other years. However, we can analyze that the Basin Head area was more affected during the years 82-83 as well as the Transfer Zone. The Intermediate Basin was affected by the period between the years 92-93 more than the other two regions. Besides, the Transfer Zone and the Basin Head have a higher average maximum intensity than the Intermediate Basin.

Table 1. Average characteristics of droughts for the three zones in Quilca-Chili basin

SPI <-1	Transfer Zone			Head basin zone			Intermediate Zone		
	SPI 3-	SPI 6-	SPI 12-	SPI 3-	SPI 6-	SPI 12-	SPI 3-	SPI 6-	SPI 12-
Frequency (%)	13.97	14.53	14.34	14.38	15.53	14.95	10.10	14.62	16.43
Duration (N° months)	4.86	7.00	13.63	4.11	7.23	16.00	3.58	7.07	16.50
Max. Intensity	-2.57	-2.95	-3.58	-2.18	-2.68	-3.71	-2.17	-2.41	-2.45
Max. Severity	-13.25	-24.84	-36.78	-15.98	-25.82	-38.05	-13.41	-23.08	-38.05

In addition, Table 1 shows that the duration of the drought is similar except in SPI 12- in the intermediate zone where it is longer. While in its SPI 3- it is shorter in relation to the transfer zone and head basin zone. In a similar way, it happens with the frequency having the same pattern as the duration of drought events.

4 CONCLUSIONS

The major conclusions of this study are: i) the SPI index calculated shows that the most intense and severe drought events occur during ENSO events. Thus, this research can be the basis for the development of further research on the correlation between ENSO events and droughts in the Quilca-Chili basin; ii) the Head Basin zone presents the average maximum intensity for SPI 12- and an average duration of 16 months similar to Intermediate zone. This is a severe problem because the zone is where most of the dams that supply water to the city are located. And iii) the events tended to last longer and showed higher intensity and severity, especially during ENSO events, suggesting that the main effects of droughts could be felt on river flows and groundwater. This research can serve as the basis for the development of drought and water management plans in the Quilca-Chili basin to face the effects of ENSO and climate change.

REFERENCES

Colotti, E., Cedeño, M., and Montañez, C. (2013). Meteorological drought and variation of agriculture land in The Margarita Island, Nueva Esparta state, Venezuela. Period 1972-2004. *Terra*. *Nueva Etapa*, 24 (45),11-53.

Edwards, D.C. and T.B. McKee (1997): Characteristics of 20th century drought in the United States at multiple time scales. *Climatology Report*, 97-2, Department of Atmospheric Science, Colorado State University, Fort Collins, Colorado.

McKee, T.B., N.J. Doesken and J. Kleist (1993): The relationship of drought frequency and duration to time scale. *In: Proceedings of the Eighth Conference on Applied Climatology, Anaheim, California*,17–22 January 1993. Boston, American Meteorological Society, 179–184.

WMO (2012). Standardized Precipitation Index User Guide. *World Meteorological Organization*, 1090, 9.

ISBN: 978-90-824846-7-0

Proceedings of the 2nd IAHR
Young Professionals Congress
30 Nov-2 Dec. 2021

Influence of the Inter-annual variation in the vegetable coverage in the Chicama River Basin, La Libertad-Perú, with SWAT modeling

Espinoza Varillas, Kithner[1,2], Yaranga Lázaro, David[3,4] & Prudencio Paredes, Fernando[5]

[1] *Master's Programme in Water Resources – National Agrarian University La Molina, Lima, Peru,*

[2] *Scientific Research Assistant at the Geophysical Institute of Peru, Lima, Peru*
alfonso.e08@gmail.com

[3] *Master's Programme in Water Resources –National Agrarian University La Molina, Lima, Peru,*

[4] *National Meteorological and Hydrological Service Peru, Lima, Peru*
davidyar7@gmail.com

[5] *Master's Programme in Applied Statistics – National Agrarian University La Molina, Lima, Peru,*
fjprudenciop@gmail.com

ABSTRACT
The study analyzed the incidence of vegetation cover change in the water response of the Chicama river basin, La Libertad, Peru, evaluating satellite images of the years 1995, 2005 and 2015 of the Landast product (5TM and 8OLI). Using the SWAT model, the monthly discharge was simulated in three scenarios: vegetation cover 1995, 2005 and 2015. The statistics show an acceptable performance in the calibration period: 1995 (NSE = 0.71, R2 = 0.87), 2005 (NSE = 0.71, R2 = 0.87) and 2015 (NSE = 0.72, R2 = 0.87); and validation (2001-2016): 1995 (NSE = 0.69, R2 = 0.8), 2005 (NSE = 0.7, R2 = 0.81) and 2015 (NSE = 0.71, R2 = 0.82). It was concluded that the reduction in coverage between 1995 and 2005 affects a better characterization (+ 3%) of the flows during the flood season, while between 2005-2015 the characterization during the flood season is reduced (-5%).

Keywords: Water availability, Climate change, PISCO v.2.1, Landast, SWAT.

1 INTRODUCTION

The latest report from the Intergovernmental Panel on Climate Change (IPCC) indicates that projections for climate change in the coming decades will increase in all regions (IPCC, 2021). Peru already suffers from this problem, and it is that in relation to extreme events (meteorological or climatic), the presence of frosts and droughts that occur annually stands out (MINAM, 2016). Soto et al. (2010), shows that during the years 2000 and 2010, 163 drought events were recorded in Peru, of which 78% occurred on the coast, 15% in the mountains and 7% in the jungle, reflecting the first impact of climate change.

2 OBJECTIVE

Analyze the incidence of interannual variability of vegetation cover in the water response of the Chicama river basin through SWAT modeling, during the period 1981-2016.

3 MATERIALS AND METHODS

3.1 Study area

The area that encloses the Chicama basin from its sources to its delivery in the Pacific Ocean is 4814.3 km² with a perimeter of 418.7 km. Geographically it is located approximately between the parallels 7°21' and 7°59' of South Latitude and the meridians 78°14' and 79°20' of West Longitude (ANA, 2015). Like most of the rivers of the Coast of Peru, in the Chicama river, the discharges present marked differences in their extreme values; reaching a maximum flow of 1,441.16 m3/s in the rainy season, and decreasing to 0.50 m3/s in the dry season, with a monthly average of 26.6 m3/s, which causes an annual discharge of 839.4 MM3 (ANA , 2003).

3.2 Data

3.2.1 Observed , gridded climatological information and Hydrometric

The daily grilled information PISCO Precipitation v2.1 and maximum and minimum temperature v1.1 were

ISBN: 978-90-824846-7-0

used, with a spatial resolution of 0.1 ° (10km) (Aybar et al. 2019), the distribution of 7 pseudo meteorological stations was characterized, 1 by delimited sub-basins, in the Chicama river basin. The analysis period ranges from January 1981 to December 2016. Hydrometric information for the calibration and validation process comprises the period 1981 -2016.

3.2.2 DEM, Land Use and Soil Type

The DEM was downloaded from the Geoserver of the Peruvian Ministry of the Environment and the soil map used was from INRENA (National Institute of Natural Resources) (INRENA, 2004), at a scale of 1: 5,00,000 rasterized in 90m x 90m. Land use was characterized considering three annual compounds (1995, 2005 and 2015) of Landast data (5TM and 8OLI) that correspond to the atmospherically corrected surface reflectivity products from the google earth engine catalog (https: // developers .google.com / earth engine / datasets / catalog / landsat).

3.3 Methodology

SWAT Hydrological Model
SWAT (Neitsch, Arnold, Kiniry, & Williams, 2011) or Soil and Water Assessment Tool. It is a model of a river basin in continuous and semi-distributed time. The process of uncertainty analysis, automatic calibration and validation of the model was used SWATcup (Abbaspour et al., 2015).
The efficiency of the model will be evaluated considering statistics such as the Nash-Sutclife efficiency method (NSE), the percentage bias method (PBIAS) and the RSR method by RMSE-Observations Standard Deviation. According (D.N. Moriasi et al. 2007) estimated as satisfactory if NSE> 0.5, RSR≤0.70 and PBIAS = ± 25% for flow.

4 RESULTS

The coverage classification was developed from a principal component analysis of the six spectral bands (VNIR and SWIR) obtaining three new predictor variables. The analysis shows that between 1995 and 2005, the areas with the highest incidence were forests (-12%), shrubs (-17%) and wetlands (-36%). While 2005 and 2015, the areas with the highest incidence were forests (-15%), Shrubby scrub (-23%). On the other hand, the monthly evaluation during the calibration process (1983-2000) of the three models were: 1995 Scenario (NSE=0.75, R2=0.83, PBIAS=-30.3), 2005 Scenario (NSE=0.76, R2=0.83, PBIAS=-29.6) and 2015 Scenario (NSE=0.76, R2=0.83, PBIAS=-27.9); while the statistics of the validation process (2001-2016) were: 1995 Scenario (NSE=0.79, R2=0.84, PBIAS=-11.4), 2005 Scenario (NSE=0.78, R2=0.84, PBIAS=-10.3) and 2015 Scenario (NSE=0.77, R2=0.84, PBIAS=-7.4).

5 CONCLUSIONS

The analysis of the water response of the Chicama basin between the coverage from 1995 to 2005 shows an improvement of 2% in the statistics, mainly during the flood season (January-April), as a result of the reduction in the vegetation cover affecting the generation of surface runoff. Between the years 2005 to 2015, it shows a reduction of approximately 6% in the statistics with respect to the months of floods, but an improvement in the response of the flows during low water, mainly due to the increase in the coverage areas that affects the recharge of the aquifer. .

REFERENCES

Abbaspour, K. C., Rouholahnejad, E., Vaghefi, S., Srinivasan, R., Yang, H., & Kløve, B. (2015). A continental-scale hydrology and water quality model for Europe: Calibration and uncertainty of a high-resolution large-scale SWAT model. *Journal of Hydrology*. https://doi.org/10.1016/j.jhydrol.2015.03.027

Aybar, C., Fernández, C., Huerta, A., Lavado, W., Vega, F., & Felipe-Obando, O. (2019). Construction of a high-resolution gridded rainfall dataset for Peru from 1981 to the present day. *Hydrological Sciences Journal*. https://doi.org/10.1080/02626667.2019.1649411

D. N. Moriasi, J. G. Arnold, M. W. Van Liew, R. L. Bingner, R. D. Harmel, & T. L. Veith. (2007). Model Evaluation Guidelines for Systematic Quantification of Accuracy in Watershed Simulations. *Transactions of the ASABE*. https://doi.org/10.13031/2013.23153

Neitsch, S. ., Arnold, J. ., Kiniry, J. ., & Williams, J. . (2011). *Soil & Water Assessment Tool: Theoretical Documentation Version 2009*. *Texas Water Resources Institute, TR-406*. https://doi.org/10.1016/j.scitotenv.2015.11.063

ISBN: 978-90-824846-7-0